# Energy Absorption Characteristics and Assessment of Failure Criteria during Ship Collisions

by

Alexandros Glykas
*Diploma Degree, National Technical University of Athens, C.Eng*

Thesis Submitted for the Degree of Doctor of Philosophy

Department of Naval Architecture and Ocean Engineering
Faculty of Engineering

University of Glasgow

May 1998

This thesis is dedicated to my Parents,

*Ioannis and Themelina*

# DECLARATION

Except where reference is made to the work of others,
this thesis is believed to be original

# ACKNOWLEDGMENTS

This thesis is the result of a study carried out in the department of Naval Architecture and Ocean Engineering at the University of Glasgow during the last three years. Within the following paragraphs I would like to acknowledge those people whose direct or indirect contribution brought me to this stage.

I would like to thank my supervisor, Dr. P.K. Das for his assistance throughout the period of the three years. The lengthy discussions, consistent supervision and advise I received from Dr. Das provided me with appropriate confidence and encouragement for my work. I wish to confess that sometimes I was not a very obedient student but this is due to my character since I always seek knowledge through my inquisition. I also appreciate my supervisor's support for my participation to ISOPE-96 conference in Los Angeles.

I'm indebted to Professor Nigel Barltrop for the interest he showed for my project and his advise regarding the modeling of my finite element model. His background in numerical analysis was very helpful for my queries. I also wish to express my appreciation for his contribution in my first two publications. I would like to wish to him all the best for the future in the department as a head.

I wish to thank Mr. Ian Winkle for his suggestions related to the presentation of this thesis. His experience as a good reader and recognized writer proved very helpful. I also wish to recognize his valuable ideas regarding the hydrostatic calculations involved in my model.

I don't forget the contribution of Professor Douglas Faulkner who initially accepted me in the department prior to his retirement. I'm also grateful to him because he

recommended me as a student member at the UK/EC team involved at the 2nd phase of the Derbyshire expedition, during March/April 1997.

I would also like to acknowledge the assistance of Professor Mike Cowling from the department of Mechanical Engineering regarding his comments about the Fracture Mechanics, related to my first Publication.

Special thanks are also addressed to Pratul Chaterjee, for his valuable help in the numerical analysis, Alberto Morandi for his guidance around ABAQUS, when I first came to the department, and Yasmine Mather for her help in installing ABAQUS EXPLICIT in NEMO.

Last, but not least from the department I would like to thank Maureen McGrady, our departmental secretary, for her assistance, David Percival, our Network and computer wizard man for his help when I was messing around with the software and Thelma Will, our secretary in the hydro lab. The presence of all three was and still is very valuable.

Special thanks are addressed to my ex-Supervisor from the National Technical University of Athens, Professor Manolis Samuelides, who first showed me the way to this thesis. Thank you very much!

I also wish to thank Trym Tveitnes for his wizardry in Excel, my honest friend Dimitris Konovessis for his general comments for this thesis. I wish you good luck in your Ph.D. degree. Tom Robertson, for his help in the English in my second publication, my cousin Michael Glykas for his assistance during the preparation of the writing work, Elizabeth Ford for the corrections she suggested about the English in the chapters included herein, and my friend Vagelis Zacharis, for his encouragement and the fun we had during our stay in Glasgow.

Special thanks are also addressed to Kyriakos Papadeas, Christos Papadimitriou and Michalis Fragiskos for their hospitality and patience during the preparation of this thesis. I wish them good luck and all the best for their future.

This thesis owes far to much to the stimulating guidance and critical advise I received from Mr. Frank Wall and all the inspiration, knowledge, experience and assistance from Mr. Robin Williams. Both these friends helped me to understand that beyond the numbers hidden in this thesis there is something more meaningful, such as the interest for human virtues like honesty, integrity, and respect to those who sacrificed their lives in order to make progress in Shipping.

Concluding, I would like to express my appreciation to both my parents Γιάννης και Θέμις whose moral support and love for the sea brought me to this position.

# LIST OF CONTENTS

# SUMMARY

Ship collision against rigid bodies is a very complex phenomenon and a large number of parameters are involved. All analytical methods developed until now consider the colliding ship as a rigid structure. This suggests that methods used to date have not considered the deformation of the ship. The potential energy derived is estimated as a function of the available kinetic energy prior to the collision. Especially in the case of grounding the response of the ship during the impact is examined with the equations of motion and kinematic relationships. The energy dissipated on the structural members and the kinetic energy lost due to the collision still remains unknown.

The use of Finite Element Methods has proved to be, one way to analyse the structural response of a ship structure during collision. It is feasible to ascertain the effect of mass inertia, strain rate hardening, complicated boundary conditions etc.. In this thesis a three-dimensional finite element model of a bow, is presented for the collision and grounding with a rigid object. The energy dissipation of the structural configuration is examined and compared with the existing empirical methods. A parametric study is performed and the results are presented in terms of velocity, the duration of the collision and the relative penetration. An evaluation for the calculation of the indentation is compared with existing empirical approaches.

Furthermore a fracture criterion is introduced on the basis of the energy released during crack propagation. A comparative study is shown involving three other failure criteria and the fracture criterion utilisation is validated on the bow model during the collision with a rigid surface. Results are generated with regard to the indentation, limit speeds and potential energy dissipated on the bow.

# NOTATION

| | |
|---|---|
| A | Cross sectional area, equation 2.44 |
| a | Distance from centre of gravity, equation 2.23 |
| a, b | Plate length, width table5.1 |
| $a_{1,2,3,4}$ | Coefficients, equation 3.31 |
| $a_1$,$a_2$ | Coefficient which depend on ice class, table 2.2 |
| $A_{MV}$ | Area of tearing |
| AP | After perpendicular |
| $A_z$ | Water plane area |
| B | Breadth of vessel, equation 2.41 |
| b | Breadth, equation 2.42 |
| B | Buoyancy |
| b | Coefficient, equation 3.36 |
| b | Distance from centre of buoyancy, equation 2.23 |
| $b_{\alpha\beta}(\omega)$ | Frequency depended on damping coefficient |
| $b_1$ | Constant, equation 1.2 |
| $b_2$ | Constant, equation 1.2 |
| $b_e$ | Effective plate width |
| $b_i$ | Width of the i-th flange, equation 2.51 |
| Bulk 1 | Notation, refer to table 3.5 and figure A3-23 |

| | |
|---|---|
| Bulk 2 | Notation, refer to table 3.5 and figure A3-23 |
| Bulk 3 | Notation, refer to table 3.5 and figure A3-23 |
| c | Half crack length |
| CASPPR | Canadian arctic waters pollution prevention act |
| $C_B$ | Block coefficient |
| $C_{DH}$ | Coefficient table 3.3 |
| $C_{MD}$ | Coefficient, equation 3.3 |
| COD | Crack opening displacement |
| d | Coefficient, equation 3.36 |
| D | Constant, equation 2.17 |
| d | Draft of vessel, equation 2.41 |
| D | Factor, equation 2.34 |
| $d_c$ | Bow collapse distance |
| Deck 1 | Notation, refer to table 3.5 and figure A3-23 |
| Deck 2 | Notation, refer to table 3.5 and figure A3-23 |
| Deck 3 | Notation, refer to table 3.5 and figure A3-23 |
| Deck 4 | Notation, refer to table 3.5 and figure A3-23 |
| Deck 5 | Notation, refer to table 3.5 and figure A3-23 |
| Deck 6 | Notation, refer to table 3.5 and figure A3-23 |
| Deck 7 | Notation, refer to table 3.5 and figure A3-23 |
| Deck 8 | Notation, refer to table 3.5 and figure A3-23 |
| Deck 9 | Notation, refer to table 3.5 and figure A3-23 |
| $d_S$ | Distance, equation 1.4 |
| DWT | Deadweight |
| E | Young's modulus |

| | |
|---|---|
| $E_\alpha$ | Plastic energy, equation 2.14 |
| $E_D$ | Energy absorbed in structural deformation |
| $E_{Ei}$ | Elastic energy of the i-th member |
| $E_{Fi}$ | Friction energy of the i-th member |
| $E_I$ | Potential energy absorbed up to i-th frame, equation 2.53 |
| $E_{kinetic}$ | Kinetic energy |
| $E_{Pi}$ | Plastic energy of the i-th member |
| f | Body force vector, equation 2.56 |
| F | Friction force, equation 2.10,2.11 |
| $F_c$ | Crippling force, equation 2.52 |
| $F_z$ | Vertical force, equation 2.38 |
| G | Energy release rate, equation 5.10-5.11 |
| g | Gravity |
| g | Number of flanges and cuts, equation 2.44 |
| h | Thickness, equation 2.42 |
| $h(\tau)$ | Unit response function, equation 2.4 |
| HAZ | Heat affected zone |
| $h_S$ | Height of broken or heavily deformed longitudinal member, equation 1.3 |
| IMO | International Maritime Organisation |
| $I_r$ | Indentation radiation |
| $I_x$ | Moment of inertia about x- axis |
| $I_y$ | Moment of inertia about y- axis |
| $I_z$ | Moment of inertia about z- axis |
| $j_{yy}$ | Dimensionless added mass for the pitch motion |

| | |
|---|---|
| k | Effective area of contact over the area of plating,, equation 1.6 |
| K | Stress intensity factor, equation 5.20 |
| K, M, N | External moments experienced at the origin |
| kDWT | 1000 DWT |
| $K_T$ | Kinetic energy |
| L | Length of vessel, $=l_{bp}$, equation 2.41 |
| $L_b$ | Length of span |
| LBZ | Local brittle zone |
| LCB(t) | Centre of buoyancy with regard to the time |
| LCF | Centre of flotation distance from AP |
| LNG | Large natural gas carrier |
| LR | Lloyd's Register of Shipping |
| m | Constant, equation 2.43 |
| M | Mass |
| m | Mass |
| $m_{\alpha\beta}$ | Added mass coefficient |
| M* | Mass of the offshore structure with added mass |
| m* | Mass of the ship with added mass |
| $m_a$ | Added mass, equation 2.54 |
| MEPC | Marine environment pollution committee |
| $M_p$ | Plastic movement capacity, equation 5.2a |
| $m_s$ | Mass of the ship |
| $M_S$ | Still water bending moment |
| $M_W$ | Wave bending moment |
| $m_{xx}$ | Added mass in x-direction |

| | |
|---|---|
| $m_{yy}$ | Added mass in y-direction |
| $m_{zz}$ | Added mass in z-direction |
| $n_1$ | Unit vector in direction 1, equation 3.6-3.9 |
| $n_2$ | Unit vector in direction 2, equation 3.6-3.9 |
| $n_{AT}$ | Number of angle and t-sections in the cross section |
| $n_c$ | Number of cruciforms in the cross section |
| NCRE | Naval Construction Research Establishment and now Defence Evaluation and Research Agency (DERA) |
| $n_f$ | Total number of flanges, angles and t-sections in the cross section, equation 2.51 |
| $n_T$ | Number of t-sections in the cross section |
| OPA | Oil Pollution Act |
| P | Change in momentum, equation 2.35 |
| P | Impact force |
| $P_c$ | Collapse load, equation 5.2a-5.2b |
| $P_c$ | Crippling force, equation 2.47 |
| $P_m$ | Mean crushing load, equation 2.51 |
| psi | Pounds square inch = 0.0689 bar = 0.0680 atm |
| r | Equivalent radius of inertia, equation 2.39 |
| r(x,t) | Reaction force distribution density, equation 4.11 |
| $R_{max}$ | Maximum reaction force, equation 4.11 |
| $R_{MV}$ | Destroyed volume |
| $R_T$ | Resistance factor |
| $r_y$ | Radius of plastic zone around crack |
| s | Second |
| $SED_{FM}$ | Strain energy density fracture mechanics |

| | |
|---|---|
| $S_{ij}$ | Component of the stress deviator tensor, equation 2.19 |
| t | Time |
| t | Thickness, equation 5.19 |
| $t_d$ | Deck thickness,, equation 1.6 |
| $t_i$ | Thickness of the i-th flange, equation 2.51 |
| $t_S$ | Associated thickness to $h_s$, equation 1.3 |
| $t_s$ | Thickness of skin, equation 2.46 |
| $t_w$ | Thickness of stiffening members, equation 2.46 |
| $\dot{U}$ | Energy release rate |
| U | Internal energy per unit mass, equation 2.56 |
| u | Velocity at x direction |
| UDL | Uniformly distributed load |
| $\overline{V_i}$ | Vector parallel to the axis of movement |
| $\vec{v}$ | Velocity vector, equation 2.56 |
| V | Speed, equation 2.12 |
| VLCC | Very large cargo carrier |
| VLNG | Very large natural gas carrier |
| $V_o$ | Initial speed prior to collision |
| $V_t$ | Speed at time t, equation 3.31 |
| $V_x$ | Speed in horizontal direction |
| $v_y$ | Velocity at y direction |
| $V_z$ | Speed in vertical direction |
| W | Specimen width, equation 5.12-5.13 |
| w | Velocity at z direction |

| | |
|---|---|
| w | Weight distribution table 3.2 |
| $W_{critical}$ | Critical deflection |
| $W_f$ | Final deflection |
| X,Y,Z | External forces on the ship along the three axes |
| $X_g$ | X-co-ordinate for the centre of gravity |
| $X_{max}$ | Maximum indentation, equation 2.77 |
| $Y_g$ | Y-co-ordinate for the centre of gravity |
| $Z_g$ | Z-co-ordinate for the centre of gravity |
| $Z_u$ | Lifted distance of the bow, equation 2.76 |
| $\alpha_{\alpha\beta}(\omega)$ | Frequency depended added mass |
| $\overline{\alpha}_{max}$ | Crack dimension, equation 5.1 |
| $\alpha$ | Stem angel, equation 1.6 |
| $\beta$ | Direction of impact force, equation 2.26 |
| $\beta$ | Plate slenderness ratio |
| $\delta_c$ | Critical COD value |
| $\delta_{\gamma_\alpha}$ | "Slip" of point a, equation 3.11 |
| $\dot{\varepsilon}$ | Strain rate |
| $\varepsilon_o$ | Elastic yield strain |
| $\theta$ | Angle of inclined surface, equation 2.29 |
| $\kappa_{\alpha\beta}$ | Surface curvature matrix |
| $\mu$ | Constant, equation 2.43 |
| $\mu$ | Friction coefficient, equation 2.25 |
| $\nu$ | Poisson ratio =0.3 |
| P | Constant, equation 2.17 |

| | |
|---|---|
| $\rho$ | Mass density |
| $\sigma_o(\dot{\varepsilon})$ | Variation of ultimate stress with respect to the strain rate |
| $\sigma_y$ | Yield Stress |
| $\tau$ | Time |
| $\varphi(t)$ | Pitching angle of the vessel |
| $\psi$ | Stem angle |
| $\omega$ | Angular velocity |
| $\nabla$ | Vessel displacement |

# CHAPTER ONE

# INTRODUCTION and LITERATURE REVIEW

## 1.1 PREFACE TO THE THESIS

A search back into the history of mankind would reveal that amongst the first human discoveries made was sailing. Boats were built during the same period (approximately 3000 BC), Chapelle (1998), as the discovery of the wheel, and other simple machines. These ultimately triggered human intelligence to investigate the question of *"how does it work?"*

Observation of the "basics" has always been the impetus of perceiving the theoretical background. Simple examples are *Archimedes "Eureka"* back in the 3rd century BC, *or Aristoteles* suggestions, in the 4th century BC, regarding the consistency of matter comprising the four elements, earth, air, fire, and water, as well as *Isaac Newton's* observations of falling apples which led to the powerful theory of gravitation back in 1687.

***How does it work?*** This has been a dominant question of scientists ever since the 18th Century. Once this question was satisfied, the transition from the *understanding* to the *creation,* promptly followed, ***"How do we make it work?"***! using the knowledge accumulated so far?

Due to the lack of accurate construction designs in engineering or in science, hazardous events occurred with catastrophic consequences, to both the community and the environment. Nevertheless engineers did not become discouraged at all when their creations ceased to perform due to the forces of nature. The challenge was always there!

The tragic loss of numerous lives and the destruction due to pollution caused, has made it necessary to study and focus on the nature of the problem. In consequence, a redefinition in the question mentioned earlier soon followed: ***"how can we make it work SAFELY, and what sacrifices are we willing to accept when safety standards are less than 100% perfect."***

## 1.2 INTRODUCTION

Of all the major accidents which a ship can incur, collisions are the most frequent. With increased speeds and displacements of modern ships, it is of consequence that collisions are commonly more serious due to the growth in kinetic energy. Contrary to the rate of major structural failures on ships, grounding and collisions are, by far, more recurrent and can result in major environmental disasters.

The analysis of ship collisions and grounding is now receiving appropriate attention due to recent major hazardous events, for example, the penetration of the ship shell which not only endangers the ship but also causes major environmental pollution. This especially applies to collisions between vessels carrying cargo such as crude oil, chemicals or liquefied gas.

Public opinion has always been sensitive to disasters at sea, but never more so than in modern times when incidents of this nature receives wide coverage through the media. Accordingly, every major casualty or series of casualties is a stimulant to the formulation of new and increasingly stringent safety regulations.

Thus the loss of 548 British ships and 3000 fatalities in 1882 led to legislation of load lines. The "TITANIC", "MORRO CASTLE", "ANDREA DORIA" and "TORREY CANYON" disasters, to name but a few, have been at the origin of regulations affecting subdivision, fire prevention, damage stability and pollution prevention.

The loss of the "TITANIC" after the collision with an iceberg was initially treated as a problem of compartment subdivision. Following this incident, the Bulkhead Committee in 1915 recommended that the collision bulkhead should be positioned at the minimum distance of one twentieth of the ship's length from the fore end of the stem, at the level of the load waterline.

Nowadays there is increasing interest in ship collision analysis. Despite the great complexity of the subject, this theoretically analyses the interaction between the

striking ship and the struck object, which could be, for example, an offshore structure, another ship, an iceberg or a rigid pier.

The design of a ship able to survive collision forces embodies the following key points:

- What is the impact force on the ship structure?
- What is the amount of energy dissipated during the collision and how is this energy dissipated in the individual ship structural members which are directly involved during the collision?
- What is the maximum indentation in the ship, if the collision is head-on?
- Is it possible to define failure criteria which are directly involved with the structural integrity and watertightness of the hull and how can these criteria be used to set limits on the impact speed?

Contrary to earlier years, nowadays, sophisticated and powerful numerical tools using finite element analysis have allowed the detailed modelling of such structures and hence, the response under various exciting forces may be predicted.

Possible collision scenarios that have been recorded during last decades are:

- Ship to ship collisions, (Both ships are in motion, or at least one of them).
- Ship to offshore structure collision.
- Ship to rigid pier, such as bridge concrete pillar base.
- Ship to artificial island (where the artificial island may absorb energy or not).
- Bottom ship collision with rigid bottom, grounding.

The head-on collision of a ship with a rigid pillar base and the collision to a rigid artificial island are both examined in this Thesis. Following the theoretical knowledge accumulated on the issue of ship collisions, a numerical example has been developed. This aims to address the key points mentioned previously. The methodology followed during the modelling and the results acquired from this analysis, presents possible guidance on the numerical procedure and potential understanding of the dynamics involved. The model is based on a 27500 tons

Deadweight tanker which is subjected to a head-on impact with a rigid wall, and alternately grounding with rigid bodies.

## 1.3 LITERATURE REVIEW

Safety in shipping has many meanings, like stability safety, structural safety, safety from fire or machinery breakdown, or in general Safety Of life at Sea. For some people the meaning to the word safety is directly translated into finance. That means: higher safety, less profit, and the opposite! In the ultimate *safety can be defined simply as freedom from danger or risks*. Although total loss of life or property is tacitly accepted as an inherent risk of air travel, this has never been so in the case of sea transport. Bates M. J. (1975)

To reduce the consequences of ship collision we should either reduce the probability of collision by adopting adequate navigation measures (PREVENTION), or choose proper structural configuration against collisions (MITIGATION), or a combination of both. It seems impossible to create a structural configuration that will be able to withstand most of the accidental loading derived during operational use, and equally impossible on the other hand, to adopt a decision strategy that will ensure prevention of a collision.

A combination of both prevention and mitigation can be met by imposing certain rules, such as, limit the speed of the vessels in areas of high collision probability. This action would allow more time of response for the officers of the ship (Prevention) as well as the amount of energy released during an accidental collision (Mitigation).

In order to provide potential guidance on the optimum structural design arrangements and the reaction of the vessel during collision, some rational approach is required which will consider all the factors involved. The outcome would be a substantial mathematical tool, which would accurately predict the limit speeds, the structural configuration response, and the energy dissipated.

Because of the number of parameters and uncertainties involved in a ship to ship collision, the prediction of the structural response of the vessel is complicated. Engineers dealing with collision analysis adopt simplifying assumptions so that the solution of the problem becomes feasible. Samouelides (1984) defines these assumptions as:

1. A collision resulting in significant damage is an inelastic problem {Minorsky V. (1959)}.
2. The behaviour of the material is ductile.
3. Structural behaviour can be decoupled from the rigid body response.
4. Structural behaviour may be treated as quasi static.
5. The main energy absorption mechanism prior to fracture of the side shell is membrane tension, Jones (1979).

Some of these assumptions have received support, e.g. {assumption 4 by Jones (1973)}, whereas others have been questioned, e.g. {assumption 5 by Woisin (1983)}.

Most of the analytical models derived for grounding or collision adopt a number of assumptions. However, modern computers and sophisticated numerical codes make it possible to eliminate a large number of assumptions and to study the topic more thoroughly.

### 1.3.1 DESCRIPTION OF A SHIP COLLISION

As mentioned above, the interaction between the two colliding ships is very complicated. Therefore, most papers studied the two extreme cases, namely,

1. A rigid bow against a deformable body for example an offshore structure.
2. A deformable bow against a rigid body,
   - Head-on Collision
   - Grounding

Scenario one describes the collision of two ships and examines the response of a struck vessel from another ship, while the second scenario examines the response of the structural members located in the bow of a ship, during a grounding or during a head on collision with a rigid body.

#### 1.3.1.1 A RIGID BOW AGAINST A DEFORMABLE BODY OR SURFACE

The pioneer in this area is Minorsky (1959) who published his solution to predict the collision of a nuclear powered ship which was based on the record experience in a number of collisions. The main assumption he adopted was that the energy absorbed by a damage structure is proportional to the volume of the damaged steel material. In two ships under a collision scenario this hypothesis presumes that all the loss of the kinetic energy is transformed only to plastic energy. The method neglects the elastic energy stored in a system thus it is not applicable in minor collisions where elastic energy is predominant.

Minorsky collected information on 26 damaged ships and identified the loss of kinetic energy ($K_T$) and the resistance factor ($R_T$) as two parameters which largely describe the structural damage associated with major ship collision. The formula Minorsky proposed is:

$$K_T = 47 \cdot R_T + 32 \qquad 1.1$$

Where the kinetic energy is expressed in MJoules and the resistance factor as defined by Minorsky (1979) in $m^3$. Through calculation, a straight-line relationship was found between the value of $K_T$ and $R_T$, shown in Figure 1.1.

Factor $R_T$ is very difficult to estimate and a method is given in the paper Minorsky (1959). It should be noted in Figure 1.1 that $K_T$ and $R_T$ do not follow a straight-line relationship near the origin. This signifies the existence of high elastic energy densities where Minorsky's relationship is not valid.

For many years designers extensively used Minorsky's formula all over the world despite its limitations. Because of it's simplicity, several engineers, in the past modified his formula. Several formulae were proposed separately by Haywood (1971), Woisin (1979 and 1986), Jones (1979), NCRE[1] (ISSC, 1967) and Vaughan (1978).

The modification proposed by Haywood (1971), resulted in a formula which was applied in the collision assessment in double hull LNG carriers. The changes he proposed consisted in the alteration the constant value in equation 1.1 in order to account for rupture of the vertically stiffened outer shell and the longitudinally stiffened inner shell,. The formula Haywood proposed was:

$$K_T = 47 \cdot R_T + b_1 + b_2 \qquad 1.2$$

where $K_T$ and $R_T$ are the same as equation 1.1

$b_1$ is equal to 32 if the hull is transversely stiffened or equal to 96 if the hull is longitudinally stiffened

$b_2$ the same as $b_1$ for a longitudinal bulkhead if it exists; otherwise it is equal to zero

Based on experimental results, and his long time working experience in this field Woisin (1979) proposed a modified formula in which he suggested that the constant

[1] Naval Construction Research Establishment and now Defence Evaluation and Research Agency (DERA)

in equation 1.1 should be replaced by a function of the height of the side-shell or longitudinal bulkhead and the square of its thickness. His formula was;

$$K_T = 47 \cdot R_T + 0.5 \sum h_s t_s^2 \qquad 1.3$$

where $h_s$ [m] is the height of broken or heavily deformed longitudinal member
$t_s$ [cm] is the thickness of the member

Recently, Woisin (1986) made a small change in his original proposal of equation 1.3 by introducing the distance $d_s$, between the nearest plate structure attached to the shell and extending in the longitudinal and transverse directions, such as decks, inner decks and ship's bottom. The modified formula was:

$$K_T = 47 \cdot R_T + 0.19 \sum d_s h_s t_s \qquad 1.4$$

where $d_s$ [m] is the between the nearest plate structure attached to the shell.

In this formula, three spatial dimensions were used but without the dimensions in the longitudinal direction, such as the distance between webframe or transverse bulkhead.

During a minor collision the membrane energy absorbed in stiffened hull plating and in stiffened decks is the dominant energy absorption within the struck ship. Jones (1979) developed a simple formula to extend Minorsky's method to minor collision problems. Considering a rigid perfectly plastic beam with fully clamped supports across a span $2L_b$ subjected to a concentrated load $P_c$ at the mid span, Jones presented the formula 1.1 as;

$$K_T = 0.030288 \cdot \sigma_y \cdot R_T \cdot \left( \frac{W_f}{L_b} \right)^2 \qquad 1.5$$

where $R_T$ is the volume of side shell assumed to be involved in membrane mechanism and is equal to $2 \cdot L \cdot B \cdot H / 144$ in $ft^2$

$\sigma_y$ is the yield stress

$W_f$ is the final deflection

This approach was used in order to estimate the energy, which could be absorbed by a struck ship before the rupture of the side shell. Equation 1.5 is plotted for various values of final deflection/span length, with a yield stress of 207 $MNm^{-2}$ in Figure 1.2. It is also compared with Minorsky's semi empirical results derived from equation 1.1. Plotting equation 1.5 with w/2L <1/3, (where w is the deflection of the beam with length L) gives a family of lines, which radiate from the origin of Figure 1.2 and traverse the entire area, which contains minor or low energy collisions.

Engineers at NCRE (1967) and Vaughan (1978), have proposed formulae for the calculation of the energy required to tear decks and/or bottoms of ship structures. NCRE (1967) proposed the following formula

$$K_T = 2 \cdot k \cdot \sigma_C \cdot t_d \left( \tan \frac{a}{2} + \psi \right) w_f^2 \qquad 1.6$$

where k is the effective area of contact over the area of plating

$t_d$ is the thickness of the deck

a is the stem angle

$\psi$ coefficient of friction

$\sigma_c$ is the crippling stress

Vaughan's formula follows as

$$K_T = 93 \cdot R_{MV} + 32 \cdot A_{MV} \qquad 1.7$$

where $R_{MV}$ is the destroyed volume in $[m^3]$

$A_{MV}$ is the area of tearing in $[m^2]$

Poudret J. et al (1981), presented a comparison against Minorsky's equation 1.1 using the data collected from a grounded LNG carrier of 130000 tons displacement, and in

this case Vaughan's formula gave the better estimation required to damage the structure. However it is mentioned in Samouelides (1984) that this result should be treated with caution since it appears to be a consequence of the way the crushed volume was calculated.

The formulae presented here are typical modifications to Minorsky's method, but are extended in two different ways. Formulae were produced from empirical and experimental data, and formulae were the outcome of analytical calculations. Woisin followed Minorsky's method with emphasis on the results from real experiments and large-scale tests, modifying Minorsky's formula to fit the statistical data. However Jones analysed the problem theoretically, using an analytical model of clear mechanical sense, and implemented an additional structural damage parameter $W_f$.

The Minorsky and other modified methods are simple to use for design purposes. For a loss of kinetic energy during the collision the total volume of material damaged in collision is estimated. These methods may always be updated since they are based on observable measurements of the volume of the damaged area involved in a collision. However these methods cannot estimate the change in the energy absorption characteristics with alternate structural configurations. Collision between ships and other marine structures is a complicated phenomenon, which involves dynamic effects, hydrodynamic forces, interaction between the two colliding ships and structural failure modes. For better comprehension of this subject and better understanding of the contribution from the individual factors, structural analysis has been integrated in both quasi-static and dynamic approaches, using empirical, analytical and numerical solutions.

#### *1.3.1.2 A DEFORMABLE BOW AGAINST A RIGID BODY OR SURFACE*

Gerard (1958) calculated the crippling strength of simple sections based upon the results of a series of panel tests with various stiffener types. His empirical formula is shown in Section 2.3.2 where extensive analysis takes place. This formula was introduced for calculating the crippling strength of multi-corner (more than two

corners) air frame sections. This method is simple and quick; it appears that it could be applied to the section of a ship's bow to give sufficient answers, accurate enough to satisfy designers interested in knowing impact forces against bridge piers.

Minorsky (1983) introduced Gerard's formula into the calculation of the impact force, during a head-on collision with a rigid pier, with a slight modification to the thickness of the members involved as will be discussed thoroughly in Section 2.3.2. Minorsky, found very good correlation, claiming accuracy to within 10% with the experimental results of "ESSO MALAYSIA", a crude oil carrier built in 1967 by Howald Werke-Deutsche Werft. The collision tests were conducted on a welded model of it's bow to a scale of 1/12.

Pedersen and Valsgaro (1993) suggest that Gerard's approach too simple because it has been derived from simple and regular plate constructions where the variation of parameters has been limited, e.g. the range of plating to stiffener thickness ratios and stiffener spacing. Ideally, Pedersen et al. (1993) suggest, that this method should be combined with a probability function for the simultaneous occurrence of load maxima of the individual panels. However such information is not provided.

Because Gerard's approach was developed for applications in the aviation industry in collisions where speed is very high the strain rate effect was introduced on the dynamic flow stress $\sigma_o$ by Marsh and Campbell (1963), based on test results from the following relationship:

$$\sigma_O\left(\dot{\varepsilon}\right) = 1.29\sigma_y \dot{\varepsilon}^{0.037} \qquad 1.8$$

where $\sigma_y$ is the static ultimate strength of the steel material

$\dot{\varepsilon}$ is the strain rate

Following Minorsky's modification to Gerard's empirical formula, Amdahl (1983) presented a formula (see Section 2.3.3), developed from the theoretical considerations of Jones N. Wierzbicki T. (1983), of the energy dissipated in steel structures subjected to deep collapse, such as T-sections and cruciforms, see Figure 1.3. The total crushing load of a specific structure is determined by adding up the

contributions from all the basic elements comprising the actual cross-section. Examples between the theoretical predictions and the experimental results are given in Amdahl (1995).

Pedersen et al. (1993) conducted a series of bow crushing load calculations on several ships listed in the appendix of the paper, and they modified Amdahl's equation in order to obtain a better fit to experimental crushing results. The modification included an increase of the deformation energy, of corner angles at intersections between the upper deck/bottom and the bow sides, on the assumption that these angles will collapse in the same mode as cruciforms.

Aldwinckle (1984) introduce a model to predict the bow collapse distance resulting from the head on high-energy collision of a ship with rigid vertical iceberg. This model has been used to derive a correlation between the energy absorbed in structural deformation, the bow collapse distance, ship-side parameters and Ice Class. The correlation extensively discussed in Section 2.3.1. Aldwinckle's method is based on the following basic assumptions;

1. Collapse occurs frame by frame, each frame remains undistorted until the preceding frame is crushed completely flat
2. The collapse load of each panel is determined by the critical buckling stress
3. The load carried by each panel decreases linearly as the panel collapses over the frame spacing

Yang & Caldwell's method (1988) is, to a large extent, based on the same deformation and energy evaluation made by Amdahl. They introduced an equivalent thickness of the longitudinal stiffeners attached on the shell plating so that the equivalent plating has plastic bending moment capacity equal to the shell plating with longitudinal stiffeners. This method is discussed further in Section 2.3.4.

Pedersen et al. (1993) adopted a comparative study using the last three empirical methods for the calculation of the penetration and energy absorption on 6 different vessels. He found good correlation between Yang & Caldwell's (1988) and the

modified Amdahl's (1983) methods, but it overestimated results produced from Gerard's formula. It should be noted however that Gerard's formula had not been applied in the form provided by Minorsky (1983) but in the authentic form from Gerard 1958. Pedersen (1993) introduced a parametric analysis into the results obtained from the results of the vessels. He proposed an expression for the maximum bow collision load, the energy absorbed by the bow, the maximum indentation and the duration of the collision.

Glykas, Das, Faulkner (1995) conducted a study on the assessment of a Forth Road Bridge ship collision where they calculated the forces induced by ships during collision with a rigid pier structure. The authors adopted Gerard's Approach for the estimation of the crippling force derived on the bow structure, and the vessel speed with respect to the energy absorbed and the penetration was shown. This work was later on {Glykas, Das, (1998)} calculated numerically and moderate agreement with Gerard's approach was found. This is further explained in Chapter 2.

In summary, the static approaches described above may be applied, provided that assumptions have been made in order to account for the dynamic effects; e.g. the inertia force of the impacting bodies is usually described through an increase of the actual mass. The energy absorbed by the ship can be determined by integrating the Force-Indentation relation. In adopting the static approach for predicting the damage of the colliding ships, the problem remaining is how to construct a force deformation curve of the individual structural members located in the bow and how to define a reliable failure criterion in order to limit the maximum deflections.

### *1.3.2 OTHER STATIC APPROACHES*

In the following pages a review of the static approaches to ship-ship collisions and grounding is made.

### 1.3.2.1 SHIP TO SHIP COLLISIONS

Hegazy (1980) developed a method for predicting the energy absorbed during a collision by adding together the energy quantities derived from the individual members of the struck vessel and the energy dissipated during the crushing of the bow from the striking ship. Comparison of the calculated and recorded energies from the scale tests which Hegazy considered, showed that the two values of the absorbed energies agreed reasonably well. However, Hegazy (1980) noticed a large discrepancy between the calculated and measured values for some of the tests and he attributed this to the premature rupture of the side plating prior to the development of significant plastic energy from membrane straining of the side plating.

Plate tearing during collision and grounding was studied by Jones N. and Jouri W. S. (1987), where they concluded that plate rupture can not be scaled geometrically between full scale and model tests. They presented a comparison of the results from a full-scale prototype plate and a ¼ scale model and found that the full scale suffers penetrations, which are 2.62 times larger. Similar conclusions had been reached in previous work of theirs in Jones N. (1984) and Jones N., Jouri, W. S., & Birch, R. S. (1984)

To simulate the ship-ship collision process, a lot of work has been done in which the structure is subjected to impact from knife-edge indentures. Akita et al. (1972) reported two distinctly different failure types in transversely framed side structure when penetrated statically by a rigid bow. One is a deformation type and the other is a crack type. The former occurred when the strain beneath the bow was less than about 0.3. The latter was observed for large strains. Various series of tests and simple theoretical analysis were carried out. In the paper of Ando and Arita (1976), experiments were reported on double-hull models penetrated statically by a rigid bow model to estimate the amount of energy absorbed in the hull plating during a minor collision. This is neglected in the design procedure proposed by Minorsky.

Ito et al. (1984 and 1985) performed static tests, leading to destruction, on large-scale models of side and bilge structures similar to those on ships with a double hull construction. The striking bow was taken as rigid and the type of collision was

classified into five groups, from a geometric point of view, between a colliding bow and hull. A simple theoretical procedure was developed using a displacement method formulated in matrix form and quite good agreement was obtained with corresponding experimental results.

Pettersen (1981) used the simplified non-linear finite element program to make a static analysis of the damaged region of a struck vessel involved in collision. The use of simplified elements reduced the computing cost but the results generated by this particular procedure have not been verified. Valsgård and Pettersen (1982) developed this procedure further to allow for interaction between the bow and side structures and for rupture of the side shell.

Ronalds and Dowling (1986) investigated the plastic behaviour of a T-shaped beam under central point loading and derived simple formulae for modelling the denting process of the beam with finite deflections. The formulae were extended to longitudinally stiffened plates and shells. Small-scale model tests on stiffened plates and shells were conducted and comparisons were made with theoretical results.

The failure of square plates under lateral load and the load carrying mechanism with restrained edges at large deflections was numerically studied by Fan Z. (1994). In his paper he adopts a finite element solution for plates under uniformly distributed load, with various boundary conditions, and he defines the difference of membrane and bending action on plates with regard to the restraining.

#### *1.3.2.2 GROUNDING*

A great amount of work has been done in the area of the collision of the bottom structure of vessel which, in simple terms is known as grounding. At the 30$^{th}$ session of the IMO Marine environment committee, (MEPC) in November 1990, the Government of the United States proposed amendments to Annex 1 of MARPOL 73/78. These amendments were aimed at making double hull construction mandatory for new oil tankers. Although this proposal received general support several

delegations expressed the view that other designs, arguably as effective as the double hull in protecting the environment, should also be accepted.

The introduction of a mandatory design in Tankers, defined new criteria related to the optimisation of the double hulled vessels; e.g. the residual strength after grounding, and the resistance characteristics derived from bottom impacts with rigid bodies.

Pedersen (1995) defines the motion of the ship under the action of the hydrodynamic forces and the grounded reaction forces, and presents a method for evaluation of the grounded reaction of a vessel. His method is based on mathematical models, for the overall motions of the involved ship structures, for determination of those forces and energies, which must be absorbed by crushing of the structure. Vredeveldt, (1995) signifies the importance of enlarging the scope of the grounding to the quantification of "accepTable risks". The necessity of applying rational risk assessments for grounding of RO/RO ships is pointed out with some considerations of the use of full scale testing.

Pedersen's work, was complemented by Östergaard (1995) in his work entitled "Collision and Grounding Mechanics". Solutions of a collision problem and various stranding cases are demonstrated, in view of potential hazards for personnel and the environment, in cases where either one of the structures involved in such a situation fails. For example, either the ship structure or the wall or seabed structure upon which the ship is stranding will fail. In the two cases risk analysis of load carrying systems is used as a rational basis for safety decisions in design and operation of load carrying structures.

Paik J. and Pedersen T. (1996) presented a study in grounded-induced sectional forces and residual strength of grounded ships. They used an analytical approach to estimate the forces derived from the ship. The extend and location of the structural damage due to grounding was defined on the basis of the American Bureau of Shipping SafeHull Guide. They calculated the possibility of hull collapse of the grounded hull as a rate of the total applied bending moment and the residual bending

strength. Amongst their conclusions is that the risk the grounding-induced sectional forces exceeding the design (wave-induced) loads is greater for grounding amidships than grounding at the fore end of the ship.

Simonsen and Wierzbicki (1996) predicted the damage of tankers during grounding, taking into account the coupling between the external ship dynamics and the local damage process of the hull girder. The model for the local damage was based on a least upper bound solution with kinematic compatibility between all structural members. Friction was considered in the model and they showed how this contributed to the horizontal resistance force and the vertical reaction force. Their model was validated by large-scale tests done by Rodd J. (1996), & Rodd J. (1997) who developed a series of results from one-fifth scale oil tanker grounding experiments.

Ohtsubo H. et al (1997) developed a simplified damage prediction method for the grounding, side impact and bow collision of oil tankers, and the results were compared with existing results from experimental work. The approximate formulas presented in this paper, were formed through application of plasticity mechanics and good correlation was shown ist with the experimental data. The advantage of this method is that calculations are simple without requiring the use of computer programs.

For the protection of bridges against collision from vessels, Ottesen et al. (1994) published an article regarding artificial islands as protection against impact. The authors used analytical methods to calculate the size of the artificial islands or 'protective works' as they were referred to. A theory of ship-soil interaction was developed for ships sliding up on slopes. In their work they showed that for low soil permeability a water build up will take place at the forward end. This will lift the ship bow resulting in the ship sliding further up the slope before being brought to a stop. For high permeability the ship will dig into the slope and be stopped by the force of the soil. Stopping lengths and frictional coefficients between bow and fill were calculated analytically. The calculations have been checked against laboratory and full-scale tests. The agreement between tests and calculations was reasonable.

They also showed that stopping lengths and frictional coefficients depended on bow type and geometry.

On the probability of grounding and collision events between ships and bridges work has been published by Pedersen (1995). The main advantage of this method is that it allows comparisons of various navigation routes and procedures by assessing the relative frequencies of collisions and grounding.

The ship collision and grounding problem was described in this Section, as it has been presented in static and analytical methods, commencing from the pioneer Minorsky back in 1959, until now. Static approaches, as mentioned earlier, do not account for dynamic phenomena, the importance of which is very significant in real scale collisions. Minorsky's formula, along with the modifications applied, was numerously used for preliminary design calculations, and could be refined, if necessary, for the case of minor collisions. Most of the dynamic approaches developed throughout the years, were based on simple small-scale testing, but their results due to the nonlinearities involved and the problem of scaling were always debatable. Nowadays the introduction of powerful numerical techniques allows to the engineers to validate the significance of these factors, which eventually leads to simple and beneficial simple truths regarding this subject. More of the importance of dynamics during ship collision and grounding follow in the next Section.

### *1.3.3 DYNAMIC AND NUMERICAL APPROACHES FOR COLLISION AND GROUNDING*

Strictly speaking, all major impacts and collisions will involve some dynamic effects. Kinetic energy will, by some mechanism, be transferred to elastic plastic friction and wave energy, during the structural deformation. The mass inertia forces, the hydrodynamic added mass, and material strain rate sensitivity are issues which have to be introduced in the examination of the global as well the local response of a vessel during a grounding or collision.

In the early 60s, a series of impact experiments were conducted in Japan, Harima et al. (1962), for beams of various shaped cross-section and stiffened plates as well as double-hull side structure models. For the fully clamped plates and stiffened plates, a ball-end striker was used to hit the plate centre dynamically. In the theoretical analysis, however only the static solution for a circular plate model was adopted.

Ueda et al. (1989) studied the dynamic elastic response of a tubular beam under collision through point contact, using an equivalent mass spring model incorporated with the Finite Element Method in which the local and bending deformation of the beam was considered. Based on the analysis, the phenomena were classified into three groups depending on the ratio of the stiffness and mass.

Pettersen (1979) used the simplified non-linear finite element program DOBL for the quasi-static analysis of the damaged region of a struck vessel involved in a low energy collision. The use of "simplified elements" reduced the computing cost but the results generated by this particular procedure have not been verified. The procedure does not allow geometrical non-linearity to be taken into account. This would appear to limit the extent of side shell damage that can be considered by the technique used for his analysis.

Soreide and Amdahl (1982) and Amdahl (1983) performed a series of static and dynamic tests on tubular members. It was observed for a certain range of impact velocity that the load indentation curve is raised by about 10 % due to dynamic effects, while very little influence is obtained on the opposite side of the cross section. This phenomenon indicates that the dynamic loading primarily affects the local deformation at point of impact, and that the increase in load carrying capacity is caused by a rise in the material stress-strain curve due to strain-rate sensitivity. Since the strain rate increase the yield stress, the dynamic yield stress is multiplied by a factor to allow for the strain rate sensitivity of yield stress in struck beams Parkes (1958) and in the side shell of a struck tanker Jones (1979).

Zhu, and Faulkner (1994) studied the dynamic inelastic behaviour of plates in minor ship collisions by adopting experiments and numerical work. In the numerical

simulation, the side structure of a struck ship is simplified as a fully clamped rectangular plate and the striking vessel as a knife-edge indenture. The collision is treated as "minor" and no rupture on the plate occurs. The striking ship is of relatively small mass but has relatively large velocities. Numerical predictions favourably match the results from impact experiments on clamped plates and on small-scale ship models. The authors present results where strain rate sensitivity is an important factor, affecting the dynamic response and they also claim that the energy analysis based on the dominant membrane behaviour can well explain the overall response of the plate. They conclude that local stress/strain analysis throws light on the investigation of plate failure and they suggest that a failure/fracture criterion should be adopted on this basis.

Samouelides (1984) made studies on the structural dynamics and rigid body response coupling in ship collision both numerically and experimentally. The proposed procedure solved the governing equation using a time-marching technique that included the hydrodynamic force acting on the struck ship. The structural analysis used, predicted the behaviour of a beam and a plate-strip. The numerical model over-estimated the deflection with the theoretical predictions being 1.5 to 2.0 times the experimental results. In the experimental work of Samouelides (1984), a V-shaped striker was used to hit the structure and the deceleration of the striker during impact was measured, using an accelerometer attached to a dummy in order to establish the history of the interactive force between the striker and the model. However, from the recorded results, it was difficult to separate the rigid body acceleration of the striker from the vibrations of the member on which the instrument was mounted.

Egge & Böckenhauer (1991) within the framework of a research program 'Tanker Safety' developed a program system for the evaluation of the absorbed plastic deformation energy in a ship to ship collision. Their program describes the internal collision mechanics on the basis of the 'substructure method'. The principles this method follows, requires that all the areas of the ramming and rammed ships affected by the collision are divided into their structural components, e.g. plates, panels, stringers, frames shell, etc. and then the ultimate loads of these components are calculated by ultimate load and load buckling theory. The program system consists of

two parts: A program for calculating the ultimate loads of the bow structure of the ramming ship and a program for calculating loads in the side structure of the rammed vessel.

For the evaluation of the membrane behaviour of the shell Egge E. & Böckenhauer (1991) used non-linear FE-analysis and they found good correlation with the theoretical examples. However for the assessment of the elongation of the shell at the point of fracture during the collision, they assumed that a 5% elongation at rupture was realistic, based on the experiments of Woisin (1976) at GKSS, in Germany.

Glykas, Samuelides, Das (1996) developed a parametric study in which the failure-fracture of plate elements under U.D.L. and Patch loading was examined on the basis of encastre or free to pull-in boundary conditions. For the evaluation of the maximum displacement of the plates four failure criteria where used. The study, which is thoroughly described in chapter 5, shows that the elongation of the plate during bending did not exceed 1% in any case and this was attributed to the local failure in areas with high strain concentration.

Shen & Jones (1993) examined the dynamic plastic response of a fully clamped beam grillage, struck transversely at the centre by a heavy mass travelling with a low speed in order to gain further insight into the importance of inertia effects. While good agreement was obtained between the corresponding experimental results and quasi-static analysis in Jones et al. (1991), for the permanent transverse displacements, Shen & Jones (1993) extended the analysis to examine the dynamic plastic response. They obtained the plastic work distribution in a grillage for the purpose of predicting materials failure. Their work reveals an interesting behaviour of the plastic hinges, including their development, movement and disappearance and they predict very good agreement with the experimental results for the permanent transverse deflections at the mid-span of the aluminium alloy and mild steel grillages.

Bai & Pedersen (1991) and (1993) presented a method for the collision analysis of offshore steel structures and bridges, using a non-linear force–displacement

relationship. This relationship was derived for the simulation of the local indentation in a hit tubular member and a three-dimensional beam-column element is developed for the modelling of the global behaviour of the struck structure. Large deformations, plasticity and strain-hardening of the beam-column elements are accounted for by combining an elastic large displacement analysis theory with the plastic node method. The dynamic elastic-plastic response of offshore platforms in typical ship collision situations is investigated. It is shown that strain-hardening plays an important role in the impact response. Bai & Pedersen showed that a large part of the impact energy is transformed into plastic deformation energy of the struck structure in a severe ship-platform collision.

Corbett & Reid (1993) presented the results of a series of experimental tests on the local loading of circular plates resting on a ring support. Both quasi-static and impact loading tests were performed using hemispherical- tipped and flat-ended cylindrical indentures. The effects of local indentation on the overall quasi- static response of the plate are investigated, and the errors that arise from neglecting these effects, when applying rigid, perfectly- plastic plate theory to the problem, are highlighted. The maximum energy absorbing capacity of the plates when subjected to impact from hemispherical-tipped and flat-faced projectiles are determined experimentally and compared with the available empirical formulae.

Many solid materials behave plastically when they are subjected to high impulse loads. This may result in locally plastic wave propagation and propagating discontinuity surfaces like shocks, i.e. jumps of stresses and strains, or material interfaces. The wave structure, Lin X. and Ballmann (1993), which has a great influence on the dynamic yield pattern and fracture processes, can only be correctly preserved by methods that taking into account the probability of physical discontinuities. Unfortunately, most practical problems of mechanical waves in solids cannot be solved analytically due to the shape of the boundaries, stress hardening effects and complicated loading functions.

Kuroiwa et al. (1994) studied the structural damage of ships due to collision and grounding using finite element program DYNA3D. They investigated the failure

mechanism and the energy absorption capacity of ship structures and correlated the numerical results with large-scale experiments at Mitsubishi Heavy Industries, Nagasaki, Japan. In the numerical simulations failure of the fillet welds and rupture of plates were taken into account. The authors found very good correlation between the experimental and numerical results.

A comparative study on side collision was presented by Kitamura (1997), who carried out a series of numerical simulations of side collisions. The energy absorption capacity of a standard double side structure of a 300 kDWT class VLCC was compared with those of alternative designs, also the contribution of each structural component or category was examined in detail. For the fracture assessment of the steel plate the author adopts a criterion based on the strain, in areas where plasticity is predominant. A comparison of the numerical values derived on the basis of global energy with respect to the indentation of the shell comes to sufficient agreement to those values obtained from Glykas, et al. (1998).

Another numerical simulation of a ship colliding against a pier structure was carried out by Kisielewicz L. T. et al (1993) who reported the numerical autopsy of an actual accident involving a 500 tons cargo ship hitting a harbour pier made of concrete segments standing on the sea bottom. The authors describe the modelling assumptions and provide useful recommendations regarding the finite element construction. The structural response presented here is shows good agreement with the one provided by Glykas et al. (1998).

### *1.3.4 THE IMPACT OF HULL STRUCTURE & OIL SPILLS*

The emergence of new maritime nations, and the continuous rise in standards of living, results in a greater demand for sources of energy and industrial products. The consequent increase in the ship population of the world has been a contributory factor to a growing concern for the safety of ships, their crews and passengers and, more recently, for the protection of the environment.

The enormous environmental penalties due to the massive oil spills which accompany tanker groundings (for example, off the Alaskan coast in 1989, the Shetland Islands in 1993, the Korean Peninsula in 1995, South in Wales 1996) and tanker collision accidents, including those off the Sumatra Coast in 1993, have established the phenomenon of crude oil tanker accidents as a matter of worldwide concern.

As stated earlier every major casualty or series of casualties is a stimulant to the formation of new and increasingly stringent safety regulations.

Tank Vessels traditionally have been designed as single skinned hulls. Depending on the size of the vessel, longitudinal bulkheads are often present and the overwhelming majority of single skinned designs are longitudinally framed. The Oil Pollution Act 1990 introduced the double hulled tankers or, in layman words, a mandatory barrier inside the hull of the ship between the cargo and the environment.

The impact of hull structure on the reduction of outflow has had more limited attention and it has come later in the cycle of the recent considerations as well. The complexity of determining the contribution of structure to cargo protection and the unpredictability of structural response under the variety of potential damage scenarios, have no doubt contributed to this set of circumstance.

The function of a tank vessel's structural system may be examined from the point of view of normal operation and casualty operation. In providing adequate strength for normal operations, the objective in structural design is to maintain structural integrity of the hull girder, of bulkheads, decks, etc. and of plating, stiffeners and details. Other considerations relate to vessel size, complexity and heaviness of structure, producibility and maintainability. In terms of casualty operations, the objective is to maintain vessel integrity and to protect cargo, or conversely to protect the environment from oil pollution in case an accident occurs. In this case the primary considerations should encompass;

- Resistance to collision and grounding damage

- Resistance to fire and explosion damage
- Containment of cargo outflow if damage does occur and
- Maintenance of sufficient residual strength after damage in order to permit salvage and rescue operation and to minimise further damage and spilling of cargo.

Daidola J. (1995) published a Table in which 50 major oil spills from tankers and other combined carriers are shown, see Appendix 1. It can be seen that the circumstances leading to the accidents are the considerations mentioned above and among these collision and grounding hold a big percentage. Summarising, the following Table displays the categories of the causes of spillages except the unknowns

| | | |
|---|---|---|
| Grounding | 13 cases | 693 000 tons |
| Collision | 11 cases | 792 000 tons |
| Fire and Explosion | 12 cases | 851 000 tons |
| Structure and Machinery | 12 cases | 653 000 tons |

**TABLE 1.1 MAJOR SPILL OILS**

Note that Amoco Cadiz accident result in an outflow of 221000 tons of oil off the coast of France, the third largest in terms of outflow of oil. This accident is classified as a structural or machinery accident. The primary failure was the loss of steering. As a secondary failure the ship stranded and failed by progressive collapse of the hull. The accident might therefore as well be classified as grounding.

A major challenge for the marine community at present, is to come up with rational procedures for design against collision and grounding. The basis for such procedures is a deeper understanding of the complete scenario of different important categories of accident. Procedures to be applied should demonstrate a proper balance between a realistic representation of the accident scenario and ability to include the statistical

nature of accidents. A large range of possible accident scenarios should be considered, and each should given a proper double hull OPA (90).

One procedure of this type has been presented by Det norske Veritas by Köhler, P. E. (1990). In this model the potential oil spill from different tankers can be compared. The ship is defined in terms of tank arrangement and main scantlings. Operational parameters can either be specified by single values or by statistical distributions. The main parameters are the ship speed, extent of damage and location of damage.

## 1.4 AIM OF THIS THESIS

Ship collision against rigid bodies is a very complex phenomenon and a large number of parameters are involved. All analytical methods developed until now consider the colliding ship as a rigid structure. This suggests that methods used to date have not considered the deformation of the ship. The total energy derived is estimated as a function of the available kinetic energy prior to the collision. Especially in the case of grounding the response of the ship during the impact is examined with the equations of motion and kinematic relationships. The energy dissipated on the structural members and the kinetic energy lost due to the collision still remains unknown.

The use of Finite Element Methods has proved to be, one way to analyse the structural response of a ship structure during collision. It is feasible to ascertain the effect of mass inertia, strain rate hardening, complicated boundary conditions etc.. In this thesis a three-dimensional finite element model of a bow, is presented for the collision and grounding with a rigid object. The energy dissipation of the structural configuration is examined and compared with the existing empirical methods. A parametric study is performed and the results are presented in terms of velocity, the duration of the collision and the relative penetration. An evaluation for the calculation of the indentation is compared with existing empirical approaches.

Furthermore a fracture criterion is introduced on the basis of the energy released during crack propagation. A comparative study is shown involving three other failure criteria and the fracture criterion utilisation is validated on the bow model during the collision with a rigid surface. Results are generated with regard to the indentation, limit speeds and total energy dissipated on the bow.

It is hoped that the proposed methodology may provide useful guidelines in gaining a better understanding of ship collision and assisting ship designers with information regarding the response of bow collision with rigid objects.

## 1.5 LAYOUT OF THE THESIS

The second chapter contains a discussion of the analytical techniques applied to the collisions, starting from the kinematic relationship of the ship-ship collision, continuing to the collision of a ship with a rigid body and then grounding. The empirical methods developed in the area of a head-on collision are presented. Using Gerard's approach the calculation of the crippling force derived during a collision of a tanker vessel with a rigid structure is examined and the results are compared with the empirical formulas with respect to the energy absorbed, and indentation during the impact.

The third chapter demonstrates the construction of the finite element model of the bow structure as this was derived from data contained in the 2nd chapter. The assumptions and parameters involved in the modelling are presented and discussed. From Section 3.3 onwards the results from the numerical experiments are presented and compared with those calculated from the empirical approaches.

In the fourth chapter similar finite element analysis results are presented for the grounding problem. Two different sliding configurations are developed and the loss of kinetic energy during the impact is examined with regard to the total energy dissipated on the structural members. A particular investigation into the effects of the grounding reaction force on the global response of the vessel with regard to the bending moments and shear forces is also shown.

In the fifth chapter, the development of a fracture criterion is presented and a comparative study involving three other existing failure criteria is examined. Sections 5.1 to 5.5 are related to the development of the fracture criterion on simple rectangular plates under lateral load, and comparison of the energy absorbed when using the other criteria takes place. The application of the fracture criterion to the finite element model follows from Section 5.6 onwards and a design appraisal on the effects of the energy absorbed by the structure is made.

In the sixth chapter conclusions from the work reported herein are discussed along with some thoughts and proposals regarding future work on the subject.

## APPENDIX 1

| Rank | NAME | Tanker Size | Spillage | | Location | Cause | | | | |
|---|---|---|---|---|---|---|---|---|---|---|
| Rating | | DWT | Tons ($10^3$) | Type | | Co | Grn | F/e | S/h | N/k |
| 1 | ATLANTIC EMPRESS | 292666 | 257 | crude | West Indies | X | | | | |
| 2 | CASTILLO DE BELLVER | 271540 | 239 | crude | South Africa | | | X | X | |
| 3 | AMOCO CADIZ | 237439 | 221 | crude | France-Atlantic | | | | | |
| 4 | ODYSSEY | 138392 | 132 | crude | mid-Atlantic | | | X | | |
| 5 | TORREY CANYON | 121000 | 124 | crude | UK channel | | X | | | |
| 6 | SEA STAR | 120300 | 123 | crude | Gulf of Oman | X | | | | |
| 7 | HAWAIAN PATRIOT | 101038 | 101 | crude | Hawaian Island | | | | X | |
| 8 | INDEPENDENTA | 152408 | 95 | crude | Turkey, Bosp | X | | | | |
| 9 | URQUIOLA | 111125 | 91 | crude | Spain, north | | X | | | |
| 10 | IRENES SERENADE | 105460 | 82 | crude | Greece | | | X | | |
| 11 | KHARK 5 | 284632 | 76 | crude | Marocco, Med. | | | X | | |
| 12 | NOVA | 239435 | 68 | crude | Iran, Persian Gulf | X | | | | |

| | | | | | | | | | | |
|---|---|---|---|---|---|---|---|---|---|---|
| 13 | WARFA | 68600 | 62 | crude | South Africa | | X | | | |
| 14 | EPIC COLOCOTRONIS | 64000 | 58 | crude | West Indies | | X | | | |
| 15 | SINCLAIR PETROLORE | 56000 | 57 | crude | Brazil | | | X | | |
| 16 | YUYO MARU NO 10 | 52836 | 4242 | Wh prod | Japan | X | | | | |
| 17 | ASSIMI | 59032 | 50 | crude | Oman | | | X | | |
| 18 | ANDROS PATRIA | 122173 | 48 | crude | Spain, north | | | X | | |
| 19 | WORLD GLORY | 45000 | 46 | crude | South Africa | | | | X | |
| 20 | BRITISH AMBASSADOR | 44929 | 46 | crude | Japan | | | | X | |
| 21 | METULA | 206719 | 45 | crude | Chile | | X | | | |
| 22 | PERICLES G.C | 59096 | 44 | crude | Qatar | | | X | | |
| 23 | MANDOIL II | 45000 | 41 | crude | US, West coast | X | | | | |
| 24 | JAKOB MAERSK | 88000 | 41 | crude | Portugal | | X | | | |
| 25 | BURMAH AGATE | 62663 | 41 | crude | US, Gulf of Mexico | X | | | | |
| 26 | J. ANTONIO LAVALLEJA | 131663 | 38 | crude | Algeria | | X | | | |
| 27 | NAPIER | 38561 | 37 | crude | Chile | | X | | | |
| 28 | EXXON VALDEZ | 2144861 | 36 | crude | US, Alaska | | X | | | |

| | | | | | | | | | | |
|---|---|---|---|---|---|---|---|---|---|---|
| 29 | CORINTHOS | 56882 | 36 | crude | US, Delaware R | X | | | | |
| 30 | TRADER | 35000 | 36 | Fuel cgo. | Greece | | | | X | |
| 31 | ST PETER | 34730 | 33 | crude | Ecuador | | | X | | |
| 32 | GINO | 48760 | 32 | Carbon blk | France Atlantic | X | | | | |
| 33 | GOLDEN DRAKE | 30004 | 32 | crude | Bermuda | | | X | | |
| 34 | IOANNIS ANGELICOUSSI | 68106 | 32 | crude | Angola | | | X | | |
| 35 | CHRYSSI | 29653 | 32 | crude | Bermuda | | | | X | |
| 36 | IRENES CHALLENGE | 34884 | 31 | crude | Pacific Ocean | | | | X | |
| 37 | ARGO MERCHANT | 28691 | 28 | Fuel cgo. | US, East Coast | | X | | | |
| 38 | HEIMVARD | 55000 | 31 | crude | Japan | X | | | | |
| 39 | PEGASUS | --- | 25 | Wh prod | US, East Coast | | | | | X |
| 40 | PACOCEAN | 30016 | 31 | Crude | Northwest Pacific | | | | X | |
| 41 | TEXACO OKLAHOMA | 35072 | 29 | Fuel cgo. | US, East Coast | | | | X | |
| 42 | SCORPIO | 42000 | 31 | crude | Mexico, east | | X | | | |
| 43 | ELLEN CONWAY | 47566 | 31 | crude | Algeria | | X | | | |
| 44 | CARIBBEAN SEA | 30661 | 30 | Crude | East Pacific Ocean | | | | X | |

| | | | | | | | | | | |
|---|---|---|---|---|---|---|---|---|---|---|
| 45 | CRETAN STAR | 30372 | 27 | Crude | India, west | | | | | X |
| 46 | GRAND ZENITH | 29930 | 26 | Fuel cgo. | South Africa | | | | X | |
| 47 | ATHENIAN VENTURE | 31016 | 26 | Wh prod | Canada Newfd | | | X | | |
| 48 | VENOIL | 330954 | 26 | Crude | South Africa | X | | | | |
| 49 | ARAGON | 238959 | 24 | Crude | Madeira | | | | X | |
| 50 | OCEAN EAGLE | 18824 | 21 | crude | Puerto Rico | | X | | | |

Fifty major oil spills from tankers and combined carriers, Source Lloyd's Shipping Index: Green Tanker guide

Codes: Co =Collision, Grn =Grounding/Stranding; F/e =Fire explosion; S/h =Structural hull or machinery failure; N/k =Not known

## FIGURES

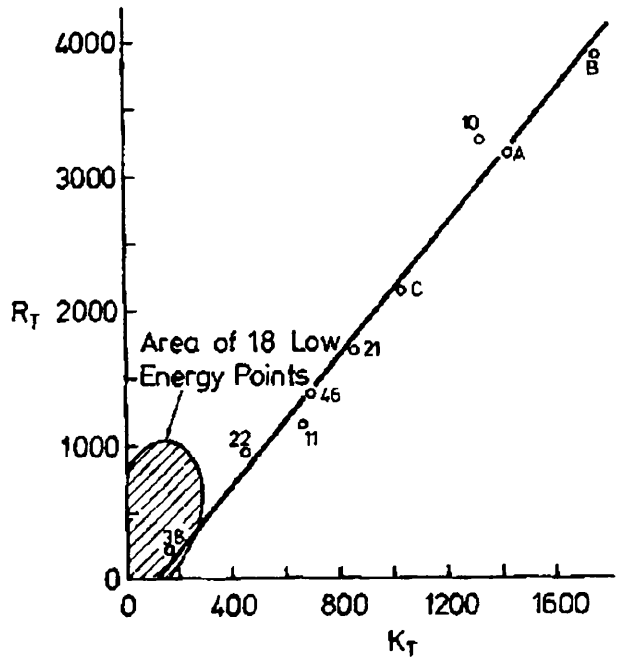


**Figure 1.1** *Minorsky's empirical correlation between resistance factor ($R_T$) and kinetic Energy ($K_T$) absorbed during a collision. $R_T$ is in $m^2$, and $K_T$ is in MJoules, Minorsky (1959)*

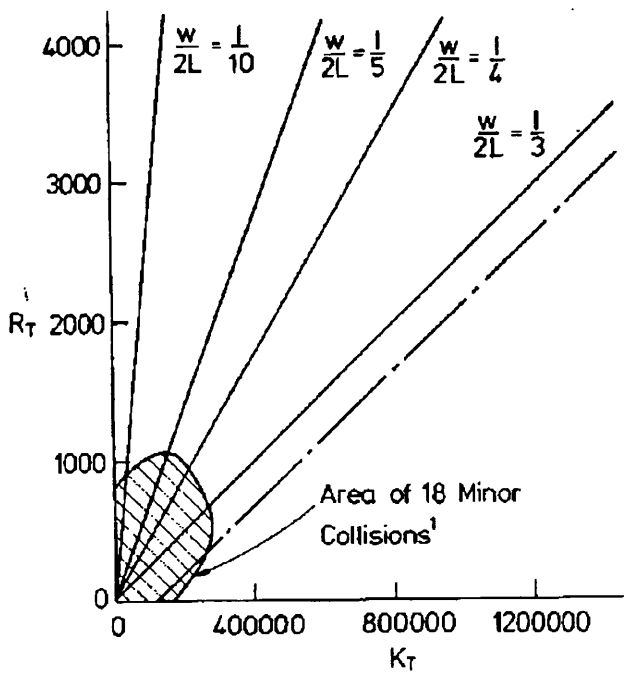


**Figure 1.2** *Comparison of the modified Minorsky method, Jones, with $\sigma_o$=30000 lbin$^{-2}$ for various values of w/2L $R_T$ is in ft$^2$ and $K_T$ is in ton knot$^2$, Jones (1993)*

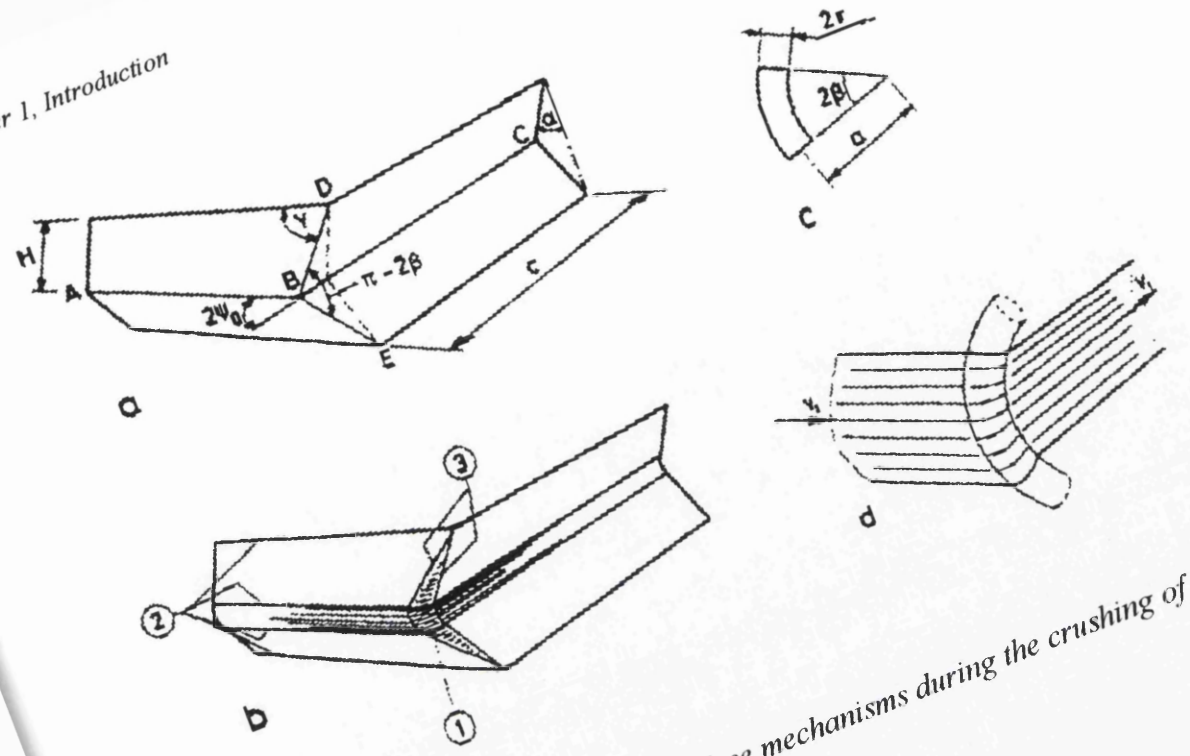


**Figure 1.3** *The sliding toroidal surface mechanisms during the crushing of simple members by Amdahl (1983)*

# CHAPTER TWO

# DYNAMICS OF SHIP'S COLLISIONS

## 2.1 GENERAL SHIP DYNAMICS DURING A COLLISION WITH A DEFORMABLE BODY

Collision response is a transient and a non-linear procedure including the continuous variation of parameters of geometric, structure boundary and material properties. There are two cases included in a collision analysis. The overall ship mechanics i.e. the ship's motion, and the internal mechanics, the deformation and damage of local structure of ship hull. The forces introduced in the collision procedure include the overall force acting on the ship hull and the local force acting at collision point. Both of them are related to the inertia and hydrodynamic forces, which act on ships. Collision leads to the deformation, damage and penetration of local structure and changes, consequently, the geometry as well as the amount and direction of components of collision forces in the collision zone.

Provided that the energy transmitted to elastic vibrations in the colliding ship hulls can be neglected, then Newton's law in six degrees of freedom describes the general motion of the rigid ship hulls. In a right-hand co-ordinate system fixed in the ship, general equations of motion for each of the ship hulls can be expresses as follows:

$$
\begin{aligned}
X &= m\left[\dot{u}+qw-rv-x_g\left(q^2+r^2\right)+y_g\left(pq-\dot{r}\right)+z_g\left(pr+\dot{q}\right)\right] \\
Y &= m\left[\dot{v}+ru-pw-y_g\left(r^2+p^2\right)+z_g\left(rq-\dot{p}\right)+x_g\left(pq+\dot{r}\right)\right] \\
Z &= m\left[\dot{w}+pv-qu-z_g\left(q^2+p^2\right)+x_g\left(pr-\dot{q}\right)+y_g\left(qr+\dot{p}\right)\right]
\end{aligned}
\qquad 2.1
$$

$$K = I_x \dot{p} + (I_z - I_y) qr + m\left[ y_g \left( \dot{w} + pv - qu \right) - z_g \left( \dot{v} + ru - pw \right) \right]$$

$$M = I_y \dot{q} + (I_x - I_z) pr + m\left[ z_g \left( \dot{u} + qw - rv \right) - x_g \left( \dot{w} + pv - qu \right) \right] \qquad 2.2$$

$$N = I_z \dot{r} + (I_y - I_x) qp + m\left[ x_g \left( \dot{v} + ru - pw \right) - y_g \left( \dot{u} + qw - rv \right) \right]$$

where:

| | |
|---|---|
| X, Y, Z | are the external forces on the ship along the three axes; |
| K, M, N | are the external moments experienced at origin; |
| u, v, w | are the velocities in x-, y-, and z-directions, respectively; |
| p, q and r | are the angular velocities about x-, y-, and z-directions; |
| xg, yg, zg | are the co-ordinates for the centre of gravity; |
| Ix, Iy, Iz | are the moments of inertia about the axes through origin; |
| m | is the mass; |
| (·) | Denotes the derivation with respect to time (acceleration) |

During a collision the most significant motions of the involved hulls will be in the water plane. If we assume that there is no coupling between the motion in the water plane and the vertical motions and, as indicated in Figure 2.1, that the co-ordinate system has its origin on the centreline, x-axis oriented longitudinally positively forward, y-axes transversely positively to the port side, and z-axis positively upwards from the ships baseline, then the equations for horizontal motions take the form:

$$X = m\left( \dot{u} - rv - x_g r^2 \right)$$

$$Y = m\left( \dot{v} + ru + x_g \dot{r} \right) \qquad 2.3$$

$$N = I_z \dot{r} + m x_g \left( \dot{v} + ru \right)$$

The external forces X, Y and N acting on the two ships during a collision are the results of propeller forces, rudder forces, wave-induced forces, forces due to current,

hydrodynamic forces and collision forces arising from deformation of material. However, the hydrodynamic pressure forces $(X^H, Y^H, N^H)$ and the collision forces $(X^C, Y^C, N^C)$ will dominate to such an extent that we can neglect other forces.

For a ship that is symmetrical about a plane through the longitudinal axis, the hydrodynamic pressure forces acting on the hull can be expressed as:

$$\begin{aligned}
X^H(t) &= -m_{xx}\dot{u} + m_{yy} v r + m_{y\psi} r_2 - \int_0^\infty h_{xx}(\tau) r(t-\tau) d\tau \\
Y^H(t) &= -m_{yy}\dot{v} - m_{y\psi}\dot{r} - m_{xx} u r - \int_0^\infty h_{yy}(\tau) v(t-\tau) d\tau - \int_0^\infty h_{y\psi}(\tau) r(t-\tau) d\tau \\
N^H(t) &= -m_{y\psi}\dot{v} - m_{\psi\psi}\dot{r} - (m_{yy} - m_{xx}) u v - m_{y\psi} u r - \int_0^\infty h_{y\psi}(\tau) v(t-\tau) d\tau \\
&\quad - \int_0^\infty h_{\psi\psi}(\tau) r(t-\tau) d\tau
\end{aligned} \qquad 2.4$$

where the terms with constant coefficients express the instantaneous hydrodynamic pressure forces when the free surface effects are absent. Due to the free surface, the ship will set up waves when it accelerates. These waves will cause fluctuations in the hydrodynamic pressure forces that are functions of the earlier motion of the ship. These memory effects are taken into account by the convolution integrals.

The constant, added-mass coefficients $m_{\alpha\beta}$ are equal to the frequency-dependent added masses, $\alpha_{\alpha\beta}(\omega)$, for infinite frequency

$$m_{\alpha\beta} = \lim_{\omega \to \infty} \alpha_{\alpha\beta}(\omega) \qquad 2.5$$

The unit response functions $h_{\alpha\beta}(t)$ can be found by cosine transformation of the frequency-dependent damping coefficients $b_{\alpha\beta}(t)$:

$$h_{\alpha\beta}(t) = \frac{2}{\pi} \int_0^\infty b_{\alpha\beta}(\omega) \cos \omega t \, d\omega \qquad 2.6$$

The adoption of convolution integrals for determination of hydrodynamic forces on ships was first made in a paper by Cummins (1962). Later on, the same expressions were found by Bishop, Burcher, and Price (1973) using Volterra series.

The frequency-dependent, hydrodynamic coefficients $\alpha_{\alpha\beta}$ and $b_{\alpha\beta}$ can be determined either by experimental or by theoretical methods.

If the surge velocity, the sway velocity, and the yaw rate before collision impact ($\tau \leq 0$) are denoted $u_O$, $v_O$, and $r_O$, respectively, then relations of the following form can be introduced for all the convolution integrals:

$$\int_0^{\infty} h_{yy}(\tau)\, v(t-\tau)\, d\tau \;=\; \int_0^{t} h_{yy}(\tau)\,(v(t-\tau)-v_o)\, d\tau \qquad 2.7$$

Based on the transient equations of motion in the horizontal plane, equation 2.4, a simulation procedure for the motion of two colliding ships is presented in Petersen (1982). This numerical procedure can deal with the general case in which two ships, both sailing, collide at an arbitrary angle of incidence and with an arbitrary location of the strike. Figures 2.2 & 2.3 illustrate the results of a simulation between two similar ships by means of this procedure.

From Figure 2.3 it can be seen that in cases where the collision point on the struck ship is situated at a relatively long distance from amidships, some of the initial kinetic translational energy is transformed into rotational energy associated with the yaw motion of the struck ship.

### *2.1.1 SHIP IMPACT ANALYSIS FOR BOTTOM SUPPORTED RIGID STRUCTURES*

In this case a central ship impact with velocity V, against a stiff bottom-supported gravity-based structure is considered. Examples of such structures are bottom-supported light houses, bridge piers (Figure 2.4), pylons and some concrete offshore production platforms.

To illustrate the procedure, Figure 2.5, we shall assume that the plastic crushing force P associated with the relative displacement between ship, with total mass

$$m_s^* = m_s + dm_s \tag{2.8}$$

and struck offshore structure with mass

$$M^* = M + dM \tag{2.9}$$

can be assumed constant. Similarly, we shall assume that the friction force, F, between the seabed and the offshore structure can be considered constant. If P<F then the impact will not cause any global displacement of the platform. Therefore, let us assume that P<F.

For the time interval, $0 \leq t \leq t_o$, where $t_o$ is the time where the ship velocity $\dot{x}$ equals the velocity of the offshore structure $\dot{y}$ after the impact, assuming that the time interval where F<P is very small, ($t_{F<P} \rightarrow 0$), we obtain the following two equations of motion:

For the ship $$m_s^* \ddot{x} = -P \Rightarrow \dot{x} = \frac{P}{m_s^*} t + V \Rightarrow x = -\frac{1}{2}\frac{P}{m_s^*} t^2 + Vt \tag{2.10}$$

For the offshore st. $$M^* \ddot{y} + F = P \Rightarrow \dot{y} = \frac{P-F}{M^*} t \Rightarrow y = \frac{1}{2}\frac{P-F}{M^*} t^2 \tag{2.11}$$

The time $t_o$ is determined from the condition $\dot{x}(t_o) = \dot{y}(t_o)$. This yields :

$$\frac{P}{m_s^*} t_o + V = \frac{P-F}{M^*} t_o \Leftrightarrow t_o = V \frac{M^* m_s^*}{P(m_s^* + M^*) - F m_s^*} \tag{2.12}$$

and the maximum crushing distance is :

$$x(t_o) - y(t_o) = -\frac{PM^* + m_s^*(P-F)}{2M^* m_s^*} \cdot \frac{V^2 M^{*2} m_s^{*2}}{\left[P(m_s^* + M^*) - F m_s^*\right]^2} + Vt_o = \frac{1}{2} Vt_o \tag{2.13}$$

The absorbed plastic energy is

$$E_a = P \cdot \left\{ \dot{x}(t_o) - \dot{y}(t_o) \right\} = \frac{V^2 M^* m_s^*}{2\left[ \left( m_s^* + M^* \right) - \frac{F}{P} m_s^* \right]} = E_{kinetic} \frac{M^*}{\left[ \left( m_s^* + M^* \right) - \frac{F}{P} m_s^* \right]} \qquad 2.14$$

where $E_{kinetic} = \frac{1}{2} m_s^* V^2$ is the initial kinetic energy of the striking ship.

When the collision point is close to the longitudinal centre line of the ship so that the yaw motion can be neglected, equation 2.4 shows that the equation of horizontal motion can be reduced to two, uncoupled, one dimensional equations of motion for surge and sway. If furthermore, we assume that the hydrodynamic forces can be modelled by a constant added mass of the ship, that is the convolution integrals in equation 2.4 can be neglected, then the external collision dynamics are reduced to the simple classical case Minorsky (1959), where the crushing energy can be determined from single momentum and energy expressions.

### *2.1.2 COLLISION WITH A RIGID SURFACE*

This situation simulates the contact of a ship with a rigid non-deformable surface e.g. the impact of a ship with a rigid pier. This impact is head on, that means that the angle between the velocity vector and the normal to surface vector is zero. Since the impact is symmetrical to the main axes of the vessel, one could use symmetry in the modelling of the structure. In the case where the interior scantlings are not symmetrical, this would not be possible. The head on collision is considered to be the most severe case, as far as the impact is concerned. Where the angle of the impact is not zero, initial kinetic energy $E_{ki}$ is transformed not only to plastic but additionally to kinetic $E_{kT}$ because of the final transverse change of the position of the vessel. Mitsubishi Industries (Kitamura 1991) developed such real scale collision tests in order to develop a side structure having crashworthiness against collision. They found very good correlation between the experiments and the numerical simulation.

The rigid surface is defined as a boundary such as beyond which, velocity of the vessels equals zero. In terms of analytical equation this yields the following vector product:

$$\|\vec{v}_i\| = 0 \qquad \text{where} \quad \vec{v}_i \cdot \vec{n} = 0$$
$$\text{and} \qquad\qquad 2.15$$
$$M^* \to \infty$$

where $\vec{v}_i$ is the i component of velocity normal to the rigid surface and

$\vec{n}$ is a parallel, to the rigid surface, vector

$M^*$ is the generalised mass of the rigid surface

The collision with the rigid body implies that:

1. $y(t_o) = 0$

2. $\lim_{M^* \to \infty} x(t_o) = \frac{1}{2} V t_o$ 2.16 (a,b,c)

3. $\lim_{M^* \to \infty} E_a = E_{kinetic}$

The emphasis, in this situation, is that a great amount of the kinetic energy of the ship is transformed to plastic energy through the plastic deformations of the structure during the impact. This energy transformation will be discussed further in the results.

### *2.1.2.1 THE STRAIN RATE*

The effect of strain rate has extensively been discussed in Samuelides (1984) where he examines the effect of strain rate in a dynamically loaded plate strip. The material of the plate strip was assumed to be elastic/visco-perfectly plastic. The material showed viscous effects in the plastic region. Figures A2-1.1, A2-1.2 in Appendix 1 show typical stress-strain curves, for the above type of material, for constant and variable strain-rates.

The relationship between the strain rate $\dot{\varepsilon}$ and the dynamic yield stress $\sigma_y$ in uniaxial tension has been investigated by Cowper & Symonds (1957). Based on tensile tests performed by Manjoine (1944) at different rates of strain, they proposed the following formula:

$$\frac{\sigma_y}{\sigma_{yo}} = 1 + \left( \frac{\dot{\varepsilon}}{D} \right)^{1/p} \qquad 2.17$$

where $\sigma_y$ is the static yield stress

D, p are material constants and take the values 40.4 $s^{-1}$ and 5 for mild steel.

The correlation between equation 2.17 and Manjoine's (1944) test results is shown in Figure A2-1.3 appendix 1, extracted from Bonder et al. (1960). For this correlation the value for static yield stress had been taken equal to 30,000 psi (207 $N/mm^2$) which corresponded to a strain rate of approximately $10^{-4}$ $s^{-1}$ according to Manjoine's original results (see Figure A2-1.3 appendix 1 taken from Manjoine). If the static yield stress had been taken to be equal to 27,5000 psi (190 $N/mm^2$), which corresponds to a strain rate of $10^{-6}$ $s^{-1}$, Figure A2-1.4 appendix 1, the comparison between equation 2.17 and the experimental results would be as shown in Figure A2-1.5, appendix 1.

For the present analysis it has been assumed that $\sigma_{yo}$ is the static yield stress at zero strain-rate. This has been experimentally measured, according to TRRC (1977), two minutes after switching off the testing machine when the strain reached the value of 0.005. The recommended strain-rate for the tensile tests was 300 μstrains per minute.

Jones (1976) has recommended the use of equation 2.17 and based on this, Symonds and Jones (1972) derived a dynamic correction factor for both the plastic bending and the plastic axial force in order to allow for the strain rate effect on the dynamic response of a fully clamped beam.

Another relationship between $\sigma_y$ and $\dot{\varepsilon}$ for mild steel has been proposed by Reckling (1977) and supported by Woisin in Samuelides (1984). According to this, for strains less than 0.02 the following relationships are shown:

$$\frac{\sigma_y}{\sigma_{yo}} = \begin{cases} 0.393 + 0.131 \cdot \log \dot{\varepsilon} & \dot{\varepsilon} \le 1 \quad s^{-1} \\ 0.393 + 0.393 \cdot \log \dot{\varepsilon} & \dot{\varepsilon} \ge 1 \quad s^{-1} \end{cases} \qquad 2.18$$

The equations indicate that strain rate effects are negligible for $\dot{\varepsilon} \le 10^{-3}$ $s^{-1}$. The restriction $\varepsilon \le 0.02$ implies that there is a significantly smaller effect of strain-rate on the ultimate tensile strength of the material than on the yield stress.

For more complicated stress systems Perzyna (1966) introduced a family of yield functions to account for the effect of rate of strain for elastic/visco-perfectly plastic materials. Jones (1972) identified a specific relationship for members of this family which relates the equivalent stress:

$$\sigma_e = \left( \frac{3}{2} s_{ij} s_{ij} \right)^{0.5} \qquad 2.19$$

where $s_{ij}$ are the components of the stress deviator tensor, to an equivalent strain-rate:

$$\dot{\varepsilon}_e = \left( \frac{2}{3} \dot{\varepsilon}_{ij} \dot{\varepsilon}_{ij} \right)^{0.5}$$

Thus:

$$\frac{\sigma_e}{\sigma_{yo}} = 1 + \left( \frac{\dot{\varepsilon}_e}{D} \right)^{1/p} \qquad 2.20$$

for the biaxial stress system:

$$\sigma_e^2 = \sigma_X^2 + \sigma_Y^2 - \sigma_X \sigma_Y \qquad 2.21$$

Equation 2.20 will be used in the analysis in chapter 3 where a bow model is analysed under dynamic loading against a rigid wall.

It is of great importance to ascertain the strain rate status in the deformed panels of the bow structure during the impact.

## 2.2 COLLISION WITH AN ARTIFICIAL ISLAND – THE GROUNDING PROBLEM

Artificial islands were created in order to absorb the collision of a vessel and thereby protect bridge legs. They are the best, most cost effective solution where large vessels are involved. The cheapest material for an island is sand, Figure 2.7, which can be pumped to site by dredger.

Sand may not be suiTable if the location is subject to a breaking surf in stormy weather, or to swift tidal currents; in both instances there may be a scouring action that will carry away part of the island. In such cases coarse gravel, stones (10-15 cm), or cobbles will be preferable.

The stopping capability of an island for any vessel is a function of the vessel speed, the bow characteristics, the loading condition i.e. full load or ballast condition, and the friction of the steel bottom sliding up the beach. For sandy soil frictional coefficients are found to 0.6-0.8 and 0.9-1.0 for bulbous bows and V-bows respectively when the frictional coefficient between steel and sand is assumed to be $\mu$=0.38. Minorsky takes this coefficient equal to 0.40.

In Ottesen Hansen (1994) friction coefficients are calculated for both V-shape and bulbous bow model vessel. The tests were made with different velocities and types of sand (fine, grained and coarse grained). Table 2.1 presents measured and calculated friction coefficients between bow and slope derived from Ottesen (1994).

| Impact Velocity (m/s) | Average Friction Coefficient Measured | Average Friction Coefficient Calculated |
|---|---|---|
| 0.265 | 0.67-0.83 | ~ 0.95 |
| 0.465 | 0.66-0.85 | ~ 0.85 |
| 0.665 | 0.68-0.79 | ~ 0.80 |

**TABLE 2.1** Comparisons between measured and calculated friction coefficient (projected on the slope of the furrows in the slope). Bulbous bow.

The theories presented in Sections 2.2.1 & 2.2.2 refer to the static and dynamic response of vessels during grounding. These methods have been developed on the hypothesis that the vessel behaves as a rigid beam and hence the maximum bending moment capacity the vessel may undergo is not incorporated. Further discussion on the bending moments, derived for the vessel as the grounding takes place, is given in chapter 4, where the maximum bending moment capacity is incorporated in the analysis with regard to the behaviour of the vessel while it slides on the slope!

### *2.2.1 GROUNDING IN CONTINUOUS SLOPE ISLAND*

In Figure 2.8 a vessel is shown first contacting an artificial island at point $O_1$, travelling up the beach a distance d, and stopping with the forefoot at the point $O_2$. If in Figure 2.8 O is any point along d between $O_1$ and $O_2$;

| | |
|---|---|
| $\nabla$ | is the ship's displacement |
| B | is the buoyancy |
| a | the distance from centre of gravity to point O |
| b | the distance from centre of buoyancy to point O |

The reaction R at point O is:

$$R = \nabla - B \qquad 2.22$$

For equilibrium, moments about O are:

$$\nabla \cdot a = B \cdot b \quad \Rightarrow \quad R = \nabla\left(1 - \frac{a}{b}\right) \qquad 2.23$$

The angle of the ship's keel with the horizontal, during the travel of the forefoot up the beach, is unknown: if several trim lines are drawn when forefoot is at point O, the corresponding ship buoyancy B and longitudinal centre of buoyancy b can be determined for the trim lines using the hydrostatic and Bonjean curves. Plotting the product B·b against the trim line angles, the trim angle for which equation 2.23 is satisfied, can be established, and knowing B, the reaction R at point O is determined. In Figure 2.9 the down slope component of R is Rsin$\vartheta$. The component normal to the beach slope is Rcos$\vartheta$. In sliding up the beach the forefoot has to overcome a force:

$$F = R\sin\vartheta + \mu R\cos\vartheta \qquad 2.24$$

where $\mu$ is the frictional coefficient. Minorsky (1983) claims that if F is plotted against distance travelled by the forefoot, the area under such curve is the work done. The stopping point is where this area equals the kinetic energy of the vessel at the moment of contact. However expression 2.24 neglects the amount of energy dissipated as elasto-plastic energy on the structure that plastically deforms during the impact. Moreover this energy conservation does not consider the potential energy lost due to the vertical displacement of the centre of gravity as well the energy lost due to the rotation of the centre of mass around the centre of flotation. Accordingly, Pedersen (1995) presents a study for grounding in discontinuous slope-island where he includes the last two energy quantities but still no reference regarding the elasto-plastic energy is made.

### *2.2.2 DYNAMICS DURING GROUNDING IN DISCONTINUOUS SLOPE ISLAND*

Three new factors are introduced in this situation, friction, gravity and the change of momentum. The sliding of the model on the inclined surface produces a severe friction which retards the ship. Additionally the trimming of the model itself during the collision results in the reduction of draft, hence the forces of buoyancy and

ground pressure are interchanged. This response also affects the inertia effect since, instead of being unidirectional, the inertia becomes bi-directional, e.g. acting on an axis vertical to the direction of the initial velocity. As a result the bow structure is compressed in the vertical axis resulting in higher $\sigma_3$ stresses compared with the models discussed earlier.

A free body diagram of a grounded ship is shown in Figure 2.10 extracted from P. T. Pedersen (1995). It is an XYZ-coordinate system fixed with respect to the sea bottom. The z-axis is pointing downwards opposite to the gravity field; the X-axis lies in the symmetry plane of the vessel's bow pointing towards the inclined rigid surface. At t=0, the grounding contact occurs, the contact point has co-ordinates $(x_c,0,0)$. The centre of gravity G has co-ordinates $(x_g,0,z_g)$ and the location of centre of flotation, LCF, is placed on a distance $x_f$ forward of the midship section.

P. T. Pedersen (1995) simplifies the grounding event into two phases. In the first phase the ship is subjected to an impulse due to the contact with the ground, see Figure 2.11, and in the second phase the ship is sliding with continuous contact with the ground, Figure 2.12.

In the first phase the soil and the structural response is assumed to be such that the impulse is completely inelastic and along with the assumption that the ship hull is stiff this impulse leads to a rapid change of the initial forward speed V such that the ship, after the impact, has a set of surge, heave and pitch velocity components, $v_x$, $v_z$, $\dot{\vartheta}_y$, which are compatible with the motion of the contact point along the sloping bottom.

In the second phase the kinetic energy, which is available after the end of the first impact, is transformed into elasto-plastic energy and into friction in the contact surface between the ground and the ship as it moves up on the sloping bottom.

### 2.2.2.1 PHASE I

At this stage, the contact of the ship with the rigid surface must change the motion of the vessel instantaneously in order to be compatible with the imposed kinematic restriction.

From Figure 2.11, Petersen (1995) in order to find the direction of the reaction force β, considered the force components to be perpendicular to the parallel with the sloping bottom, $F_g$ and $F_f$, respectively. If we assume that Coulomb's friction law;

$$F_f = \mu F_g \tag{2.25}$$

is valid. The direction β is found to be

$$\tan\beta = \frac{\mu\cos\alpha + \sin\alpha}{-\mu\sin\alpha + \cos\alpha} \tag{2.26}$$

P. T. Pedersen showed that with the direction of the acting impulse known, the equations which express the conservation of momentum in a direction perpendicular to the acting impulse in conjunction with the angular momentum around the contact point can be expressed as:

$$V \cdot M(1+m_{xx})\cos\beta = v_x \cdot M(1+m_{xx})\cos\beta + v_z \cdot M(1+m_{zz})\sin\beta \tag{2.27}$$

$$V \cdot M(1+m_{xx})z_g = M\,R^2(1+j_{YY})\dot{\vartheta}_y + v_x \cdot M(1+m_{xx})z_g + v_x \cdot M(1+m_{zz})(x_c - x_g) \tag{2.28}$$

R denotes the radius of inertia of mass around the centre of gravity, $m_{xx}$ and $m_{yy}$ are dimensionless virtual masses of water for surge and heave motions and $J_{yy}$ is the dimensionless virtual mass of water moment for the pitch motion.

The velocities $v_x$, $v_z$, $\dot{\vartheta}_y$, immediately after the moment of impact can be determined as:

$$v_X = V\left\{1 - \frac{R^2\alpha_1\alpha_2\tan\alpha\tan\beta}{D\,x_\alpha}\right\} \tag{2.29}$$

$$v_Z = V\frac{R^2\alpha_2 \tan\alpha}{D\, x_\alpha} \tag{2.30}$$

$$\dot{\vartheta}_y = -V\frac{\alpha_1 x_\beta \tan\alpha}{D\, x_\alpha} \tag{2.31}$$

where $\alpha_1$ and $\alpha_2$ are dimensionless added mass ratios:

$$\alpha_1 = \frac{1+m_{zz}}{1+m_{xx}} \quad \text{and} \quad \alpha_2 = \frac{1+j_{YY}}{1+m_{xx}} \tag{2.32}$$

$x_\alpha$ and $x_\beta$ are two normally nearly equal effective distances between the centre of gravity and the contact point:

$$\begin{aligned} x_\alpha &= (x_C - x_g) - z_g \tan\alpha \\ x_\beta &= (x_C - x_g) - z_g \tan\beta \end{aligned} \tag{2.33}$$

and the factor D is given by the following relation:

$$D = \alpha_1 x_\beta + \frac{R^2\alpha_2(\alpha_1 \tan\alpha \tan\beta + 1)}{x_\alpha} \tag{2.34}$$

Since the velocities immediately after the impact are known the change in momentum P can be determined:

$$\begin{aligned} P = \int_0^t F(t)dt &= M(1+m_{xx})(V - v_x)\sin\beta + M(1+m_{zz})v_z\cos\beta \\ &= VM(1+m_{xx})R^2\alpha_2\alpha_1\frac{\tan\alpha}{x_\alpha D\cos\beta} \end{aligned} \tag{2.35}$$

The maximum value of the force F(t) associated in this impulse will depend on the hardness of the ground, the bow form, the bow structural response and the flexibility of the ship hull. For impacts against rigid walls, $\alpha = 0.5\cdot\pi$, Pedersen (1993) gives expressions for the variation of F with time for a number of different ship types.

#### *2.2.2.2 PHASE II*

In phase II it is of great importance to calculate the ground reaction force while the ship slides up the rigid slope. The distance that the ship will cover upon sliding is shown in Figure 2.12 where the energy balance is satisfied.

Pedersen (1995) shows that even in this second phase of the grounding event, although it is a dynamic problem, the vertical acceleration forces are relatively modest for normal merchant ships. Hence, it is reasonable to neglect inertia forces associated with heave and pitch. In order to further simplify the problem and obtain analytical expressions we shall approximate the hydrostatic forces and moments by linear expressions in the heave and pitch displacements and only consider the effect of the vertical force component, $F_z$. As a consequence of these assumptions the relation between the vertical grounding force component $F_z$. acting at a distance

$$\ell = (x_C - s) - x_F \qquad 2.36$$

from the centre of flotation LCF leads to a vertical displacement w of the centre of flotation which can be found from:

$$F_Z = \rho\, g\, A_Z\, w \qquad 2.37$$

where $A_z$ is the area of the waterplane. The distance l is equal to $(x_c - x_f)$ when the slope is continuous. The vertical force component can also be expressed as:

$$F_Z = \rho\, g\, A_Z \frac{z}{\left(1 + \ell^2 / r^2\right)} \qquad 2.38$$

where z is the vertical displacement of the hull section at the location where the force $F_z$ is acting and where

$$r = \left( \frac{\nabla \cdot GM_L}{A_Z} \right)^{0.5} \qquad 2.39$$

is the radius of gyration. $\nabla$ is the displacement volume and $GM_L$ the longitudinal metacentric height. If we introduce the water plane area coefficient $C_w$ and the block coefficient $C_B$ we also have:

$$F_Z = \frac{Mg}{T}\frac{C_W}{C_B}\frac{Z}{\left(1+\ell^2/r^2\right)} \qquad 2.40$$

Pedersen (1995) notes that the above relation between the contact force and z is valid only for small values z/T. Therefore unless the actual motion of the ship is confined to small perturbations of the initial draft, the linear expression should be replaced by more accurate relations obtained from the ship's hydrostatics.

# 2.3 EMPIRICAL AND STATISTICAL METHODS FOR ESTIMATING THE ENERGY DURING A HEAD–ON COLLISION

## 2.3.1 D.S. ALDWINCKLE'S APPROACH

Aldwinckle (1984) developed a model to predict the bow collapse distance resulting from the head-on, high energy, collision of a ship with a rigid, vertical iceberg. This model has been used to derive a correlation between the energy absorbed in structural deformation, the bow collapse distance, ship size parameters and Ice class. The correlation derived is the following:

$$\frac{E_D}{L \cdot B \cdot d} = a_1 d_c^2 + a_2 d_c^4 \qquad 2.41$$

where :

$E_D$ = Energy absorbed in structural deformation (Joules)

L = Length between perpendiculars (m)

B = Moulded breadth (m)

d = Draft (m)

$d_C$ = Bow collapse distance (m)

$a_1$, $a_2$ = Coefficients which depend on Ice class, see Table 2.2

| CASPPR Ice Class | a1 | a2 |
|---|---|---|
| 1 | 57.0 | -0.09 |
| 1A | 106.5 | -0.24 |
| 2 | 171.3 | -0.58 |
| 3 | 230.8 | -0.92 |
| 4 | 282.6 | -1.21 |
| 6 | 330.4 | -1.43 |
| 7 | 372.0 | -1.58 |
| 8,10 | 392.0 | -1.64 |

**TABLE 2.2** Coefficient $a_1$ and $a_2$ for equation 2.41

The limitations inherent in the methodology used to derive this correlation are discussed in the report (1984). Notwithstanding these limitations, the derived correlation is considered to be valuable in Arctic Shipping Probability Evaluation

Network {ASPEN} for comparing the possible damage extent, resulting from high energy collision, for ships of differing sizes and Ice Classes. Particulars of the ships used in this study follow in Table 2.3. The energy absorbed versus the penetration distance on the bow is shown in Figure 2.13. Furthermore a correlation was sought to reduce the curves to a single curve that would be independent of the ship size.

| Ship Name | Ship Type | LBP | B | D | d | Deadweight | CASPPR Ice class or Equivalent |
|---|---|---|---|---|---|---|---|
| A | Tanker | 160.33 | 24.77 | 12.60 | 9.69 | 24240 | E |
| B | General Cargo | 135.62 | 20.65 | 12.73 | 9.25 | 16050 | E |
| C | General Cargo | 129.75 | 19.21 | 11.00 | 8.22 | 10160 | E |
| D | Tanker | 103.00 | 17.49 | 9.1 | 7.88 | 8470 | E |
| E | General Cargo | 78.48 | 13.8 | 8.11 | 5.77 | 2380 | E |
| F | Bulk Carrier | 196.63 | 22.86 | 15.24 | 10.97 | 28540 | 2 |

**TABLE 2.3** The vessels used for Aldwinckle's method

The results follow on Figures A2.2.1 and A2.2.2 in appendix 2. Figure A2.2.1 shows a plot of $E_D$ as a function of the product of the ship parameters length, breadth and draft (L B d). for various values of collapse distance. A linear dependency can be seen. This is confirmed in Figure 2.13 where $E_D/L \cdot B \cdot d$ is shown as a function of $d_c$. As Aldwinckle showed the results for ships, B, C, D and E reduce to a single curve with little scatter. The results for ship A do not fit on this curve.

### *2.3.2 GERARD'S APPROACH*

One of the most well-known, and generally accepted model, for the estimation of the crushing load of structures has been developed by Gerard (1958). The method was originally developed for aircraft structures but has found application in automobile and ship engineering.

His semi-empirical formula has been established on the basis of the correlation against results of a series of panel tests with various stiffener types. The method postulates that the maximum strength is a function of the plate slenderness ratio defined as

$$\beta = \frac{b}{h}\sqrt{\frac{\sigma_y}{E}} \qquad 2.42$$

so that

$$\frac{\sigma_{max}}{\sigma_y} = \mu\left(\frac{1}{\beta}\right)^m \qquad 2.43$$

where

| | |
|---|---|
| b | is the width of the element considered |
| h | thickness of the element |
| $\sigma_y$ | is the compressive yield stress |
| E | is the Young's modulus |
| m, $\mu$ | constants subject to fitting with experimental data |

A clear distinction is made between elements where unloaded edges remain straight during post buckling and those where the unloaded edges are free to warp in the plane of the plate. For straight edges a best fit was obtained with $\mu$=0.67 and m=0.40, and for distorted edges, $\mu$=0.56 and m=0.85.

Complex members belong to the first category (straight edges) if two or more flanges meet at a common junction and to the second group (distorted edges) when only two elements meet at a junction. A generalisation of equation 2.43 is made by substituting the width to thickness ratio by:

$$\frac{b}{h} = \frac{A}{2h^2} = \frac{A}{gh^2} \qquad 2.44$$

Where

| | |
|---|---|
| A | is the cross sectional area. |
| g | represents the number of flanges and cuts required to reduce the section to a series of flange elements. Typical values for g are shown on 2.14 |

From the above equations the maximum crushing strength according to Gerard can be estimated as:

$$\sigma_{max} = \sigma_y \mu \left[ \left( \frac{g \cdot t^2}{A} \right) \sqrt{\left( \frac{E}{\sigma_y} \right)} \right]^m \qquad 2.45$$

The virtue of this scheme is that the results of several tests are reduced to a single equation for the ultimate load.

Minorsky (1983) adopts Gerard's formula and predicts the energy absorbed by the bow structure of a ship when this hits a rigid body which has a concrete based bridge leg. Gerard's formula is based on a variety of tests which were performed on stiffened plating using many stiffeners and different materials, including a number of aluminium alloys, steel, copper and titanium. The interpretation of crippling strength is given as the stress at which secondary instability occurs for thin wall compression members, in the form of a local failure in buckling which exceeds the elastic buckling load.

Equation 2.45 applies also to stiffened panels and built-up cross sections, with different thickness and yield strength providing a weighting factor is introduced. The thickness effect is often sufficiently accounted for by the modified equation:

$$\sigma_{max} / \sigma_y = \mu \left[ \left( \frac{g \cdot t_w \cdot t_s}{A} \right) \left( \frac{E}{\sigma_y} \right)^{1/2} \right]^m \qquad 2.46$$

where $t_W$ is the thickness of stiffening members

$t_S$ is the thickness of the skin

In the simple sections considered by Gerard it was thought that an average value for $t_W$ and $t_S$ would provide sufficient accuracy. Most crippling methods, such as the ones that follow, involve subdivision of the cross section of the formed section into a series of plates and angle sections. The crippling strength of the section is obtained as a weighted average of the crippling strengths of the subdivided elements.

The total crushing load is then given by:

$$P_c = \sigma_{max} \cdot A \qquad 2.47$$

The strain rate is taken as:

$$\frac{de}{dt} = \frac{v_x}{S} \qquad 2.48$$

Where $v_x$ velocity in longitudinal direction during impact

S frame spacing

Based on test results published by Marsh and Campbell (1963), the magnitude of the flow stress $\sigma_0$ is calculated from the following relationship:

$$\sigma_O\left(\dot{\varepsilon}\right) = 1.29\sigma_{OS}\,\dot{\varepsilon}^{0.037} \qquad 2.49$$

Where $\sigma_{os}$ is the static ultimate strength of the steel material.

The load formula 2.47 predicts the maximum crushing load of plated structures within ±10% of the experimental results. The disadvantage of this method is the fact that it has been derived from the crushing of fairly simple, and regular, plate constructions, where the variation of the parameters incorporated has been limited, e.g. range of plating to stiffener thickness ratios and stiffener spacing. Normal bow structures will consist of a number of plate panels of different geometry and scantling arrangement. Using Gerard's approach, adding up the maximum crushing load of individual panels to determine the maximum load for the complete structure is expected to yield relatively comprehensive results. The application of Gerard's empirical formula should, ideally be combined with probabilistic function for estimating those load maxima occurring in individual panels.

However, even with its existing shortcoming, Gerard's approach has been frequently utilised in many applications where head on, bow collisions, have been investigated for the ship design. It mostly applies to accidental load assessments, which should reflect the maximum load magnitude that occurs.

### *2.3.3 NUMERICAL METHODS BASED ON AMDAHL'S METHOD.*

Other collision empirical formulas have been established on the basis of theoretical considerations and correlation of results against model test results. The theoretical basis may vary from simplified energy assessments and buckling considerations.

Amdahl's (1983) empirical formula has been established on the theoretical considerations, *of the energy dissipated during plastic deformation of basic structural elements such angles, T-sections and cruciforms*. The total crushing load is determined by a minimisation of the deformation energy absorbed during the folding process. Amdahl's procedure leads to the formula 2.50 for the prediction of the average crushing strength,

The total crushing load is determined by multiplying the crippling stress with the associated cross-sectional area of the deformed steel material.

$$\sigma_c = 2.42\sigma_0\left[\frac{n_{AT}t^2}{A}\right]^{0.67}\left(0.87+1.27\frac{n_C+0.31n_T}{n_{AT}}\left[\frac{A}{(n_C+0.31n_T)t^2}\right]^{0.25}\right)^{0.67} \qquad 2.50$$

Where $\sigma_C$ is the Average crushing strength of the bow

$\sigma_0$ is the ultimate strength of steel. For elastic material-fully plastic $\sigma_o=\sigma_y$, where $\sigma_y$ is the static yield stress

t Average plate thickness of the cross section under consideration

A is the cross-sectional area of the deformed steel material

$n_C$ Number of cruciforms in the cross-section under consideration

$n_T$ Number of T-sections in the cross section

$n_{AT}$ Number of angle and T-sections in the cross-section.

In the numerical examples, presented in appendix 3, a slight modification to equation 2.50 has been introduced in order to obtain a better fit to experimental crushing results of small-scale bow models.

The modification includes an increase of the deformation energy of corner angles at intersections between the upper deck/bottom and the bow sides on the assumption

that these angles will collapse in the same mode as cruciform, i.e. a corner angle =1/2 cruciform. Amdahl indicates that this crushing mode represents an upper bound solution for angles. In addition, the effective crushing distance of the structure is taken equal to 0.75 times the folding length in case of longitudinally stiffened structures, and 0.85 times the folding length in case of transversely stiffened structures. These values have been selected on the basis of appearances of local peaks in load-indentation curves for the small scale bow models mentioned previously. Furthermore, the characteristic steel strength $\sigma_0$ has been taken equal to the mean value of the yield and the ultimate strengths of the steel.

### *2.3.4 YANG & CALDWELL'S METHOD*

The crushing model proposed by Yang & Caldwell (1988) is, to a large extent based on the same deformation and energy evaluation made by Amdahl. Both methods make use of the folding mechanisms proposed by Wierzbicki (1983).

Compared to the slightly modified Amdahl method, the following differences can be identified.

Yang & Caldwell assume somewhat different energy dissipation during deformation of the structure under consideration. Amdahl determines the folding strength and crushing load by a minimisation of the deformation energy absorbed by the folding process. Yang & Caldwell on the other hand propose taking the folding length H equal to the spacing between transverse frames, provided that the frame spacing is less than the theoretical folding length.

Furthermore, Yang & Caldwell suggest that longitudinal stiffeners may be included along with an equivalent thickness of the shell plating, so that the plastic bending moment of the equivalent plating equals the plastic bending moment of the shell plating with longitudinal stiffeners.

The result is the following formula for the estimation of the crushing load of a section of a complex bow structure:

$$P_M = \sigma_O \left[ 1.178 \cdot H \sum^{n_f} b_i t_i^2 + 0.215 \cdot H \sum^{n_{AT}} t_i + 6.935 \cdot H \sum^{n_{AT}} t_i^2 + 0.265 \cdot H \sum^{n_T} t_i + 0.589 \sum^{n_T} t_i^2 + 0.750 \sum^{n_C} \sum^{4} t_i^2 + 0.375 \sum^{n_C} \sum^{4} t_i^2 \right]$$

2.51

where :

| | | |
|---|---|---|
| | $P_M$ | Mean crushing load of the structure |
| | $\sigma_o$ | Flow stress based on the mean value of the yield and the ultimate strength of the steel. For elastic material-fully plastic $\sigma_o=\sigma_y$, where $\sigma_y$ is the static yield stress |
| | $b_i$ | Width of the I-th plate flange |
| | $t_i$ | Thickness of the I-th plate flange |
| | H | Folding length of the distorted plate flanges |
| | $n_c$ | Number of cruciforms in the cross section under consideration |
| | $n_T$ | Number of T-sections in the cross-section |
| | $n_{AT}$ | Number of angle- and T-sections in the cross section |
| | $n_f$ | Total number of flanges of angles, T-sections and cruciforms |

### *2.3.5 DISCUSSION ON THE EMPIRICAL METHODS*

As a result of the uncertainties involved in a collision assumption, simplifications have been necessary in Aldwinckle's (1984) method. These impose limitations on the accuracy of the results.

The most important assumption in Aldwinckle's from the point of view of the influence on the results is that the iceberg presents a rigid barrier to the bow of the ship. This assumption means that no allowance has been made for energy absorbed in crushing the ice. Therefore the bow collapse distances calculated are likely to be an over-estimate. Hence, this is a conservative assumption from the point of view of pollution risks.

The other major assumptions embodied in the collision damage model, namely that collapse occurs only by buckling and that the iceberg presents a rigid vertical barrier to the ship, are felt to have lesser influence on the results. However, it must be stated that the relative contribution of each has not been assessed in this study.

The assumption that the structure collapses by buckling means that the model is only valid for collision energies sufficient to initiate this type of collapse. Hence the model is only applicable for high-energy collisions.

In Figures A2-3.1-A2-3.3 in appendix 3, crushing loads predicted by Gerard's method, Amdahl's and Yang & Caldwell's have been compared with experimental results from the crushing of bow models. In all the cases considered, it was found that Gerard's load predictions are significantly higher than the experimental results obtained by the crushing of both longitudinally and transversely stiffened bow models. Thus, Figure A2-3.1 shows that for the longitudinally stiffened Amdahl bow No. 5, Gerard's method predicts loads that are approximately 50% higher than the experimental results.

However is should be stated that Amdahl in his test used the original Gerard formula and not the modified one, introduced by Minorsky (1983). The latter in his example

indicates accuracy of 10% with experimental results. Thus, the significance, of splitting the thickness of the simple structural members into the thickness of the shell and the scantlings is very important as will be discussed later on, in Section 2.4.4.

In several cases, Gerard's method predicted crushing loads and average stresses in the deformed cross-section of the bow, which are close to the yield strength of the steel material. Due to these unreasonably high loads Gerard's method is not applied in the models shown in the Figures beyond A2-3.1.

The results presented in Figure s A2-3.1- A2-3.3, indicate that equation 2.50 predicts crushing loads similar to the ones produced from the results for transversely stiffened bow structures. For longitudinally-stiffened bows, the application of the modified Amdahl formula may lead to somewhat conservative estimates of the crushing loads, while on the other hand corresponding estimates of the Yang & Caldwell method are somewhat low.

Figure A2-3.4 shows the calculated crushing load-indentation curves for a 150000 DWT bulk carrier, using Amdahl's modified method and Yang and Caldwell's method. The total collision load is estimated as the sum of the crushing load of the deformed part of the stem. For indentations of the bow exceeding the length of the bulb, the two locations of deformations will be reduced to one crushing area similar to that of the conventional bow collision. The applied procedure of adding up the load contributions of the bulb and bow will not always be correct. For a bulb/bow structure with a heavily-reinforced forward part followed by a weaker rear part, the deformations may start in the rear part of this structure, resulting in lower crushing load of the bow than that predicted by the present approach. Such a deformation process has been observed during several model tests as well as in cases of full scale collision.

Figure A2-3.5 shows similar results for a 40000 DWT, container vessel, for a head-on collision against a rigid wall at an initial speed equal to 12.9 m/s

Using Amdahl's method, Figure A2-3.6 shows similar calculated crushing loads for the 3000 DWT general cargo carrier during a head on collision against a rigid wall at an initial speed equal to 7.5m/s.

Figure A2-3.7 shows calculated results using Amdahl's modified procedure for the 2000 DWT tanker. First the results for a normal head on collision at an initial velocity equal to 7.0 m/s are presented. Then the total crushing load is presented from a calculation where the strain rate effect represented by equation 2.49 is neglected. It can be seen that strain rate effects result in a considerable increase of the crushing force.

Figure A2-3.8 shows the calculated bow crushing loads for a 1000 DWT pallet carrier at an initial velocity to 5.5 m/s and a 500 DWT coaster at an initial velocity equal to 5.0 m/s. It can be seen that even though the kinetic energy to be absorbed by these two vessels is quite different, the maximum collision forces do not differ to a great extent.

Figures A2-3.9, A2-3.10, & A2-3.11 show collision forces, indentation and collision duration at two speeds, $V_o$=12m/s and $V_o$=5m/s, as functions of ship's dead-weight tonnage.

Figure A2-3.12 shows the calculated collision force for a supply vessel with rule L=64m, breadth B=15.9m, depth to main deck D=8.0m, displacement 4590 tons, and a velocity before head-on impact against a vertical rigid wall V=6m/s.

## 2.4 HEAD-ON COLLISION OF A VESSEL WITH A RIGID BODY

### 2.4.1 GENERAL

A ship impact risk evaluation has been carried out by Burness Corlett & Partners (IOM) Ltd. (1995) with respect to the main tower piers of the Forth Road Bridge. It has been shown that, with one of the typical vessels, the risk of impact by a tanker of 27500 tonnes displacement is 1 in 5.5 years for the North Pier and 1 in 12 years for the South Pier.

The work carried out so far only predicts risk of collision by a ship and consequent damage to it. It does not identify the damage of the structure due to impact force. Therefore, a study was initiated, which is reported here, to provide an estimate of forces induced by ships in collision with a rigid pier and to evaluate the extent of damage of the bow of the ship when hitting the rigid pier with a certain speed and, thereby, the energy absorbed in the structure. This information is required in order to assess the extent of damage and the protection requirement for the piers.

The scope of the study is limited to the following situations:

A ship's bow striking a wall such that:

- the wall absorbs no kinetic energy and is entirely rigid
- the ship expends all the kinetic energy in deforming the bow and no rebound from the wall occurs
- the ship strikes the wall such that the angle between its centreline and the face of the wall is $90^{\circ}$ and this angle remains between throughout the collision

### 2.4.2 BACKGROUND

The methods used for the assessment of collision resistance of ships are classified according to whether they are applied to minor or major collisions. A minor collision (or low energy collision) is defined as a collision where the full damage of a ship (sustained by whatever means) is accommodated by elastic and inelastic material

response without rupturing. On the other hand, a major collision is defined as a collision which causes inelastic strains and fracture of the struck ship's hull in way of cargo tanks or even including the fuel tank forward of the collision bulkhead.

In this report the procedure developed by Minorsky (1983) for ship collision with a rigid body is applied and provides a simple method to calculate impact forces delivered by ships when hitting relatively immovable objects, such as bridge piers.

### *2.4.3 METHODOLOGY*

In the work reported herein, the calculation of the collision energy absorbed by the bow structure of a tanker vessel while it impacts with a rigid body, is discussed, in order to establish a relationship between the energy absorbed by the vessel and the penetration distance from the forward end.

The calculation of the energy absorbed, based on the crippling force imposed on the bow structure, emanates from the impact with a rigid body and, therefore, leading to the collapse of both the scantlings and the shell involved in the design of the ship compartments forward of the collision bulkhead.

Minorsky adopts Gerard's formula and proposes a method for predicting the energy absorbed by the bow structure of a ship when this hits on a rigid body such as a concrete basis of a bridge leg. A simple method to calculate forces delivered by ships is presented as well as some thoughts on the hydrodynamic reasons for such collisions, and gives a method for calculating the ship stopping capacity of artificial islands. Gerard's method is based on a variety of tests which were performed on stiffened plating using many stiffeners and different materials, including a number of aluminium alloys, steel, copper and titanium. *The interpretation of crippling strength is given as the stress at which secondary instability occurs for thin wall compression members, in the form of a local failure in buckling which exceeds the elastic buckling load.* It is calculated through the formula shown on equation-2.46.

Since the Crippling stress is defined, the Crippling force $F_C$ is the product of the crippling stress and the Area of the Frame, A.

$$F_c = \text{Crippling stress} \cdot \text{Area} \qquad 2.52$$

Therefore the energy absorbed up to Frame i is defined through the following integral:

$$E_i = \int_{lastFrame}^{i} F_C \, da \qquad 2.53$$

where
- last frame = the frame related to the forward end
- a = the distance of the frame i from the forward end in (m)
- $F_C$ = The crippling Force. (kN)
- $E_i$ = Energy absorbed up to frame i in (kNm)

Distance "a" is shown on Figure 2.15

The elements of each bulkhead, which contribute to the strengthening, taken into account in Gerard's formula are only the longitudinal scantlings, including decks, mid bulkheads ect. Further information for the elements participating in the modelling are included in the individual calculations of each Frame. The energy absorption, in relation to the indentation, is shown in Figure 2.18.

The Kinetic Energy of the moving Vessel is given as :

$$E_K = \frac{1}{2}(m + m_a) \cdot v^2 \qquad 2.54$$

where:
- m = is the displacement of the ship in (tons)
- $m_a$ = is the added mass in surge condition in (tons)
- v = is the speed of the ship in (m/s)
- $E_k$ = is the kinetic Energy in (kNm)

### *2.4.3.1 ADDED MASS*

Minorsky (1993) in his work adopted a value of 40% of the struck ship's displacement in the ship to ship collision study. In this work, added mass refers to the sway condition, i.e. the lateral movement. The ship is striking the side shell of the vessel. No allowance is made for the added mass of the striking ship. When the ship is striking the rigid pier, at head on, the added mass to be considered refers to the surge condition. Added mass in surge is a small fraction of the displacement, probably less than 10%. Pedersen (1995), Minorsky (1983)

In this study the added mass of the vessel is taken as 5% of the Displacement.

Substituting the Energies derived from formulas 2.53 and 2.54 and solving 2.54 in respect of v, yields to:

$$v = \sqrt{\frac{2E_K}{(m+m_a)}} = \left[\frac{2}{(m+m_a)} \cdot \int_{last\,Frame}^{i} F_C\, da\right]^{1/2} \qquad 2.55$$

Formula 2.55 is the result expected and it is anticipated to give a good appraisal of a *critical speed* of the vessel since the penetrating position, expressed in term of Frame numbering, is given.

### *2.4.4 RESULTS*

The detailed characteristics of the tanker vessel are as follows:

| | |
|---|---|
| Displacement | 27500 tons |
| $L_{OA}$ | 161,5 m |
| Breadth | 24,99 m |
| Depth | 12,57 m |
| Draft | 9,25 m |

**TABLE 2.4** Tanker Characteristics

The bow structure is shown in Figure. 2.15 in which frame 77 is the collision bulkhead.

For other frames, as before, it has been assumed that these are of similar construction to their neighbouring frames, and for crippling force calculation, a linear interpolation according to the frame breadth and depth is assumed. The following Table 2.5 shows the section areas with the crippling stresses.

| Frame No. | **Crippling stress Kgf/cm$^2$ Gerard** |
|---|---|
| 80 | 2326.11 |
| 84 | 1540.76 |
| 87 | 941.76 |
| 88 | 965.86 |
| 91 | 1095.27 |
| 93 | 857.27 |
| 97 | 864.90 |

**TABLE 2.5** Crippling stress as it was calculated from Gerard's approach

With Yield stress = 2530 kgf/cm$^2$, and E= 2098483.2 kgf/cm$^2$

In certain frames, some assumptions had to be made regarding some of the scantling section sizes, as they are not shown on the drawings. In Figure 2.16 the results of the tanker ship are shown in which the crippling force is plotted in kN against indentation, i.e. from collision bulkhead a =15.6m to frame No. 101, a =0 m. Except Gerard's formula, modified Amdahl's and Yang & Caldwell formula has been used.

As expected, the crippling force increases with the depth of penetration. The result shown on Figure 2.16 is similar to Figure A2-3.1 produced by Amdahl in appendix 3. Gerard's approach produces higher values than the other two. Comparing these values from those of Amdahl's the significance of the modification Minorsky (1983) introduced into Gerard's approach can be seen. It is expected that the energy quantities being derived from these formulas will have significantly lower values than Gerard's and therefore they can be ignored. Minorsky has shown that Gerard's method produces results with ±10% tolerance.

The integration of the crippling force in respect to the indentation produces Energy. This is shown in Figure 2.17. For example a collision incident with a resultant indentation of 9m will theoretically absorb 1.0 GJoule.

Considering the size of this tanker and comparing it with ship *A* from Table 2.3 it can be assumed that according to Aldwinckle's equation both ships can be included in the same class and hence a comparison of the energy absorbed is shown in Figure 2.18.

Very good correlation is shown with Aldwinckle's equation, contrary to that derived from to Amdahl's and Yang & Caldwell formulas.

In Figure 2.19a, b, are shown the curves of energy absorbed and the final resting time for the ship. In the finite element analysis these curves will be compared to the numerical results. Figure 2.19c displays the indentation.

## 2.5 ENERGY BALANCE

### 2.5.1 COLLISION WITH A RIGID BODY WHEN $\alpha=\pi/2$

The conservation of energy implied by the first law of thermodynamics, states that the time rate of change of kinetic energy and internal energy for a fixed body of material is equal to the sum of the rate of work done by the surface and body forces. This is depicted in equation 2.56 as:

$$\frac{d}{dt}\int_V \left(\frac{1}{2}\rho\vec{v}\cdot\vec{v}+\rho U\right)dV = \int_S \vec{v}\cdot\vec{t}\;dS + \int_V \vec{f}\cdot\vec{v}\;dV \qquad 2.56$$

where:

| | |
|---|---|
| ρ | is the mass density |
| v | the velocity vector |
| U | is the internal energy per unit mass |
| $\vec{t}$ | is the surface force per unit of the area |
| $\vec{f}$ | is the body force vector |
| $\vec{n}$ | is the normal direction vector on boundary S |

Using Gauss' theorem and the identity that $\vec{t}=\vec{\sigma}\cdot\vec{n}$ on the boundary S, the first term of equation 2.56 can be rewritten as:

$$\begin{aligned}\int_S \vec{v}\cdot\vec{t}\;dS &= \int_V \left(\frac{\partial}{\partial x}\right)\cdot(\vec{v}\cdot\vec{\sigma})\,dV \\ &= \int_V \left[\left(\frac{\partial}{\partial x}\cdot\vec{\sigma}\right)\cdot\vec{v}+\frac{\partial v}{\partial x}\times\vec{\sigma}\right]dV \qquad 2.57 \\ &= \int_V \left[\left(\frac{\partial}{\partial x}\cdot\vec{\sigma}\right)\cdot\vec{v}+\dot{\varepsilon}\times\vec{\sigma}\right]dV\end{aligned}$$

since it is also known that

$$\frac{\partial v}{\partial x}\times\vec{\sigma} = \dot{\varepsilon}\times\vec{\sigma} \qquad 2.58$$

where $\dot{\varepsilon}$ is the total, elastic and inelastic strain rates. Substituting equation 2.57 into equation 2.56 yields

$$\frac{d}{dt}\int_V \left(\frac{1}{2}\rho\vec{v}\cdot\vec{v}+\rho U\right)dV = \int_V \left[\left(\frac{\partial}{\partial x}\cdot\vec{\sigma}+\vec{f}\right)\cdot\vec{v}+\vec{\sigma}\times\dot{\varepsilon}\right]dV \qquad 2.59$$

From Cauchy's equation of motion, we have

$$\frac{\partial}{\partial x}\cdot\vec{\sigma}+\vec{f}=\rho\frac{dv}{dt} \qquad 2.60$$

substituting this into equation 2.59 gives

$$\frac{d}{dt}\int_V \left(\frac{1}{2}\rho\vec{v}\cdot\vec{v}+\rho U\right)dV = \int_V \frac{d}{dt}\left[\left(\frac{1}{2}\rho\vec{v}\cdot\vec{v}\right)+\vec{\sigma}\times\dot{\varepsilon}\right]dV \qquad 2.61$$

from this the energy equation is obtained:

$$\rho\frac{dU}{dt}=\vec{\sigma}\times\dot{\varepsilon} \qquad 2.62$$

The internal energy, $E_U$, is then defined as:

$$E_U=\int_V \rho U dV=\int_0^t\left(\int_V \vec{\sigma}\times\dot{\varepsilon}dV\right)dt \qquad 2.63$$

To make the energy balance equation 2.56 more convenient to use it is integrated in respect to the time t:

$$\frac{d}{dt}\int_V \left(\frac{1}{2}\rho\vec{v}\cdot\vec{v}+\rho U\right)dV=\int_0^t \dot{E}_{WF}dt+\text{constant} \qquad 2.64$$

where $\dot{E}_{WF}$ is the rate of work done to the body by external forces and contact friction forces between the contact surfaces, defined as

$$\dot{E}_{WF} = \int_S \vec{v} \cdot \vec{t}\, dS + \int_V \vec{f} \cdot \vec{v} dV \qquad 2.65$$

The force t may be further split into the surface distributed load $t^l$, and the frictional $t^f$. $\dot{E}_{WF}$ can be then written as:

$$\dot{E}_{WF} = \left(\int_S \vec{v} \cdot \vec{t}^{\,l} dS + \int_V \vec{f} \cdot \vec{v} dV\right) - \left(-\int_S \vec{v} \cdot \vec{t}^{\,f} dS\right) = \dot{E}_W - \dot{E}_F \qquad 2.66$$

where $\dot{E}_W$ is the rate of work done to the body by external forces and $\dot{E}_F$ is the rate of energy dissipated by contact friction forces between the contact surfaces. An energy balance for the entire model may be written as

$$\sum F_i + \sum E_{Pi} + \sum E_{Ei} - E(u)_i = 0 \qquad 2.67$$

where:

**$E(u)_i$** is the initial kinetic energy

**$\Sigma E_{Pi}$** is the summation of the plastic energy quantities absorbed from the various parts of the bow.

**$\Sigma E_{Fi}$** is the summation of the friction energy.

**$\Sigma E_{Ei}$** is the summation of the elastic energy quantities absorbed from the various parts of the bow, after the collision.

From these quantities the important ones for the current analysis are the elastic and plastic energy dissipated in the structure since a comparison with the initial kinetic energy is being developed.

### 2.5.2 COLLISION WITH A RIGID BODY WHEN $0<\alpha<\pi/2$

The impact of the ship with a rigid surface with slope $\alpha$ is assumed to be fully plastic. Therefore, during the grounding, the ship will lose some kinetic energy during the first phase as described earlier. At the end of this phase the kinetic energy can be expressed as:

$$E^1_{kinetic} = 0.5M(1+m_{xx})v_x^2 + 0.5M(1+m_{zz})v_z^2 + 0.5MR^2(1+j_{YY})\dot{\vartheta}_Y^2 \qquad 2.68$$

or:

$$E^1_{kinetic} = E^0_{kinetic}\left[\left(\frac{v_x}{V}\right)^2 + \alpha_1\left(\frac{v_z}{V}\right)^2 + \alpha_2\left(\frac{R\dot{\vartheta}_Y}{V}\right)^2\right] \qquad 2.69$$

where:

$$E^0_{kinetic} = \frac{1}{2}M(1+m_{xx})V^2 \qquad 2.70$$

From Figure 2.20 it is seen that for slope angles $\alpha$ less than around 0.10 rad, the loss of kinetic energy during the initial impact phase can be neglected. But when the slope is around $\pi/4$ nearly all the kinetic energy is lost in this phase. In this case the impact is comparable to bow impact against a rigid wall.

At the end of this phase the kinetic energy of the ship can be determined as:

$$E^t_{kinetic} = E^1_{kinetic} - \int_0^{u(t)} F_f du - \int_0^{z(t)} F_z dz \qquad 2.71$$

where u is the distance the bow slides along the slope. This can be reduced to:

$$E^t_{kinetic} = E^1_{kinetic} - \int_0^{z(t)} \frac{\tan\beta}{\tan\alpha} F_z(z) dz \qquad 2.72$$

since $dx \cdot \tan\alpha = dz$ it can be seen that the last term in equation 2.72 expresses the loss in kinetic energy due to the horizontal force. However it should be noted that the loss of kinetic energy accounts only for the frictional forces while it assumes that the

elasto-plastic energy stored on the bow is negligible. This assumption will be evaluated further more in the fourth chapter where the finite element model for a tanker vessel during grounding is developed.

If the initial velocity is assumed to be very large so that the bow will reach the flat plateau of the ground, then the kinetic energy will decrease as a function of the distance s which the ship slides over the horizontal surface:

$$E^t_{kinetic} = E^1_{kinetic} - \int_0^{T_f+h} F_f(z)\frac{1}{\sin\alpha}dz - \int_0^{T_f+h} F_z(z)dz - \mu\int_0^s F_z(s_1)ds_1 - \int_0^s F_z\frac{T(s_1)+h-w(s_1)}{\ell(s_1)}ds_1 \qquad 2.73$$

where $T_f$ is the forward draught

$h$ is the height of the horizontal plane above the sea surface

If the angle $\alpha_2$ is introduced for the ship bottom $s_1$ to the horizontal x-axis:

$$\alpha_2 = \alpha\sin\left(\frac{T(s_1)+h-w(s_1)}{\ell(s_1)}\right) \qquad 2.74$$

substituting $\alpha_2$ for the slope $\alpha$ of the island in equation 2.26 and denote the resulting reaction inclination $\beta_2$ then the instantaneous kinetic energy in the situation when the ship slides on the edge of the island can also be expressed as:

$$E^t_{kinetic} = E^1_{kinetic} - \int_0^{T_f+h}\frac{\tan\beta}{\tan\alpha}F_f(z)dz - \int_0^s \cos\beta_2(s_1)\tan\beta_2(s_1)\cdot F_z(s_1,z)ds_1 \qquad 2.75$$

This is the final resting situation which represents the worst loading case for the ship hull. In the simplified case where the ship does not reach the flat plateau of the ground and where the linear approximation equation 2.38 can be used for the ground reaction $F_z$ as function of the lifted distance z we find from equation 2.72 that when the ship comes to rest $E_{kinetic}(t)=0$ the bow will be lifted the distance :

$$z_u = \left\{ \frac{2E^1_{kinetic} C_B T \left(1 + \ell^2 / r^2\right) \tan\alpha}{C_w M\, g \tan\beta} \right\}^{0.5} \qquad 2.76$$

or

$$x_{max} = V \sqrt{\left(1 + \frac{\ell^2}{r^2}\right) \frac{RTC_B}{C_w M \tan\alpha \tan\beta}} \qquad 2.77$$

Where V and R can be found from the system 2.27, 2.28

Since the kinetic energy $E^1_{kinetic}$, see equation 2.69, is proportional to the square of the initial velocity V, it is observed from equation 2.76 that $z_u$ and hence also the sliding distance $x_{max}$ is proportional to V.

# APPENDIX I

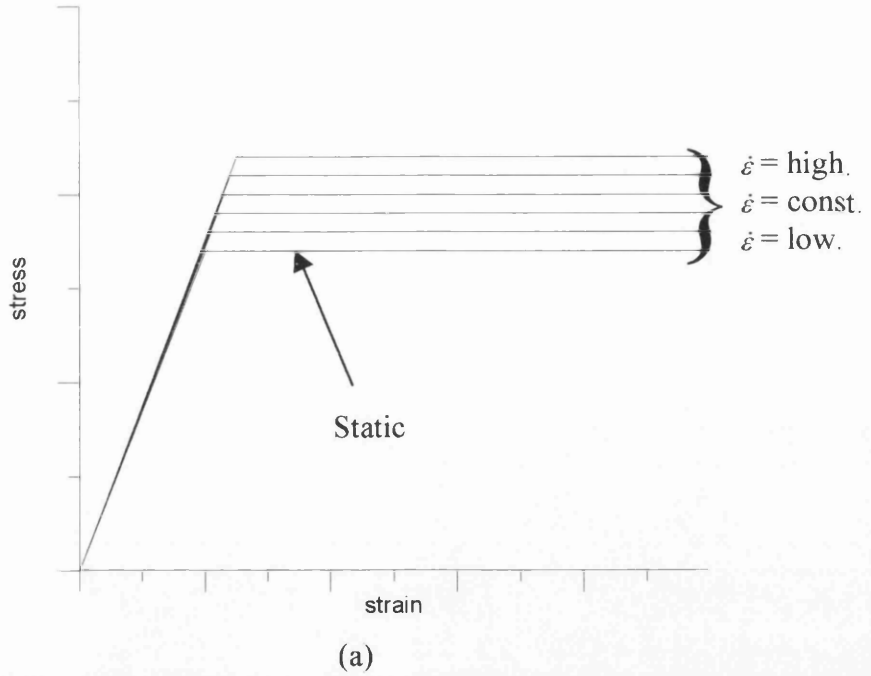


***Figure A2-1.1*** *Stress Strain curves for elastic/visco-perfectly plastic material.* $\dot{\varepsilon}$ *remains constant, in (b)* $\dot{\varepsilon}$ *varies. Samuelides (1984)*

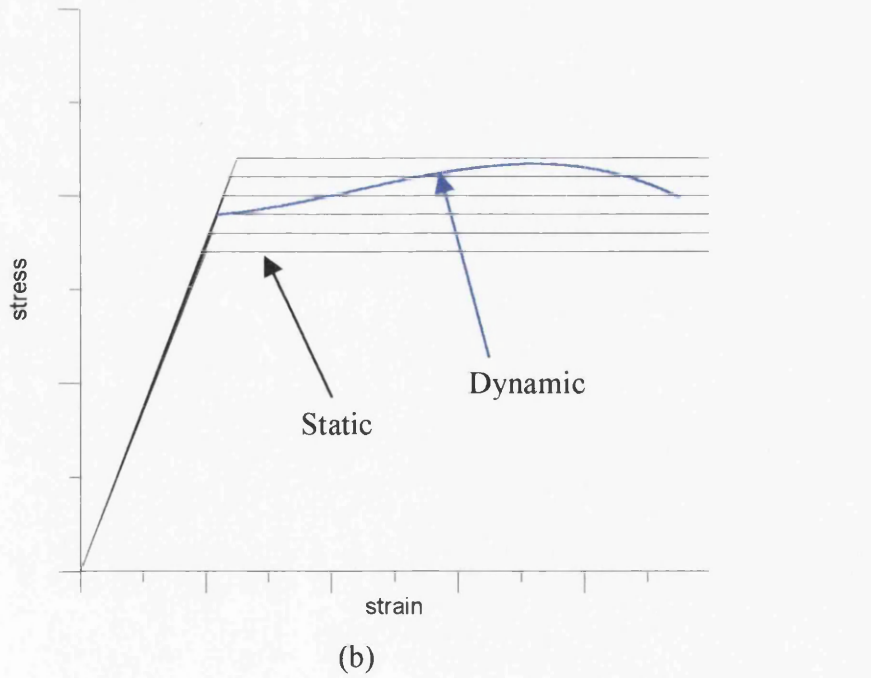


***Figure A2-1.2*** *Stress Strain curves for elastic/visco-perfectly plastic material.* $\dot{\varepsilon}$ varies, Samuelides (1984).

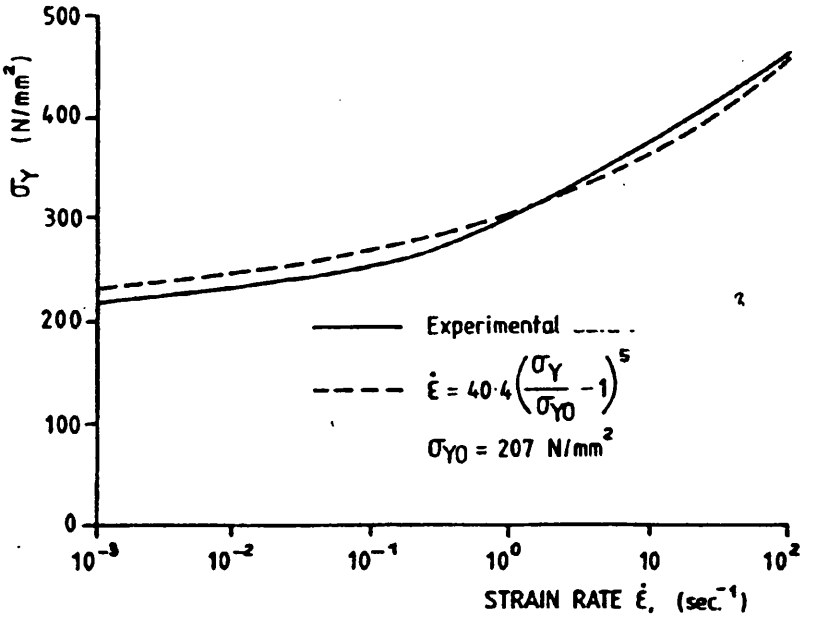


*Figure A2-1.3* *Comparison between the results obtained from equation 2.20 and Manjoine's (1944) experimental results.*

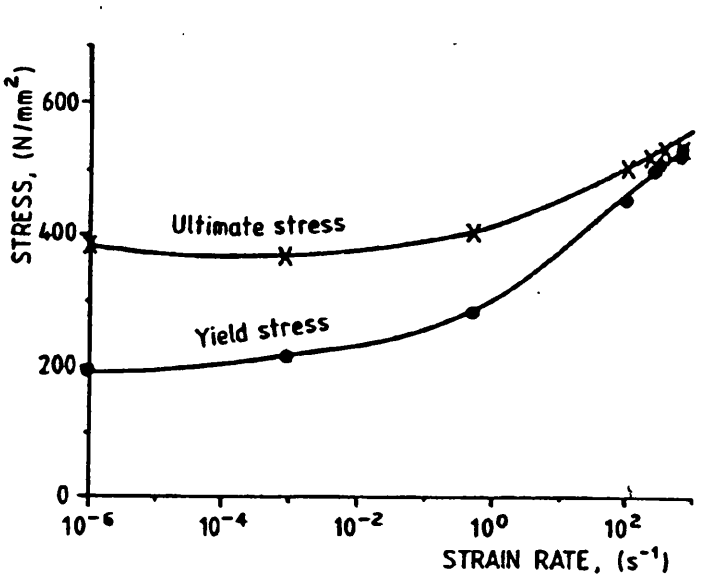


*Figure A2-1.4* *Strain rate effect on yield and ultimate stress. Samuelides (1984)*

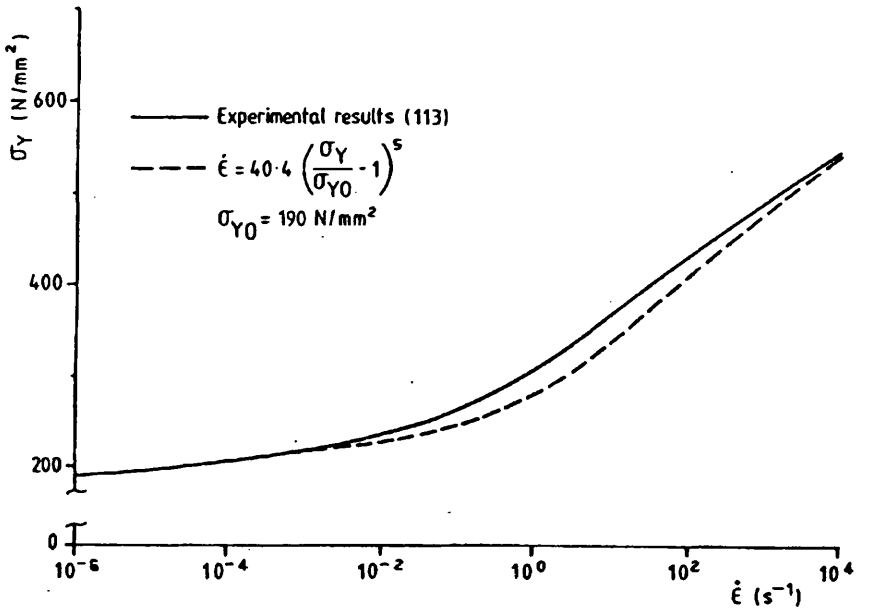


***Figure A2-1.5*** *Strain rate effect on yield stress: Correlation between experimental and theoretical results.*

# APPENDIX II

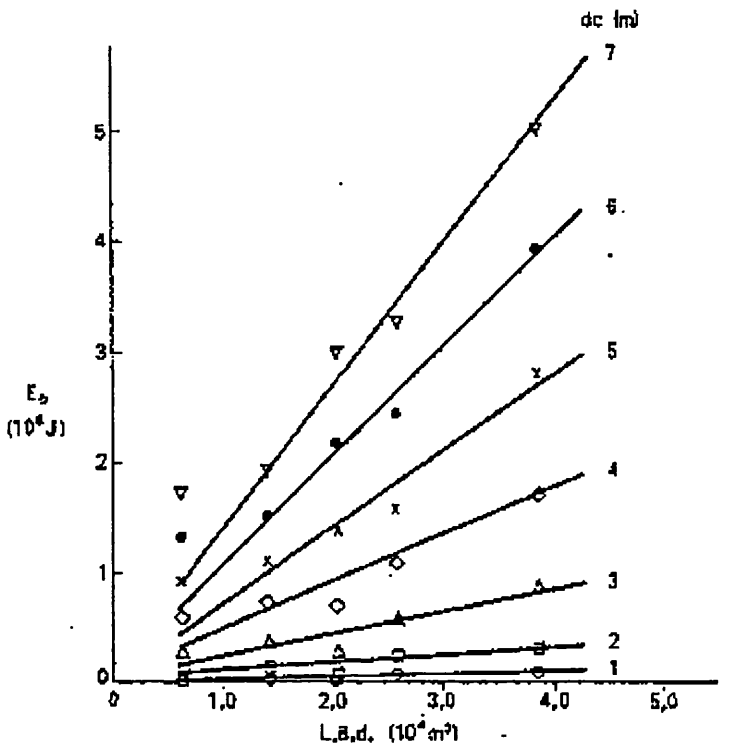


***Figure A2-2.1*** *$E_D$ and collapse distance as a function of ship size parameters. Aldwinckle (1984)*

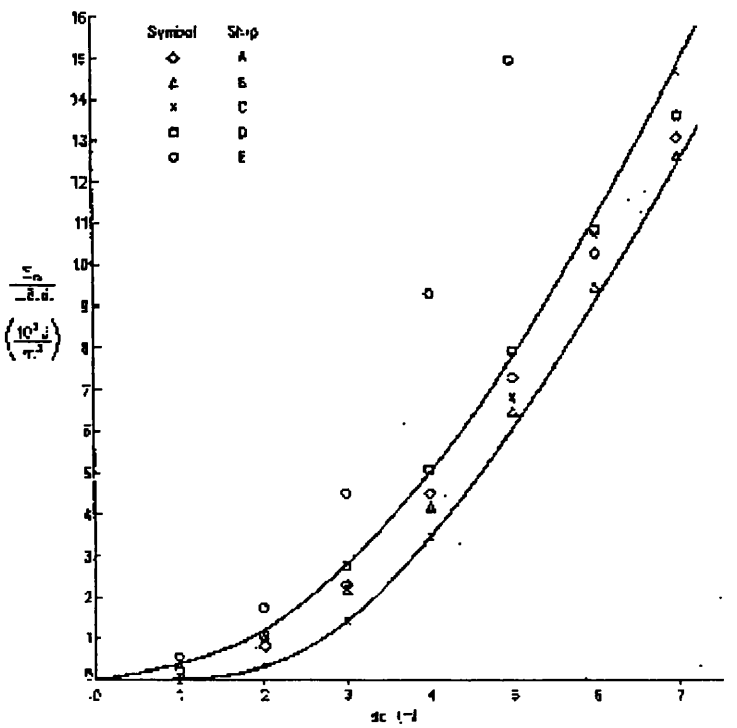


***Figure A2-2.2*** *Collision Model – Correlation with ship size parameters Aldwinckle (1984)*

# APPENDIX III

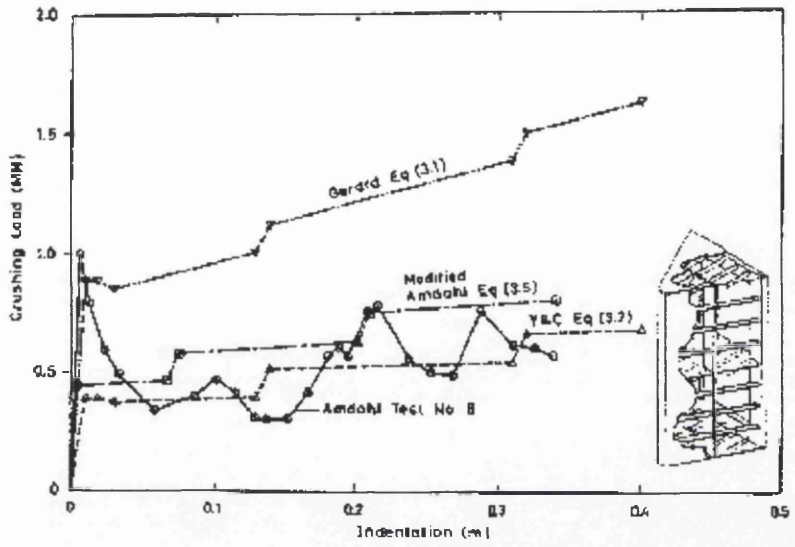


***Figure A2-3.1*** *Comparison between numerical predictions and Amdahl test no. 5, presented in Pedersen (1995)*

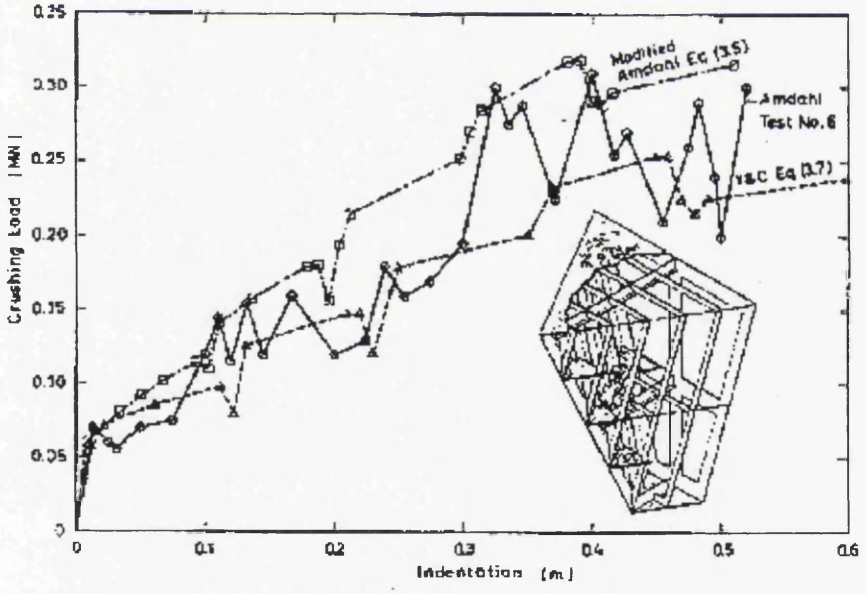


***Figure A2-3.2*** *Comparison between numerical predictions and Amdahl test no. 6, presented in Pedersen (1995)*

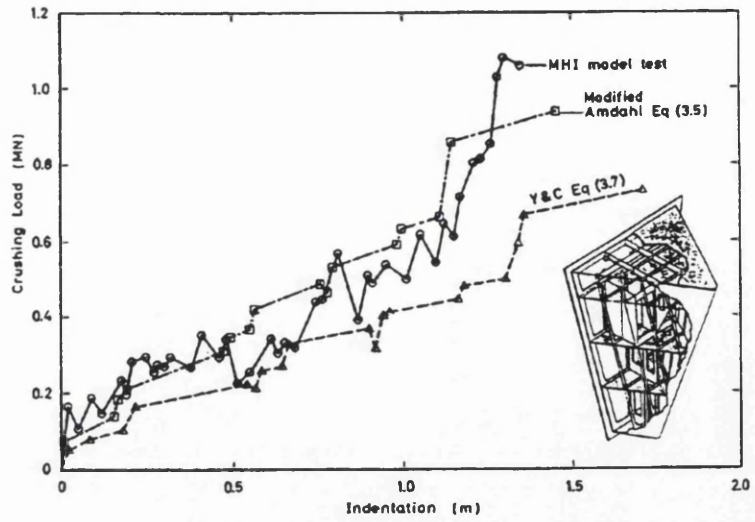


*Figure A2-3.3* *Comparison between numerical predictions and model test by Hagiwara et al (1982). Pedersen (1995)*

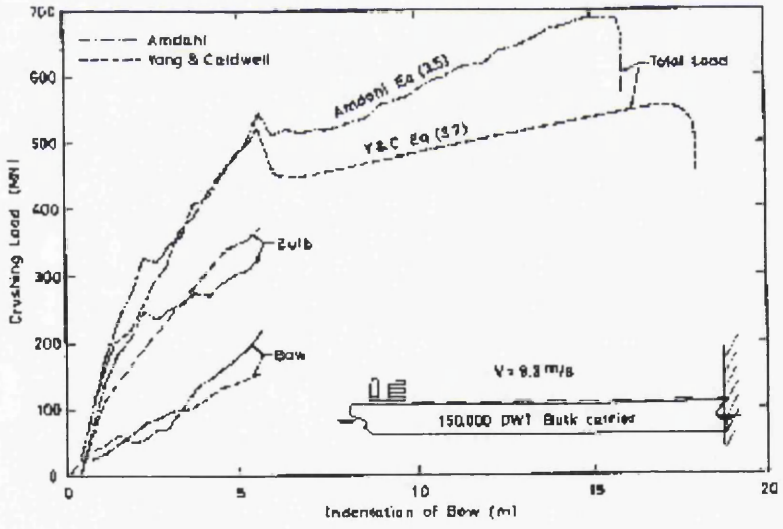


*Figure A2-3.4* *Calculated load deflection curves for 150,000 DWT bulk carrier at an initial speed of 9.3 m/s colliding head-on with an infinitely rigid half space, Pedersen (1995)*

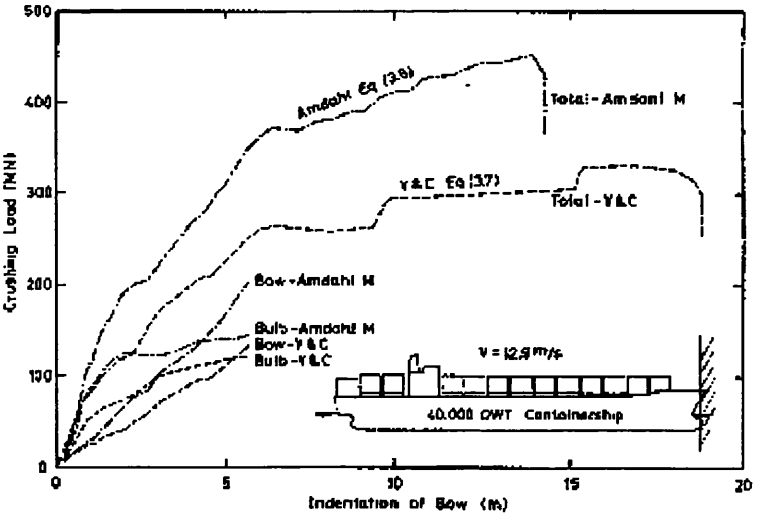


*Figure A2-3.5* *Calculated load deflection curves for 40,000 DWT container vessel at an initial speed of 12.9 m/s, Pedersen (1995)*

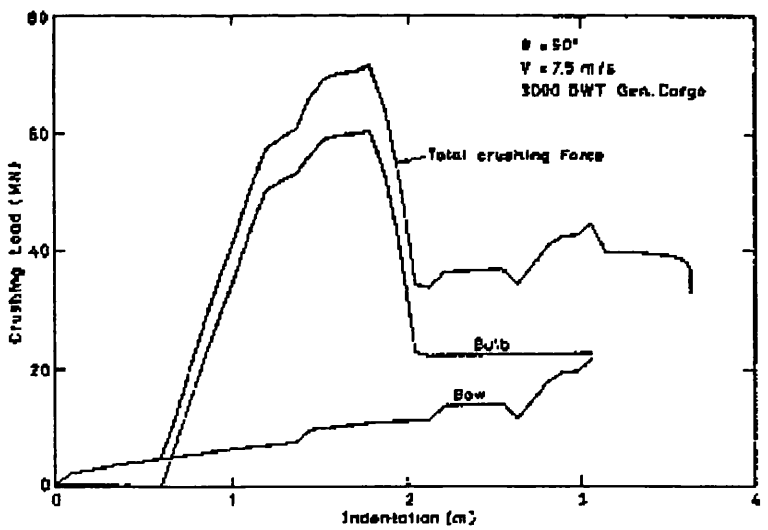


*Figure A2-3.6* *Calculated load deflection curves for 3,000 DWT general cargo vessel at an initial speed of 7.5 m/s, using Amdahl's modified procedure, Pedersen (1995)*

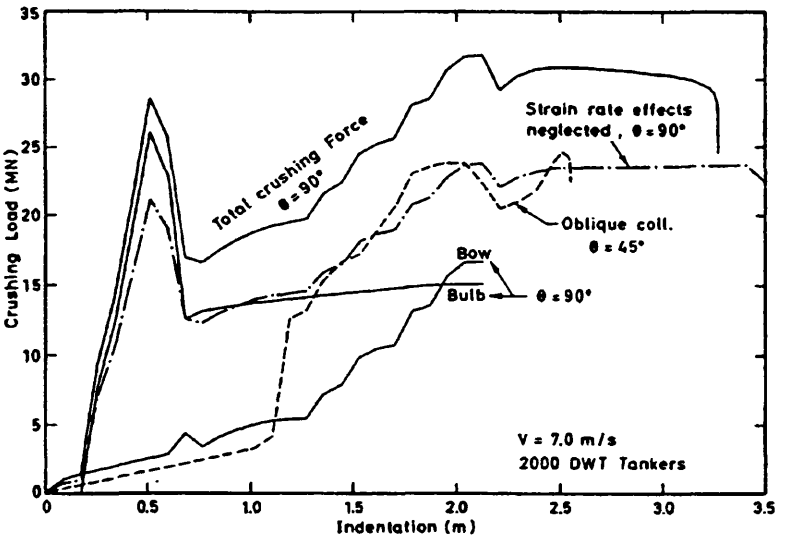


***Figure A2-3.7*** *Calculated bow crushing loads for 2,000 DWT tanker, Pedersen (1995)*

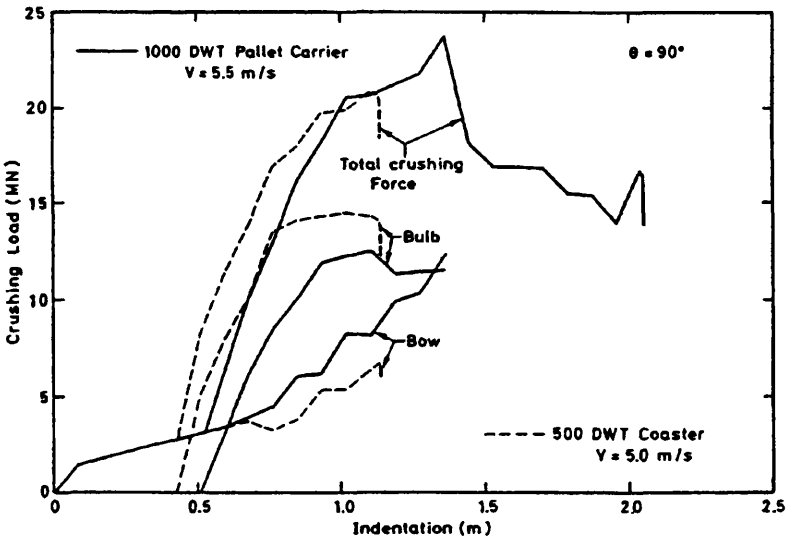


***Figure A2-3.8*** *Calculated bow crushing loads for 1,000 DWT pallet carrier (Vs=5.5 m/s and 500 DWT coaster (Vo=5.0 m/s), Pedersen (1995)*

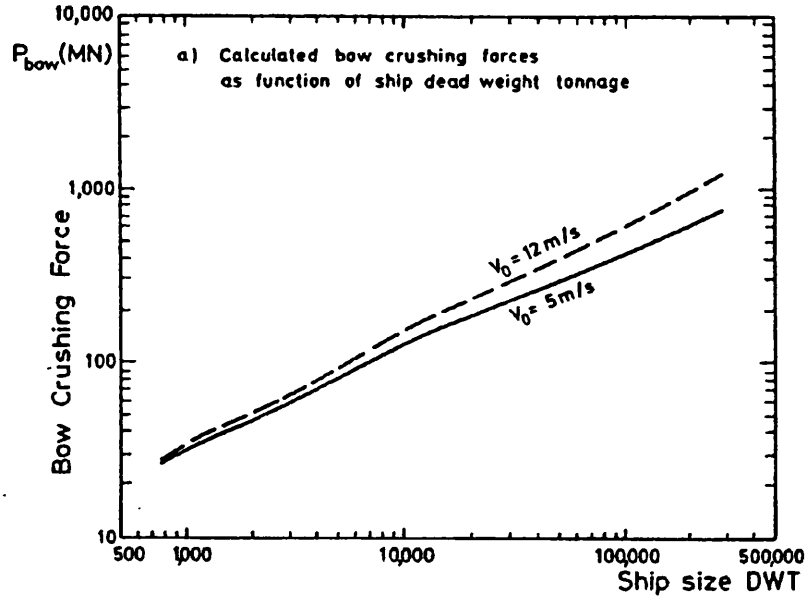


*Figure A2-3.9* *Calculated collision forces, indentation and duration for average merchant vessels in head-on collision against a fixed wall. Pedersen (1995)*

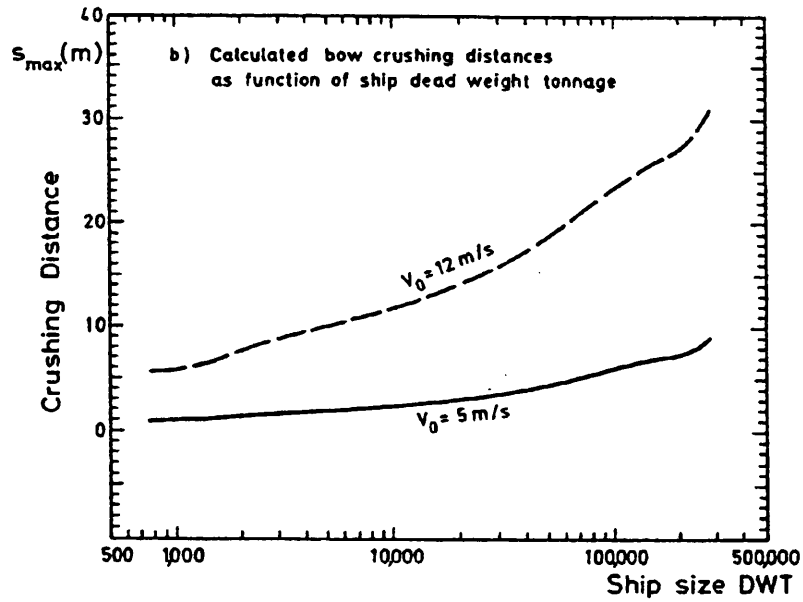


*Figure A2-3.10* *Calculated collision forces, indentation and duration for average merchant vessels in head-on collision against a fixed wall Pedersen (1995)*

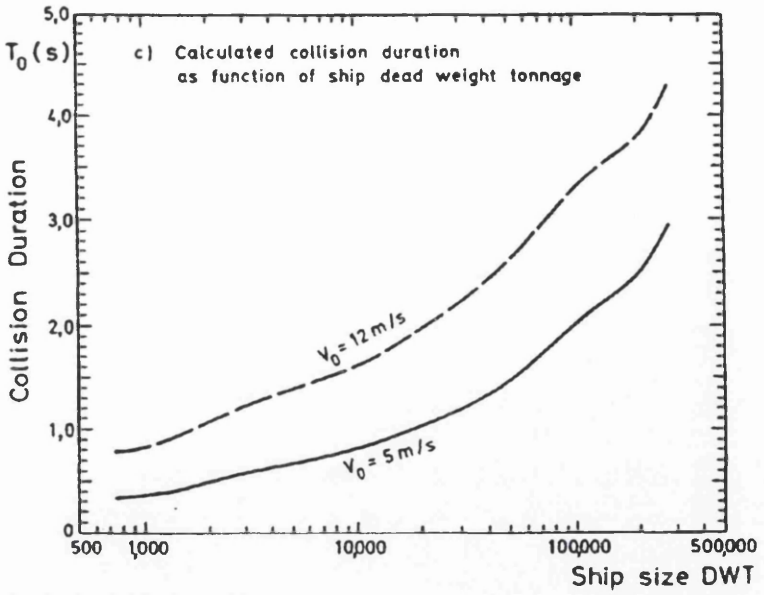


***Figure A2-3.11*** *Calculated collision forces, indentation and duration for average merchant vessels in head-on collision against a fixed wall. Pedersen (1995)*

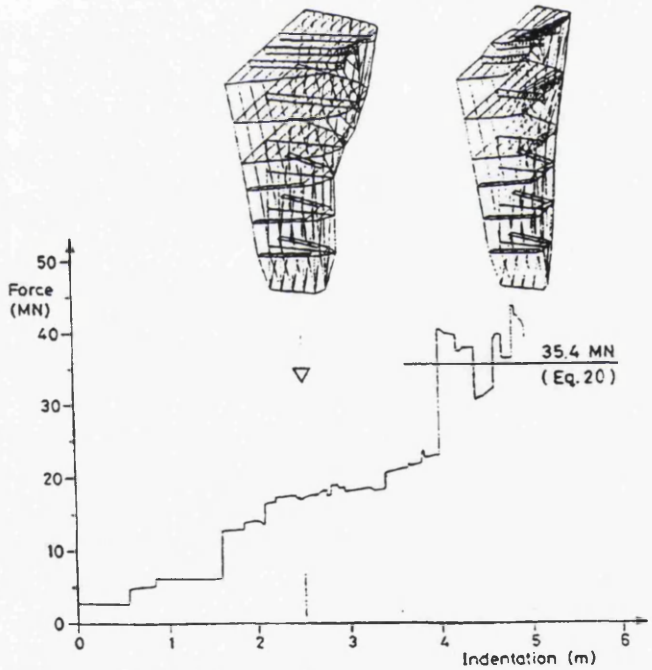


***Figure A2-3.12*** *Head on collision force calculated for a supply vessel (4590 tons displacement) with 6.0 m/s impact velocity against a rigid wall, Pedersen (1995)*

# FIGURES

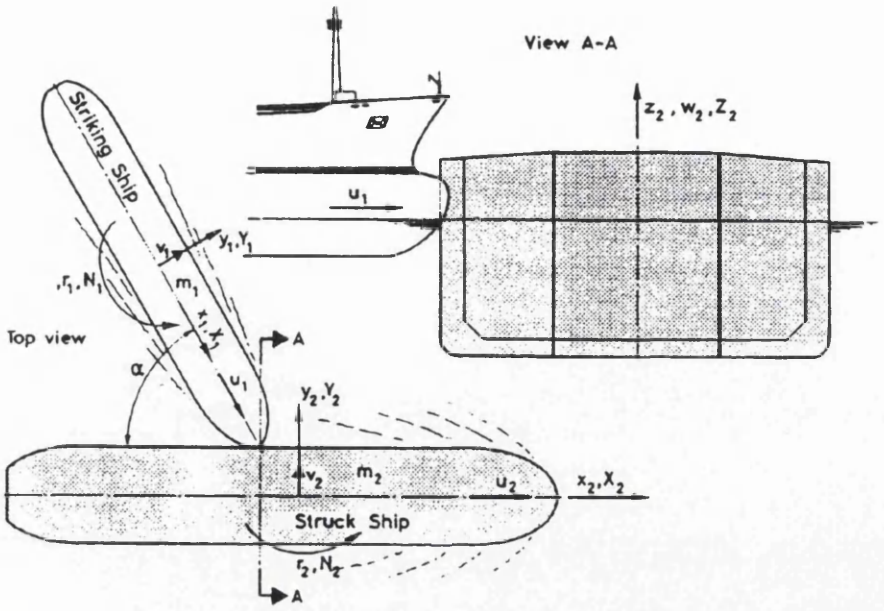


***Figure 2.1.*** *Definition of co-ordinate systems for horizontal, rigid body motions*

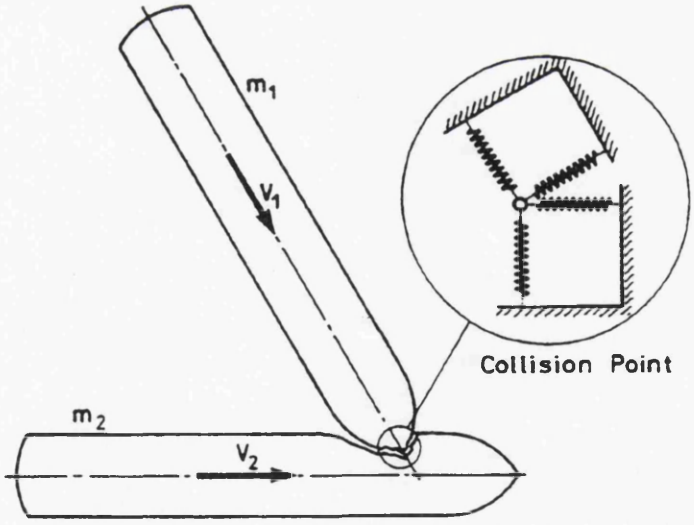


***Figure 2.2.*** *A general ship-ship collision time simulation model, Pedersen (1995)*

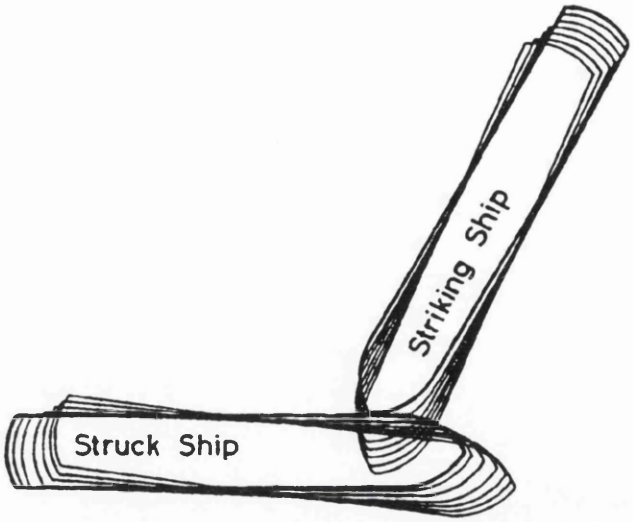


***Figure 2.3.*** *Simulation of an oblique collision between two similar ships, Pedersen (1995)*

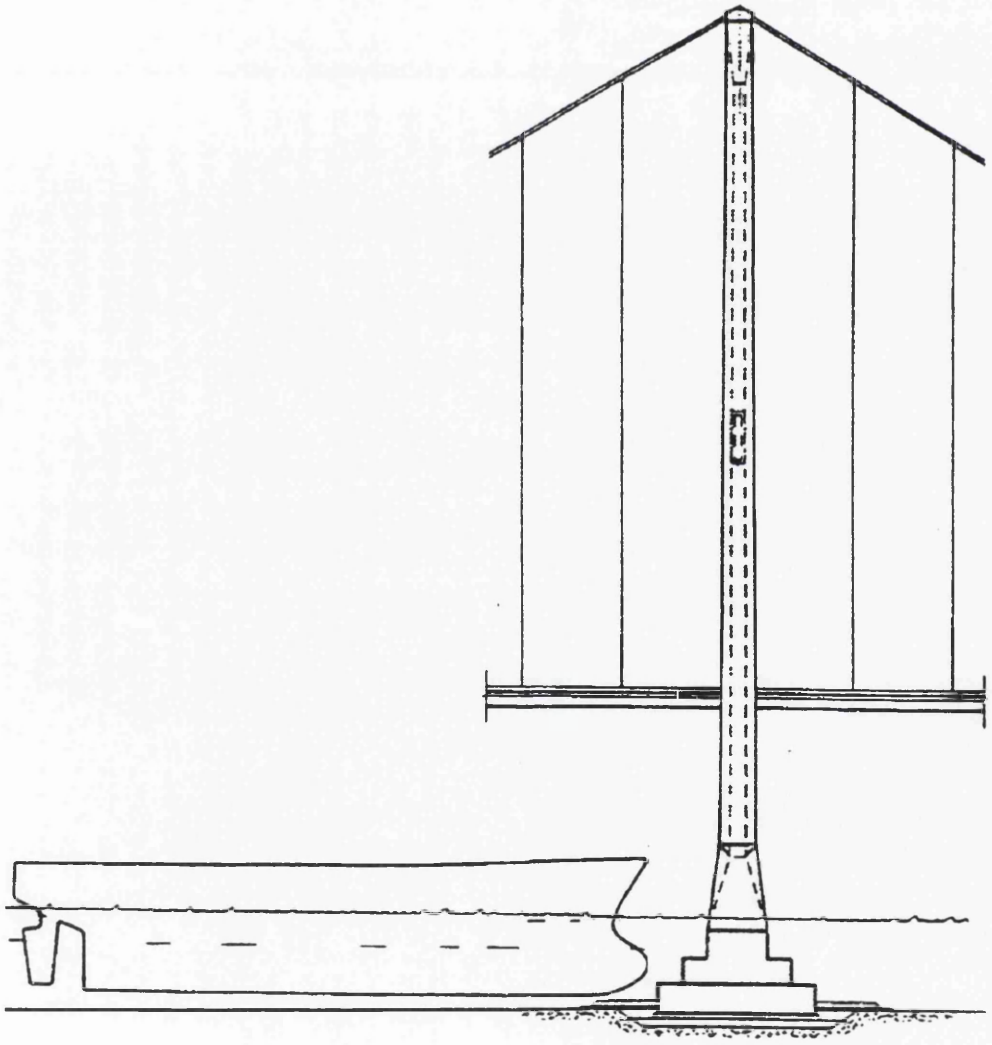

***Figure 2.4.*** *Head on Collision against a bridge pylon.*

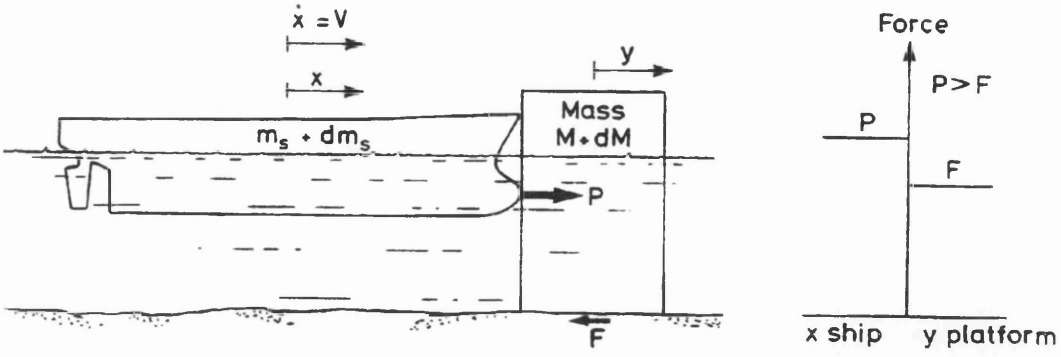


***Figure 2.5.*** *Ship Impact against offshore structure*

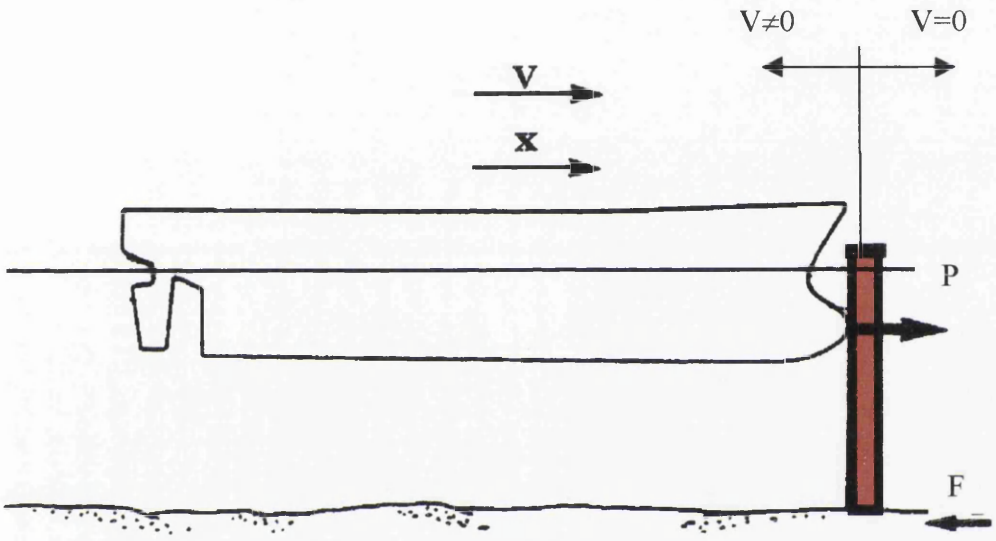


***Figure 2.6.*** *Ship Impact against rigid surface*

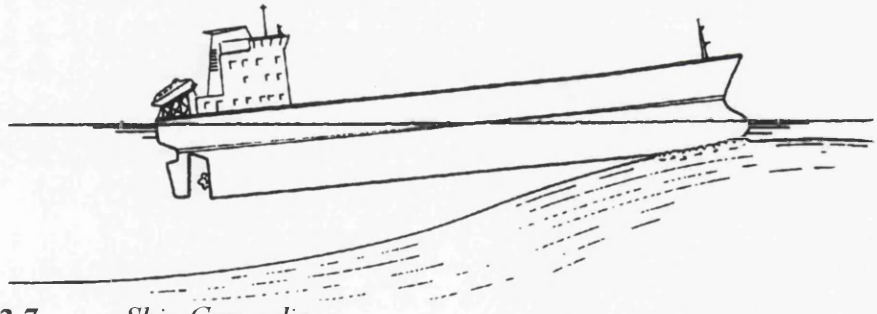

***Figure 2.7.*** *Ship Grounding*

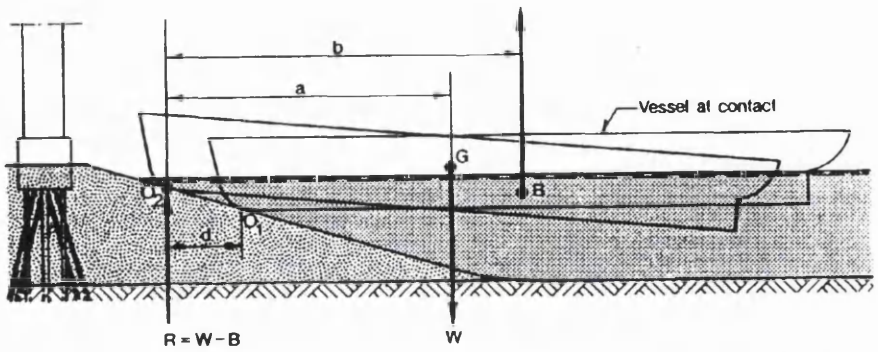


*Figure 2.8* *Weight buoyancy equations for ship meeting artificial island*

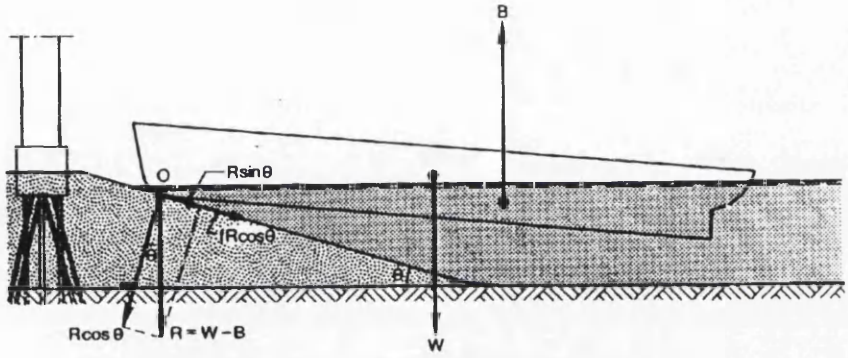


*Figure 2.9* *Forces on ship forefoot, Minorsky (1983)*

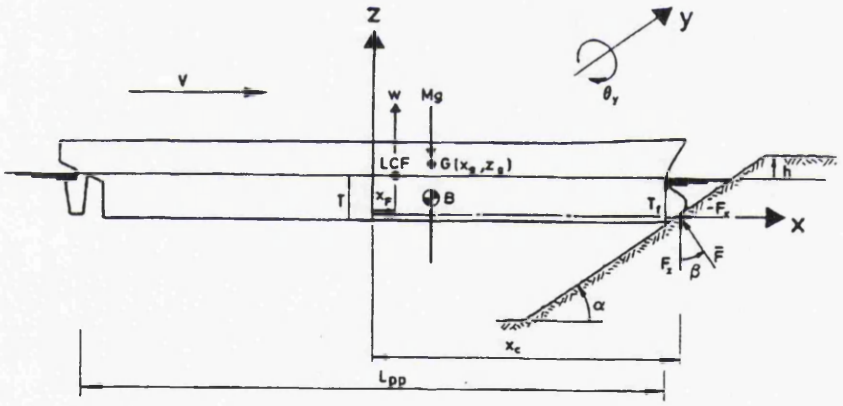


*Figure 2.10* *Initial contact with the ground, Pedersen (1995)*

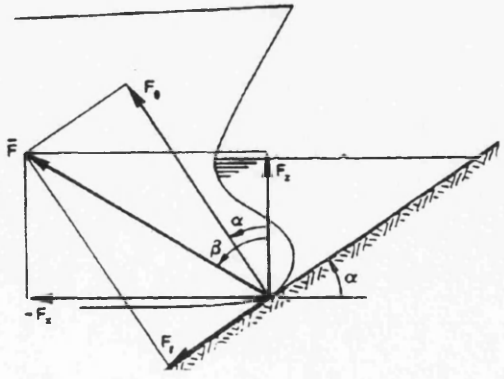


*Figure 2.11* *Resulting force acting on the bow at initial impact, Pedersen (1995)*

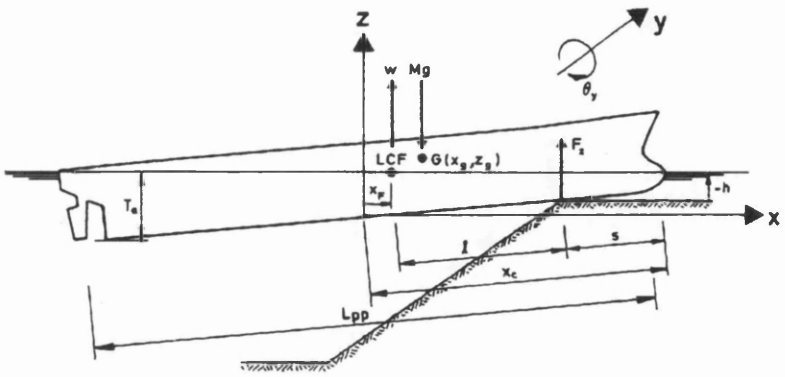


***Figure 2.12*** *Sliding on a subsea island, Pedersen (1995)*

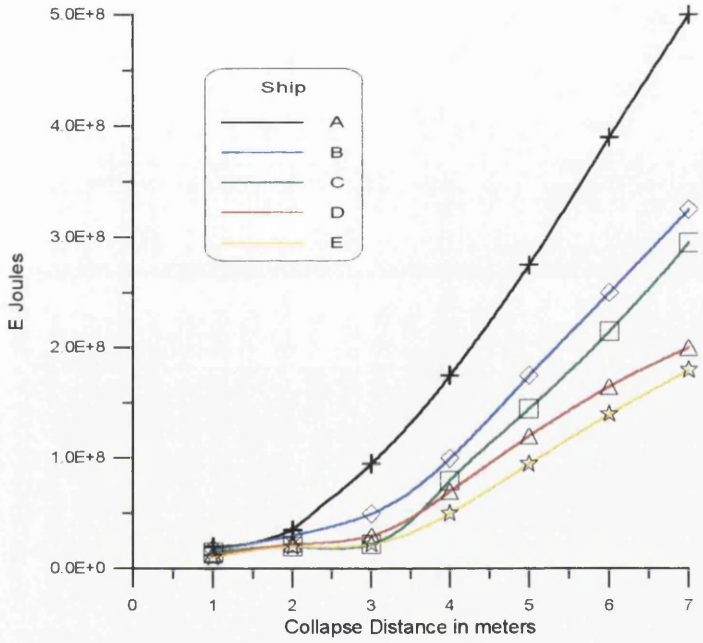


***Figure 2.13*** *The total Energy absorbed by those ships shown on Table 2.3 in respect to the penetration distance*

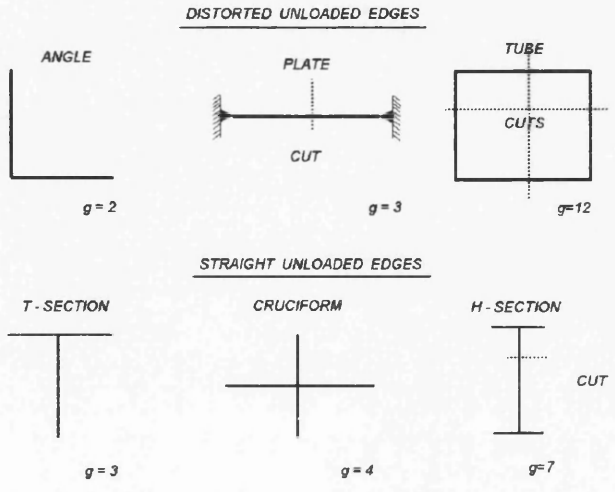


***Figure 2.14*** *Methods of cutting simple elements in order to determine the value of the g factor in equation 2.45*

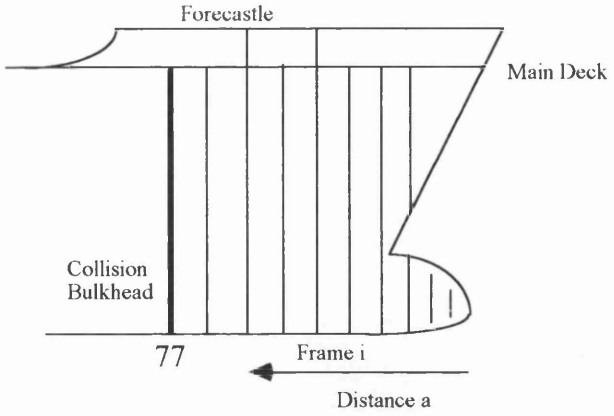


***Figure 2.15.*** *The Bow Frame structure*

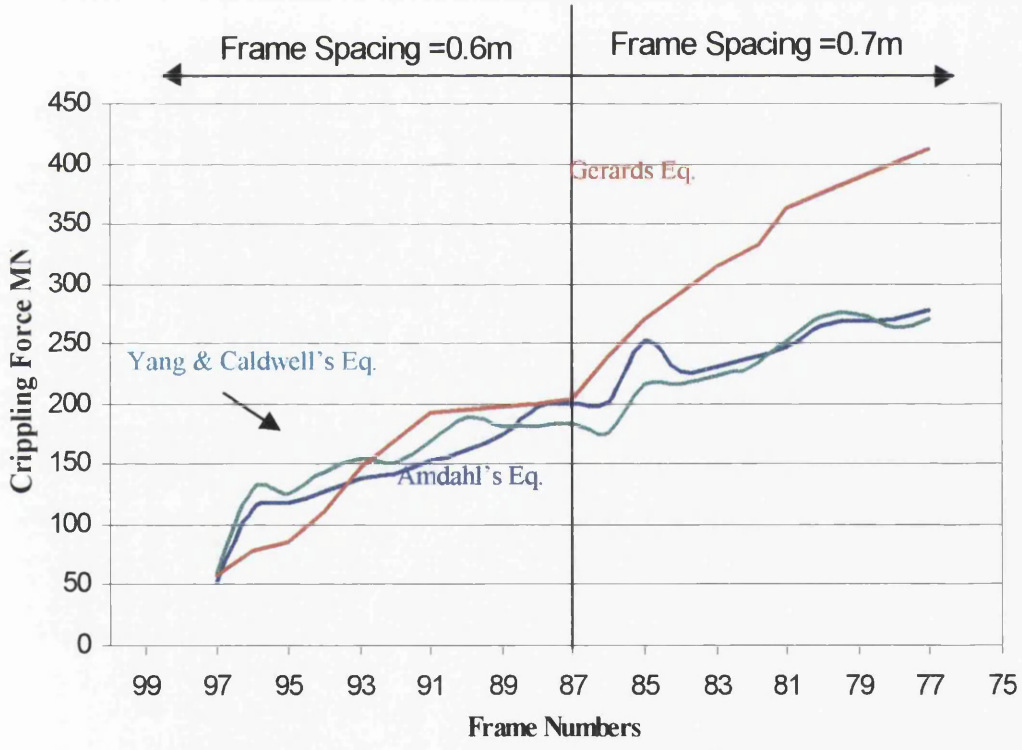


***Figure 2.16*** *Crippling Force versus indentation using the empirical methods provided by Gerard, Amdahl and Yang & Caldwell's Equations*

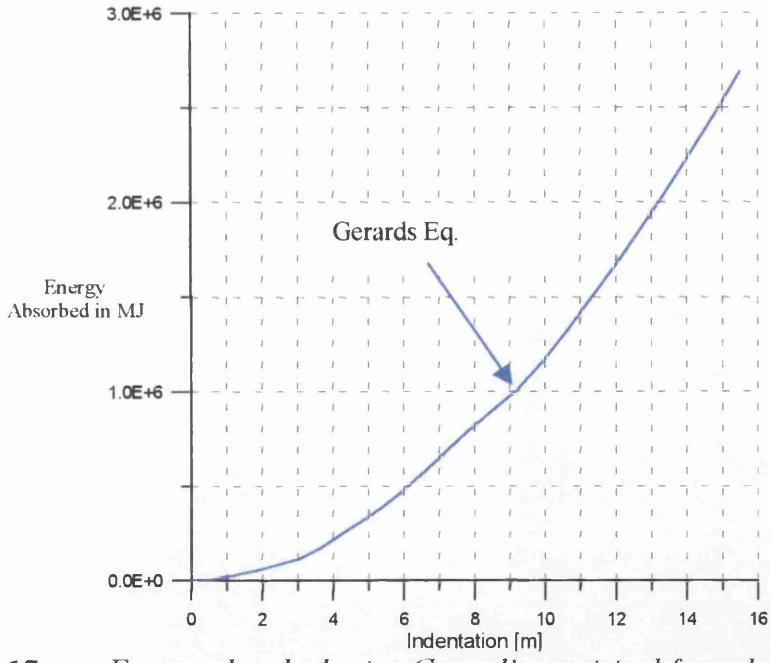


***Figure 2.17*** *Energy absorbed using Gerard's empirical formula*

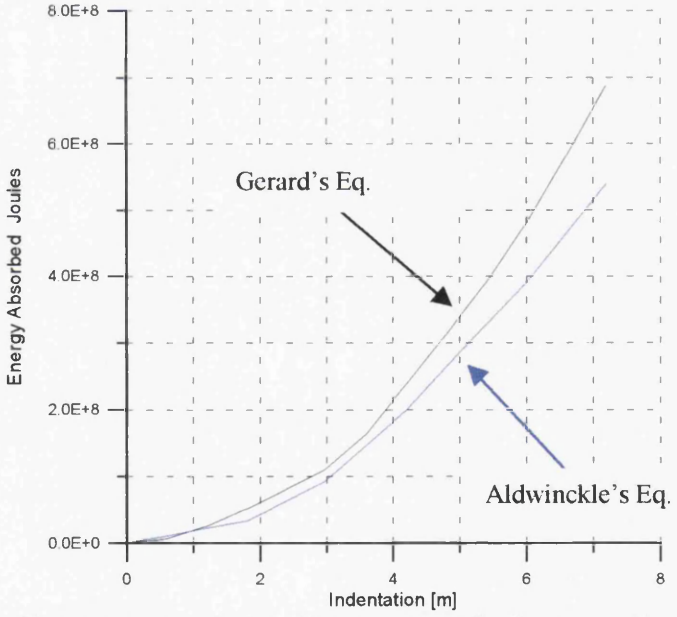


***Figure 2.18*** *Comparison of the Energy absorbed using Gerard's empirical formula and Aldwinckle's equation*

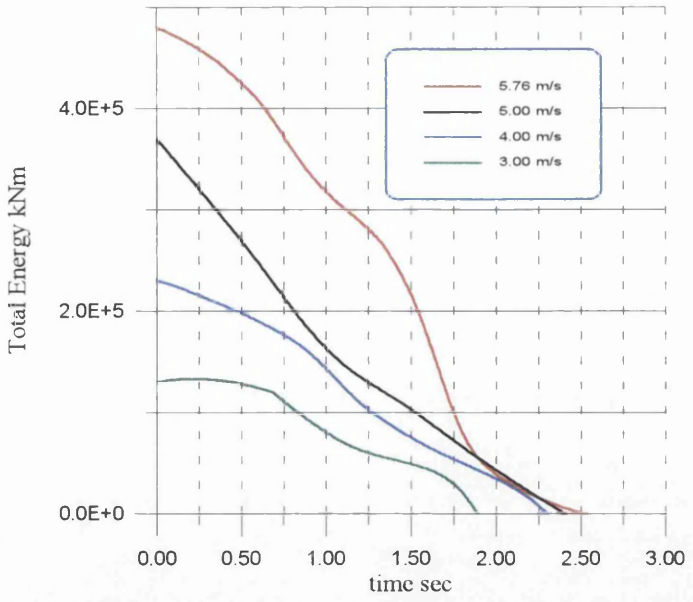


***Figure 2.19a*** *The total resting time with initial speeds 5.76, 4.00, 3.00, 2.00m/s, versus the energy absorbed.*

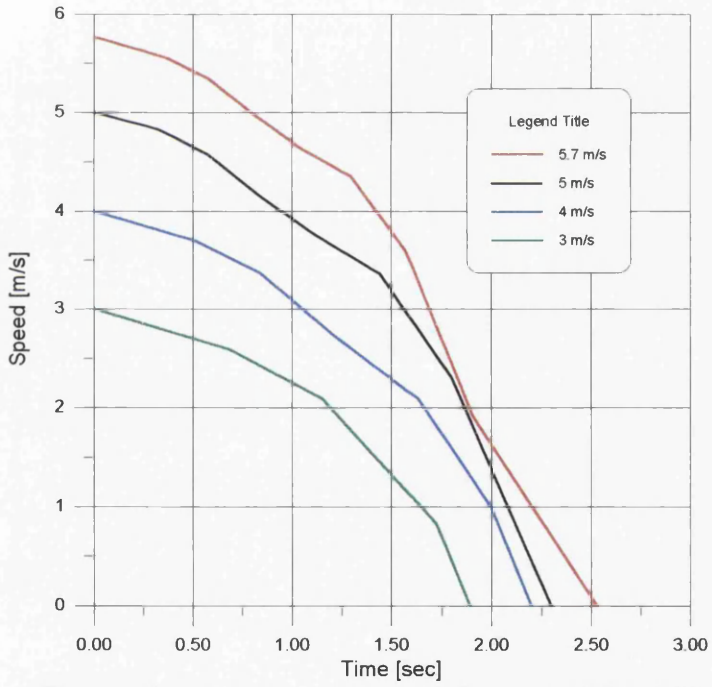


***Figure 2.19b*** *The total resting time with initial speeds 5.76, 4.00, 3.00, 2.00m/s, versus the speed of the ship*

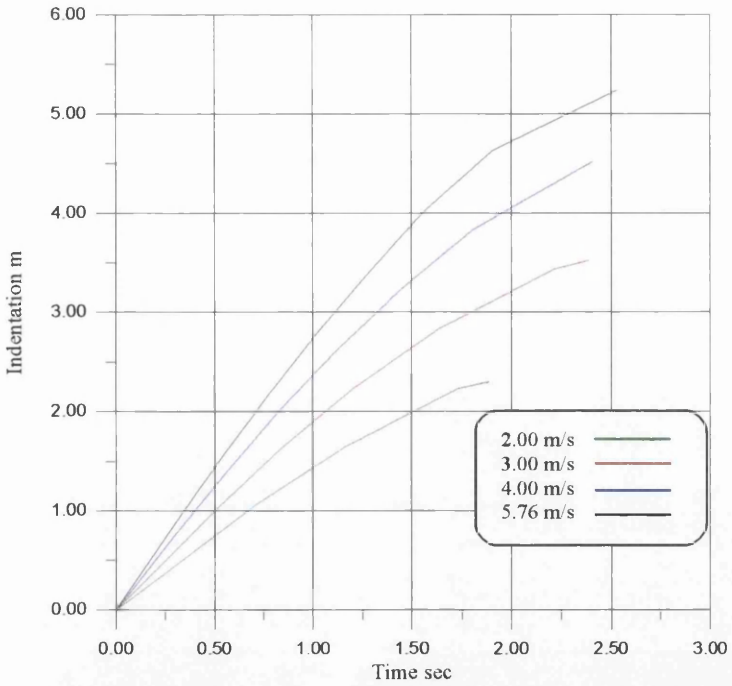


***Figure 2.19c*** *The indentation with initial speeds 5.76, 4.00, 3.00, 2.00m/s, versus the time of the ship*

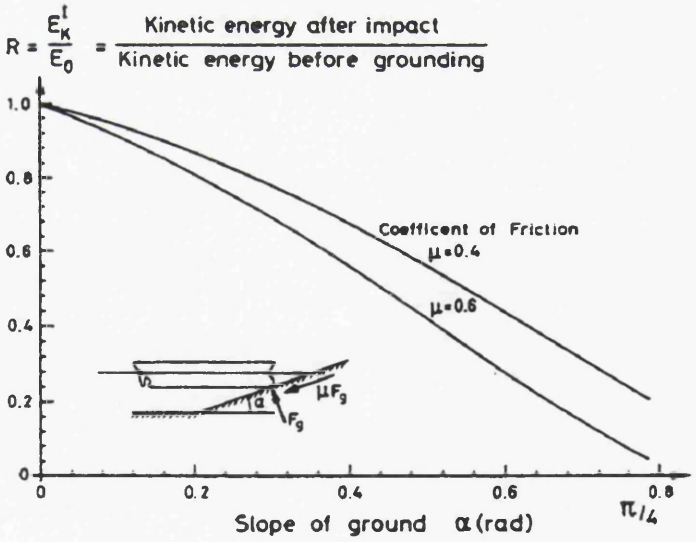


***Figure 2.20*** *Energy after initial impact as function of slope $\alpha$. Added mass ratio $\alpha_1=\alpha_2=1.82$*

# CHAPTER THREE

# THE FINITE ELEMENT ANALYSIS OF THE HEAD-ON COLLISION

---

## 3.1 INTRODUCTION

In Chapter 2 a description of the current empirical approaches for the estimation of crippling force was shown. The basis of these theories is based on the degree at which elements of the bow structure, such as *angles, T-sections and cruciforms,* exceed its maximum load carrying capacity, under axial load. Gerard's method is based on *the stress at which secondary instability occurs for thin wall compression members, in the form of a local failure in buckling which exceeds the elastic buckling load.* Amdahl's and Yang and Caldwell's method is established on *the energy dissipated during plastic deformation of basic structural members.* Their calculations predict that the plastic energy absorbed by these members is less than that of Gerard's theory. This is clearly shown in Figure 2.28, appendix 3, in Chapter 2.

All three theories have been developed on the assumption that structural members that are deformed during buckling load do not distract from the structural stability of the neighbourhood members. Considering the elements of Figure 3.1 one can see that if the system of elements $S_{1\text{-}8}$ travels with an initial speed of V at $t_0$ towards the rigid wall on the left-hand side. The member 1-8 consists of material and geometric properties P1-P8.

At time $t_1$, member 1 has been distorted while offering to the system a plastic energy equal to $E_1$. Following this sequence element number 2 is being distorted at time $t_2$, element 3 at time $t_3$ etc. Presuming the system comes to rest at time $t_8$, after element 8 has offered its buckling energy, the energy conservation of this system shows that:

$$At \quad time\ t = t_i \rightarrow E_{KINETIC} = \sum_{i=1}^{m} E^{t_i}_{PLASTIC(i)} \qquad 3.1$$

where m is the number of the $m^{th}$ member which has reached the rigid surface. Hence at time $t_1$ we have $E_{KINETIC}=E_{plastic\text{-}1}$ and at time $t_2$ we have $E_{KINETIC}=E_{plastic\text{-}1}+E_{plastic\text{-}2}$

The applied procedure of adding up the load contributions of the members 1-8 will not always be correct. In a structure with a heavily-reinforced forward part, (that means that the stiffness properties P1> P2 >P3 >....>P8), followed by a weaker rear part, the deformations may start in the rear part of this structure as well, resulting in different energy absorption on the system, than that predicted by the present approach. Figure 3.2 shows a schematic approach to this scenario.

In this case equation 3.1 is being altered as follows:

$$At \quad time\ t = t_i \rightarrow E_{KINETIC} = \sum_{i=1}^{m} E^{t_i}_{(i)} + E^{t_i}_{(i-1)} + E^{t_i}_{(i-2)} \ldots + E^{t_i}_{(i-[m-8])} \qquad 3.2$$

Such a deformation process is very complex, because the members 1-8 carry geometric restrictions at their nodes.

This problem of energy dissipation can only be examined in full-scale where the response of a detailed bow structure, under impact, is numerically explained. Such an analysis follows in this Chapter.

## 3.2 THE FINITE ELEMENT MODEL.

For the purpose of the numerical solution the drawings was provided by Burness Corlett & Partners (IOM) Ltd (1995), who assigned the assessment of the collision evaluation with a bridge rigid pier. The vessel itself is a tanker the characteristic's of which are shown on Table 2.4 in Chapter 2. The size of this tanker has been chosen on the grounds that it belongs in a "size" classification, which is critical for passages through particular bridges.

### *3.2.1 MODEL DEFINITION*

From the whole tanker, the model was developed for the bow construction, from the peak of the bow aft to the collision bulkhead, number 77 (from this point onwards the collision bulkhead will be referred as B77) as shown on Figure 3.3.

The rest of the vessel is incorporated in the analysis as lumped masses attached on B77.

The vertical distribution of the lumped masses is derived from a weight calculation on a full load condition.

| | **Weight {tonnes}** | **VCG {m}** |
|---|---|---|
| Dead-weight | 20833 | 5.941 |
| Light ship | 6667 | 5.190 |
| **Total Ship** | **27500** | **5.758** |
| **EXCLUDING THE BOW** | | |
| Bow Section | 884.3 | 6.976 |
| **Total aft Part** | **26615.7** | **5.717** |

**TABLE 3.1 WEIGHT CALCULATION EXCLUDING THE BOW**

Thus the total lumped mass on B77 must be 26615.7 tonnes with a Vertical Centre of Gravity equal to 5.717 meters.

Furthermore the distributed lumped masses are divided into three sections along the depth of the cross sectional area at B77, as shown in Figure 3.4.

The difference on the weight of each individual lump mass has been derived on the grounds of the following weight information:

| Sign | CATEGORY | Value tonnes |
|---|---|---|
| $W_{dd}$ | The weight of the dead-weight | 20833 |
| $W_{ac}$ | The weight of the accommodation | 270 |
| $W_{me}$ | The weight of the main engine and pumproom spaces | ≈599 |
| $W_{pp}$ | The weight of the piping on the main deck | ≈55.54 |
| $W_{pp}$ | The weight of the piping on duct keel | ≈44.32 |
| $W_{lb}^{T}$ | The weight of the longitudinal bulkheads over the length of the cargo section of the ship on the top | 284.4 |
| $W_{lb}^{M}$ | The weight of the longitudinal bulkheads over the length of the cargo section of the ship on the middle | 802.08 |
| $W_{lb}^{B}$ | The weight of the longitudinal bulkheads over the length of the cargo section of the ship on the bottom | 340.00 |
| $W_{md}$ | The weight of the main deck | 875.36 |
| $W_{sk}^{T}$ | The weight of the skin shell along with its girders on the top part | 450 |
| $W_{sk}^{M}$ | The weight of the skin shell along with its girders on the middle part | 882 |
| $W_{sk}^{B}$ | The weight of the skin shell along with its girders on the bottom part | 600 |
| $W_{db}$ | The weight of the double bottom plating | 580 |

**TABLE 3.2 THE INDIVIDUAL WEIGHTS FOR THE TANKER VESSEL**

Most of the weights stated on the previous Table have been derived by calculation from area and steel thickness. In cases where empirical formulas were available they have been used.

As far as the main engine weight is concerned Watson's-Gilfillan's (1976) formula has been used where:

$$W_M[tonnes] = C_{MD}\, P_D^{0.83} \qquad 3.3$$

where: $P_D$[kW] is the Break Horse Power of the engine

$C_{MD}$ is a coefficient = 0.21 low revolution diesel

0.3-0.5 medium rev. diesel

For the weight of the piping simple approximation depended on the length of pipes according to the LBP, number of cargo holds (5 for this vessel), and average weight of the pipe per meter length.

For the calculation of the weight of the accommodation, Figure 3.5 Müller-Köster's (1978) formula has been applied, where:

$$W_{DH}\,[kg] = C_{DH} \cdot A_w \cdot h \cdot k_1 \cdot k_2 \cdot k_3 \qquad 3.4$$

$C_{DH}$[kg/m$^3$] is a volumetric weight coefficient according to the Table 3

$A_w$ is the area of the deck$_I$ $=0.5(A_0+A_U)$

h is the height of the deck

$k_1$, $k_2$, $k_3$ Corrections

| Position Ao/Au | I | II | III | IV | Pilot House |
|---|---|---|---|---|---|
| 1,00 | 57 | 55 | 52 | 53 | 40 |
| 1,25 | 64 | 63 | 59 | 60 | 45 |
| 1,50 | 71 | 70 | 65 | 66 | 50 |
| 1,75 | 78 | 77 | 72 | 73 | 55 |
| 2,0 | 86 | 84 | 78 | 80 | 60 |
| 2,25 | 93 | 91 | 85 | 86 | 65 |
| 2,50 | 100 | 98 | 91 | 93 | 70 |

**TABLE 3.3 $C_{DH}$ COEFFICIENT FOR EQUATION 3.4**

After defining the weight locations on the vessel an attempt to distribute these factors along the depth of the collision bulkhead follows. It can be seen that the major contribution of the weight comes from the dead weight, which covers the 75.7% of the total weight. This mass is distributed at a vertical distance between the double bottom and the main deck. The rest of the masses are distributed as shown in the schematic diagram of appendix 1. As can be seen there is a tendency of the weight to be dragged towards the keel of the ship. If we have the individual loads summed along the depth, the diagram in Figure 3.6 is created.

In the x-axis the weight is shown in tonnes and on the y-axis the depth of B77 including the forecastle. Integration of the weight distribution below the red curve produce the individual amounts of weight for the three areas (area 1, area 2, area 3.) along the depth. Thus:

$$\begin{aligned} Total\ Weight &= \int_{0}^{2.39} w(h)dh + \int_{2.39}^{11.20} w(h)dh + \int_{11.20}^{15.37} w(h)dh \\ &= 11900tons + 9392.5tons + 5323.2tons \\ &= \approx 0.45\nabla \quad + \approx 0.35\nabla \quad + \approx 0.20\nabla \end{aligned}$$

The above distribution is converted to lumped masses on the nodes of bulkhead 77 as shown on Figure. The distribution is shown in the following Table:

| Location | Number of lumped masses | Individual mass Weight [tns] | Total area weight [tns] |
|---|---|---|---|
| Area 1 | 34 | 350.00 | 11900 |
| Area 2 | 35 | 268.35 | 9393.5 |
| Area 3 | 27 | 197.16 | 5323.2 |

**TABLE 3.4 LUMPED MASSES AS SHOWN IN FIGURE 3.4**

As can be seen in Figure 3.4, the values for the lumped masses are larger than those shown in Table 3.4. This difference is explained due to the effect of added mass in surge motion of the ship. The issue of added mass during the head-on collision will be further examined in a section 3.2.3.6.

### *3.2.2 THE BOUNDARY DEFINITION ON B77*

Using the above process in the creation of the model, the detachment of the bow structure from the rest of the vessel directly implies a geometrical constraints on B77.

Let us consider the forces applied on B77 because of the impact, as shown in Figure 3.7

Force G forms a torque around the impact point P, which is equal to G times h, where h is the vertical distance between P and the centre of Gravity of the vessel. This rotation implies a bending mechanism on B77.

The boundary on B77 should be modelled in order to withstand this bending mechanism during the impact, since the lumped masses tend to apply a rotational deformation around the impact point, as one can see in Figure 3.8. Additionally B77 should be supported in the z-direction so that the z-displacement would be conserved throughout the collision period.

This restriction on the Z-axis is too trivial to be modelled since the numerical solution provides the user with this boundary function.

The rotational status on the other hand is conserved through the introduction of a rigid structure attached on the back side of B77 reflecting the structure of the midship section shown in Figure 3.9. On the aft side of B77, the members that maintain the connectivity of the vessel's structure consist of two longitudinal bulkheads plus the shell, the main deck and the double bottom. These added members behind B77 are shown in Figure 3.10

The advantage of this technique, constraining B77, focuses on the fact that B77 is restrained only in the geometrical locations that match the true vessel construction. Consequently, the members of B77 that have not been restrained are free to any subjected reaction mode, as an outcome of the impact load.

### *3.2.3 STRUCTURAL DEFINITION*

In Appendix II Figure A3-2.1 a sketch of the side view of the bow structure is shown. It consists of 9 deck and 3 bulkhead members along with the outer shell. All the inner members are reinforced with longitudinal and vertical girders, and the shell is reinforced with transverse webs as well. Figures A3-2.2, 2.3, 2.5 in Appendix II depict these configurations. The various thicknesses of the previously described structures are shown in the following Table.

| *Members* | *Description Code* | *Thickness Values in [mm]* |
|---|---|---|
| **Collision Bulkhead** | Bulk1 | 9.5, 11.0, 12.0 |
| **Longitudinal Bulkhead** | Bulk3 | 9.0, 11.0, 12.5 |
| **Double Bottom Deck** | Deck9 | 12 |
| **Trsv. Diaphragm Bulkhead** | Bulk2 | 11.5, 13.0, 14.0 |
| **Bulbous Deck** | Deck7 | 12 |
| **Bulbous Deck** | Deck8 | 12 |
| **Lower main deck** | Deck6 | 10 |
| **Main Deck** | Deck2 | 10 |
| **Upper Forecastle Deck** | Deck1 | 9 |
| **Front Deck 1** | Deck3 | 10 |
| **Front Deck 2** | Deck4 | 10 |
| **Front Deck 3** | Deck5 | 10 |

**TABLE 3.5 THE THICKNESS OF THE DECKS SHOWN IN FIGURE A3-23.**

The description Codes shown in Table 3.5 are shown in Figure A3-2.3 in Appendix II. Dimensions of the interior configuration will not be discussed at this stage. A scale is shown in sketch 3A-2.1 in appendix II, from which the reader can get a feeling of size. In order to get an idea of the size of the model, the distance between B77 and B101 is 15.4 meters and the maximum breadth of the bow at B77 is 24.99 meters.

The geometry of the decks and bulkheads includes some details in the construction drawings, like angle brackets, liner plates, lightening holes, man access holes, etc. These are of minor significance and have not been embodied in the design since the discritisation and the complexity of the mesh did not allow for such accuracy.

There is a significant issue in the design of Deck4, as can be seen in Figure 3A-2.3. On the starboard side of this deck there is a rectangular opening, which allows access to a pump at the bottom of the deep tank, located between frame 77 and 87. This opening modifies the buckling characteristics of Deck4 and introduces a structural asymmetry, with the starboard side being weaker than the port as the results show later on. Figure 3.11 displays this deck from a plan view.

#### *3.2.3.1 EXPLICIT AND IMPLICIT SOLUTION*

Dynamic integration operators are broadly characterised as implicit or explicit. Explicit schemes, as used in ABAQUS/ Explicit, obtain values for dynamic quantities at $t+\Delta t$ based entirely on available values at time t. The central difference operator, which is the most commonly used explicit operator for stress analysis application, is only conditionally stable, the stability limit being approximately equal to the time for an elastic wave to cross the smallest element dimension in the model. The validity of the results of the explicit solution should be examined since this method is not based on the solution of equilibrium equations. Implicit schemes remove this upper bound on time step size by solving for dynamic quantities at time $t+\Delta t$ based not only on values at t, but also on these same quantities at $t+\Delta t$. But because they are implicit, non-linear equilibrium equations must be solved. In structural problems, implicit integration schemes usually give acceptable solutions with time steps typically one or two orders of magnitude larger than the stability limit of simple explicit schemes, but the response prediction will deteriorate as the time step size increases relative to the period of typical modes of response.

For the dynamic finite element analysis of this model explicit solution has been used.

### *3.2.3.2 THE SHELL ELEMENT*

The deck and bulkhead plating is modelled using shell elements. These elements were chosen in preference to plate elements because they consider a linear distribution of the stresses through their thicknesses. They take both bending and membrane stresses, contrary to plate elements that can generate only uniformly distributed stresses through their thickness.

In more detail, the shell elements utilised herewith this study, are "shear flexible" shells with 9 integration points uniformly distributed along the thickness, in which transverse shear deformation is allowed. These elements can be used for both thick and thin shell analysis. When they are thin, the transverse shear stiffness acts as a penalty function to impose the Kirchoff constraints approximately. The Kirchoff constraints require a line that is originally normal to the shell's reference surface, to remain normal to that surface throughout the deformation, as shown on Figure A3-2.4 These constraints are one of the fundamental postulates of classical "thin" shell theory.

The shell theory incorporated in the numerical analysis allows for finite strains and rotations of the shell. The strain measure used is chosen to give a close approximation to logarithmic strain. Thus, the theory is intended for direct application to cases involving inelastic deformation where the stress-strain behaviour is given in terms of true stress and logarithmic strain, such as metal plasticity denoted by the Pradle model in this analysis. The theory is approximate, but the approximations are not rigorously justified in ABAQUS, they are introduced for simplicity, and seem reasonable. These approximations are incorporated herein for completeness. These are:

1. A "thinness" assumption is made. This means that, at all times, only terms up to first order with respect to the thickness direction are included.

2. The thinning of the shell caused by stretching parallel to it's middle surface is assumed to be uniform through the thickness, and defined by an incompressibility condition on the reference surface of the shell. Obviously

this is a relatively coarse approximation, especially in the case where a shell is subjected to pure bending. It is adopted because it is simple, and models the effect of thinning associated with membrane straining: this is considered to be of primary importance in the type of applications envisioned, such as the failure of pipes and vessels subjected to over-pressurisation.

3. The thinning of the shell is assumed to occur smoothly, that is to say, gradients of the thinning with respect to position on the middle surface are assumed to be negligible. This means that localisation effects, such as necking of the shell, are only modelled in a very coarse way. Again, the reason for adopting this approximation is simplicity details of localisation effects are not important to the type of application for which the elements are designed.

4. All stresses except those parallel to the reference surface, see Figure A3-2.4, are neglected, and, for the non-negligible stresses, plane stress theory is assumed. As with no. 3 assumption, this precludes detailed localisation studies, but introduces considerable simplification into the formulation.

5. Plane sections remain plane. This has been shown to be consistent with the thickness assumption, no. 1 above, for most material models. Here it is simply assumed without further justification.

6. Transverse shears are assumed to be small and the material response to such deformation is assumed to be linear elastic. Transverse shear is introduced because the elements used are of the "reduced integration, penalty" type. In these elements position relative to the reference surface, and rotation of lines initially orthogonal to the reference surface, are interpolated independently: the transverse shear stiffness is then viewed as a penalty term imposing the necessary constraint at selected (reduced integration) points. The transverse shear stiffness is the actual elastic value for relatively thick shells. For thinner cases the penalty must be reduced for numerical reasons; -this is done in ABAQUS in the manner described in Hughes (1983) et al.

In large deflections, the geometric non-linearity is accounted by using three basic formulations;

- Total Lagrangian
- Updated Lagrangian
- Eulerian

All three formulations are valid for arbitrary large deformations. If rotational degrees of freedom are present, then rotations must be small for Total Lagrangian, but may be large for Updated Lagrangian or Eulerian (provided that they are small within each load increment). All three formulations are valid for small strains. For SHELL elements the Updated Lagrangian formulation is valid for moderately large strains. The Eulerian formulation is generally valid for large (finite) strains. In general, the Total Lagrangian is the most stable formulation, and can usually cope with substantial load increments (except in the presence of plasticity). The Updated Lagrangian, and particularly Eulerian formulations generally require smaller load increments in order to avoid divergent solution.

Standard geometrically non-linear formulations account for the change in position of the loading, but not the change in direction relative to the deformed configuration. Loading is always conservative for the Total Langrangian geometrically non-linear formulations (that is, the load is always applied in the same direction as was initially prescribed). Using an Updated Langrangian formulation, the geometry is updated at the end of each increment. The applied loads maintain the same relative orientation as to the original surface. Non-conservative loading is therefore increment size dependent. True non-conservative loading may only be achieved by using the Eulerian formulation.

#### *3.2.3.3 MODELLING OF THE STIFFENERS*

As far as the configuration of the beam elements is concerned, these are classified in seven different categories according to the drawings of the tanker's bow, as in the sketch of frame 80 in Figure 3.12. The configuration of the beam element is shown in Figure A3-2.6, 2.7

The following Table shows this division.

| Type | Dimensions |
|---|---|
| B1 | 300x150x13,5 |
| B2 | 100x75x8 |
| B3 | 100x75x8 |
| B4 | 900x10+150x12 |
| B5 | 100x75x8 |
| B6 | 250x150x13.5 |
| B7 | 150x90x10 |

**TABLE 3.6 BEAM ELEMENT DIMENSIONS**

For the modelling of the stiffeners, 3D beam elements have been used. The dimensions have been taken from the data of the ship adding also the effect of the effective plate thickness $b_e$. The $b_e$ has been calculated from the following formula, taken from Hughes (1983):

$$\frac{b_e}{b} = 1.9\frac{t}{b}\sqrt{\frac{E}{\sigma_y}} \qquad 3.5$$

where:

| | | |
|---|---|---|
| | $b_e$ | is the effective plate width |
| | b | is the distance between stiffeners |
| | t | is the plate thickness |
| | E | is the Young's modules {=211E9 N/mm$^2$} |
| | $\sigma_y$ | Yield stress {=245E6 N/mm$^2$} |

The diagram in Figure 13 shows the effective area, where $b_e$ is valid for this model.

Initially, an attempt of adding the inertia of the individual effective plate width into the actual stiffener's one, took place, without affecting the dimensions and hence the weight of the bow structure. Unfortunately the formulation of the beam element as it is described by ABAQUS, does not allow such action.

However, incorporating the effective plate width in the geometry of the stiffeners, leads to an increase of the total weight of the ship. Thus this phenomenon has to be

controlled through the *density* of the material. For this intention different properties data have been used for the steel material, which compose the stiffeners in order to have the total mass, including the added mass, equal to the actual mass.

#### *3.2.3.4 THE BEAM ELEMENT*

For the stiffeners shown in Table 3.6, beam elements have been used in the modelling. Beam elements in general are elements in which assumptions are made so that the problem is reduced to one dimension, Figure A3-2.6, and in mathematical terms one would say that the primary solution variables are functions of position along the beam axis only.

The simplest approach to beam theory is the classical Euler-Bernoulli assumption i.e. that plane cross sections initially normal to the beam's axis remain plane, normal to the beam axis, and undistorted. The beam elements in ABAQUS, Figure A3-2.7, which use cubic interpolation, all use this assumption, implemented in the context of arbitrarily large rotations but small strains. For the Euler – Bernoulli elements it assumed that (Hibbit, Karlsoon & Sorensen (1995)):

1. *The internal virtual work rate is associated with axial strain and torsional shear only.*
2. *The cross section is taken not to deform in its plane, or warp out of it's plane, and that*
3. *This cross-sectional plane remains normal to the beam axis.*

These are the classical assumptions for the Euler-Bernoulli beam theory, which provides satisfactory results for slender beams.

If (S, g, h) are material co-ordinates such that S locates points on the beam axis and (g, h) measures distance in the cross section. Also, let $\mathbf{n}_1$, $\mathbf{n}_2$ be unit vectors normal to the beam axis in the current configuration: $\mathbf{n}_1=\mathbf{n}_1(S)$, $\mathbf{n}_2=\mathbf{n}_2(S)$. Then the position of a point of the beam in the current configuration is

$$x^f = x + gn_1 + hn_2 \qquad 3.6$$

where, x=x(S) is the point on the beam axis of the cross-section containing $x^f$. Then:

$$\frac{dx^f}{dS} = \frac{dx}{dS} + g\frac{dn_1}{dS} + h\frac{dn_2}{dS} \qquad 3.7$$

and the length on the fibre at (S, g, h) is measured in the current configuration as

$$(dl^f)^2 = \frac{dx^f}{dS}\frac{dx^f}{dS}(dS)^2 = \left(\frac{dx}{dS} + g\frac{dn_1}{dS} + h\frac{dn_2}{dS}\right)\left(\frac{dx}{dS} + g\frac{dn_1}{dS} + h\frac{dn_2}{dS}\right)(dS)^2 \qquad 3.8$$

Since the beam element is slender, terms of second-order in g and h are neglected, the distance measuring material co-ordinates in the cross-section. Thus:

$$(dl^f)^2 = \left(\frac{dx}{dS}\frac{dx}{dS} + 2g\frac{dx}{dS}\frac{dn_1}{dS} + 2h\frac{dx}{dS}\frac{dn_2}{dS}\right)(dS)^2 \qquad 3.9$$

#### *3.2.3.5 ASSESSMENT OF THE STIFFENER-PLATE BEHAVIOUR*

In this Section an evaluation of the behaviour of the mesh used for the modelling of the structure takes place. A part of the shell between one frame spacing with two beam element along the sides is subjected under buckling load, as shown in Figure A3-2.8-a. The energy absorbed from this mesh is compared to the energy absorbed from a fine mesh of the same size and same material properties as shown in Figure A3-2.8-b.

Figure A3-2.9 displays the total elasto-plastic energy dissipated on both models. Comparison of these two curves indicates that good representation of the structural response of the bow is achieved with the use of the model (a).

Approximations in the size of the elements comprising the model of the structure must take place due to the limited number of elements used in the analysis. Example (a), in Figure A3-2.8, provides a good model since the tolerance shown in graph A3-2.9 is almost 10%.

### *3.2.3.6 THE RIGID SURFACE-KINEMATICS OF THE INTERACTIVE SURFACES*

The numerical integration utilised for the modelling of the collision episode provides two formulations for the modelling of the interaction between a deformable body and an arbitrary shaped rigid body that may move during the time history.

The first formulation allows relatively small sliding of the interacting surfaces relative to each other. Arbitrary rotation is permitted on the surfaces.

The second formulation is a finite-sliding formulation where separation and sliding of finite amplitude, and arbitrary rotation of the surfaces, may arise. This formulation is examined in this Section.

Consider the ship colliding with a rigid surface as shown in Figure 3.14.

Let A be the point on the deforming mesh, with current co-ordinates $x_A$, Hibbit, Karlsoon & Sorensen (1995). Let C be the rigid body reference node, (the node that defines the position of the rigid body) with current co-ordinates $x_c$. Let A' be the closest point on the surface of the bulbous bow to point A at which the normal to the surface of the rigid body, **n**, passes through A. **r** is the vector from C to A'. Let h be the distance from A' to A along **–n**: the "overclosure" of the surfaces. From the above definitions we have

$$nh = -x_A + x_C + r \qquad 3.10$$

If h is smaller than –c, (h<-c), there is no contact between the surfaces at A, and no further surface interaction calculations need to take place at this point. C is the "clearance" below which contact occurs.

If h≥-c the surfaces are in contact. To enforce the contact constraint the first variation of h, δh, and the second variation dδh, are introduced.

Let $S^{\alpha}$, $\alpha$=1,2 be locally orthogonal, distance measuring surface co-ordinates on the surface at A'. The $S^{\alpha}$ measure distance along the tangents $\mathbf{t}_{\alpha}$ to the surface at A'.

As the point A and the rigid body move, the projected point A' will move along. The movement consists of two parts: movement due to motion of the rigid body and motion relative to the body. This forms the *contact equation*:

$$\delta x_{A'} = \delta x_C + \delta r|_{\gamma_\alpha} + \delta r|_{\phi_C} = \delta x_C + \delta\phi_C \times r + t_\alpha \delta\gamma_\alpha \qquad 3.11$$

where, $\delta\gamma_\alpha$ is the "slip" of point A'.

The normal **n** will also change due to rotation of the rigid surface and due to slip along the surface

$$\delta n = \delta n|_{\gamma_\alpha} + \delta n|_{\phi_C} = \delta\phi_C \times n + \frac{\partial n}{\partial S_\alpha}\delta\gamma_\alpha \qquad 3.12$$

The linearised form of the contact equation 3.11 thus becomes

$$n\delta h + h\left(\delta\phi_C \times n + \frac{\partial n}{\partial S_\alpha}\delta\gamma_\alpha\right) = \delta x_{A'} - \delta x_C + \delta\phi_C \times r + t_\alpha \delta\gamma_\alpha \qquad 3.13$$

For initial overclosure equals to 0, the contact is defined as hard with h=0. The linearised form of the contact equation 3.13 then becomes:

$$n\delta h = -\delta x_A + \delta x_C + \delta\phi_C \times r + t_\alpha \delta\gamma_\alpha \qquad 3.14$$

This equation can be split into normal and tangential components, which yields the contact equation:

$$n\delta h = -n(\delta x_A - \delta x_C) + (r \times n)\cdot\delta\phi_C \qquad 3.15$$

and the slip equations:

$$\delta\gamma_\alpha = t_\alpha(\delta x_A - \delta x_C) - (r \times t_\alpha)\cdot\delta\phi_C \qquad 3,16$$

In order to obtain the second variation of h, it will again be assumed that the initial overclosure is equal to zero (h=0) and in addition it will be assumed that dh=δh=0, which is accurate for relatively "hard" contact. It then directly follows that

$$nd\delta h = d\delta r \qquad 3.17$$

From the linearised kinematic equation 3.14 follows:

$$nd\delta h = d(\delta\phi_C \times r)|_{\gamma_\beta} + \delta\phi_C \times dr|_{\phi_C} + dt|_{\gamma_\beta}\,\delta\gamma_\alpha + dt|_{\phi_C}\,\delta\gamma_\alpha + t_\alpha d\delta\gamma_\alpha \qquad 3.18$$

Where the use of $d\delta x_A = d\delta x_C = d\delta\phi_C = 0$. The first term corresponds to a second-order variation on the vector r for rigid body rotations around point C and is given by

$$d(\delta\phi_C \times dr)|_{\gamma_\beta} = \delta\phi_C \cdot d\phi_C r - \frac{1}{2}\delta\phi_C d\phi_C \cdot r - \frac{1}{2} r \cdot \delta\phi_C d\phi_C \qquad 3.19$$

The second term in the equation 3.19 for the second variation is obtained with the previously used expression for the "slip" along the surface:

$$\delta\phi_C \times dr|_{\phi_C} = \delta\phi_C \times t_\alpha d\gamma_\alpha \qquad 3.20$$

The third term follows from the expression for the rigid body rotation:

$$dt|_{\gamma_\beta}\,\delta\gamma_\alpha = d\phi_C \times t_\alpha d\gamma_\alpha \qquad 3.21$$

Finally, the fourth term is obtained by differentiation along the surface co-ordinates:

$$dt|_{\phi_C}\,\delta\gamma_\alpha = \frac{\partial t_\alpha}{\partial S_\beta} d\gamma_\beta \delta\gamma_\alpha = \delta\gamma_\alpha \kappa_{\alpha\beta} d\gamma_\beta \qquad 3.22$$

where,

$$\kappa_{\alpha\beta} = \frac{\partial t_\alpha}{\partial S_\beta} = \frac{\partial t_\beta}{\partial S_\alpha} = \frac{\partial^2 r}{\partial S_\alpha \partial S_\beta} \qquad 3.23$$

is the surface curvature matrix.

For dynamic applications we need the velocity and acceleration terms $\dot{h}$ and $\ddot{h}$, in order to calculate impact forces and impulses correctly. These terms are

$$\dot{h} = -n \cdot \left( \dot{x}_A - \dot{x}_C - \dot{\phi}_C \times r \right) \qquad 3.24$$

$$\ddot{h} = -n \cdot \left( \ddot{x}_A - \ddot{x}_C - \ddot{\phi}_C \times r \right) + n \cdot \dot{\phi}_C r \cdot \dot{\phi}_C - n \cdot r \dot{\phi}_C \cdot \dot{\phi}_C$$
$$- \left( \dot{x}_A - \dot{x}_C - \dot{\phi}_C \times r \right) \cdot \left( \dot{\phi}_C \times n + \frac{\partial n}{\partial S_\alpha} t_\alpha \cdot \left( \dot{x}_A - \dot{x}_C - \dot{\phi}_C \times r \right) \right) \qquad 3.25$$

The size of the rigid surface is taken such that it fits the scenario of the vessel colliding with a bridge leg. The scenarios have been taken from the work done in the bridge collision assessment Das et al. (1995). Figures 3.15 and 3.16 depict such scenarios.

The first Figure displays the vessel in ballast condition and the second in full load condition. The worst credible condition is the full load condition since the mass of the ship is greatest. This position corresponds to a maximum draught of 9.65m. At mean high water springs the bulbous bow will collide first with the rigid pier.

### *3.2.3.7 MATERIAL PROPERTIES*

The material used in the numerical analysis is steel with the following characteristics:

| | |
|---|---|
| **Young's Modulus E** | 207E9 N/m$^2$ |
| **Yield stress $\sigma_{yield}$** | 245E6 N/m$^2$ |
| **Poisson's Ratio $\nu$** | 0.3 |
| **Density $\rho$** | 7850 kg/m$^3$ |

**TABLE 3.7 MATERIAL PROPERTIES**

The material is taken as elastic visco-perfectly plastic with zero hardening similar to the one shown in Figure A2-1.1 in appendix 1 of the Chapter 2. The yield criterion used is the Von-Mises criterion and the plasticity flow is modelled through the Prandle model for visco-perfectly plastic behaviour with zero hardening.

This material model is very commonly used for metal plasticity calculations, either as a rate dependent or as a rate independent model, and has a particularly simple form.

In this dynamic analysis a rate dependent model is used. A rate depended yield strength is introduced in the material model. This is implemented for relatively high strain rate applications. One way of having this material non-linearity introduced (Manjoine (1944)) is via the following over-stress power law:

$$\dot{\bar{\varepsilon}}^{plastic} = D\left(\frac{\bar{\sigma}}{\sigma_y} - 1\right)^P \quad for \quad \bar{\sigma} \geq \sigma_y \tag{3.26}$$

where:

- $\dot{\bar{\varepsilon}}^{plastic}$ is the equivalent plastic strain rate
- $\bar{\sigma}$ is the yield stress at nonzero plastic strain rate
- $\sigma_y$ is the static yield stress
- D, p are material parameters which may be functions of temperature and, possibly, of other predefined state variables.

### *3.2.3.8 ADDED MASS*

Due to the free surface, the ship will set up waves when it accelerates. These waves will cause vibrations in the hydrodynamic pressure forces that are functions of the earlier motion of the ship. These memory effects are taken into account by the convolution integrals as shown in equation 2.4.

These effects deal with the surrounded amount of water around the vessel, which continues to move for duration $t = t_{collision}$, with a resultant added pressure and friction, driving the ship towards the rigid surface.

Consider the colliding scenario shown in Figure 3.17. When the ship collides with the rigid surface, at t=0 , an allowance for the force being excited by the surge motion of the ship is achieved by adding an amount of constant mass on the mass of the striking ship. Valsgard (1982) has assumed that this mass equals to 10% of the vessels displacement. In other references, Petersen has chosen an added mass equal to 5%. The difference from these two values for the tanker vessel under consideration in this study is shown in Figure 3.18.

Minorski (1983), presents experimental work done for a model of "Esso Malaysia" where good correlation was achieved (within 10%) using an added mass 5%. W. J. Liang (1991) also shows that the hydrodynamic forces relating to the surge motion of the ship cannot be found by strip method. He assumes the force in surge motion is

$$X_H(t)=-m_{11}n_1, \qquad 3.27$$

where $m_{11}$ is the added mass. This is taken later as

$$M_{11}=0.05\cdot M, \text{ where M is the vessel's mass} \qquad 3.28$$

Pedersen et al (1993) uses an added mass of 5% for the calculation of crushing load, versus indentation, using Amdahl's (1983) empirical formula. In his analysis, he defines the effective mass for longitudinal translation equal to $1.05\cdot\nabla$ for all six different vessels with DWT from 500 to 150,000 tonnes.

### *3.2.3.9 ABAQUS INPUT AND RESULTS FILES*

The ABAQUS input file is included in appendix IV. It includes all the individual issues described in Section 3.2.3 of this Chapter. The diagram in Figure 3.19 shows the way the input file has been constructed.

Unfortunately due to the size of the accompanying files, it was not possible to include them in the input file. For this reason a floppy disk is enclosed at the end of this thesis with all the data files mentioned in the input file.

## 3.3 RESULTS AND DISCUSSION

The numerical solution is accomplished with ABAQUS. It is a finite element analysis program with a very good capability in transient dynamics. The main parameter in this analysis is the initial speed of the vessel. Four speeds have been selected. The maximum speed is not considered because it is assumed that *the vessel is sailing in restricted straits, thus it's not sailing at full speed.* These are shown on the subsequent Table, along with the Kinetic energy:

| Concept | Speed [kn] | Speed [m/s] | Initial Kinetic Energy MNm |
|---|---|---|---|
| 1 | 5.83 | 3.00 | 129.937 |
| 2 | 7.78 | 4.00 | 231.000 |
| 3 | 9.72 | 5.00 | 360.937 |
| 4 | 11.20 | 5.76 | 480.000 |

**TABLE 3.8 THE FOUR CONCEPTS USED IN THE F.E.A**

The model is taken with initial distance to the obstruction equal to zero. Thus the speeds shown above are at time $t^-$, ($t^-$ means the time exactly prior to impact with the rigid surface). The energy of the ship was computed using equation 2.54 with $m_a$= $0.05 \cdot \nabla$ (where $\nabla$ is the displacement of the loaded tanker equal to 27500 tons).

Figures A3-3.1 to A3-3.4 in appendix 3 show "thumbnails" of the deformed bow in time frames, when output data have been extracted from the results file. One can see the penetration on the bulbous bow at the beginning, and the main bow arrangement thereafter, until the structure comes to rest. The first thumbnail is always taken at 0.2 as this is the first time increment results have been extracted from the results file. For time t=0 there are no results as at that initial stage the ship has it's initial values, as these have been incorporated in the input file. The last thumbnails shown in each one of A3-3.1 to A3-3.4 are not necessarily the resting positions, because the outputs have been extracted every 0.2 seconds. The resting position is somewhere between the last and second from the end frame.

An example picture is shown in Figure 3.20. It comes from the output of the model with initial speed of 5.7 m/sec, at time 1.2 sec. The red mesh indicates the undeformed bow, contrary to the green mesh, which denotes the deformed shape. The rigid wall is not shown on these thumbnails but its location can be easily seen. On the above Figure the vertical white line shows the rigid wall.

The indentation of the bow, towards the wall, is measured from the undeformed position of B77 to the deformed location of the collision bulkhead B77. A scale of the shift during the collision can be drawn from these thumbnails, as follows. The model is vertically divided into frames. These frames have length 700 mm from B77 until B87 and 600 mm from B87 onwards (Figure A3-2.1). For example, for the shot in Figure 20, the indentation is 8 frames plus. This is translated to about $5.6^{+}$ meters.

Figures 3.21 presents a typical 3D view of the collided bow. In Figure 3.21b can be seen the deformed interior construction of the bow. It is worth while to point out to the reader that although the deck constructions forward of B87 have been totally destroyed, contrary to those rearward of B87. The condition of DECK 4 (refer to Figure A3-2-3, where the arrangement of the internal decks is shown) is affected by the void hole in the attachment with B77. This will be examined later on.

### *3.3.1 SPEED VS. TIME*

Figures A3-3.5 and A3-3.6 show the speed and acceleration versus time for the four concepts. The following Table shows the final resting times.

| Concept Initial Speed m/sec | Time to Rest (sec) ABAQUS | Time to Rest (sec) GERARD | Difference % |
|---|---|---|---|
| 3.00 | 1.920 | 1.88 | -6.25% |
| 4.00 | 2.208 | 2.22 | +0.54% |
| 5.00 | 2.300 | 2.27 | -1.30% |
| 5.76 | 2.748 | 2.52 | -8.30% |

**TABLE 3.9 RESTING TIMES FOR BOTH ABAQUS AND GERARD'S METHOD**

Column 2 has the results from ABAQUS, column 3 shows the results from Gerard's approach, derived from equation 2.46 and shown in Figure 2.19b. The tolerance between the two analysis is displayed in column three. The application of Gerard's formula have reported an accuracy within 10%. This is verified herein as well.

It is interesting to compare not only the time needed to the final rest but to track the speed as the vessel retards during the period $t=0 \rightarrow t_{resting}$. For this purpose Figure A3-3-5 is combined with 2.19b and Figure 3.22 is produced.

It can be seen that although the final time of rest is approximately the same for both ABAQUS and equation 2.46, the rate of speed reduction varies. Possible reasons for this discrepancy in the path of velocity are given below:

- The effect of the global bending of the forward part of the bow structure, Figures A3-3.1 to A3-3.4, is not taken into account in Gerard's approach. This action allows more load/energy to be absorbed by the structure and therefore for a given time t, the speed predicted from ABAQUS is smaller than the one from the empirical formula

- The deck collapsing during the impact is taken into account in such a way as the one shown in Figure 3.1. The numerical analysis produces buckling modes similar to the one shown in Figure 3.2. There is a difference in the way the energy is being dissipated between the scenarios. This aspect will be examined later on.

- The effect of the transverse scantlings, have not been incorporated in Gerard's formula since only the longitudinal components are embodied in the calculations. In the numerical calculation all the scantlings are present and therefore the structure is expected to experience a different response.

As it can be seen from Figure A3-3.5, the speed-time relation can be interpolated with a 3$^{rd}$ degree polynomial. If regression analysis interpolates the data from Figure A3-3.5 we derive the pattern shown in Figure 3.23.

The relations derived from the above curves are

$$\begin{aligned} V_o = 5.76m/\sec &\rightarrow y = 0.2417t^3 - 1.1241t^2 - 0.8563t + 5.8228 \\ V_o = 5.00m/\sec &\rightarrow y = 0.1931t^3 - 1.1131t^2 - 0.5824t + 4.8757 \\ V_o = 4.00m/\sec &\rightarrow y = 0.4637t^3 - 1.9093t^2 - 0.2227t + 3.8553 \\ V_o = 3.00m/\sec &\rightarrow y = 0.2431t^3 - 1.3174t^2 - 0.1238t + 2.8933 \end{aligned} \qquad 3.29$$

If we have the coefficients of the above set of equations non-dimensionilised, then these are transformed to the following set :

$$\begin{aligned} V_o = 5.76m/\sec &\rightarrow V_t = 0.0420V_o t^3 - 0.1950V_o t^2 - 0.1486V_o t + 1.011V_o \\ V_o = 5.00m/\sec &\rightarrow V_t = 0.0390V_o t^3 - 0.2220V_o t^2 - 0.1165V_o t + 0.9751V_o \\ V_o = 4.00m/\sec &\rightarrow V_t = 0.1159V_o t^3 - 0.4770V_o t^2 - 0.0557V_o t + 0.9638V_o \\ V_o = 3.00m/\sec &\rightarrow V_t = 0.0810V_o t^3 - 0.4391V_o t^2 - 0.0413V_o t + 0.9644V_o \end{aligned} \qquad 3.30$$

The above equations are of the following form

$$V_t = (a_1 V_0)t^3 - (a_2 V_0)t^2 - (a_3 V_0)t + a_4 V_0 \qquad 3.31$$

Where $V_t$ is the speed at time t

$a_1, a_2, a_3, a_4$ are coefficients

Plotting $a_1$ and $a_2$ in respect of $V_o$, and interpolating the data using 2nd order polynomials, as shown in Figure 3.24 we acquire a relation between $a_1$, $a_2$, $a_3$, $a_4$, and $V_o$

The following relations are found.

$$\begin{aligned} a_1 &= 0.0369V_0^3 - 0.4987V_0^2 + 2.1604V_0 - 2.9083 \\ a_2 &= 0.0982V_0^3 - 1.3254V_0^2 + 5.6805V_0 - 7.3266 \\ a_3 &= -0.0122V_0^3 + 0.1699V_0^2 - 0.7227V_0 + 1.0101 \\ a_4 &= 0.0052V_0^3 - 0.057V_0^2 + 0.2041V_0 + 0.7231 \end{aligned} \qquad 3.32$$

The set of equations 3.31 and 3.32 produce a 4th degree system between the initial speed of the vessel $V_0$ and the speed at time $V_t$. The accuracy of this calculation is dependent on the number of individual concepts modelled in ABAQUS. Under the

current configuration there is definitely a small error, derived from the regression, shown in equations 3.30 and 3.32.

Limitation of the above analysis arise from the fact that the Deadweight of the ship is not included in the analysis, contrary to the empirical analysis presented in Pedersen (1993), in order to produce curves similar to A2-2.13. Similar work with this is proposed for future work.

### *3.3.2 THE INDENTATION*

The relation for the indentation, derived from ABAQUS, is shown in Figure A3-3.7. This analysis shows that the indentation as numerically calculated is far different from the one predicted from the empirical approach. Figure 3.25 shows the comparison in the results.

This big difference in the indentation is probably caused by the simplification in the Gerard model. As discussed by Pedersen (1993) the real collapse modes involve mechanisms which cripple the members behind the indent position, where the Gerard mechanism assumes that they behave independently. This is very clearly shown in Figure 3.26 where Deck 8 is shown during its collapse.

The empirical methods adopt a model as the one shown in Figure 3.1. This means that the sequence of the collapse of the joint members in any longitudinal deck, which comes in contact with the rigid *surface is an ascending process in which the crippling on the member i does not affect the stability of member i+1.*

On the contrary the finite element analysis showed that the collapse mechanism of such a deck segment affects the elements which are connected together and have not come in contact with the rigid surface. In Figure 3.26 one can see that at time t=0.2 there is a buckling mechanism on the elements following those already crippled on the wall. Thereafter, this non-linear folding develops in buckling in both longitudinal and transverse direction, times t=0.4-0.6. From 0.6 seconds onwards, buckling is predominant and finally this mechanism leads the structure to collapse.

This difference in the collapse process does not imply that Gerards approach is wrong, only an over simplification. In fact this probably accounts for the major portion of the difference between the results of the two analyses. In the context of overall engineering design of bridge structures the difference is small. The same occurs with the conservation of energy, as will be discussed later on.

The behaviour of stiffened plates under predominantly compressive loads is relatively complicated due to the number of possible combinations of plate and stiffener geometry, boundary conditions and loading.

It is possible to carry out accurate prediction of collapse load for any type of plate configuration using a finite element formulation, Soreide (1978). More simplified formulations have also been developed, based on a beam-column concept mainly due to Ostapenko (1974). The main feature of the method is the consideration of one isolated stiffener with associated width of plating, as a representative of the whole panel behaviour.

Some of the approaches solve the equilibrium equations of the beam-column in an iterative way by accounting for the decreased contribution of the plate flange in the post-buckling region, Little, (1976), & Moolani et al. (1977). This is normally accounted for by using load-shortening curves produced by finite difference or finite element methods, Frieze et al. (1977), Ueda et al. (1979), Little (1980), Crisfield, (1975), Harding (1977), Soreide (1977).

All these theoretical studies together with various experimental programs, Smith (1975), Horne et al.(1976), Horne et al (1977), Faulkner (1977), have provided the present knowledge of the main features of stiffened plate behaviour.

As systematised by Smith (1979), one may consider three main types of collapse, plate collapse, interframe flexural buckling and overall grillage collapse. A stiffened panel is dominated by the plate failure when it is short, with a length approximately equal to the width of the plate between stiffeners.

In ships, the panels are generally much longer than the stiffener spacing and therefore the possibility of having plate failure exists only in the case of a panel with high strength stiffeners and relatively low strength and nearly perfect plates. Under these conditions the plates show a very steep unloading characteristic so that the stiffeners are not able to accommodate the drop in load after plate failure.

An overall column type of plate failure can occur in long uniaxially stiffened panels. In orthogonaly stiffened panels the corresponding mode is the grillage collapse, which involves both longitudinal and transverse stiffeners. This collapse mode can be influenced by local buckling of the plate on the stiffener and is generally avoided in ships. However, it may be relevant for highly stiffened panels that can be found in superstructure decks.

Some design studies led to the conclusion that the optimum design of a compressed stiffened plate would be obtained whenever the strength of the overall buckling mode would be equal to the strength of the local buckling mode. However, it has been shown that such panels show an interaction between local and global modes that makes them very much "imperfection sensitive" and with a violent collapse, Tvergaard et al. (1975). These characteristics are undesirable from a safety point of view and therefore the stiffened plates are generally designed so as to exhibit an interframe type of collapse. The interframe collapse is specially stimulated by the presence of heavy transverse girders, which is often the case in ships. This is a typical type of interactive collapse, Reis (1977) in which the overall collapse of the beam is usually triggered by local buckling of the plate or stiffener.

This mode of failure shown in Figure 3.26 absorbs the energy prescribed by equation 2.63, or the integration of 2.46. The issue is the progress of the energy being dissipated in the structure.

This will be discussed in energy conservation, later on. The difference on indentation from both methods is shown on the following Tables.

| Concept | Time in seconds | | | | |
|---|---|---|---|---|---|
| | **0.5** | **1.0** | **1.5** | **2.0** | **2.5** |
| **Vo=3** | 0.75 | 1.44 | 1.63 | --- | --- |
| **Vo=4** | 1.00 | 1.90 | 2.65 | 3.21 | --- |
| **Vo=5** | 1.25 | 2.36 | 3.32 | 4.05 | --- |
| **Vo=5.76** | 1.43 | 2.83 | 3.88 | 4.72 | 5.20 |

**TABLE 3.10 INDENTATION DERIVED FROM GERARDS METHOD**

| Concept | Time in seconds | | | | |
|---|---|---|---|---|---|
| | **0.5** | **1.0** | **1.5** | **2.0** | **2.5** |
| **Vo=3** | 1.407 | 2.540 | 3.270 | --- | --- |
| **Vo=4** | 1.892 | 3.458 | 4.487 | 4.945 | --- |
| **Vo=5** | 2.327 | 4.278 | 5.658 | 6.418 | --- |
| **Vo=5.76** | 2.747 | 5.083 | 6.803 | 7.889 | 8.38 |

**TABLE 3.11 INDENTATION DERIVED FROM ABAQUS**

| Concept | Time in seconds | | | | |
|---|---|---|---|---|---|
| | **0.5** | **1** | **1.5** | **2.0** | **2.5** |
| **Vo=3** | 53% | 57% | 50% | --- | --- |
| **Vo=4** | 53% | 55% | 59% | 65% | --- |
| **Vo=5** | 54% | 55% | 59% | 63% | --- |
| **Vo=5.76** | 52% | 56% | 57% | 60% | 62% |

**TABLE 3.12 DIFFERENCE BETWEEN GERARD'S AND ABAQUS**

Table 10 displays the penetration derived from the empirical calculation. Table 3.11 shows the indentation derided from ABAQUS, and Table 3.12 shows the difference from these two methods.

It can be seen that if Gerards, results are almost doubled then we get a close approximation with ABAQUS. Moreover this issue ratio $I_r$ is introduced which shows the magnitude of the indentation as calculated from Figure 2.19c, over the indentation predicted by ABAQUS. This is defined as:

$$I_r = \frac{E_I}{N_I} \tag{3.33}$$

If we plot the ratios Ir, shown in Table 12, we get graph 3.27.

It is shown that the ratio $I_r$ varies significantly in the case, where the initial speed is 3.00 m/s, in comparison to the other concepts. Regression analysis is being applied on the above $I_r$ curves in order to obtain an analytical variation. Second degree polynomials produce sufficient accuracy. These polynomials follow here:

$$\begin{aligned} Ir_{5.76} &= -0.006t^2 + 0.065t + 0.492 \\ Ir_{5.00} &= -0.030t^2 + 0.013t + 0.538 \\ Ir_{4.00} &= -0.040t^2 + 0.020t + 0.530 \\ Ir_{3.00} &= -0.220t^2 + 0.410t + 0.380 \end{aligned} \tag{3.34}$$

Merging equations 3.33 and 3.34 produce a correction factor for the calculation of indentation using Gerards, approach.

With reference to Figure 3.25 one may derive a relation of the ratios presented, with regard to the actual indentation of the vessel. Similarly, with reference to Figure 3.82 the relation of the ratios with regard to the total energy dissipated is shown.

## 3.4 ENERGY CONSERVATION

Conservation of energy, defined by by the first law of thermodynamics, and respectively applied to this case states that the time rate of change of kinetic energy and internal energy, for a fixed body of material, is equal to the sum of the rate of work done by the surface and body forces, Hibbit, Karlsoon & Sorensen (1995). This is depicted in equation 2.56, which eventually yields to the following energy conservation theorem:

$$\Sigma E_{Pi} + \Sigma E_{Ei} + E_{Fr} - E(u)_i = 0 \qquad 3.35$$

where:

$E(u)_i$ is the initial kinetic energy

$\Sigma E_{Pi}$ is the summation of the plastic energy quantities absorbed from the various parts of the bow.

$\Sigma E_{Ei}$ is the summation of the elastic energy quantities absorbed from the various parts of the bow, after the collision.

$E_{Fr}$ Friction energy

All the energy derived on the structure during the impact comes from the kinetic energy including the augment due to the added mass at the surge condition. The relevant equation 2.54, exhibits the initial state of energy on the structure. Figure A3-3.8 depicts the kinetic energy variation throughout the collision time. It can be seen that a similar form of reduction is drawn from the curves. What really makes these curves interesting is to examine the rate of energy reduction in relation to the time.

Figure 3.28 displays this variation versus the time. It is interesting to see that the maximum slope is not the same for all the cases. Thus the kinetic energy is reducing faster for the impact condition with the highest initial velocity. The maximum slope is shown in Figure 3.28 whereas there is a vertical line. The following Table displays the times, where the maxima occur.

| 3.00 m/s | 4.00 m/s | 5.00 m/s | 5.70 m/s |
|---|---|---|---|
| 0.79 sec | 0.90 sec | 0.79 sec | 0.69 sec |

**TABLE 3.13 TIME WHERE MAXIMUM RATE OF KINETIC ENERGY OCCUR**

For conditions with 3.0m/s and 5.0m/s initial speeds the maxima occur at the same time 0.79 sec.

The kinetic energy on the initiation of the impact will be transformed to the following forms of energy:

1. Elastic Energy
2. Plastic Energy
3. Potential energy because of the change of vertical state.
4. Thermal energy because of the friction contact of the various steel parts
5. Acoustic Energy

From these quantities the last two energy factors are ignored primarily since they would be very small compared to the others.

The energy absorbed by the structure is calculated on the basis of volume integration on all individual members (Decks & Bulkheads), Hibbit, Karlsoon & Sorensen (1995). The energy absorbed by the webs and girders, has been added to the plate to which they are attached. The energy calculated from ABAQUS is energy per unit volume. The integration of this energy in the volume of the distorted material produces the Figure A3-3.9. Here the energy, including the plastic and elastic, is shown in respect to the time during the impact. These curves have a symmetrical shape compared to those in the previous Figure A3-3.8, where the kinetic energy is displayed.

It is verified that the final total energy derived on the structure equals the amount of the initial kinetic energy. It is interesting to examine the rate of change of the energy. This is shown in Figure 3.29.

One can see that the maximum rates are similar to the ones shown on Table 13. In Table 14 , a comparison between the rates is shown. Contrary to the rates derived from the 3.00m/s condition the others are exactly the same. This is shown in Table 14.

The difference at the case of 3.00m/sec is only 0.02 sec or 2.5% and it may be due either to the small initial speed, or numerical errors, or even to a lag in the energy transition from elastic to plastic.

| | 3.00 m/s | 4.00 m/s | 5.00 m/s | 5.70 m/s |
|---|---|---|---|---|
| Kinetic Energy | 0.79 sec | 0.90 sec | 0.79 sec | 0.69 sec |
| Elasto-plastic Energy | 0.81 sec | 0.90 sec | 0.79 sec | 0.69 sec |

**TABLE 3.14 COMPARISON BETWEEN THE MAXIMUM RATES IN ENERGIES**

It must be noted at this point that the energy transition from the elastic stage to the plastic is very much depended on the kinetic energy released from the system during the impact. The more kinetic energy that remains the faster and more determined the mechanism is and faster the elastic energy is transformed to plastic. It should be noted that the elastic energy is almost 10% of the plastic. Therefore the conversion of the elastic to plastic does not require much kinetic energy for it to be released from the ship.

The elastic and plastic energy quantities are shown in Figures A3-3.10 and A3-3.11 for all the scenarios. The forms of these graphs are similar to the one of A3-3.9 since this is the superposition of the former two curves. A comparison of the rates from A3-3.10 and A3-3.11 show much higher slopes for the elastic energy, as expected, and this elastic energy while increasing as the penetration increases, shows a reducing rate.

It is of great interest to compare the elastic and plastic energy quantities for the individual members of the structure. These are included in images from 3.30 to 3.68.

The main conclusion is that the elastic energy is approximately 100-1000 times smaller than the plastic. The compartments which predominantly have been destroyed by the crushing loads show larger plastic energy quantities than elastic. On the other hand, members which still retain their structural integrity below plasticity, show elastic energy quantities higher than the plastic. Further discussion follows.

### *3.4.1 DISCUSSION*

From the above curves the following conclusions are drawn.

- The Elastic energy dissipated on the structural members is much smaller than the plastic energy, except in the case of the collision bulkhead 77 or Bulk1 as shown in Figure A3-2.3. This is attributed to the fact that the indentation is not enough to produce large local deflections on bulkhead 77. Figures 3.69, 3.70 show the elastic and plastic energy dissipated on bulkhead 77, for the case with initial speed 5.7 m/sec

- From Figure 3.69 it is obvious that the plastic energy is mostly concentrated on the top starboard side of the bulkhead; in Figure 3.70, elastic energy is most concentrated in the central part of the bulkhead where the connection with the longitudinal diaphragm, Bulk3, takes place. This member transfers the highest part of energy from the bulbous bow to the after part. The shell also transfers some part of energy, but this is very small due to its mode of failure. The shell due to its curvature fails under buckling loads, most of which are derived from the transverse diaphragm bulkhead 87 or Bulk2, shown in Figure A3-2.3.

- The Figures displaying the elastic energy show a variation of this during the impact period. This is attributed to the variation of the plastic mechanisms that develop on the members, which are closer to the rigid wall. It is similar to the phenomenon described by Figure 3.1 and 3.2. While member i is collapsing plastically, member i+1 absorbs elastic energy which is released when member i collapses.

- This variation in the elastic energy is very predominant in the bulkhead 77 case, Figure 3.31, because this energy is much greater than the plastic. On the other members where plastic energy is much greater this variation is not predominant. In Figure 3.31 one can also see that at time t=1.6 sec the elastic energy is much higher for the case with initial velocity 3.0 m/sec. This is owing to the fact that more elastic energy is stored in the system while in the other cases this energy could be released while other members were plastically deformed. Additionally,

as mentioned in Lindbergh (1986) the impact force creates travelling stress waves in the structure, and each discontinuity divides the incoming stress waves in a transmitted and a reflected wave. All the stress waves interact with each other such that there will be areas with stress waves whose superposition creates higher accelerations and consequently higher elastic energy concentration such as bulkhead 77, compared to the other concepts.

- Decks 7 and 8 as shown in Figures 3.57-3.62 absorb a great deal of plastic energy since they directly come in contact with the rigid surface. As it is shown on the above Figures the plastic energy dissipated is 100-1000 times greater than the elastic. It is though, very interesting to see elastic energy stored in such a folded and destroyed pattern. As mentioned previously, Gerard's approach produces results similar to the finite element analysis results as far as the energy absorption is concerned.

Gerard's approach estimates the crippling forces derived on the structural elements of the structure. The integration of the crippling force with respect to the penetration produces the curve displayed in Figure 3.71. One can see the correlation of the two methods. ABAQUS calculates slightly higher quantities.

ABAQUS estimates somewhat 10% higher elasto-plastic energy, similar difference in the other quantities calculated in the second Chapter. The linear form of the Energy Indentation curve is a general tendency of the ship during the impact. This indicates that strain rates are relatively small as shown in Figures 3.72, 3.73;

As shown in earlier topic, in Chapter 2, strain rates smaller than $10^{-3}$ $s^{-1}$ are negligible, according to Reckling (1977). In this case we examine the strain rate for Deck8 for the condition with initial speed 5.7 seconds, the most forceful case, on the Deck which is the inner part of the bulbous bow and the section which crashes on the rigid surface with the highest speed. It is expected that the highest strain rates will develop on this as well as Deck7 which is located exactly above in the same volume. However Figures 3.72 and 3.73 display very small strain rates which diminish after 0.6-0.8 seconds when the frontier's decks

collapse completely. Contrary to these results Pedersen in Yong Bai & Pedersen (1993) has shown that in the case of a side collision of a vessel with a one leg jack-up offshore structure, the strain hardening effects on the deck of the vessel produce higher impact forces, but of no more than 10%. In this case however, the membrane action on the side shell is predominant, contrary to the case study developed herein, in which the membrane action is very small. The strain rates shown on the above Figures are taken from eight points along the length of the deck. Rather than displaying the number of the elements it is more interesting to include the location with respect to the rigid surface at the initiation of the collision.

- As shown in Figures A3-3.8 and A3-3.9 the energy is conserved during the impact. The summation of the individual elastic and plastic energy quantities is of great interest in order to ascertain how this energy is dissipated on the structure for the four cases of initial speed. Thus, it would be feasible to establish critical members which can absorb most of the energy.

For the concept with 5.7 m/s initial speed we acquire the following;

| Member | Elastic Energy Nm | Plastic Energy Nm | Total Energy Nm |
|---|---|---|---|
| BULK1 | 4.80E+05 | 2.09E+05 | 6.89E+05 |
| BULK2 | 3.59E+05 | 1.93E+07 | 1.96E+07 |
| BULK3 | 1.68E+05 | 7.63E+00 | 1.68E+05 |
| DECK9 | 8.91E+04 | 7.29E+06 | 7.38E+06 |
| DECK6 | 5.00E+04 | 1.80E+07 | 1.80E+07 |
| DECK7 | 1.82E+05 | 3.26E+07 | 3.28E+07 |
| DECK2 | 1.62E+05 | 4.95E+06 | 5.11E+06 |
| DECK8 | 9.30E+04 | 4.00E+07 | 4.01E+07 |
| DECK3 | 5.06E+04 | 5.09E+06 | 5.14E+06 |
| DECK4 | 1.36E+05 | 2.77E+07 | 2.79E+07 |
| DECK1 | 1.12E+05 | 1.43E+06 | 1.54E+06 |
| DECK5 | 2.81E+05 | 1.63E+07 | 1.66E+07 |
| SHELL | 1.84E+07 | 2.75E+08 | 2.93E+08 |
| **TOTAL** | **2.05E+07** | **4.48E+08** | **4.680 E+08** |

**TABLE 3.15 ENERGY QUANTITIES FOR THE 5.7M/S INITIAL SPEED**

For the concept with 5.0 m/s initial speed we acquire the following;

| Member | Elastic Energy Nm | Plastic Energy Nm | Total Energy Nm |
|---|---|---|---|
| BULK1 | 8.70E+05 | 2.29E+05 | 1.10E+06 |
| BULK2 | 3.66E+05 | 4.12E+06 | 4.48E+06 |
| BULK3 | 1.87E+07 | 1.77E+06 | 2.05E+07 |
| DECK9 | 1.27E+05 | 8.67E+05 | 9.94E+05 |
| DECK6 | 6.28E+04 | 1.32E+07 | 1.32E+07 |
| DECK7 | 9.76E+04 | 2.86E+07 | 2.87E+07 |
| DECK2 | 2.56E+05 | 6.93E+05 | 9.49E+05 |
| DECK8 | 8.78E+04 | 4.01E+07 | 4.02E+07 |
| DECK3 | 7.84E+04 | 1.67E+06 | 1.74E+06 |
| DECK4 | 2.66E+05 | 1.14E+07 | 1.16E+07 |
| DECK1 | 1.56E+05 | 1.66E+05 | 3.22E+05 |
| DECK5 | 2.56E+05 | 1.15E+07 | 1.18E+07 |
| SHELL | 2.46E+07 | 1.98E+08 | 2.23E+08 |
| **TOTAL** | **4.59E+07** | **3.12E+08** | **3.580 E+08** |

**TABLE 3.16 ENERGY QUANTITIES FOR THE 5.0M/S INITIAL SPEED**

For the concept with 4.0 m/s initial speed we acquire the following;

| Member | Elastic Energy Nm | Plastic Energy Nm | Total Energy Nm |
|---|---|---|---|
| BULK1 | 4.99E+05 | 2.36E+05 | 7.35E+05 |
| BULK2 | 4.88E+04 | 5.13E+04 | 1.00E+05 |
| BULK3 | 2.66E+04 | 2.32E+04 | 4.98E+04 |
| DECK9 | 3.08E+04 | 2.75E+04 | 5.83E+04 |
| DECK6 | 5.35E+04 | 8.35E+06 | 8.40E+06 |
| DECK7 | 1.19E+05 | 2.41E+07 | 2.42E+07 |
| DECK2 | 2.97E+04 | 1.21E+04 | 4.18E+04 |
| DECK8 | 1.13E+05 | 3.48E+07 | 3.49E+07 |
| DECK3 | 2.42E+04 | 2.39E+04 | 4.81E+04 |
| DECK4 | 8.36E+04 | 2.90E+06 | 2.98E+06 |
| DECK1 | 1.02E+04 | 7.76E+01 | 1.03E+04 |
| DECK5 | 2.66E+05 | 7.05E+06 | 7.32E+06 |
| SHELL | 1.81E+07 | 1.33E+08 | 1.51E+08 |
| **TOTAL** | **1.94E+07** | **2.11E+08** | **2.300E+08** |

**TABLE 3.17 ENERGY QUANTITIES FOR THE 4.0 M/S INITIAL SPEED**

For the concept with 3.0 m/s initial speed we acquire the following;

| Member | Elastic Energy Nm | Plastic Energy Nm | Total Energy Nm |
|---|---|---|---|
| BULK1 | 7.35E+05 | 3.84E+05 | 1.12E+06 |
| BULK2 | 7.89E+03 | 2.21E+02 | 8.11E+03 |
| BULK3 | 1.08E+04 | 3.51E+04 | 4.59E+04 |
| DECK9 | 9.08E+03 | 2.63E+04 | 3.53E+04 |
| DECK6 | 2.77E+04 | 2.69E+06 | 2.72E+06 |
| DECK7 | 8.51E+05 | 1.53E+07 | 1.61E+07 |
| DECK2 | 1.53E+04 | 1.12E+04 | 2.64E+04 |
| DECK8 | 8.02E+04 | 1.93E+07 | 1.94E+07 |
| DECK3 | 2.91E+02 | 0.00E+00 | 2.91E+02 |
| DECK4 | 2.06E+04 | 2.46E+05 | 2.66E+05 |
| DECK1 | 1.12E+04 | 6.89E+01 | 1.12E+04 |
| DECK5 | 4.47E+04 | 1.23E+06 | 1.28E+06 |
| SHELL | 1.10E+07 | 7.48E+07 | 8.58E+07 |
| **TOTAL** | **1.28E+07** | **1.14E+08** | **1.280E+08** |

**TABLE 3.18 ENERGY QUANTITIES FOR THE 3.0 M/S INITIAL SPEED**

- The Energy conservation between the initial kinetic energy and the energy dissipated on the structure is shown in the following Table

| Concept Initial Speed | ABAQUS M joules | Initial Kinetic Energy M joules | Difference % |
|---|---|---|---|
| 5.79 | 468 | 469 | 0.21 |
| 5.00 | 358 | 360 | 0.56 |
| 4.00 | 230 | 231 | 0.43 |
| 3.00 | 128 | 129 | 0.78 |

**TABLE 3.19 ENERGY CONSERVATION**

The difference is small and it is attributed to the Kirchoff thermal energy from the friction developed between the members of the structure and the rigid surface.

- The higher contribution in energy absorption comes from the outer shell, along with the transverse webs and frames as one can see in the above Tables 15-18. The shell contributes in the transition of the forces from the incident area in the bulbous bow to the upper part of the bow, decks 1, 2, 3, and 4. As a result, it is

expected that there will be areas on the shell *where plastic strains will be predominant*. This mode of response is very well shown in Figures A3-3.1 to A3-3.4 where the bending of the top part of the bow is shown. Most of the structural members fail under buckling loads, contrary to the shell and Bulk2, which fail under bending mechanism.

- In Figure A3-3.15 the reaction force-indentation relation is shown for the four initial speeds. It can be seen that all the curves are very close. This fact explains that the energy absorption-indentation relation, shown in Figures A3-3.13 and A3-3.14 is non depended on the initial speed

- Similar areas with high strains are shown on the longitudinal diaphragm as well as the transverse bulkhead 87. These structural planes are responsible for keeping the water bulkhead tightness for the forepeak tank. The longitudinal diaphragm Bulk3 transmits most of the energy in Deck2, Deck4, Deck9, and Bulk1. Bulk2 bulkhead transfers a great deal of energy to Bulk3, and all the horizontal decks located behind. Most critical area of Bulk2 is the lower one, since it is directly connected to Deck7 and Deck8. The following Table displays the percentages in the energy contribution for these members. The values shown are % of the energy without the contribution of the shell. Otherwise the numbers would have been much smaller. Usually the outer shell along its reinforcements absorbs the 60-65% of the total energy.

| Concept Initial Speed | Bulk2 % | Bulk3 % |
|---|---|---|
| 5.79 | 11.20 | 9.6 |
| 5.00 | 3.31 | 15.18 |
| 4.00 | 0.13 | 0.06 |
| 3.00 | 0.02 | 0.01 |

**TABLE 3.20 THE CONTRIBUTION OF BULK2 AND BULK3**

As one can see these percentages are not big as one would expect. The members which absorb most of the energy are the Deck4, 7 and 8, as shown on the Tables 15-18.

The energy dissipated on the structure is presented very graphically in Figures 3.74-3.77, where the elastic and plastic energy dissipated on the structure is shown. All these Figures are drawn with the same colour contours.

#### *3.4.1.1 LOSS OF SYMMETRY DURING THE IMPACT*

It is observed that during the collision the bow loses it's symmetry, although the angle of impact on the rigid surface is 0°. This reaction may be attributed to two factors.

The first one, and the most obvious, is the fact that the reaction is not only dependent on the initial conditions but also on the geometrical properties developed within the structure itself, during the impact. Thus the collapse of the primary members which come in contact with the rigid surface create asymmetrical geometrical boundary reactions.

The second factor is that the centre of mass and material is slightly shifted to the port side of the bow due to the existence of a hatch opening on the starboard side of deck DECK4 shown in Figure. 3.11. This provides a structural asymmetry, with the starboard side weaker than the port. The buckling and total collapse of the bulbous bow decks provides the structure with asymmetrical stiffness towards the main axis of the bow. This phenomenon occurs 1.12 seconds after the initiation of the impact as it is shown in Figure 3.78, where port and starboard denote the elements 164 and 194 on the port and starboard side of the ship as shown in Figure 3.11.

This non-linear response due to the rotation affects the buckling mode of the decks. Figure 3.78 shows the buckling displacement on DECK4 at time 1.6 sec for the condition with 5.7 m/s initial speed. It can be seen, that the buckling deflection developed on the port side, along the length of the Deck4, becomes less than the one on the starboard side immediately after the change of the symmetrical properties of the bow. It is shown that collapse of the stiffening structure is not symmetrical, similar to the DECK4.

This lack of symmetry shows that the structure experiences greater loads on the starboard side, as it delivers greater axial and bending loads on the parallel body of the vessel, located exactly behind the bow.

This is clearly shown on the stress curve displayed in Figure 3.80, where the stresses on elements 164, 194 are shown in respect to the time. Since the structure is loaded and unloaded during the impact period because of the formation of local plasticity, the stresses in both intercostal elements are varying. Maximum value reached from the starboard side at time t=1.8 sec and exceeds the yield strength, with value 250 $MN/m^2$.

However, the port side doesn't undergo such large stresses as the maximum value does not exceed the 125 $MN/m^2$

The effect of the loss of symmetry is shown on the collision bulkhead, on the elastic and plastic energy contours, Figures 3.69, 370. The top starboard side is "overloaded" with plastic energy, part of which will induce local buckling on the parallel body located exactly behind.

### *3.4.1.2 ENERGY-INDENTATION*

In Amdahl's experimental tests Amdahl's (1983). pp 140-141, there is an energy penetration relation for the pallet carrier M/S Fjord grounded in 1983 on Byneset close to Trondheim harbour, Figure 3.81. The ground on the spot is characterised by a steep cliff down to several meters of depth.

Thus, a virtually rigid barrier stopped the ship with a great similarity to the boundary conditions in the present numerical experiments. The replaced region of the vessel is indicated in Figure 3.81 showing that only the bulbous section of the bow was damaged.

An examination of the energy indentation curve will reveal a shape, which has a linear response in respect to the penetration, as shown in Figure 3.82. This denotes that the rate of the energy dissipated in the structure is not dependent on the initial speed.

Thus if we know the energy dissipated on the ship for a collision with 6 knots initial velocity, one can predict the energy which will be absorbed for an initial speed of 7, 8, or 10 knots.

As shown earlier in Figures 3.72, 3.73 the strain rate effect is not large enough to produce strain hardening in the stress strain curve of the impacted structural elements.

For the vessel involved in this analysis, similarly to the previous example, the energy indentation curve is shown in Figure 3.83.

The shape of the E-I (energy-indentation) curve is very similar to the one of Figure 3.83 and to those produced from Aldwinckle (1984) shown in Figure 2.13. This indicates that the numerical solution for the specific problem produces a response with a very linear "character", although it consists of a dynamic nature. The non-linear area of the curve is concentrated on the first 3.5 meters where the change of

the bow shape is significant. It is expected that vessels with bulbous bow will generate non-linear reactions similar to the one shown in Figures 3.82 and 3.83. If we examine Figure A3-3.12 we can see that for the first 3.5 meters of distance the kinetic energy versus indentation relation has a non-linear character which can only be attributed to the projected transverse area of the bulbous shape which comes in contact with the rigid wall. Figure A3-3.13 displays the elastic energy dissipated on the structure versus the penetration. In this case the non-linear response is very predominant contrary to the plastic energy dissipated as shown in, Figure A3-3.14.

If we apply regression analysis on the E-I curve we acquire a 3rd degree polynomial which fits the curve with a tolerance less than 1E-3. When the polynomial fitted it is of the following form;

$$Energy = a \cdot i^3 + b \cdot i^2 + c \cdot i + d \qquad 3.36$$

where : Energy is the total energy absorbed in MNm

i is the indentation in meters

a, b, c, d are constants

a = -0.73

b = 12.67

c = -0.79

d = 8.10

Equation 3.36 produces a relation E-I for the specific vessel. If instead, we are interested in high-speed collisions, i.e. the assumption that the crushing of the bulbous bow is taken for granted then the non-linear area can be ignored and draw the same E-I for indentations larger than 3 meters. As a consequence, linear regression produces a function E-I which is of the following form;

$$Energy = c \cdot i + d \quad \text{with} \quad i > 3.0 \text{ m} \qquad 3.37$$

where :

c = 68.74

d = -110.97

This approach is much simpler for estimating the energy dissipated for high speed collisions which exceed the bulbous bow length, provided, always that we can define one point on the curve.

### *3.4.1.3 A STATIC APPROACH*

It appears that from dynamic tests on stiffened plate arrangements, which were reported by Akita et al. (1972) and Zhu & Faulkner (1994), that energy absorbing mechanisms and fracture types had a greater energy capacity than those observed in the corresponding static tests. A circumstance which is attributed to the influence of material strain-rate sensitivity.

It should be remarked that this increase in capacity might not be realised in a ship during a collision because this is a highly non-linear phenomenon, which is very sensitive to size. Moreover the influence of material strain rate sensitivity can't be properly scaled up from a model to a full sized structure which is made from the same material, Duffey, (1971). Furthermore, it appears that no investigation on real scale tests, have been undertaken in order to ascertain the mode of the structural response of ships; i.e. may the response be considered to be static or whether it is necessary to retain the influence of inertia forces. It was suggested in Jones (1973) that the structural response of a panel in a marine vehicle during a severe slam could be accurately predicted with a static analysis, provided the duration of the pressure pulse is longer than the fundamental period of elastic vibration. Indeed, encouraging agreement was obtained between the theoretical predictions according to a static analysis and some experimental results that were recorded on a one-quarter scale model of a section of the bottom of a coast guard cutter Jones (1973). However, the inertia terms must be retained when the duration of a pressure pulse is short.

It would therefore appear worthwhile to develop further these simple ideas in order to provide guidelines, which indicate when static analysis could be used with no sacrifice in accuracy. According Jones (1975) it is likely that the retention of inertia terms would be unavoidable, when analysing even minor collisions of high-speed marine vehicles.

It will be shown herein that even with static analysis, without inertia effect, the results in terms on energy conservation and plastic energy dissipation on the structural members of the bow does not vary from the dynamic ones.

The quasi-static analysis consists of the same model definition, but instead of applying initial velocity of the bow towards the rigid wall, the ship is rigidly clamped on the axial displacement in the direction of the main axis of the bow, and the rigid wall progressively travels towards the bow. This scenario is displayed in the Figure 3.84

With the static analysis neither inertia effects are incorporated, nor strain rate effects since the problem is not time dependent. The boundary on the rigid surface is used in order to prescribe magnitudes of prescribed displacements. Because the mesh is complicated and the quadratic convergence of the quasi-Newton solution technique is depended to a series of improved approximations to the Jacobian matrix, the displacement function was selected in such a way so that the displacements were not exceeding $10^{-3}$ meter at each iteration. If the reaction forces delivered on the rigid wall, are compared with those from the dynamic method with 5.7 m/sec initial speed, it can be seen that although they are of the same magnitude, Figure 3.85, the reaction for the static case varies during the increase of the penetration. Notice that more data points could be printed out for the static analysis than for the dynamic analysis. The reason is the capacity of the output file, which is much smaller in the case of the static. The fact that the reaction force is higher for the static case, for an indentation higher than 6.8 meters, is attributed to the stiffness retained by the bow until this penetration level. Contrary to this, in the dynamic analysis the frequency of the structural member's vibration and the stress wave propagation may reduce the total reaction force due to superposition of the waves. In Figure 3.86 the variation of the reaction force is shown for the concept with 5.7 m/s initial speed. The reason this speed was selected is due to the fact that it would probable produce faster propagating stress waves on the members of the structure. It can be seen that there are areas of relaxation of the reaction force, from 0.6 to 1.0 seconds and 1.78 to 2.0 seconds. This is attributed to the progressive variation on the global stiffness of the

structure, the reduction in the speed of the vessel and the stress waves derived on the structure.

As far as the energy dissipated in the structure is concerned, Figure 3.87 displays a comparison between the two concepts. It is shown that very good correlation in the results is achieved and this fact establishes a poignant significance regarding the head on collision of conventional ships and the attribute of mass inertia and strain hardening effects. This concept has to be integrated in a wide area of vessels covering more vessels in order to derive an empirical expression, which will take into account the vessel size and initial speed.

One of the differences between the dynamic and static analysis, is the inertia of the upper part of the bow, which doesn't come in contact with the rigid surface. It was found that this inertia does not affect the energy dissipation on the structure as shown in Figure 3.87

The static analysis showed very similar results to those of the dynamic. There was a big difference in the computing time, since the static analysis required 60% of the time required for the dynamic analysis. The size of the output file of the static analysis is approximately the 70-75% of the size of the dynamic analysis.

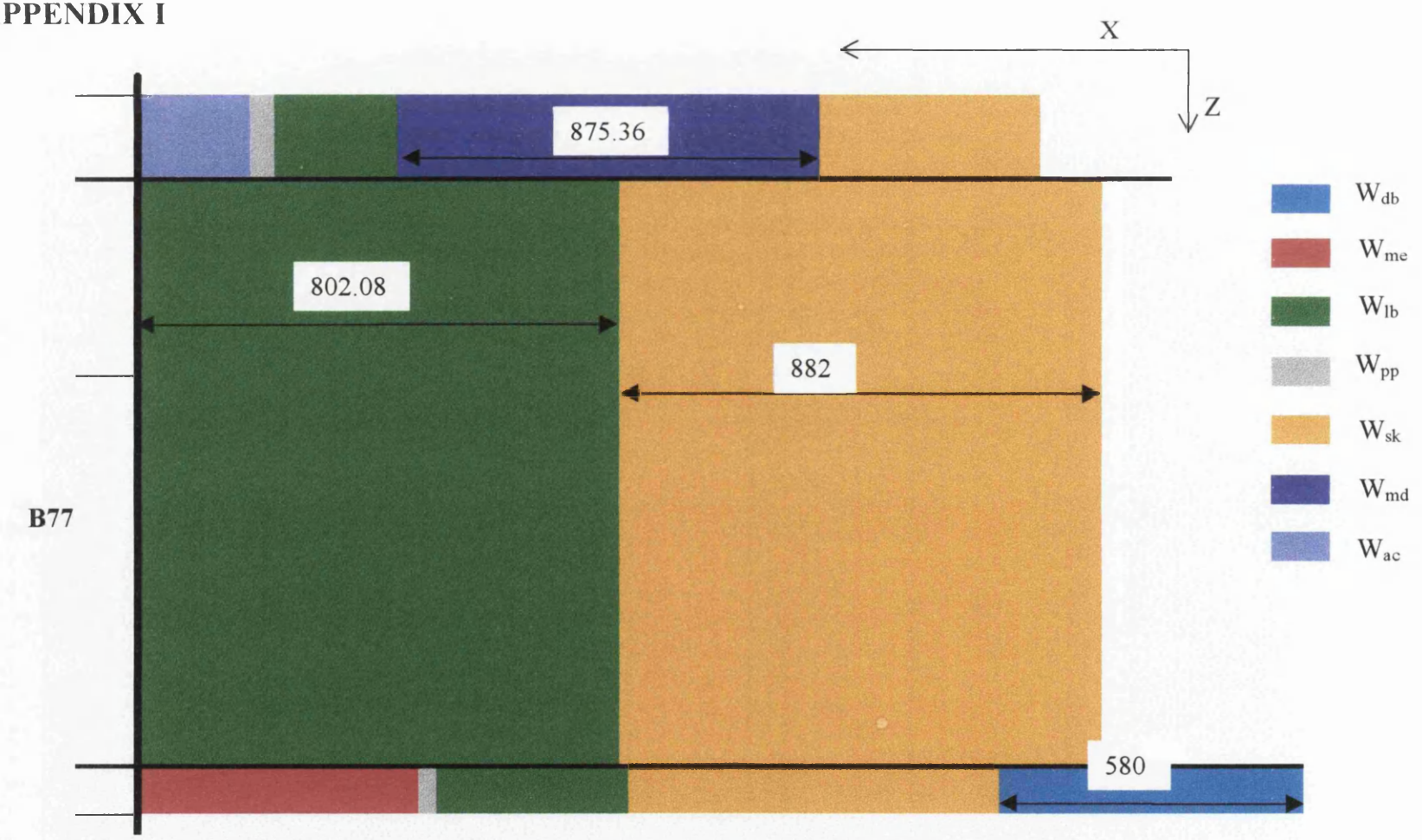


**Figure A3-1.1** *A Schematic diagram of the mass distribution along the depth of the ship*

# APPENDIX II

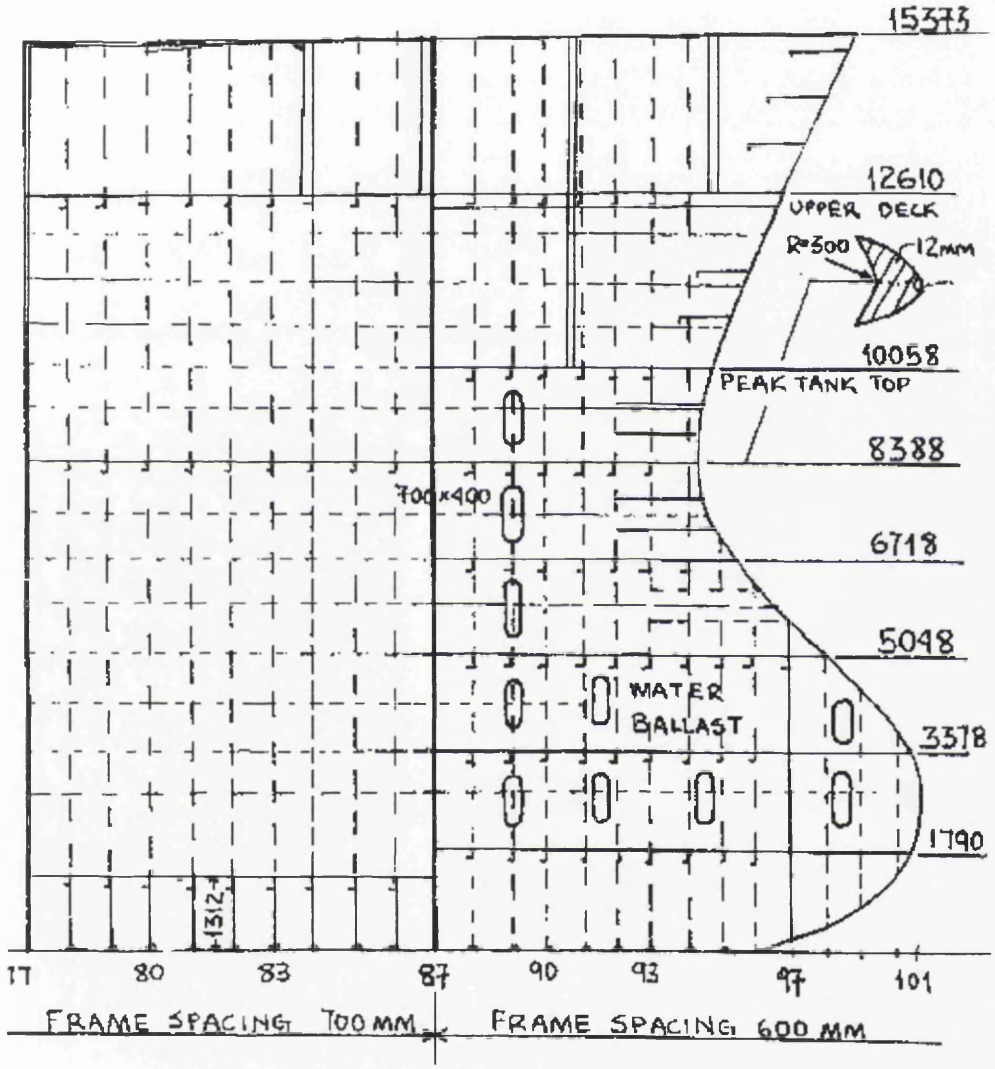


**Figure A3-2.1** *Sketch of the profile of the bow. The frame spacing is shown from which a scale can be extracted*

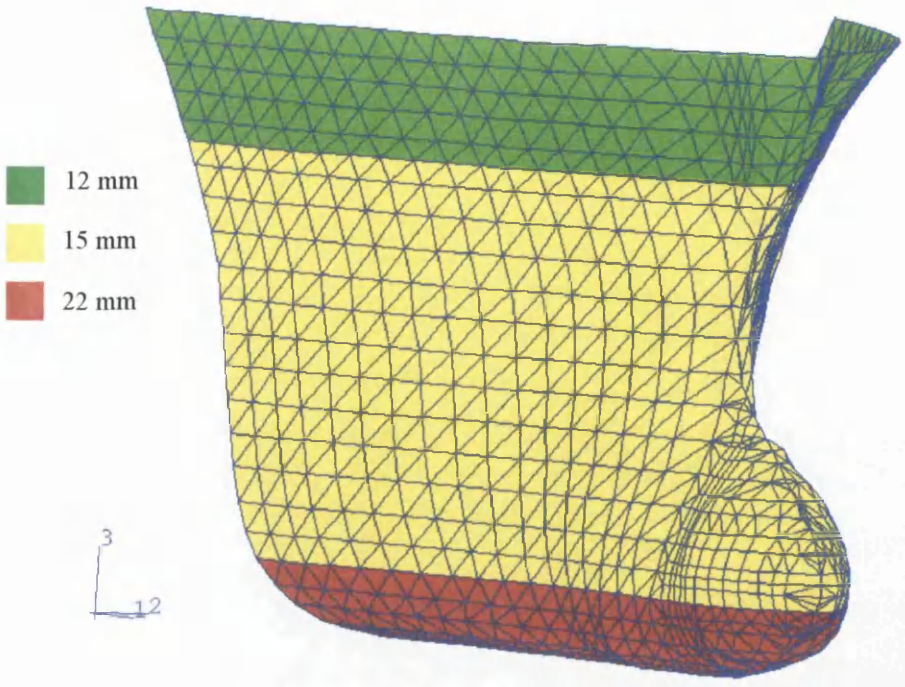


**Figure A3-2.2** *The shell of the bow with the three different levels of thicknesses*

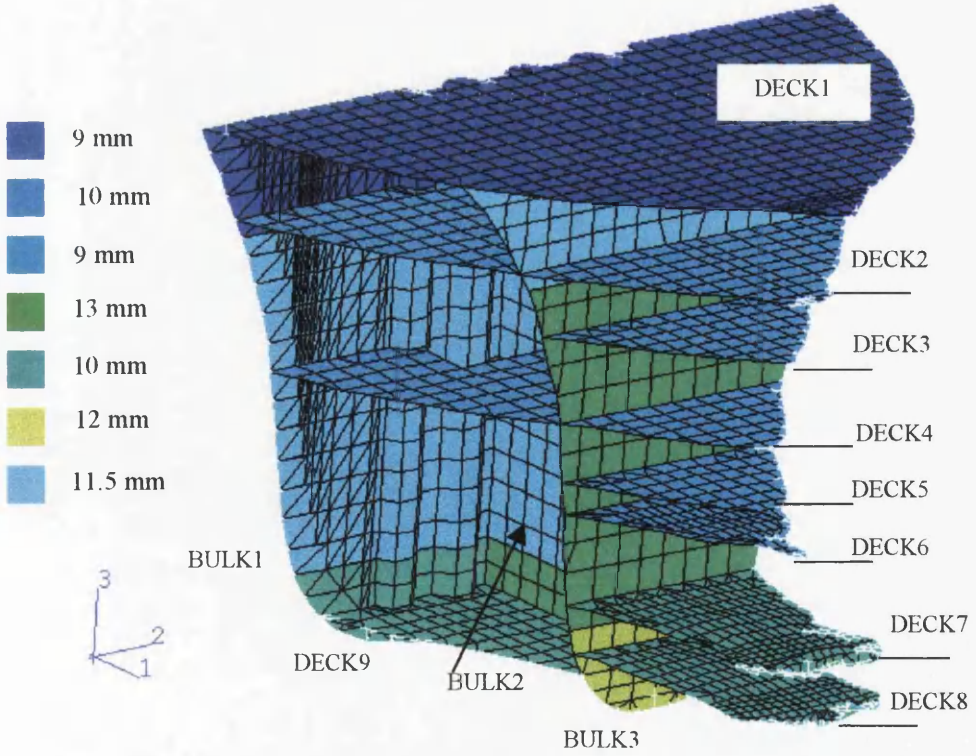


**Figure A3-2.3** *The inner members of the bow with the different levels of thicknesses*

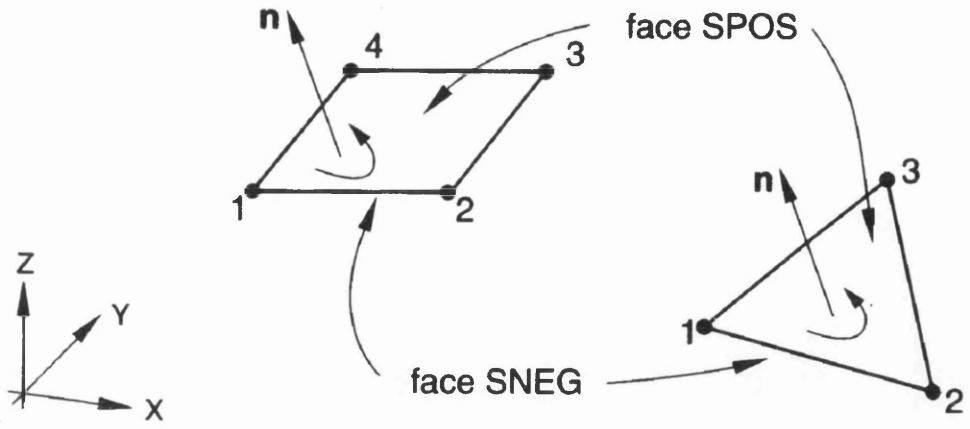


**Figure A3-2.4** *The triangular and rectangular configuration of the shell element. The normal vector n displays the positive surface of the element*

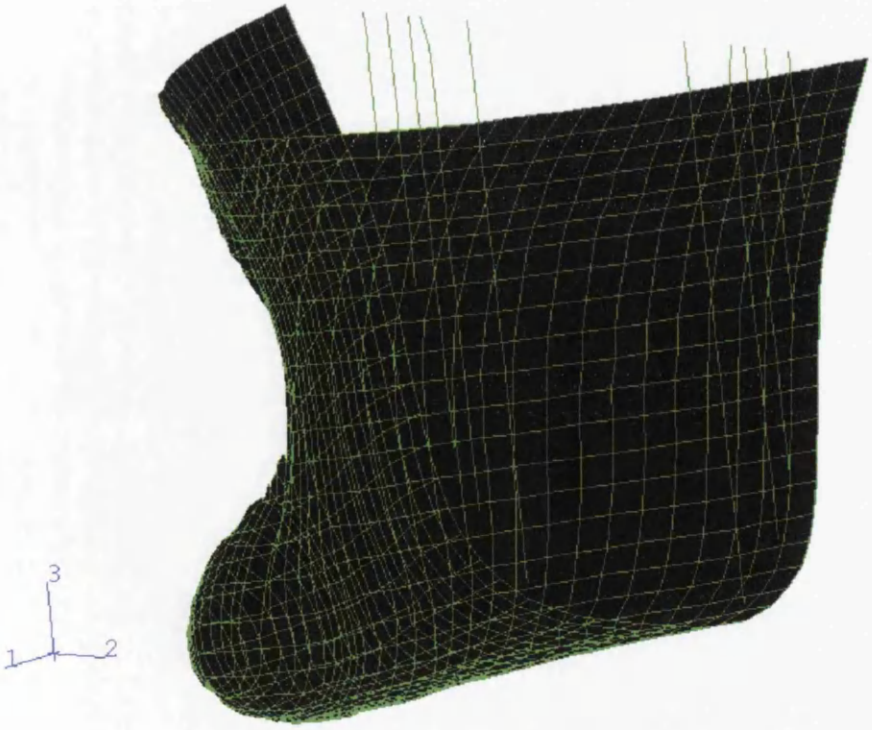


**Figure A3-2.5** *The transverse and longitudinal webs and frames, supporting the shell. These members are modelled as beam elements*

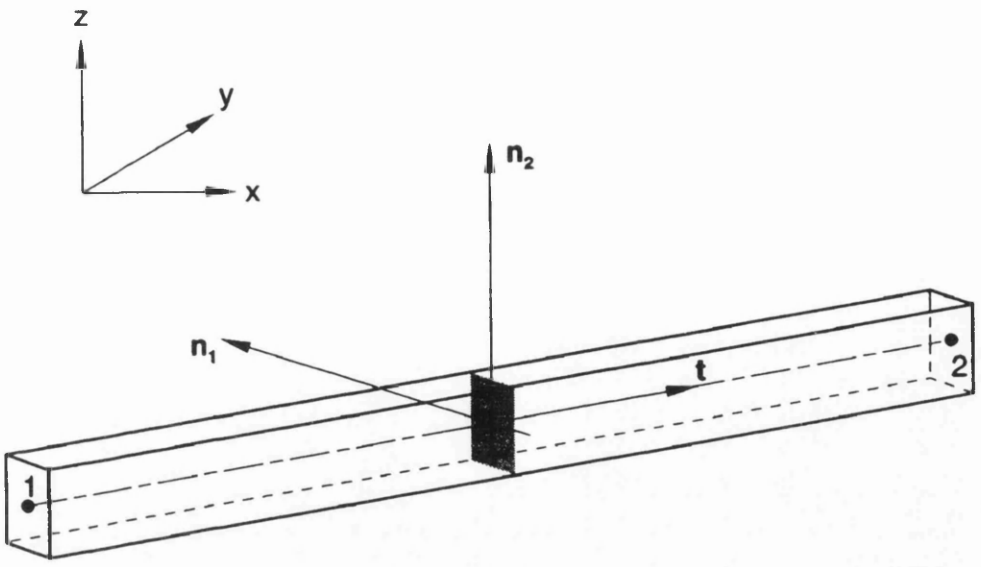


**Figure A3-2.6** *The beam element configuration along with the three principle axes*

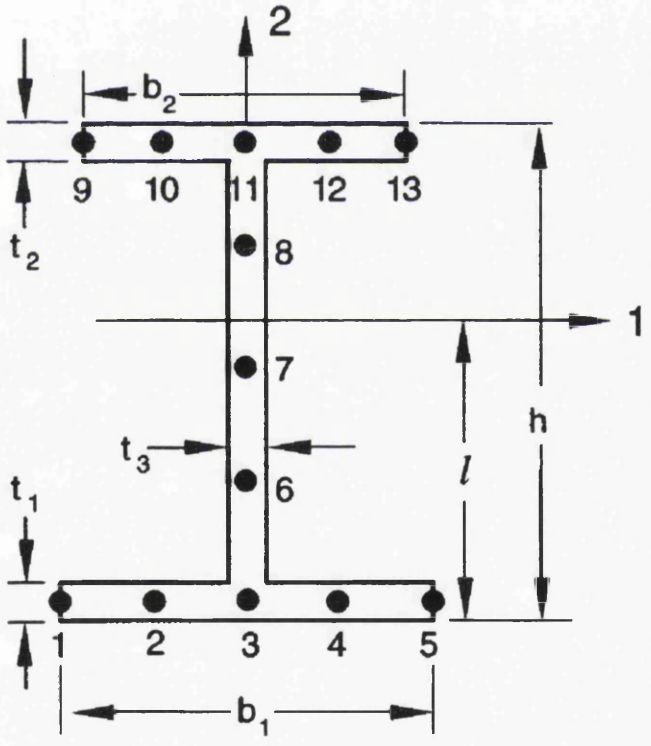


**Figure A3-2.7** *The beam element transverse area configuration. The integration points are shown*

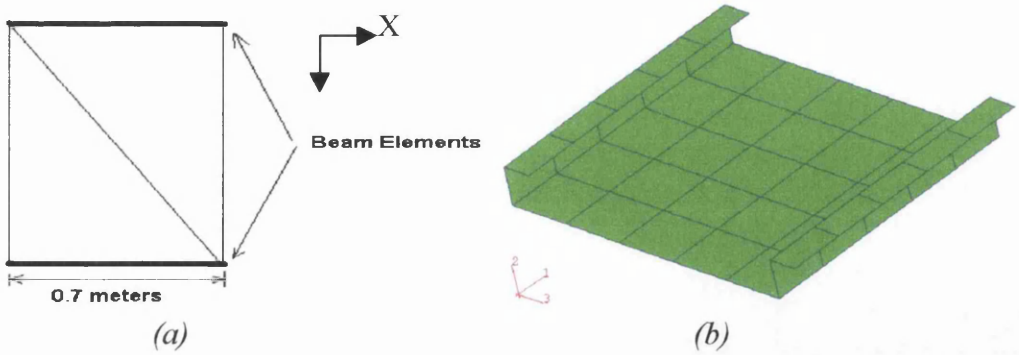


**Figure A3-2.8** *Part of the shell structure, the length of which is equal to one frame spacing. Two different models where adopted in order to evaluate the response of the coarse mesh shown in (a). The fine mesh shown in (b) was modelled using shell elements.*

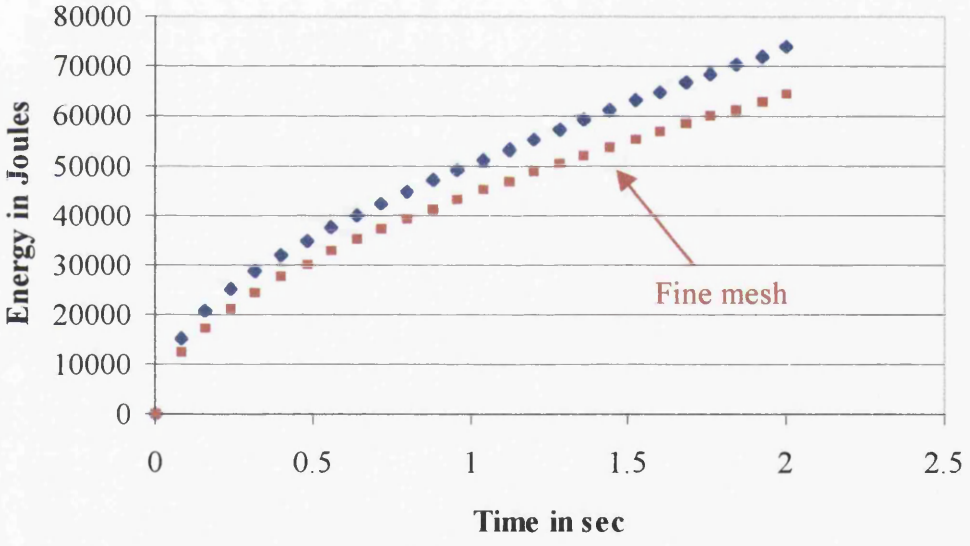


**Figure A3-2.9** *The total energy absorbed by the coarse and fine mesh. The blue dotted line denotes the energy dissipated in the coarse mesh and the red dotted line the energy from the fine mesh.*

# APPENDIX III

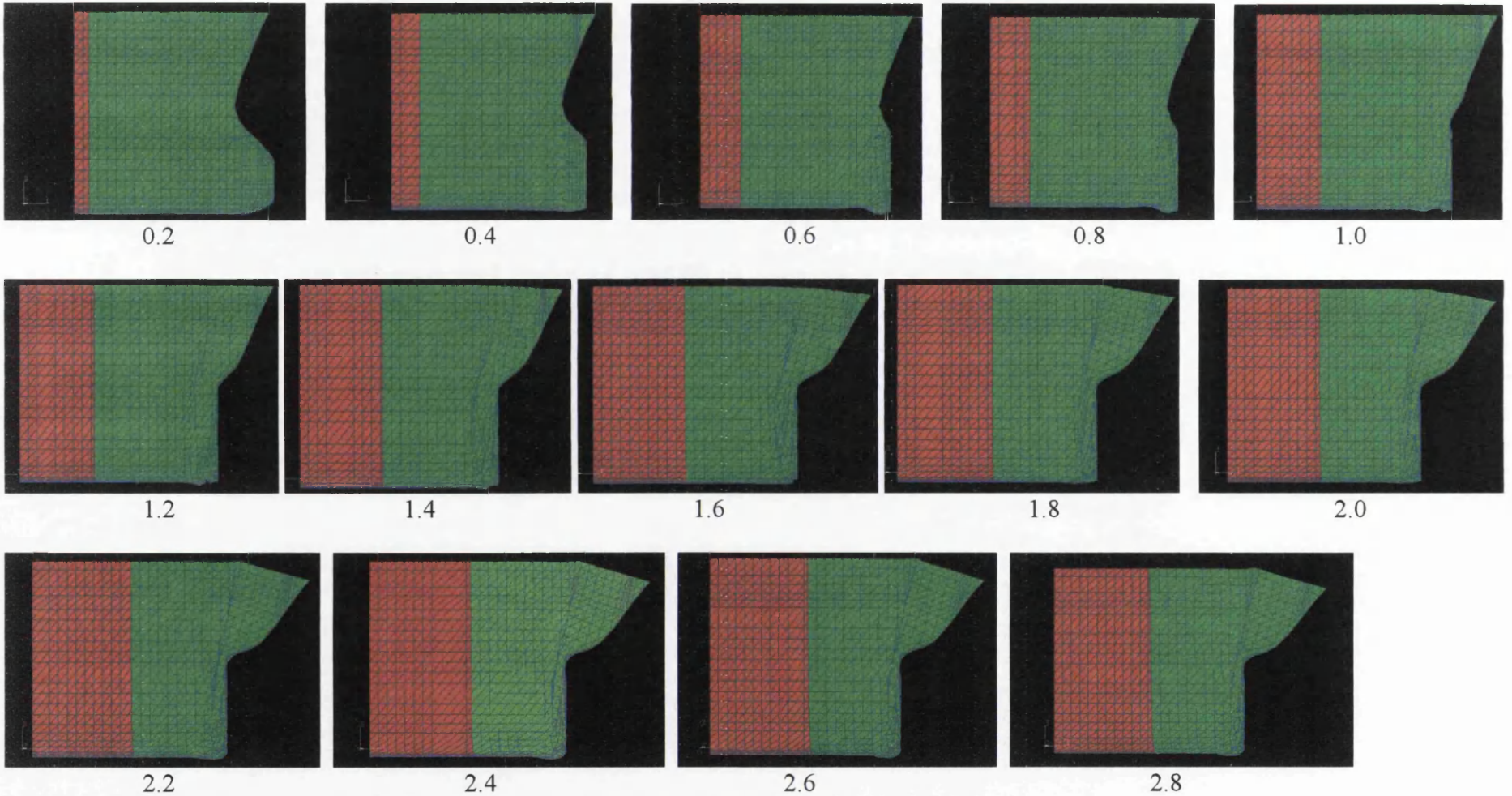


**Figure A3-3.1** *Thumbnails for the concept with initial speed of 5.7 m/sec*

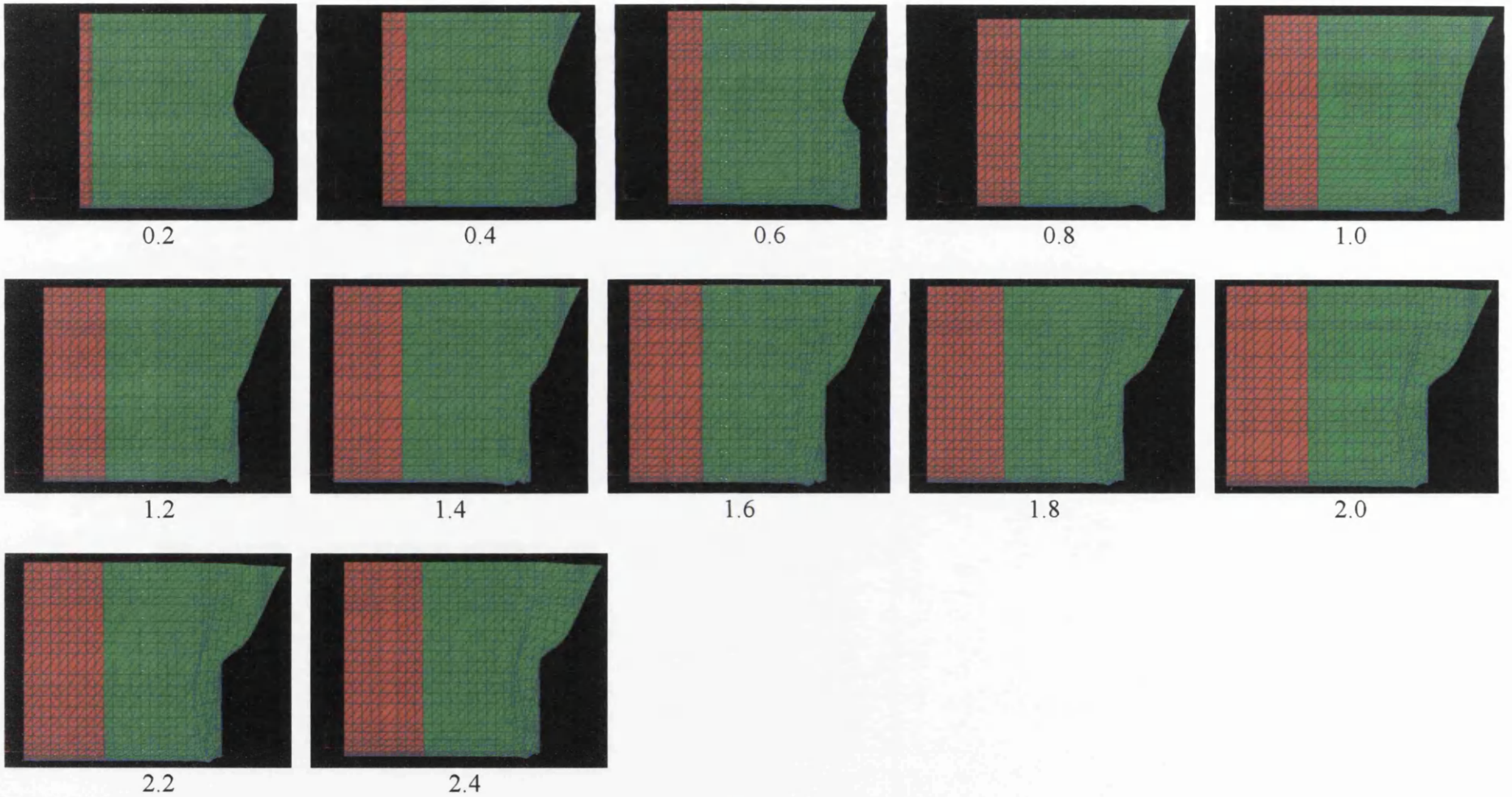


**Figure A3-3.2** *Thumbnails for the concept with initial speed of 5.0 m/sec*

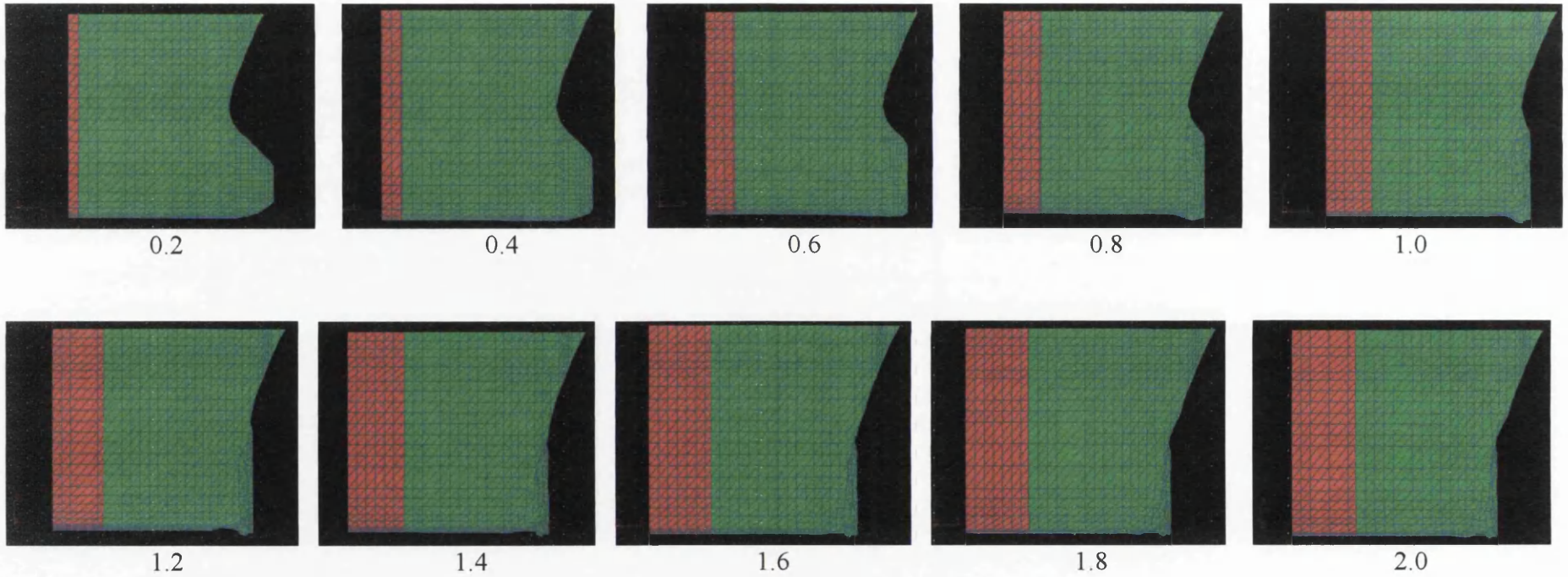


**Figure A3-3.3** *Thumbnails for the concept with initial speed of 4.0 m/sec*

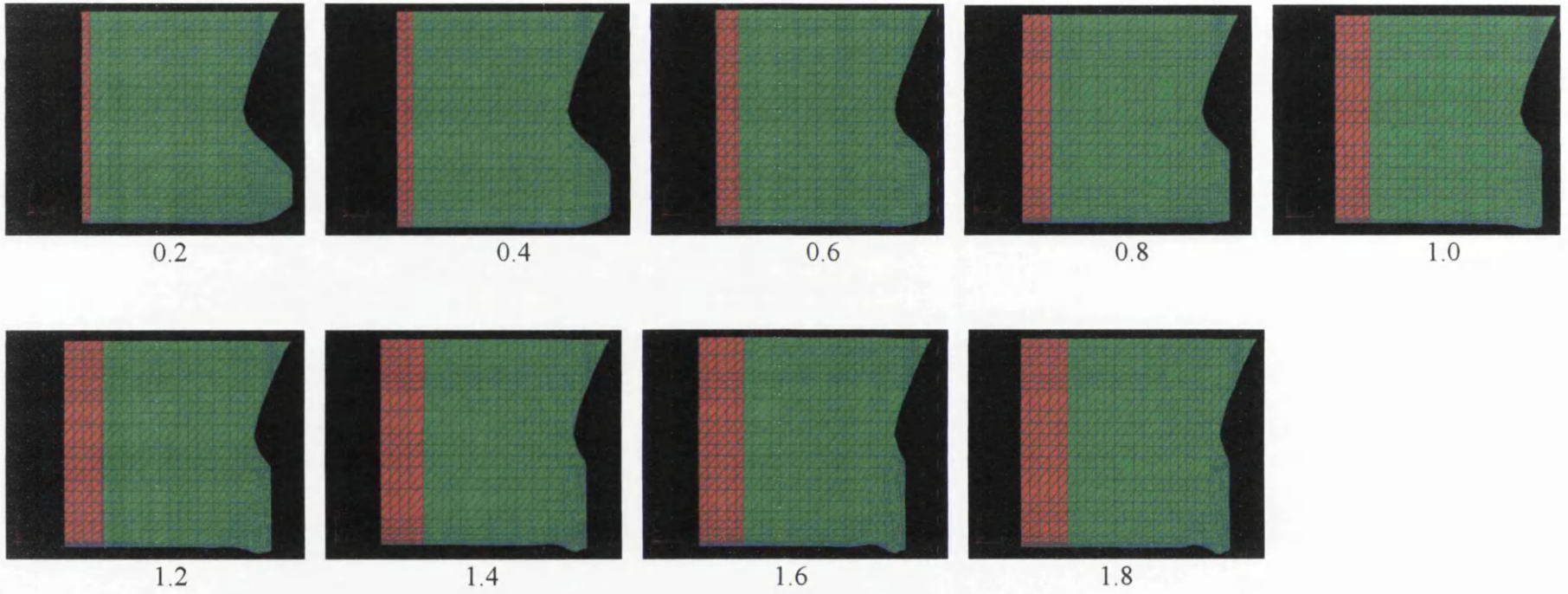


**Figure A3-3.4** *Thumbnails for the concept with initial speed of 3.0 m/sec*

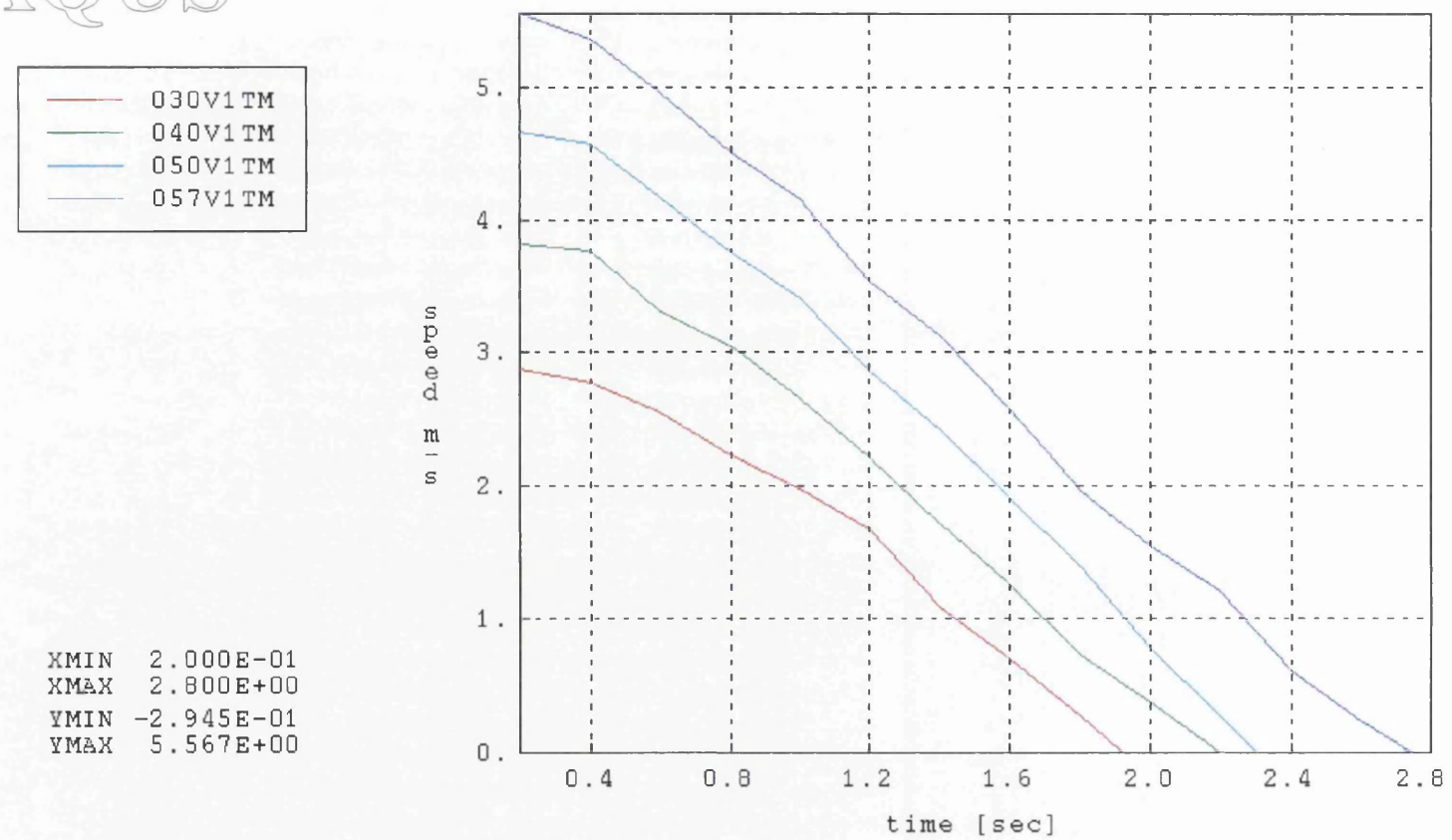


**Figure A3-3.5** *Speed Time relation for all the concepts*

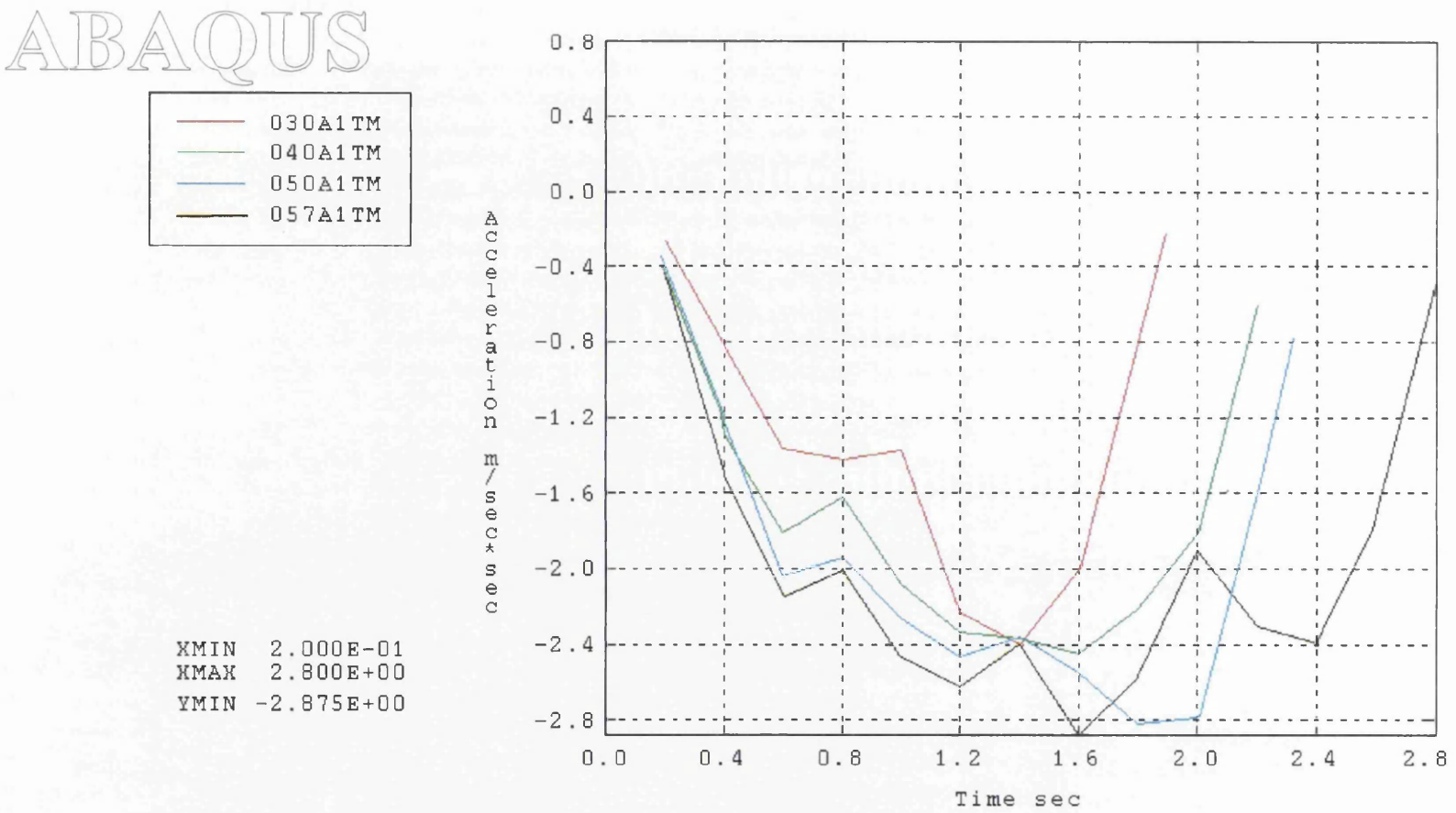


**Figure A3-3.6** *Acceleration Time relation for all the concepts*

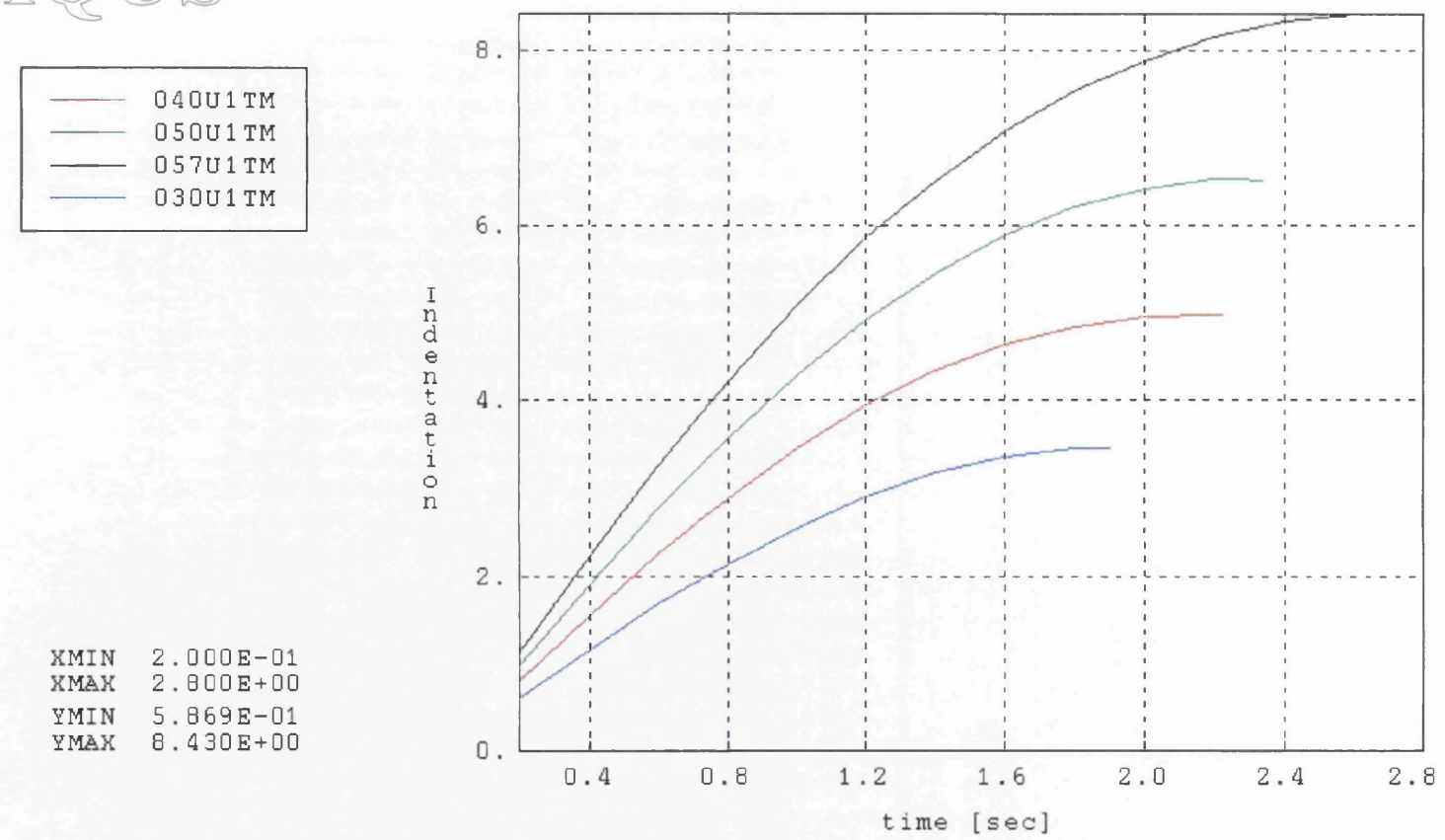


**Figure A3-3.7** *Indentation Time relation for all the concepts*

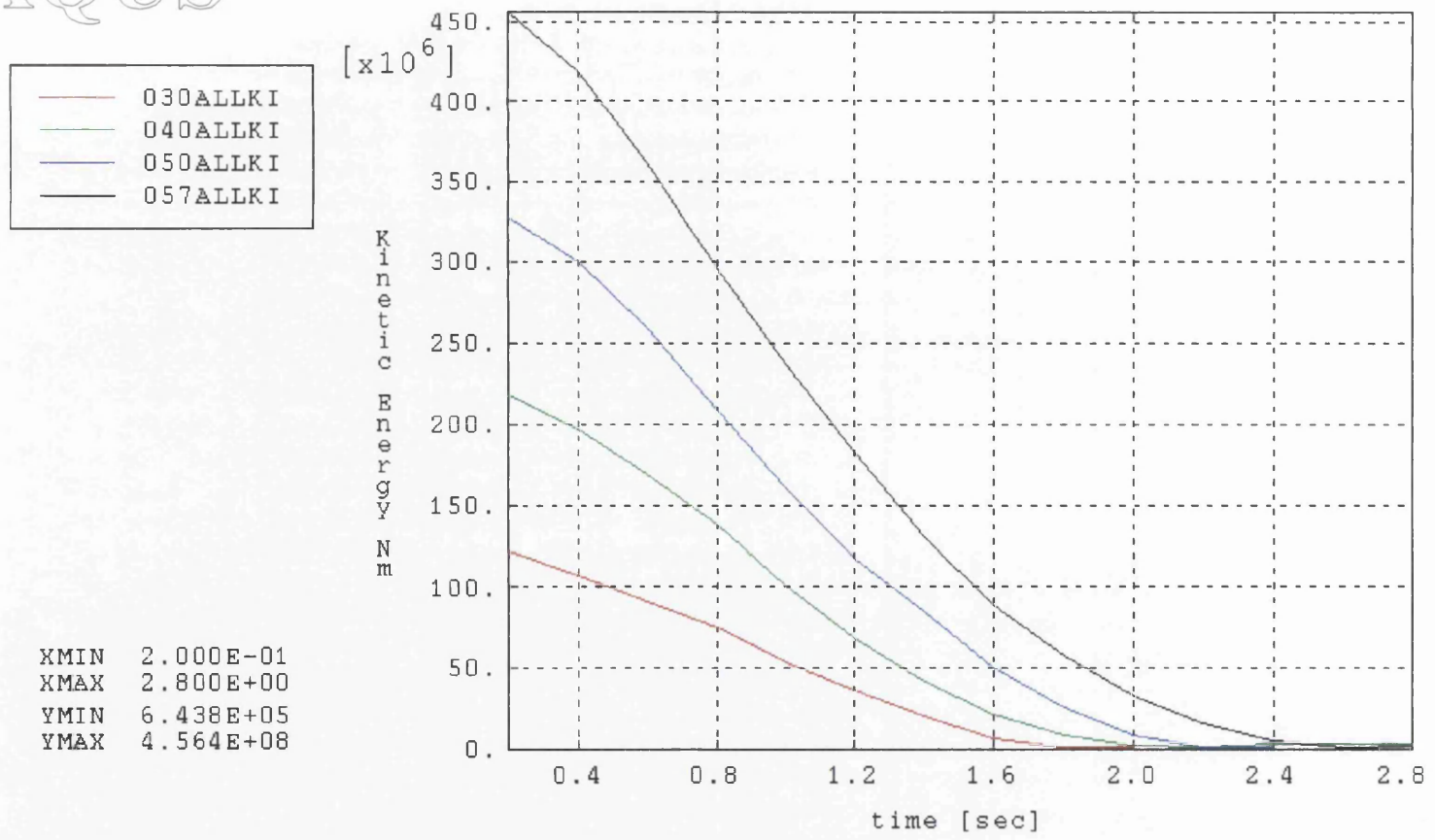


**Figure A3-3.8** *Kinetic energy versus Time for all the concepts*

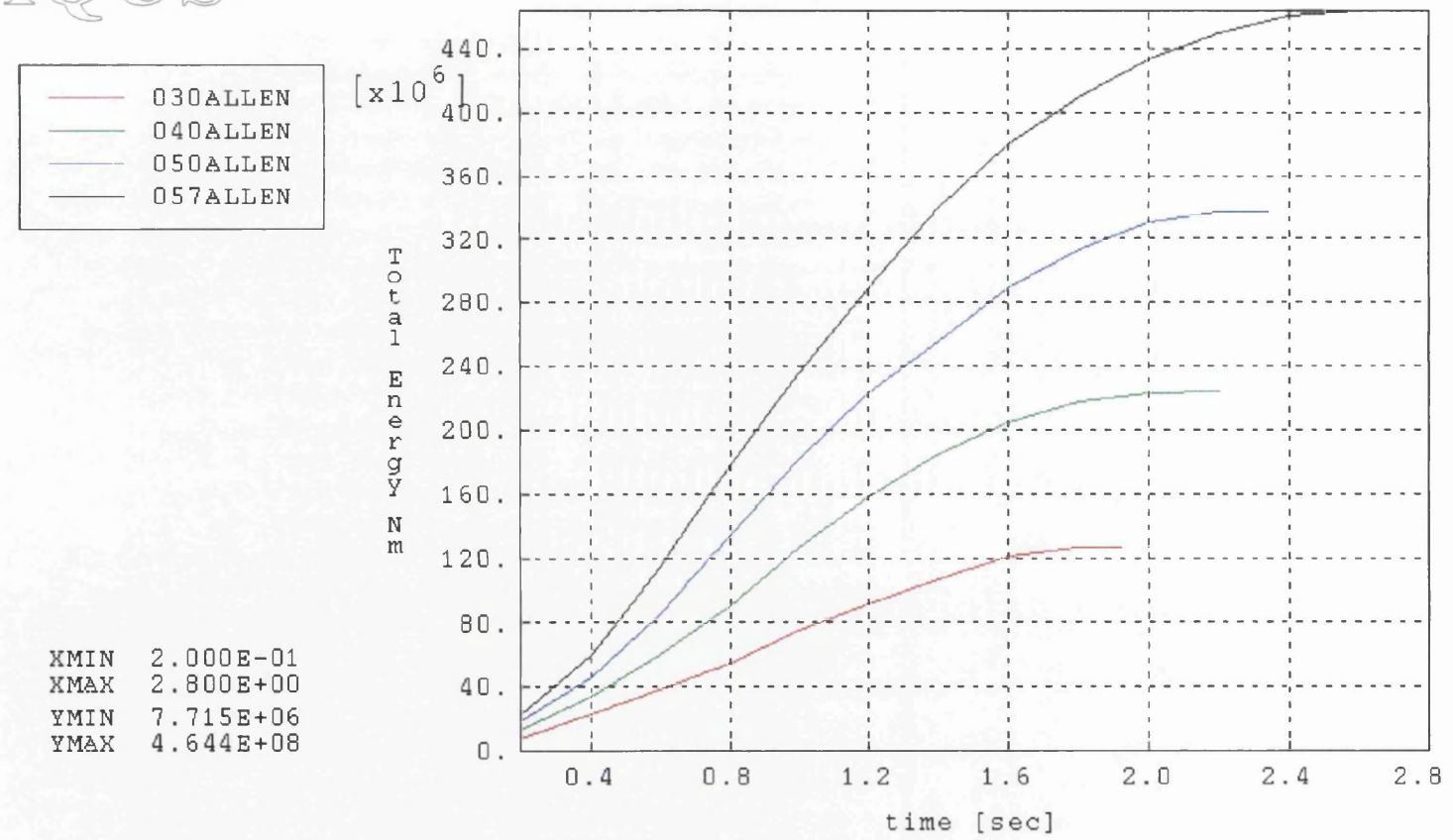


**Figure A3-3.9** *Total energy versus time for all the concepts*

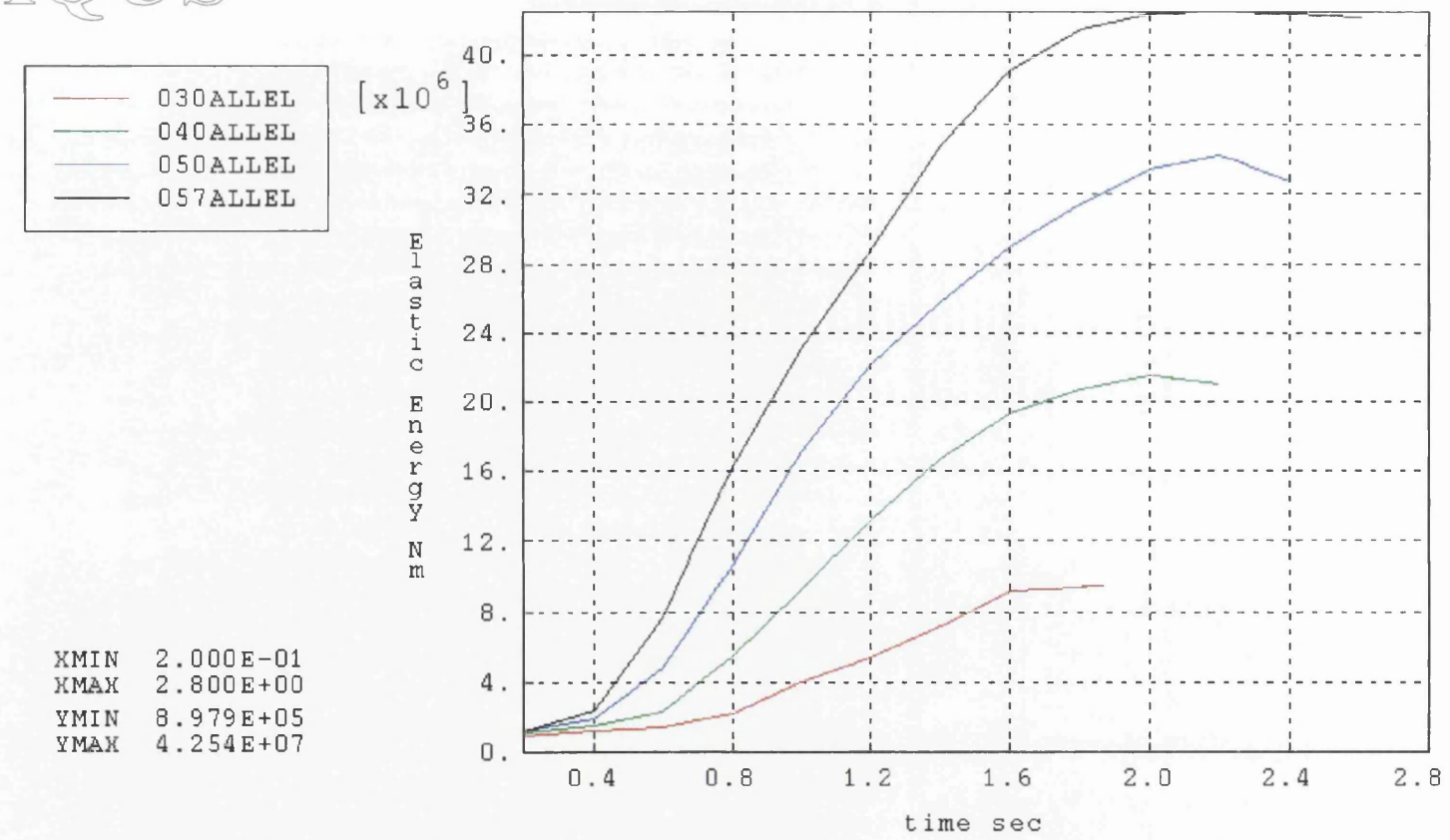


**Figure A3-3.10** *Elastic energy versus Time for all the concepts*

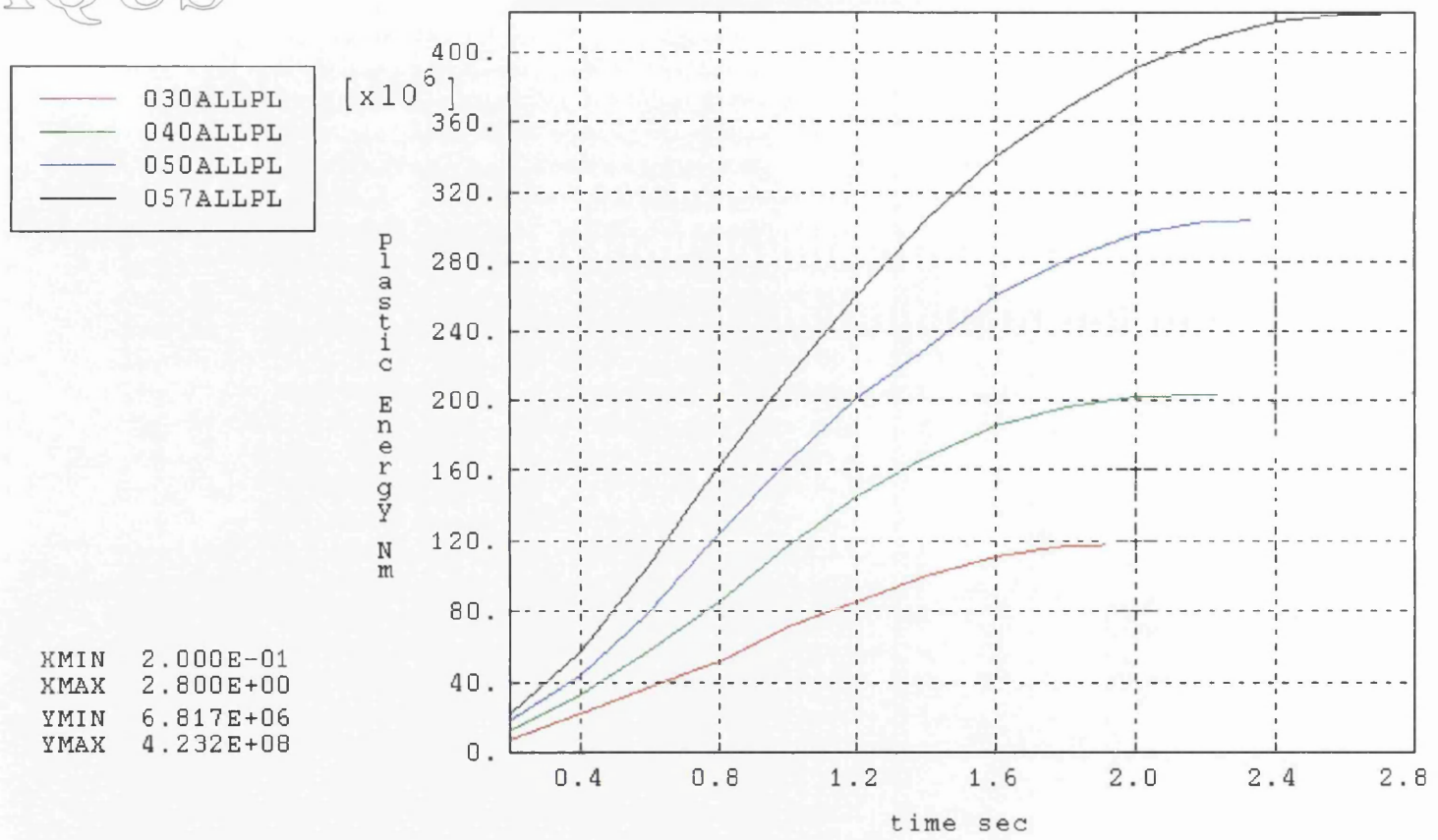


**Figure A3-3.11** *Plastic energy versus Time for all the concepts*

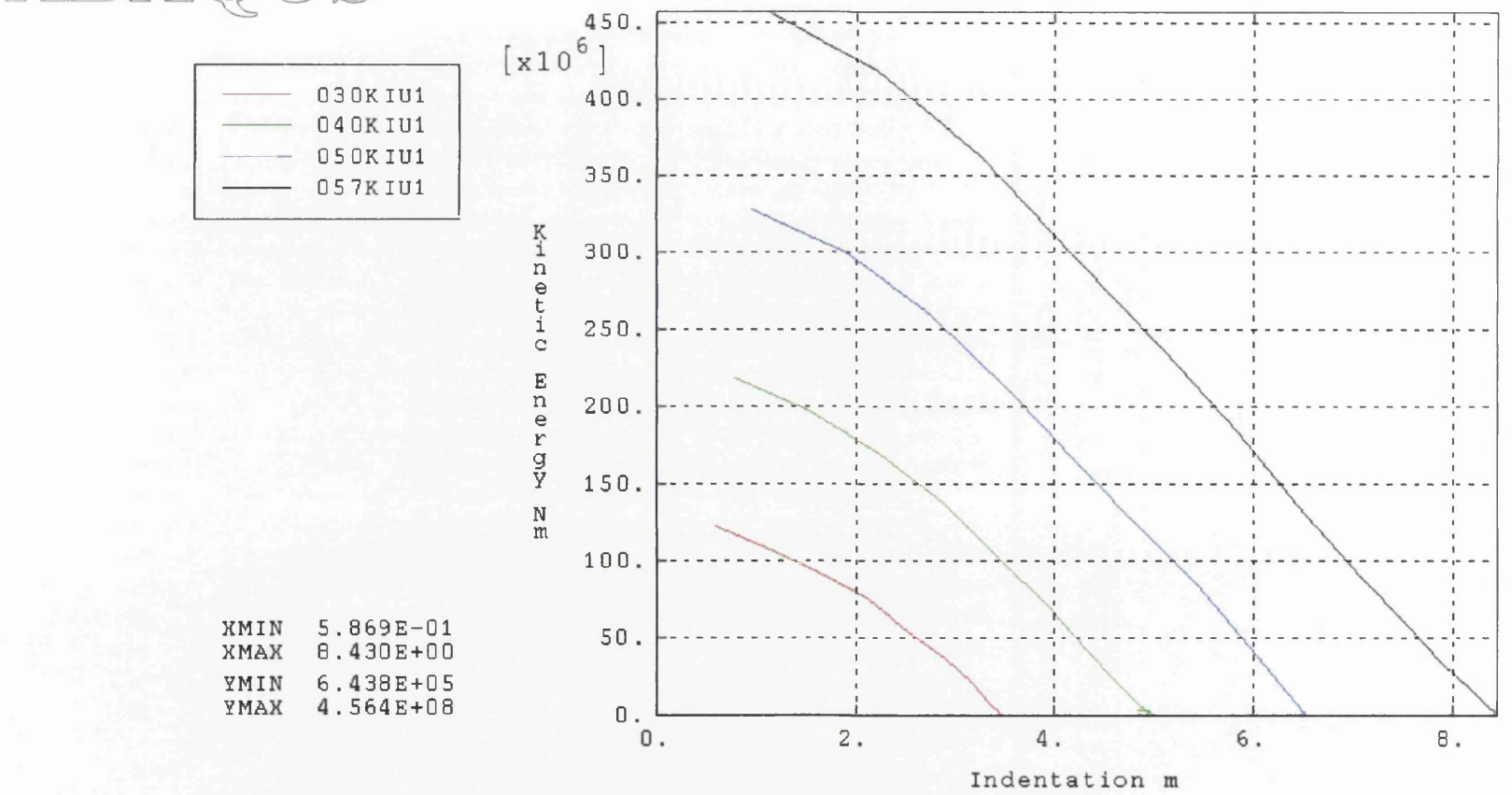


**Figure A3-3.12** *Kinetic energy versus Indentation for all the concepts*

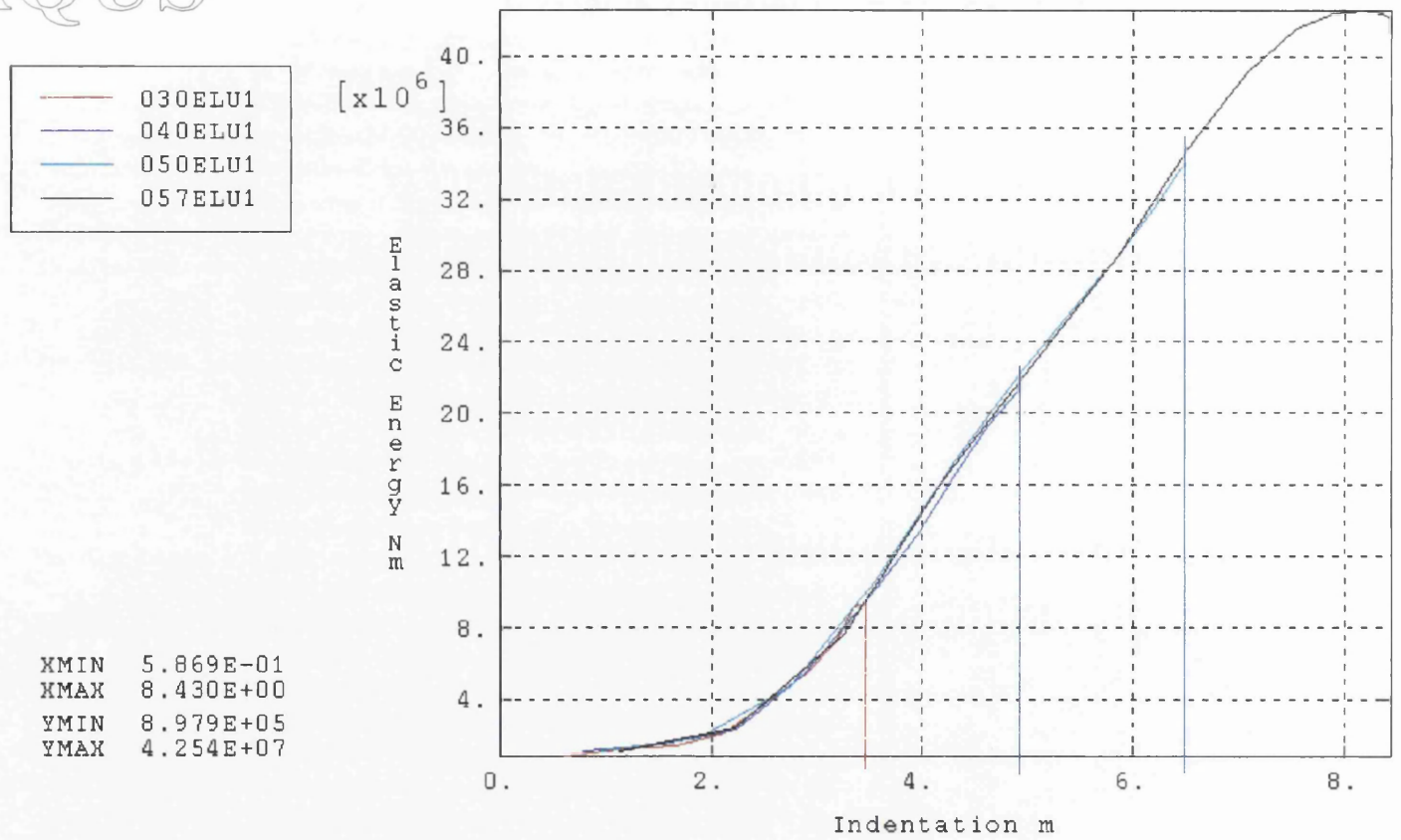


**Figure A3-3.13** *Elastic energy versus Indentation for all the concepts*

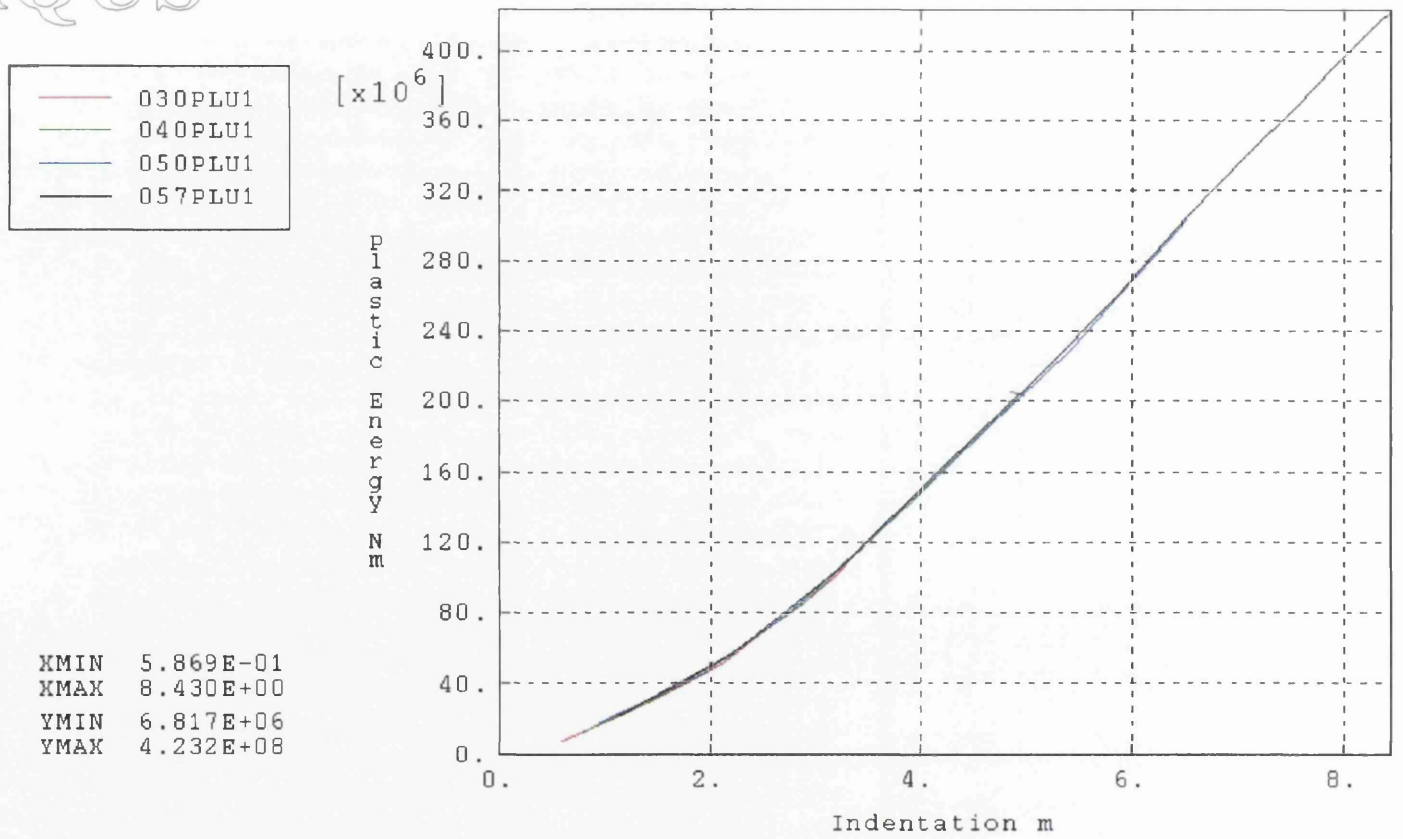


**Figure A3-3.14** *Plastic energy versus Indentation for all the concepts*

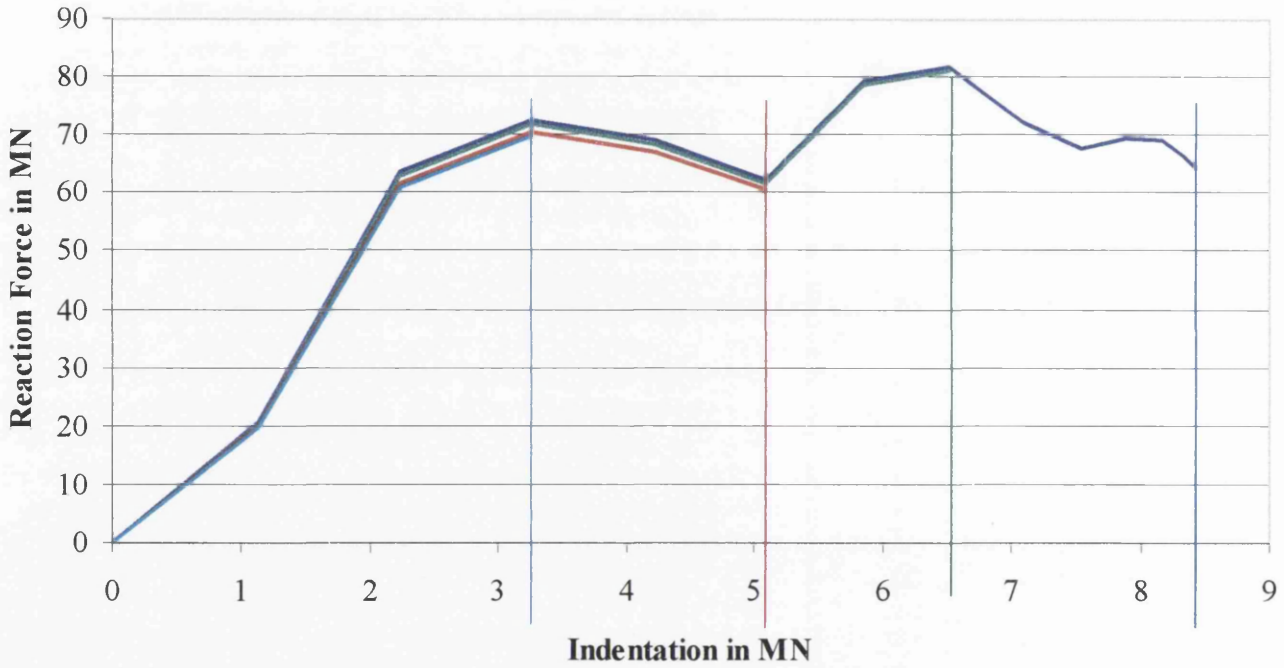


**Figure A3-3.15** *Reaction Force versus Indentation for all the concepts*

# APPENDIX IV

## ABAQUS Input File

```
*heading
collision
*node, nset=wallref
15000,15.400,-5.000,-2.000
*node, nset=main,      input=3dshell.dat
*node, nset=bowstrip, input=bolbus.dat
*node, nset=auxbar,    input=auxbar.dat
*node, nset=auxplwr1, input=auxplwr1.dat
*node, nset=auxblong, input=auxblong.dat
*node, nset=wallnode, input=wallnode.dat
*node, nset=nbulk77,   input=nbulk77.dat
*node, nset=nbulk87,   input=nbulk87.dat
*node, nset=centbulk, input=centbulk.dat
*node, nset=coreg,     input=coreg.dat
*node, nset=dck3378,   input=dck3378.dat
*node, nset=dck1790,   input=dck1790.dat
*node, nset=dck5048,   input=dck5048.dat
*node, nset=dck1250,   input=dck1250.dat
*node, nset=dck1261,   input=dck1261.dat
*node, nset=dck1537,   input=dck1537.dat
*node, nset=dck1058,   input=dck1058.dat
*node, nset=dck6718,   input=dck6718.dat
*node, nset=dck8257,   input=dck8257.dat
*node, nset=bulk,      input=bulk.dat
***************
***************
*nset,nset=boundar0, generate
1,51,1
*nset,nset=boundary
boundar0,coreg,nbulk77
*nset, nset=all1
main,bowstrip,nbulk77,coreg,dck8257,centbulk,nbulk87,
dck3378,dck1790,dck5048,dck1250,dck1261,dck1537,dck1058,
*nset, nset=all
all1,dck6718,bulk
*nset, nset=col, generate
9,43,1
60,94,1
111,145,1
162,196,1
213,247,1
264,298,1
```

```
315,349,1
366,400,1
417,451,1
470,500,1
519,553,1
573,601,1
624,652,1
675,703,1
726,754,1
777,805,1
828,856,1
879,907,1
5000,5011,1
5013,5040,1
5101,5443,1
2001,2010,1
2014,2029,1
2033,2176,1
1081,1210,1
2619,2623,1
2625,2633,1
2635,2651,1
2653,2660,1
2662,2669,1
2671,2677,1
2679,2684,1
2686,2692,1
2693,2698,1
2700,2704,1
2706,2709,1
2711,2715,1
3001,3213,1
3252,3264,1
3266,3461,1
3502,3516,1
3518,3578,1
3601,3609,1
3611,3627,1
3629,3644,1
3646,3660,1
3662,3674,1
3676,3686,1
3688,3697,1
3699,3707,1
3709,3716,1
3718,3721,1
3731,3967,1
*******
***** beams
*******
```

```
*element,type=b31,input=stifbulk.dat,  elset=stifbulk
*element,type=b31,input=bar.dat,       elset=b21
*element,type=b31,input=plwri2.dat,    elset=b21b
*element,type=b31,input=longbar.dat,   elset=longbar
*element,type=b31,input=longbar2.dat,   elset=longbar2
*******
***** shell
*******
*element,type=s3r,input=shel22.dat,    elset=shel22
*element,type=s3r,input=shel15.dat,    elset=shel15
*element,type=s3r,input=shel12.dat,    elset=shel12
*element,type=s4r,input=shel154.dat,   elset=shel154
*element,type=s4r,input=shel224.dat,   elset=shel224
***element,type=s4r,input=blbshell.dat,elset=blbshel
***element,type=s3r,input=blbshel3.dat,elset=blbshel3
***element,type=s3r,input=bowshel3.dat,elset=bowshel3
*******
***** bulkheads
*******
*element,type=s4r,input=ecoreg.dat,    elset=ecoreg
*element,type=s3r,input=btmcoreg.dat,  elset=btmcoreg
*element,type=s4r,input=ebulk377.dat,  elset=ebulk77
*element,type=s3r,input=ebulk873.dat,  elset=ebulk873
*element,type=s4r,input=ebulk87.dat,   elset=ebulk87
*element,type=s4r,input=ecntbulk.dat,  elset=ecntbulk
*element,type=s4r,input=ebulk.dat,     elset=ebulk
*******
***** decks
*******
*element,type=s4r,input=edk8257.dat,   elset=edk8257
*element,type=s3r,input=edk82573.dat,  elset=edk82573
*element,type=s4r,input=edk3378.dat,   elset=edk3378
*element,type=s3r,input=edk33783.dat,  elset=edk33783
*element,type=s4r,input=edc1790.dat,   elset=edk1790
*element,type=s3r,input=edc17903.dat,  elset=edk17903
*element,type=s4r,input=edc5048.dat,   elset=edk5048
*element,type=s3r,input=edc50483.dat,  elset=edk50483
*element,type=s4r,input=edk1250.dat,   elset=edk1250
*element,type=s3r,input=edk12503.dat,  elset=edk12503
*element,type=s4r,input=edk1261.dat,   elset=edk1261
*element,type=s3r,input=edk12613.dat,  elset=edk12613
*element,type=s4r,input=edk1537.dat,   elset=edk1537
*element,type=s3r,input=edk15373.dat,  elset=edk15373
*element,type=s4r,input=edk1058.dat,   elset=edk1058
*element,type=s3r,input=edk10583.dat,  elset=edk10583
*element,type=s4r,input=edk6718.dat,   elset=edk6718
*element,type=s3r,input=edk67183.dat,  elset=edk67183
*******
***** Mass
*******
```

```
*element, type=mass, input=mass1.dat, elset=mass1
*element, type=mass, input=mass2.dat, elset=mass2
*element, type=mass, input=mass3.dat, elset=mass3
*******
***** rigid body
*******
*element,type=r3d4,input=wall.dat,elset=rigid
***************
***************
*elset,elset=ship
shel12,shel15,shel22,shel154,shel224
*elset,elset=scant
ecoreg,btmcoreg,ebulk77,ebulk873,ebulk87,ecntbulk,edk8257
,
edk82573,edk3378,edk33783,edk1790,edk17903,edk5048,
edk50483,edk1250,edk12503,edk1261,edk12613,edk1537,edk153
73
edk6718,edk67183,edk1058,edk10583
*elset,elset=bars
b21,b21b,stifbulk,longbar
*elset,elset=ola
scant,ship,bars
***************
*elset,elset=cor95,generate
3320,3324
3000,3079
2000,2369
3341,3345
*elset,elset=cor11,generate
3325,3336
3080,3271
2370,2847
3346,3357
*elset,elset=cor12,generate
3337,3339
3272,3319
2848,2879
7150,7174
3358,3360
*elset,elset=cent9,generate
5500,5544
5698,5702
*elset,elset=cent11,generate
5545,5652
5703,5715
*elset,elset=cent125,generate
5653,5697
5715,5717
7175,7177
*elset,elset=dia115,generate
```

```
6007,6011
6210,6211
6200,6201
5985,5989
5801,5870
*elset,elset=dia13,generate
5871,5968
6212,6214
6202,6204
5990,6001
6012,6023
*elset,elset=dia14,generate
5969,5984
6024,6028
6002,6006
6215,6219
6205,6209
*nset,nset=edge,generate
1,51
*beam section,elset=b21,material=steel1,section=i
0.05,0.10,0.075,0.70,0.0135,0.0135,0.0135
*beam section,elset=b21b,material=steel1,section=i
0.15,0.30,0.15.0.65,0.0135,0.0135,0.0135
*beam section,elset=stifbulk,material=steel1,section=i
0.45,0.90,0.15,0.65,0.0120,0.0100,0.0220
*beam section,elset=longbar,material=steel1,section=i
0.125,0.25,0.15,0.65,0.0135,0.0135,0.014
*beam section,elset=longbar2,material=steel1,section=i
0.075,0.15,0.09,0.65,0.0100,0.0100,0.009
*shell section,elset=shel22,material=steel
0.022
*shell section,elset=shel15,material=steel
0.015
*shell section,elset=shel12,material=steel
0.012
*shell section,elset=shel154,material=steel
0.015
*shell section,elset=shel224,material=steel
0.022
*shell section,elset=ebulk,material=steel
0.060
*shell section,elset=cor95,material=steel
0.0095
*shell section,elset=cor11,material=steel
0.011
*shell section,elset=cor12,material=steel
0.012
*shell section,elset=cent9,material=steel
0.009
*shell section,elset=cent11,material=steel
```

```
0.011
*shell section,elset=cent125,material=steel
0.0125
*shell section,elset=dia115,material=steel
0.0115
*shell section,elset=dia13,material=steel
0.013
*shell section,elset=dia14,material=steel
0.014
*shell section,elset=edk8257,material=steel
0.010
*shell section,elset=edk82573,material=steel
0.010
*shell section,elset=edk3378,material=steel
0.012
*shell section,elset=edk33783,material=steel
0.012
*shell section,elset=edk1790,material=steel
0.012
*shell section,elset=edk17903,material=steel
0.012
*shell section,elset=edk5048,material=steel
0.010
*shell section,elset=edk50483,material=steel
0.010
*shell section,elset=edk1250,material=steel
0.012
*shell section,elset=edk12503,material=steel
0.012
*shell section,elset=edk1261,material=steel
0.010
*shell section,elset=edk12613,material=steel
0.010
*shell section,elset=edk1537,material=steel
0.009
*shell section,elset=edk15373,material=steel
0.009
*shell section,elset=edk1058,material=steel
0.010
*shell section,elset=edk10583,material=steel
0.010
*shell section,elset=edk6718,material=steel
0.010
*shell section,elset=edk67183,material=steel
0.010
*rigid body, elset=rigid, ref node=15000
*material, name=steel
*density
7850.
*elastic
```

```
211e9,0.3
*plastic
245e6,0
*material, name=steel1
*density
3925.
*elastic
211e9,0.3
*plastic
245e6,0
****
**        total mass+added mass =28875.00 10^3 kgr
**        mass of bow section   =  884.30 10^3 kgr
**        ------------------------------------
**        mass remaing          =27990.71 10^3 kgr
**
**     BOTTOM     mass1= (45 %) =370465.28 x 34
**     MIDDLE     mass2= (35 %) =279907.10 x 35
**     TOP        mass3= (20 %) =207338.59 x 27
**
*mass, elset=mass1
370465.28
*mass, elset=mass2
279907.10
*mass, elset=mass3
207338.59
*initial conditions, type=velocity
all,1,5.76
******boundary conditions
***
*boundary
15000,1,6
boundary,zsymm
*restart,write,num=25
*step
*dynamic,explicit
,5.0
*surface definition,name=wall
rigid,spos
*contact node set, name=collo
col,
*contact pair
wall,collo
*history output,time=0.05
*node history,nset=nbulk87
u,v,a
*end step
```

# FIGURES

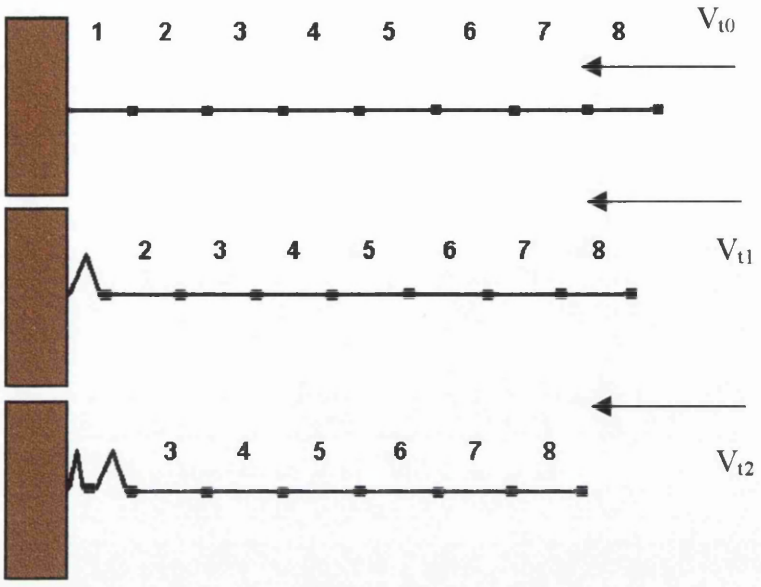


**Figure 3.1** *Collapse of a structural member on a rigid wall. Members 1-8 are collapsing one after the other.*

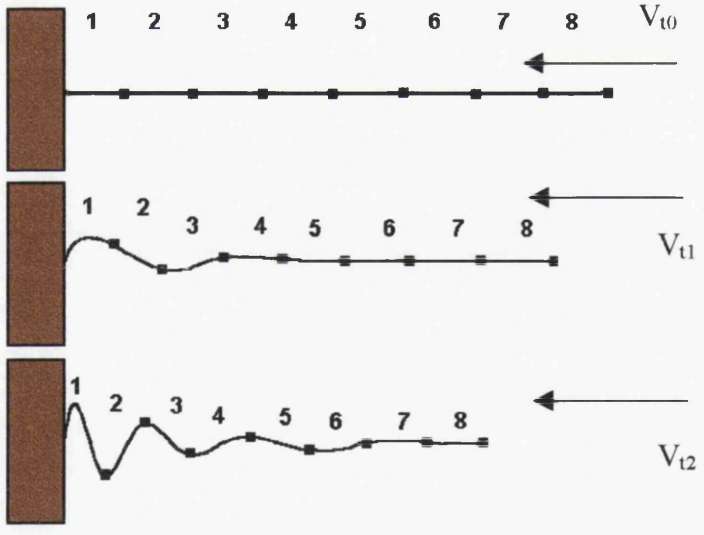


**Figure 3.2** *Collapse of a structural member on a rigid wall. The collapse of member I is affecting member i+1*

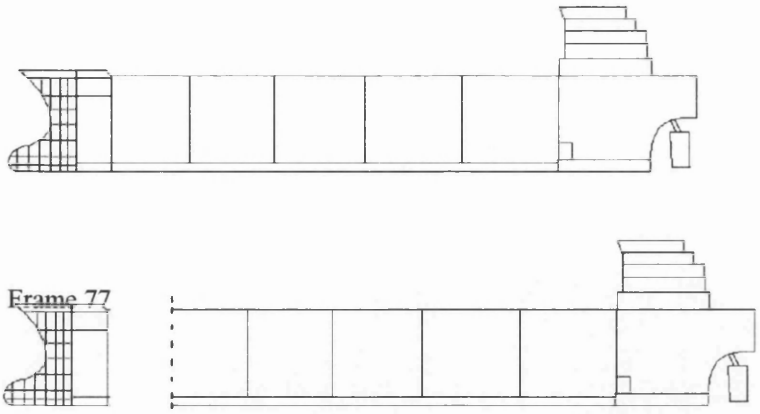


**Figure 3.3** *The detachment of the bow from the whole vessel*

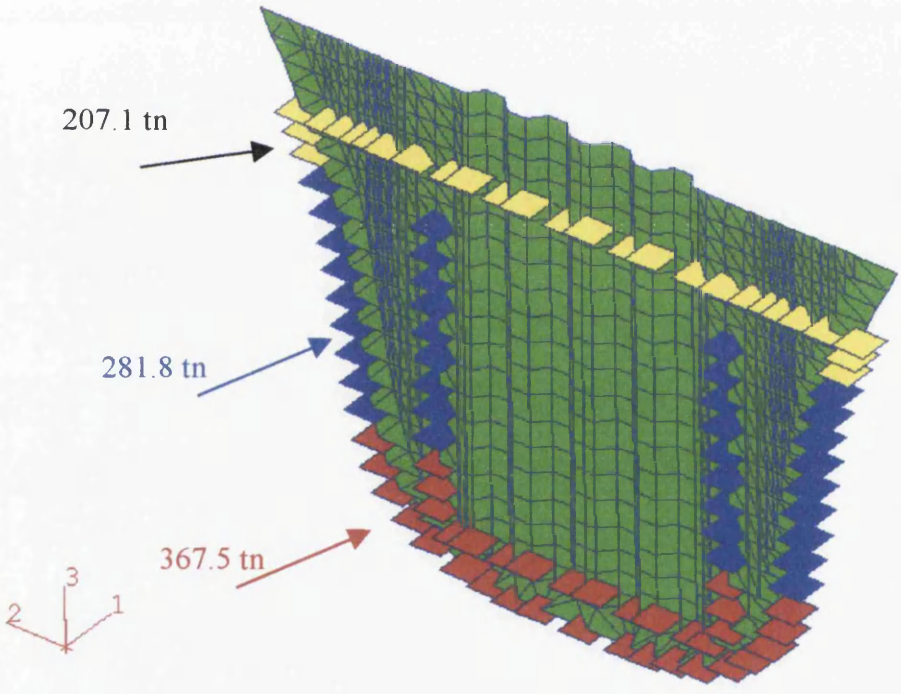


**Figure 3.4** *The collision bulkhead 77, with the lumped masses attached on it. Three different types of lumped masses have been considered. The values shown include the added mass effect.*

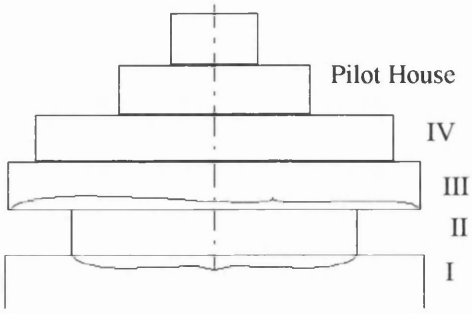


**Figure 3.5** *Typical Accommodation Block*

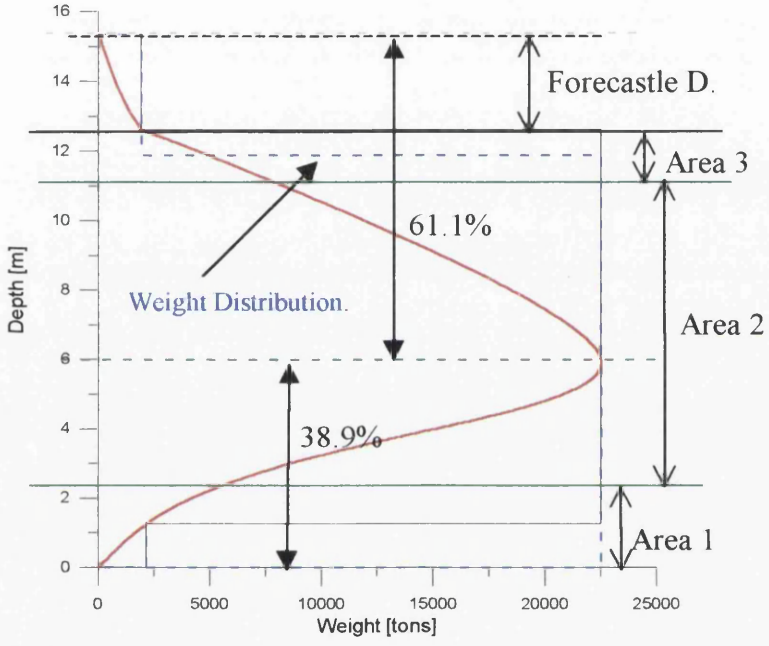


**Figure 3.6** *Weight distribution along the depth. The red curve denotes the interpolated weight distribution along the depth of the vessel. The blue curve displays the actual weight distribution, while the green dotted line shows the mean vertical centre of gravity.*

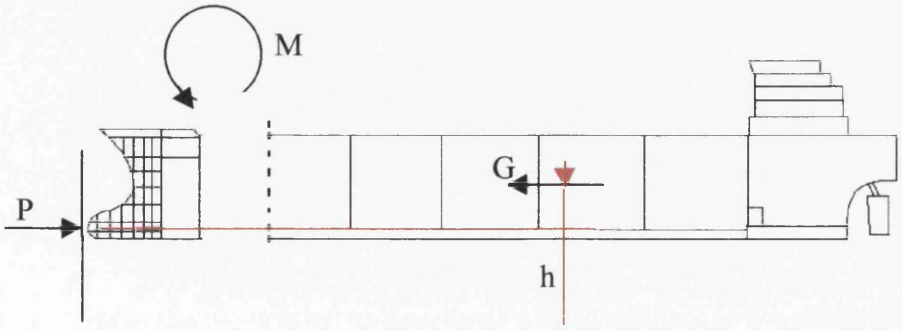


**Figure 3.7** *Forces acting on the tanker and moment on B77*

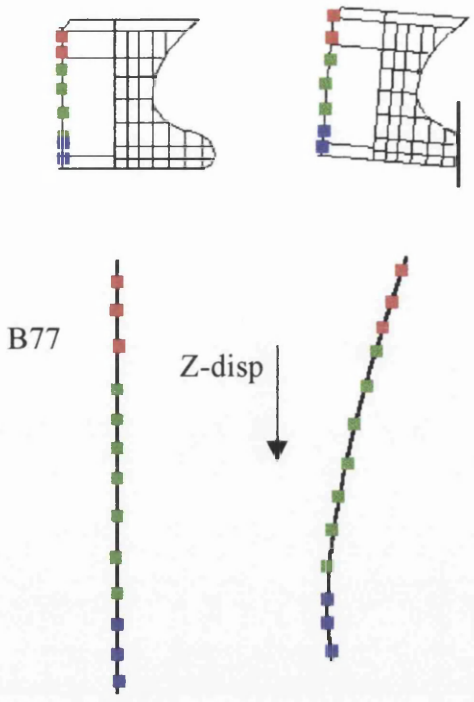


**Figure 3.8** *Rotational deformation and vertical translation on B77*

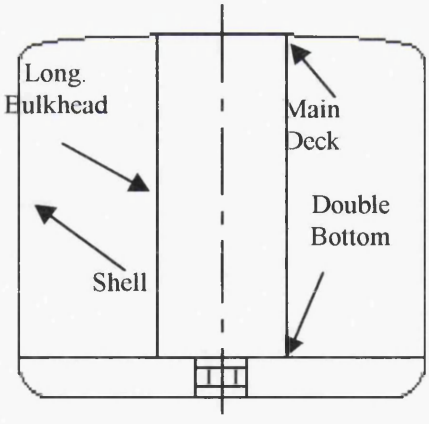


**Figure 3.9** *Midship section*

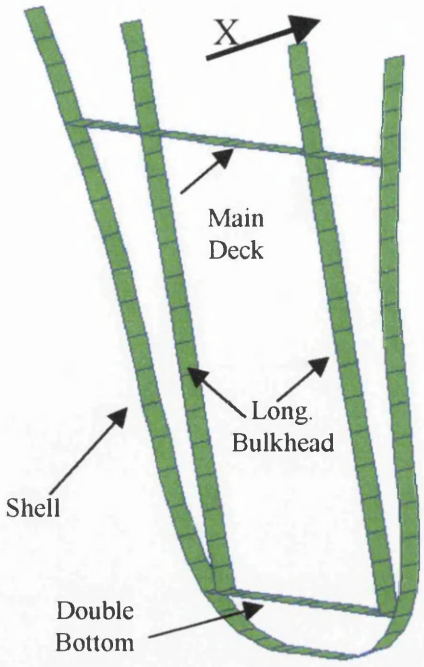


**Figure 3.10** *Structural members behind B77 following relevant arrangement with the midship section*

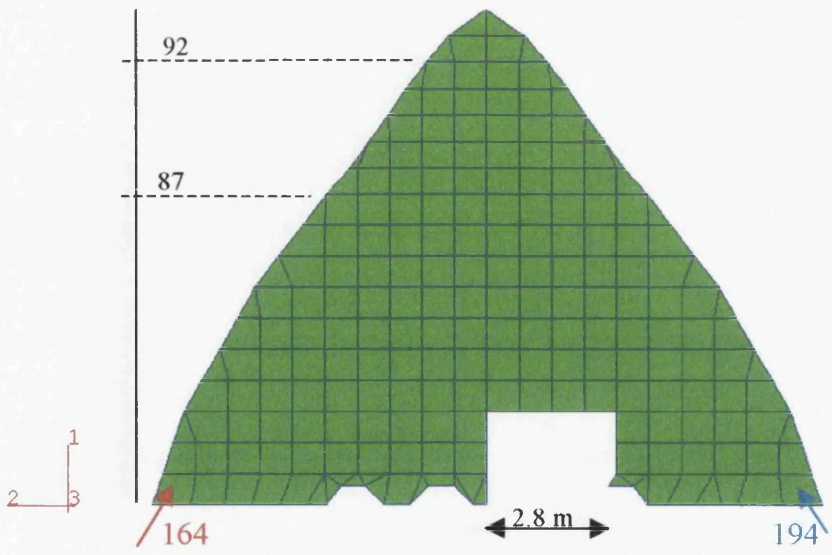


**Figure 3.11** *Top View of Deck 4. Intercostal element 164, 194 show different displacement on axis 1, during the impact. The non-symmetrical geometry of this deck is accounted as a reason for this phenomenon.*

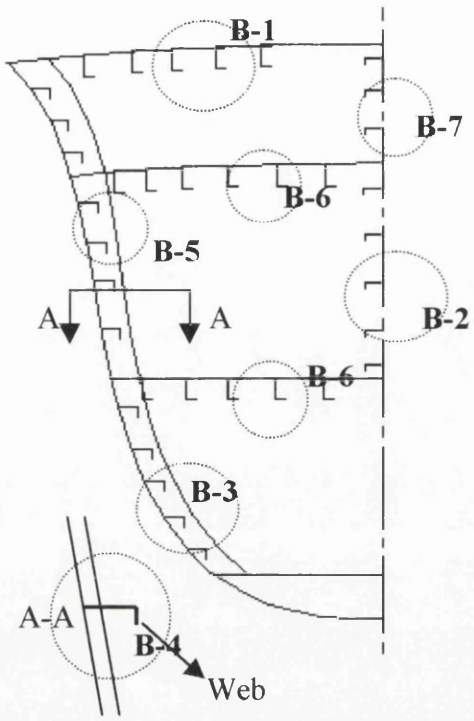


**Figure 3.12** *Frame 80. 7 different categories of Beam Elements are shown. Beams shown as B6 are the same on both decks.*

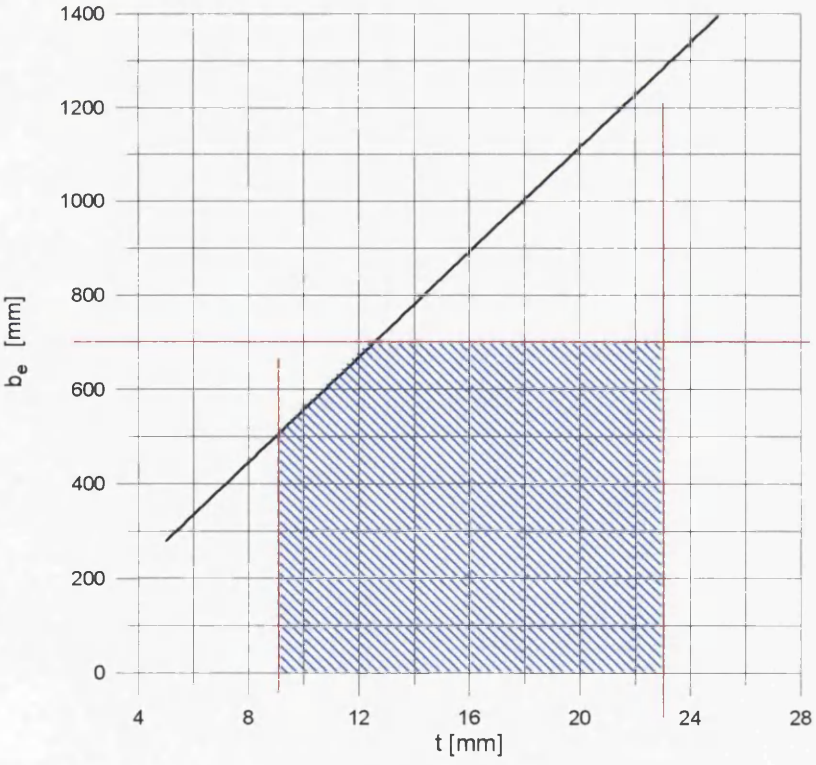


**Figure 3.13** *Effective plate width $b_e$ versus plate thickness t in mm. Whereas $b_e > b$ then $b_e = b$. In this model $b_{max} = 700$mm, hence $b_{e\,\{MAX\}} = 700$ mm. From $t = 9$mm to $t = 12.5$mm $b_e = 55.76 \cdot t$ [mm] from equation 3.5.*

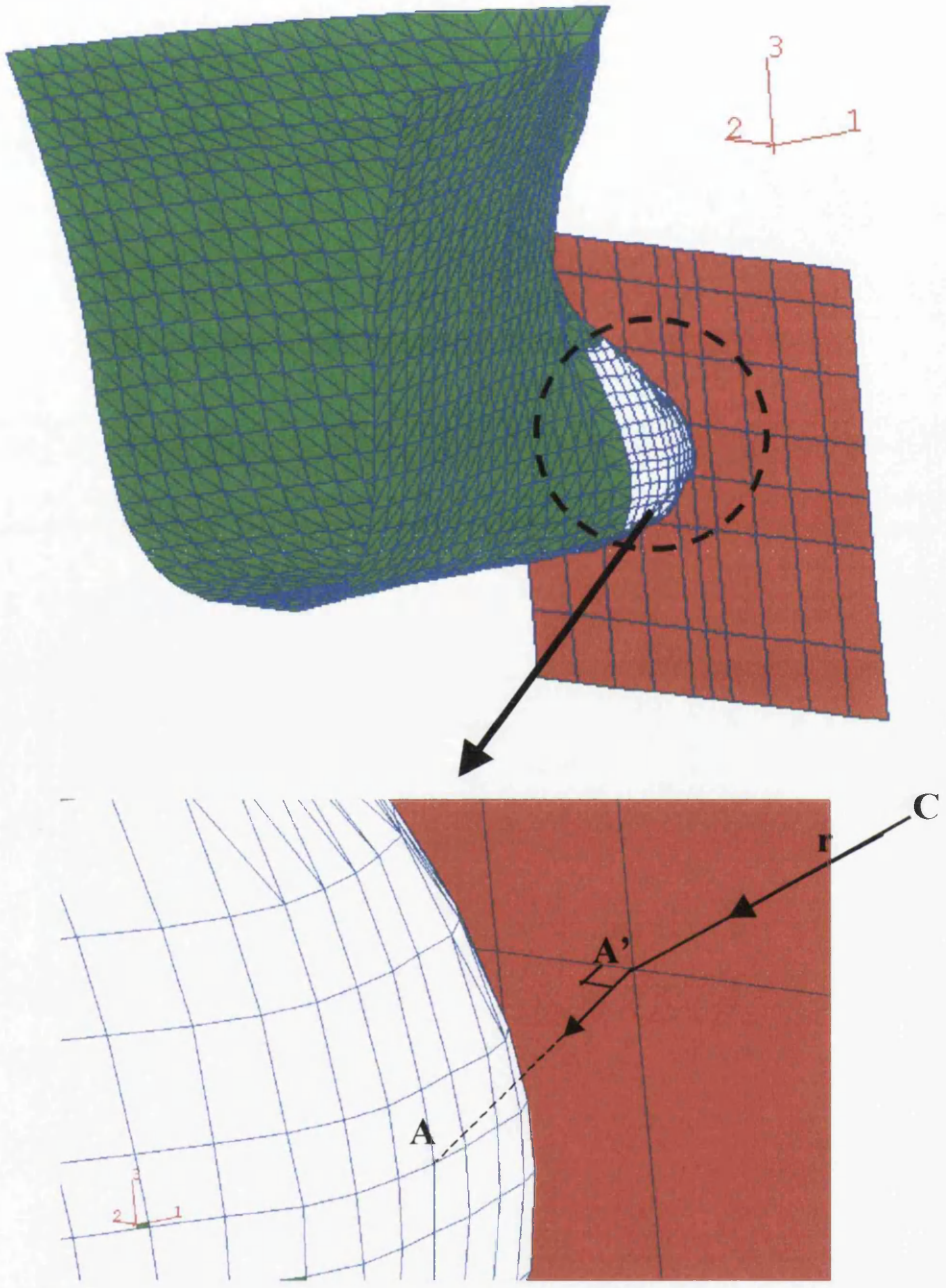


**Figure 3.14** *The red surface denotes the rigid surface, in which the bow collides. The rigid surface is non-deformable and does not absorb any energy.*

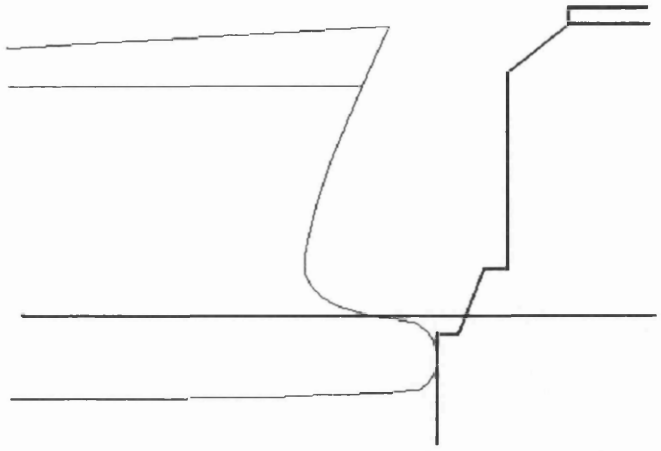

**Figure 3.15** *The ship in ballast condition and the rigid wall*

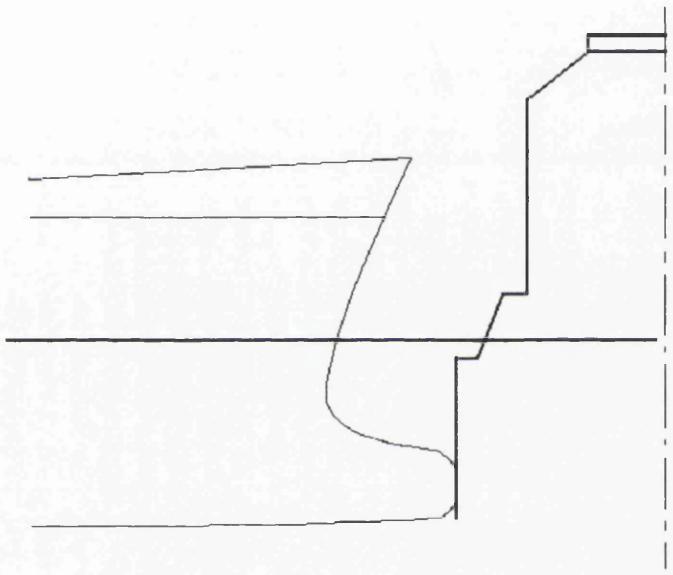

**Figure 3.16** *The ship in full load condition and the rigid wall*

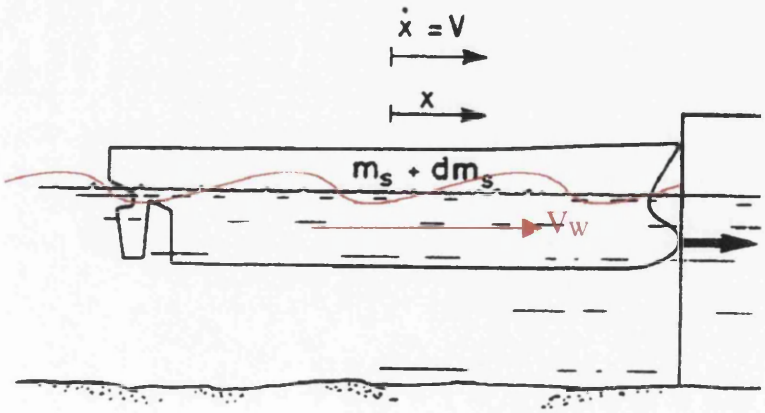


**Figure 3.17** *The free surface on the water along with the following wave in surge motion, during the collision*

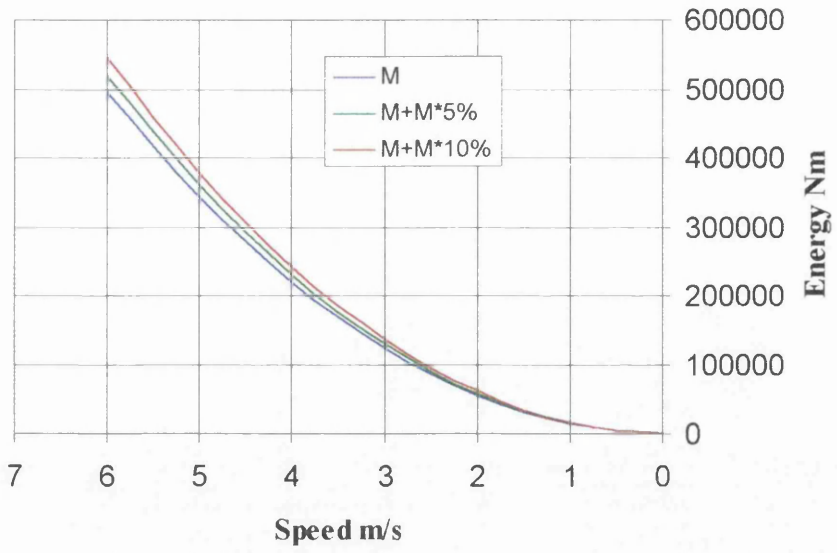


**Figure 3.18** *Kinetic energy at time t versus the added mass effect*

| ABAQUS MAIN FILE | | AUXILIARY FILES |
|---|---|---|
| NODAL CO-ORDINATES | } | 20 Individual Files |
| ELEMENT TOPOLOGY | | 42 Individual Files |
| GEOMETRIC PROPERTIES | | |
| MATERIAL PROPERTIES | | |
| RIGID SURFACE DEFINITION | | |
| INITIAL CONDITIONS | | |
| DYNAMIC PROPERTIES | | |
| RESULTS REQUEST | | |

**Figure 3.19** *The ABAQUS input file construction*

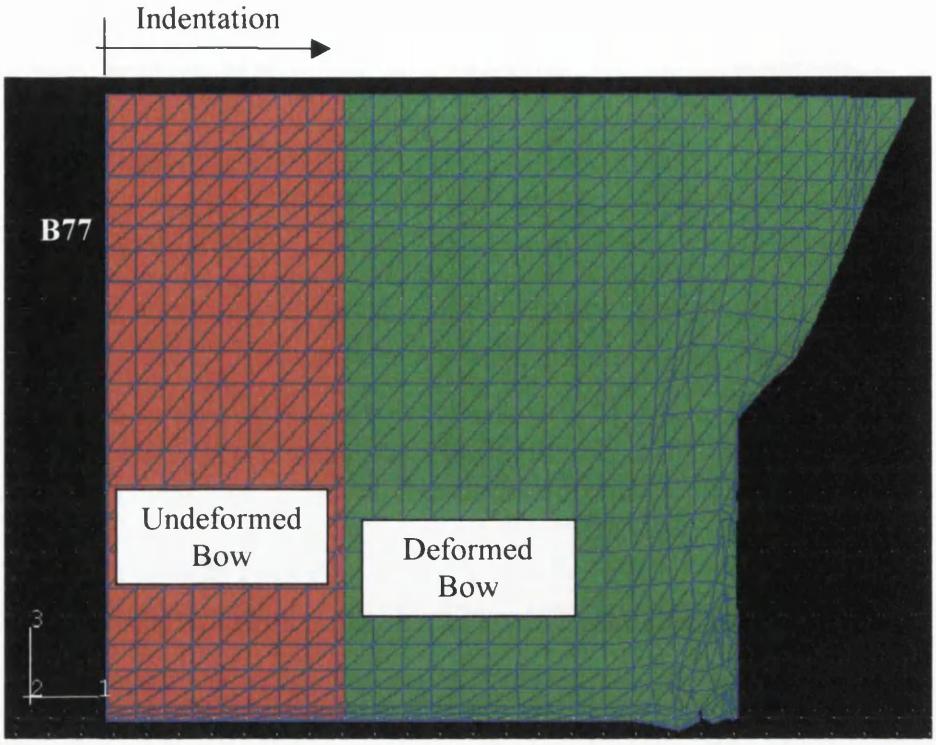


**Figure 3.20** *Example picture of a side view of the collided bow as those included in Figures A3-3.1 to 3.4*

Figure 3.21 a

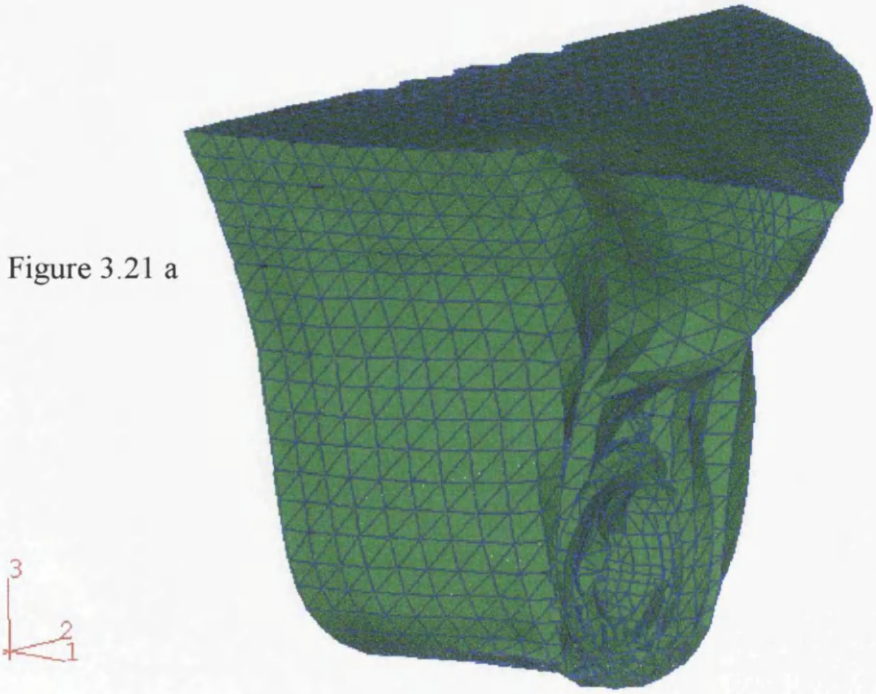

Figure 3.21 b

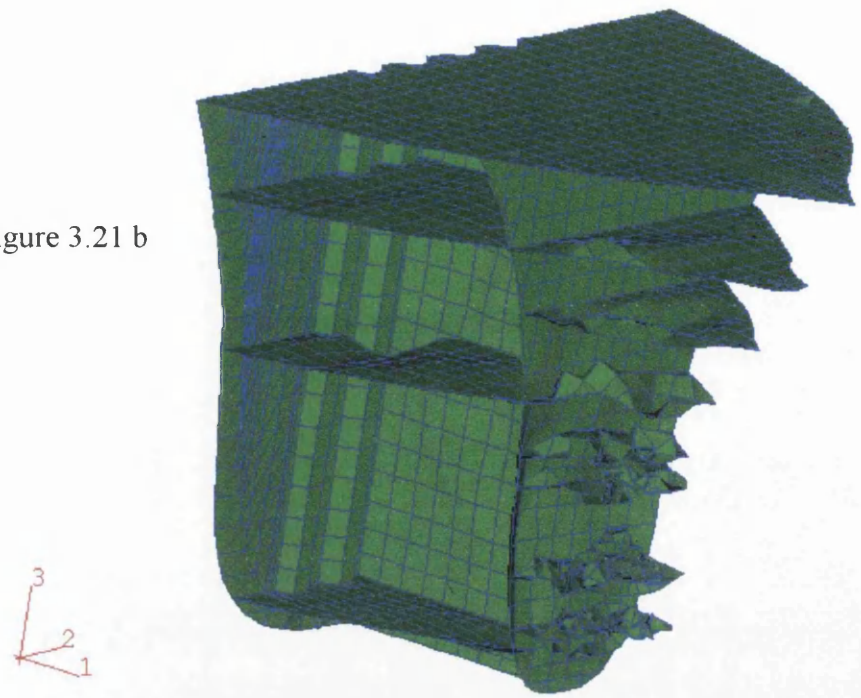


**Figure 3.21** *a, b Typical deformed 3D bow shape. The first one shows the outer skin, and the second one shows the inner arrangements.*

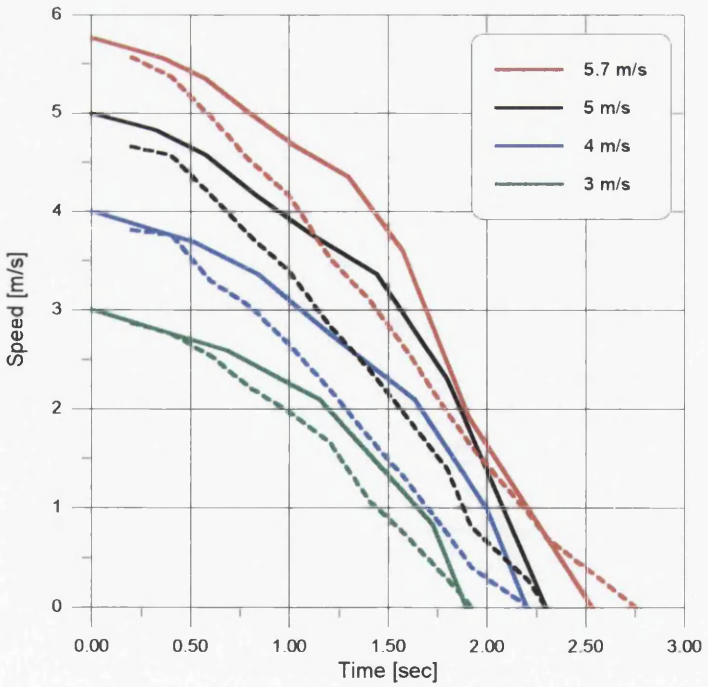


**Figure 3.22** *Comparison of the V-t curves for both ABAQUS and Gerard's empirical approach. The straight lines show the ABAQUS results and the dotted lines show the application of Gerard's formula.*

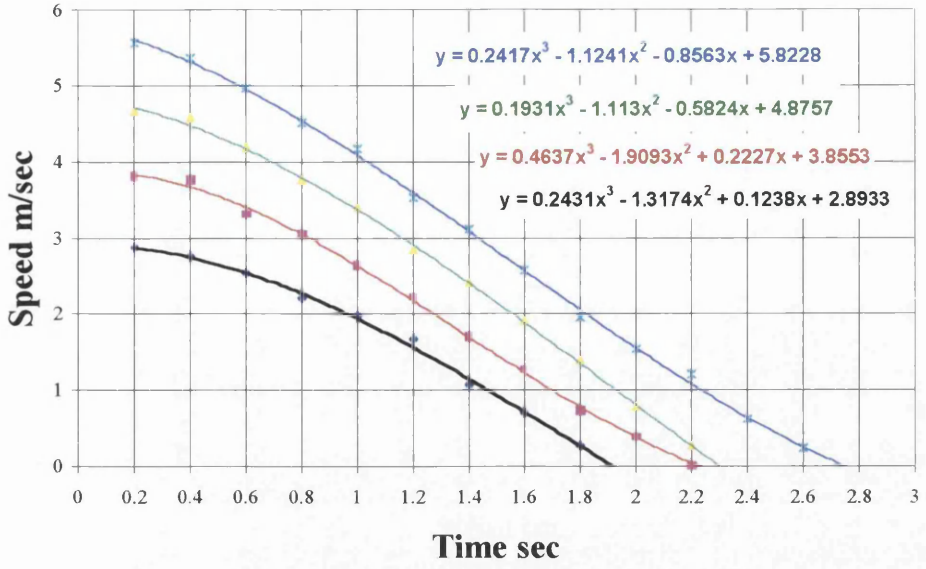


**Figure 3.23** *Regression analysis on the V-t curves derived from ABAQUS. The 3rd degree polynomials derived can are shown.*

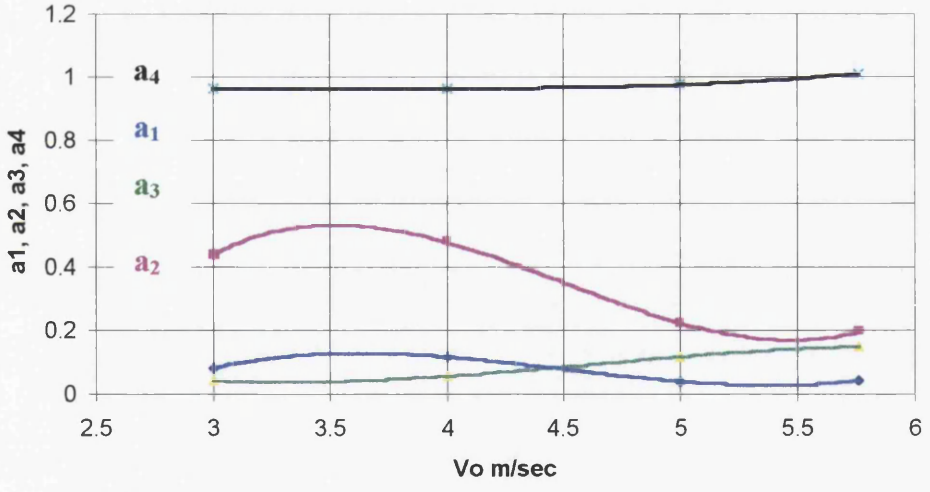


**Figure 3.24** *Coefficient $a_1$, $a_2$, $a_3$, $a_4$ in respect of the initial speed $V_o$. The 3rd degree regression polynomials are shown on Figure 3.32. These coefficients are valid for this vessel or one of a similar DWT*

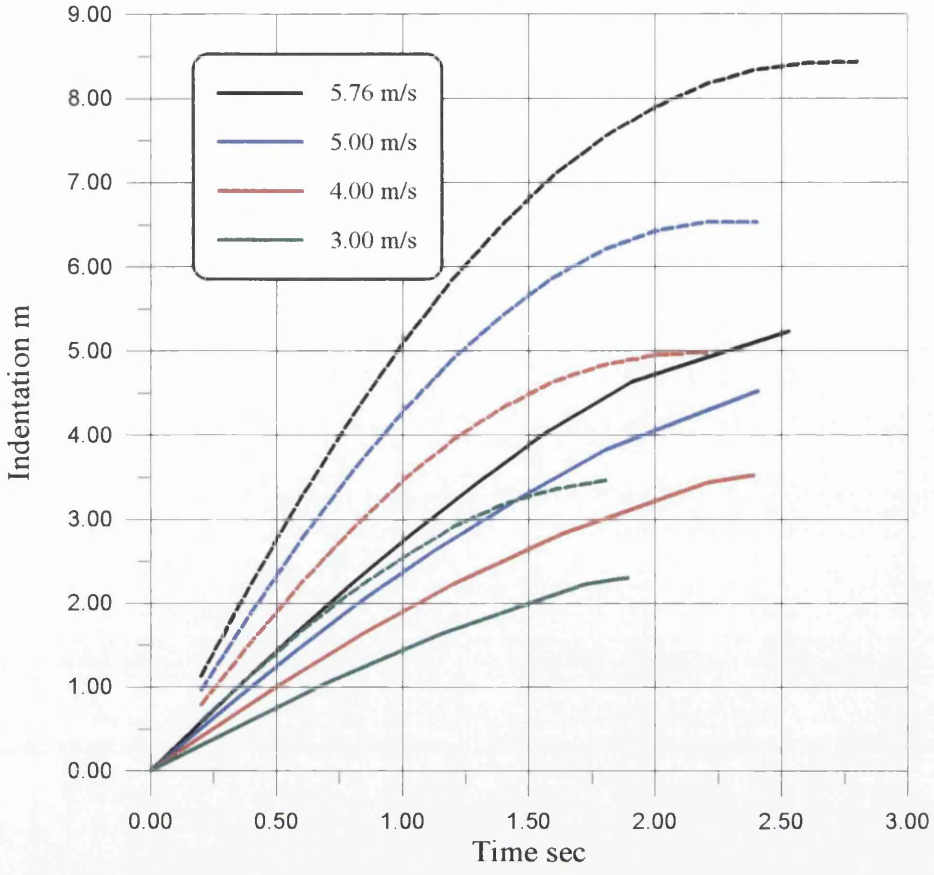


**Figure 3.25** *The time-Indentation curves for both the empirical approach and ABAQUS. The dotted lines are the numerical results*

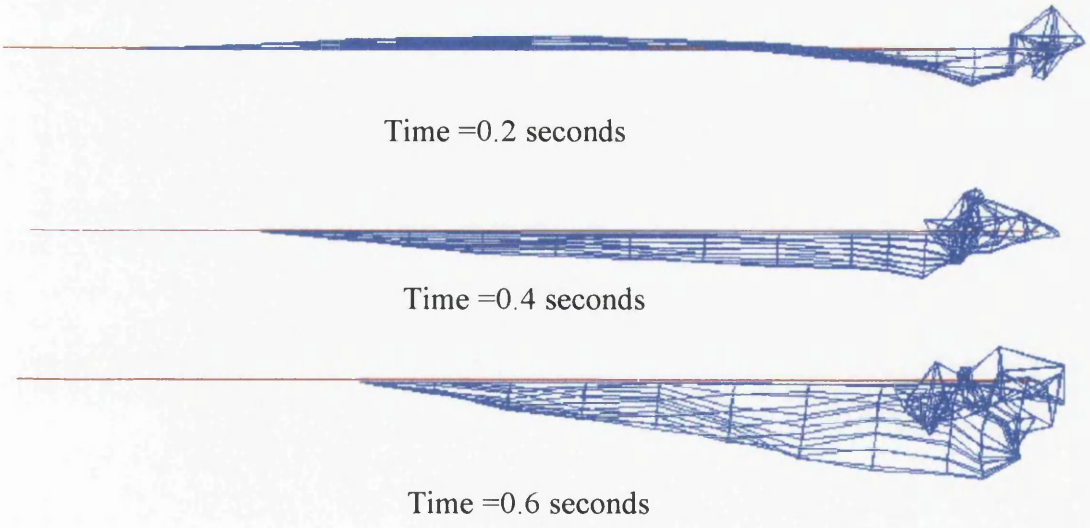

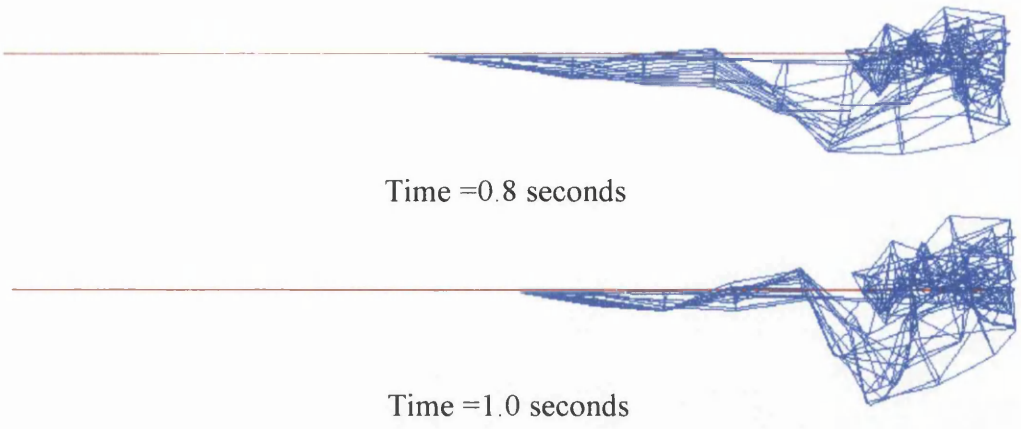


**Figure 3.26** *Folding mechanism of Deck 8 during the impact*

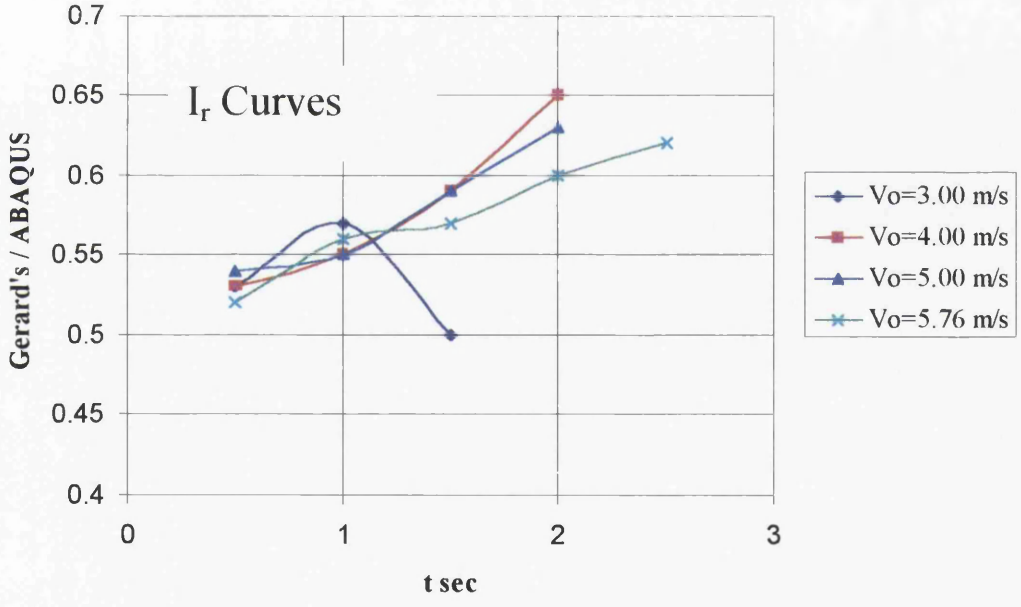


**Figure 3.27** *Ratio $I_r$, as interpolated from the finite element analysis.*

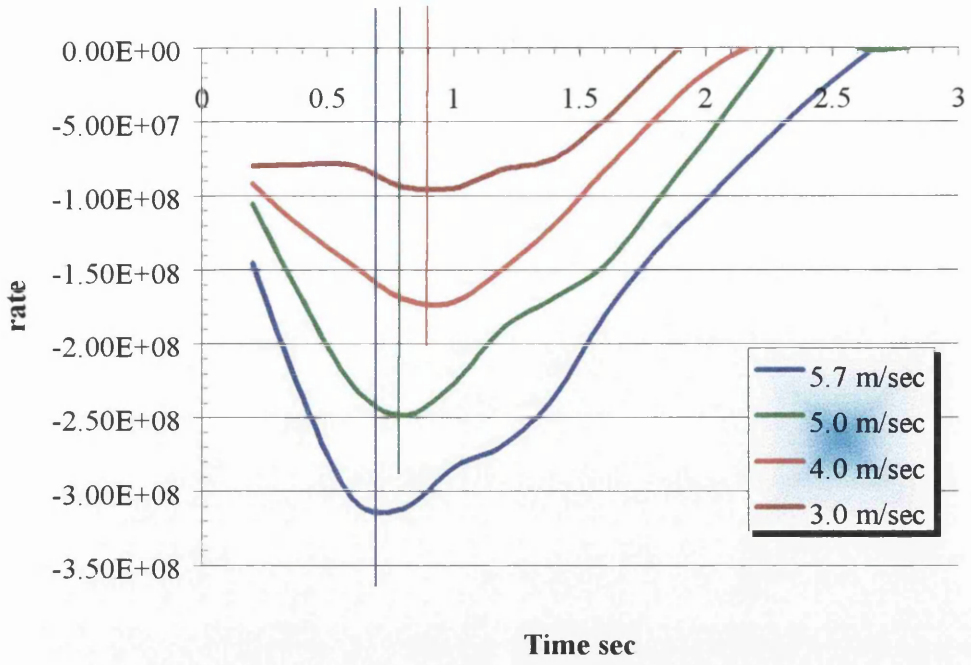


**Figure 3.28** *The rate of change in the kinetic Energy. The vertical lines show the times where the maxima occur. Conditions for 3.0 and 5.0 seconds have the maxima at the same time.*

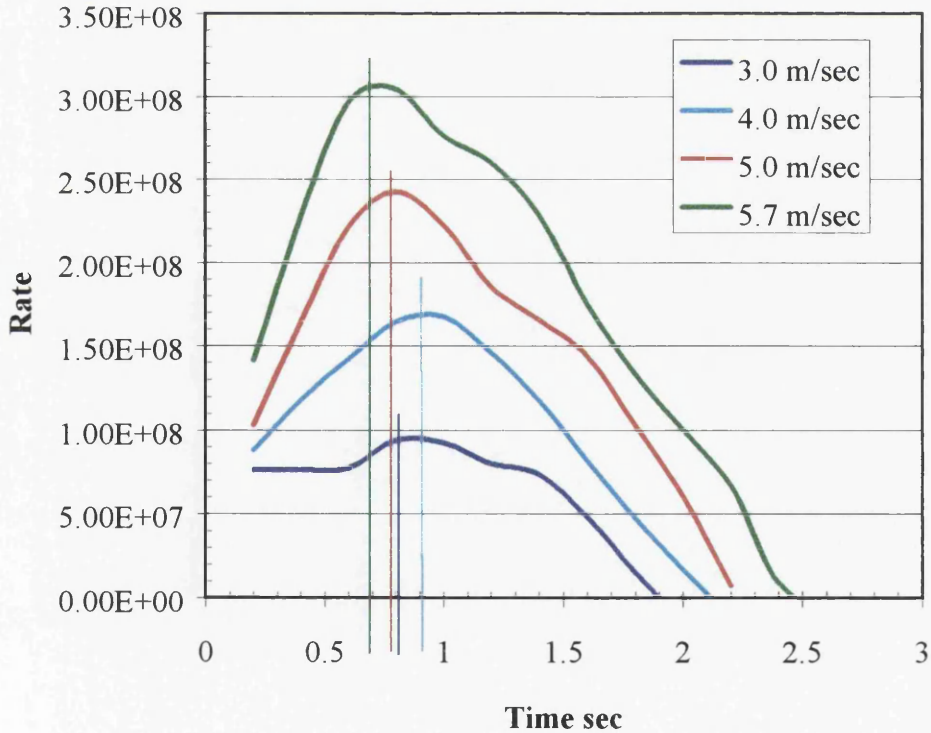


**Figure 3.29** *The rate of change in the energy. The vertical lines show the times where the maxima occur.*

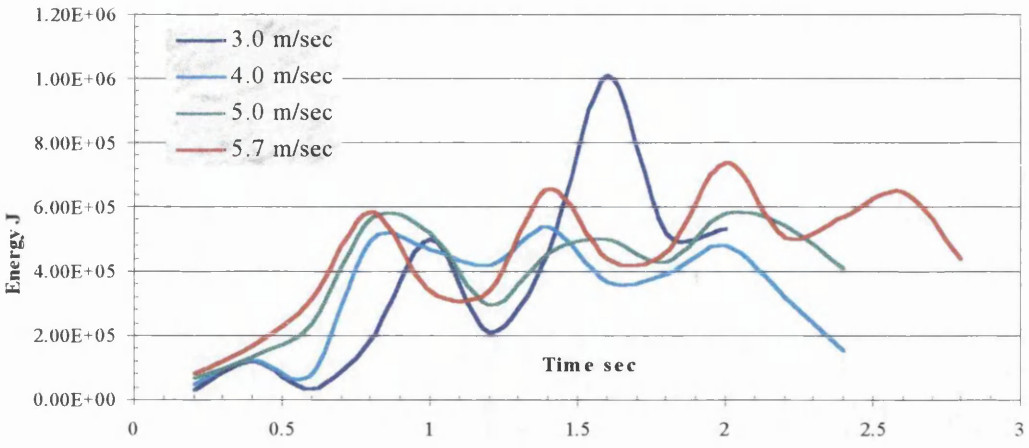


**Figure 3.30** *Total Energy for Bulk1, Bulkhead 77*

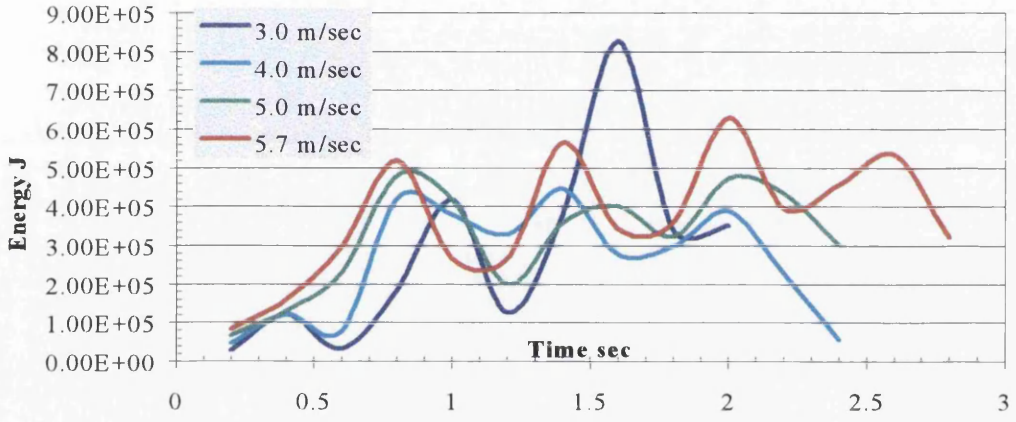


**Figure 3.31** *Total Elastic Energy for Bulk1, Bulkhead 77*

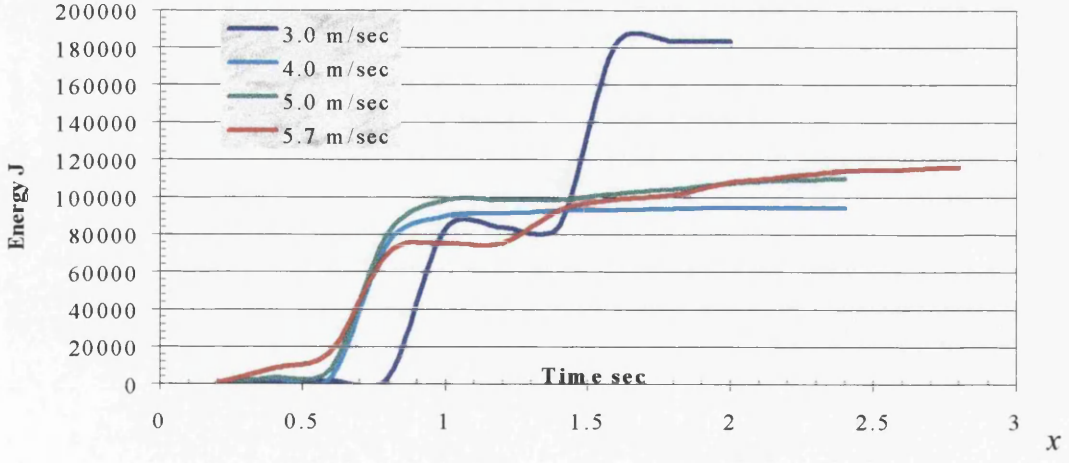


**Figure 3.32** *Total Plastic Energy for Bulk1, Bulkhead 77*

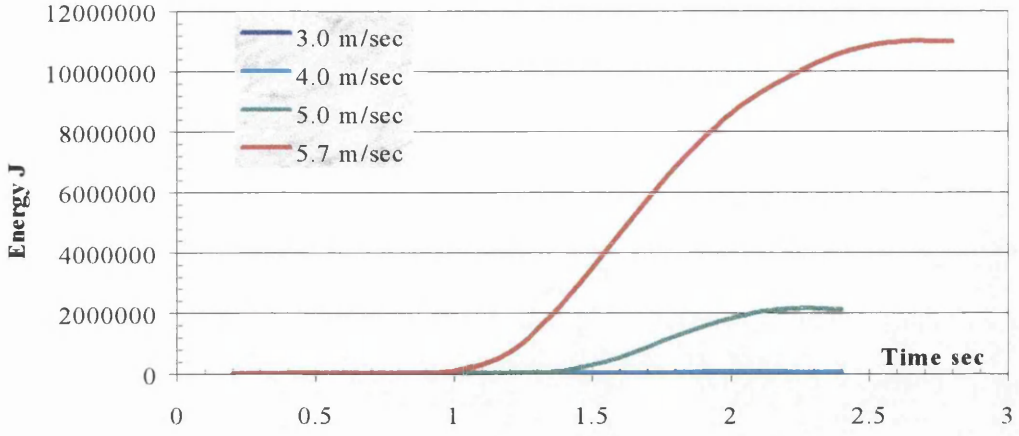


**Figure 3.33** *Total Energy for Bulk2, Bulkhead 87*

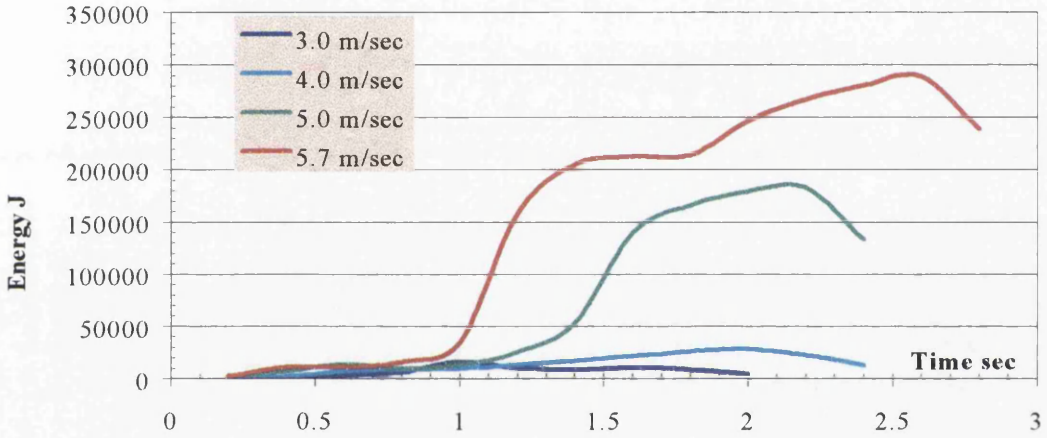


**Figure 3.34** *Total Elastic Energy for Bulk2, Bulkhead 87*

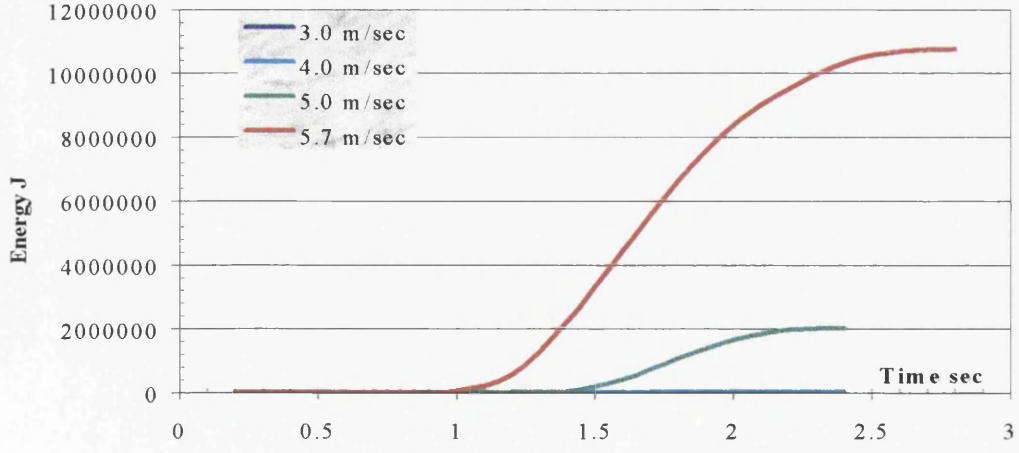


**Figure 3.35** *Total Plastic Energy for Bulk2, Bulkhead 87*

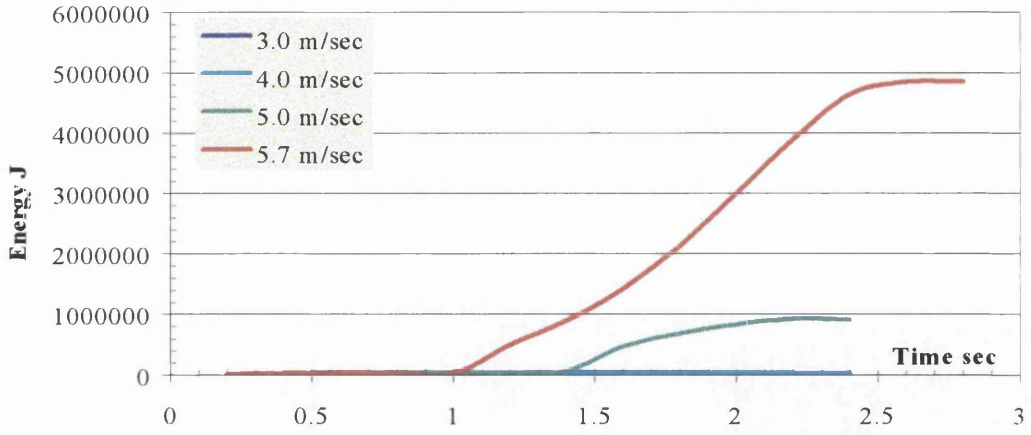


**Figure 3.36** *Total Energy for Bulk3, Centre Bulkhead*

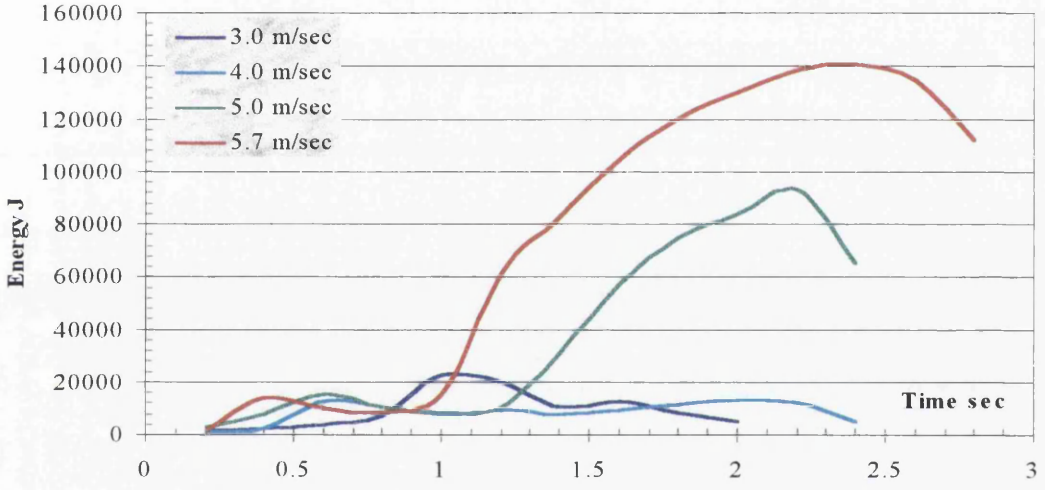


**Figure 3.37** *Total Elastic Energy for Bulk3, Centre Bulkhead*

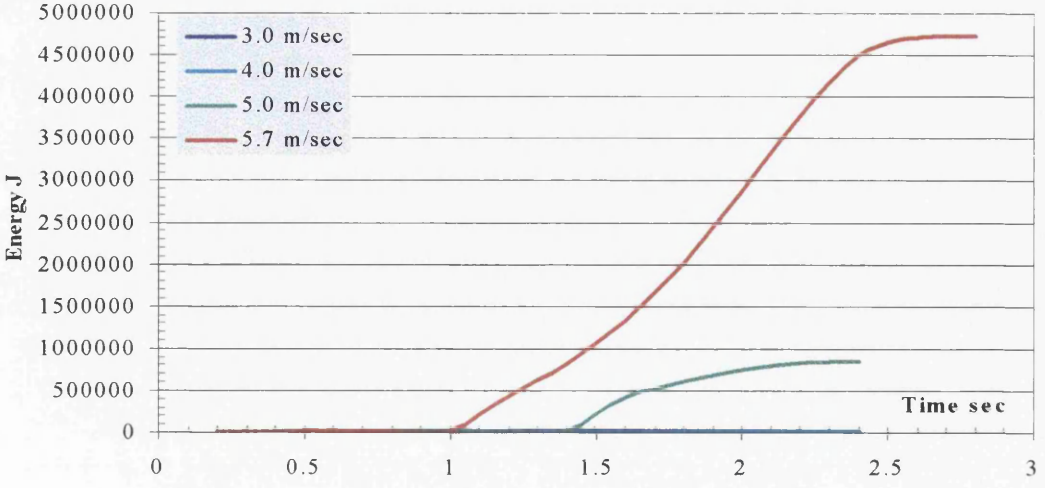


**Figure 3.38** *Total Plastic Energy for Bulk3, Centre Bulkhead*

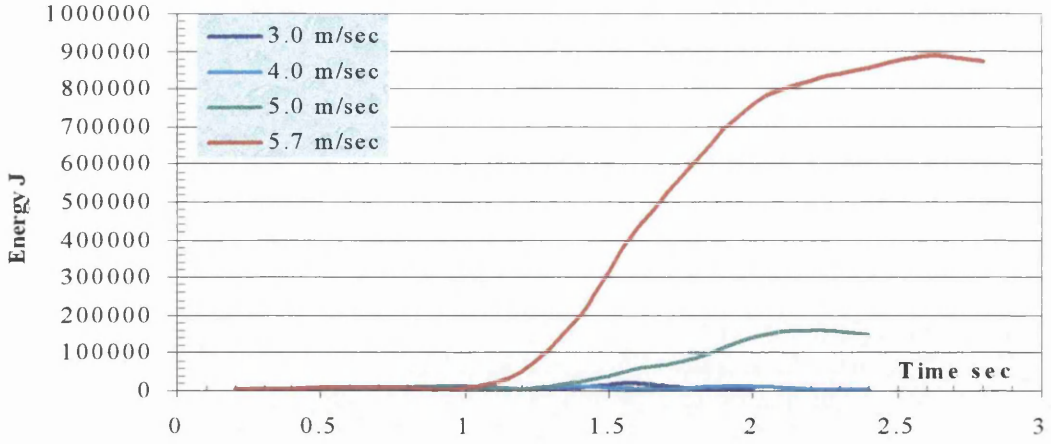


**Figure 3.39** *Total Energy for Deck1.*

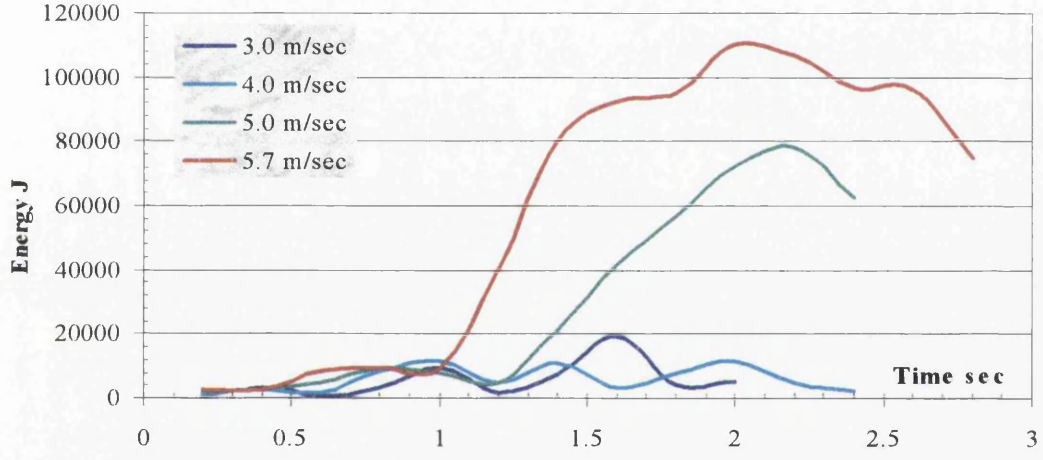


**Figure 3.40** *Total Elastic Energy for Deck1.*

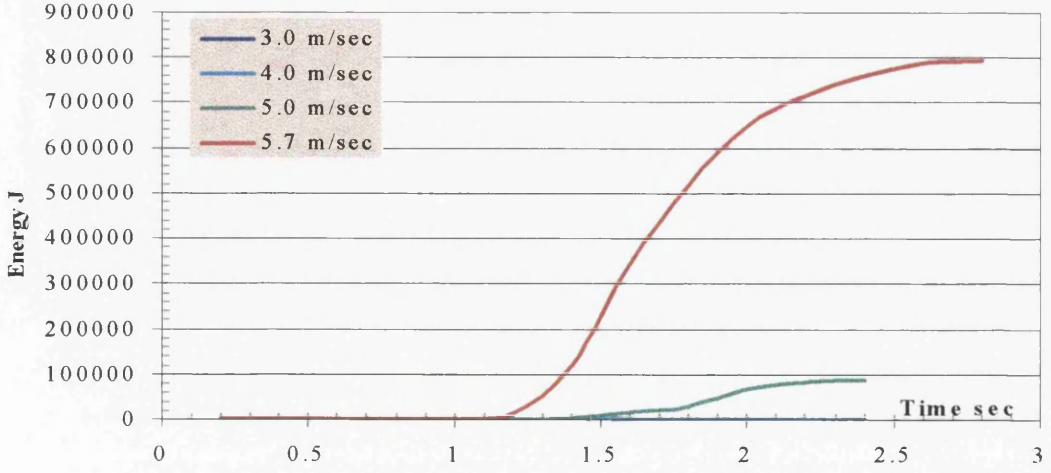


**Figure 3.41** *Total Plastic Energy for Deck1.*

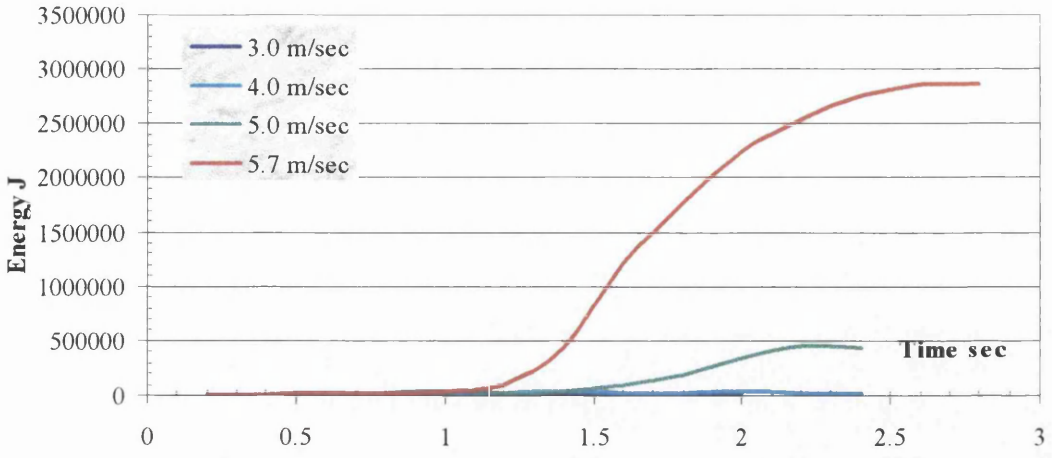


**Figure 3.42** *Total Energy for Deck2.*

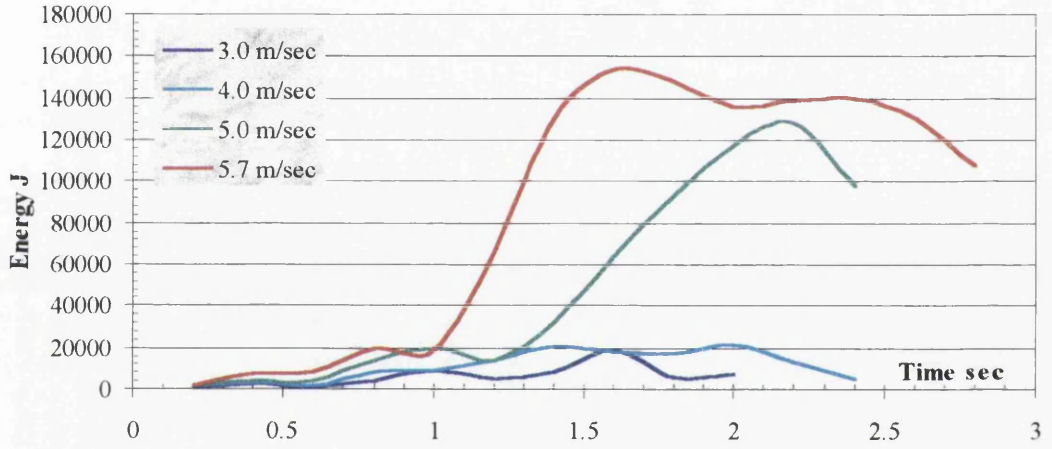


**Figure 3.43** *Total Elastic Energy for Deck2.*

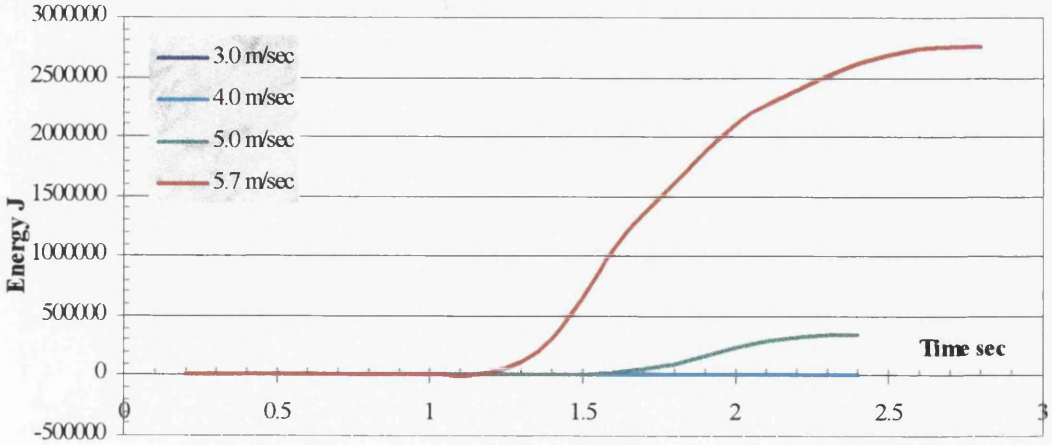


**Figure 3.44** *Total Plastic Energy for Deck2.*

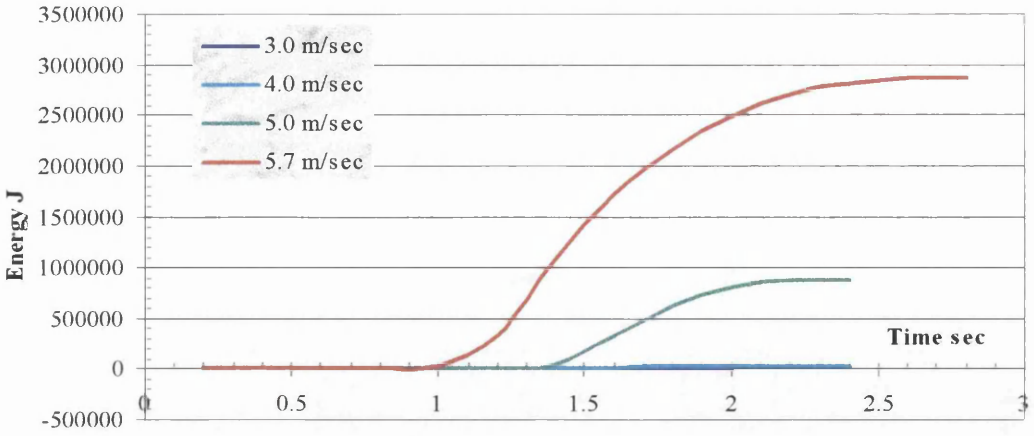


**Figure 3.45** *Total Energy for Deck3.*

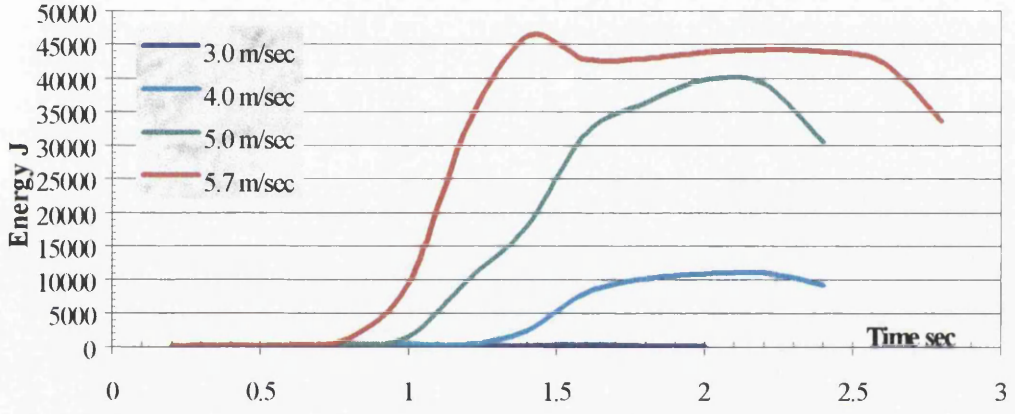


**Figure 3.46** *Total Elastic Energy for Deck3.*

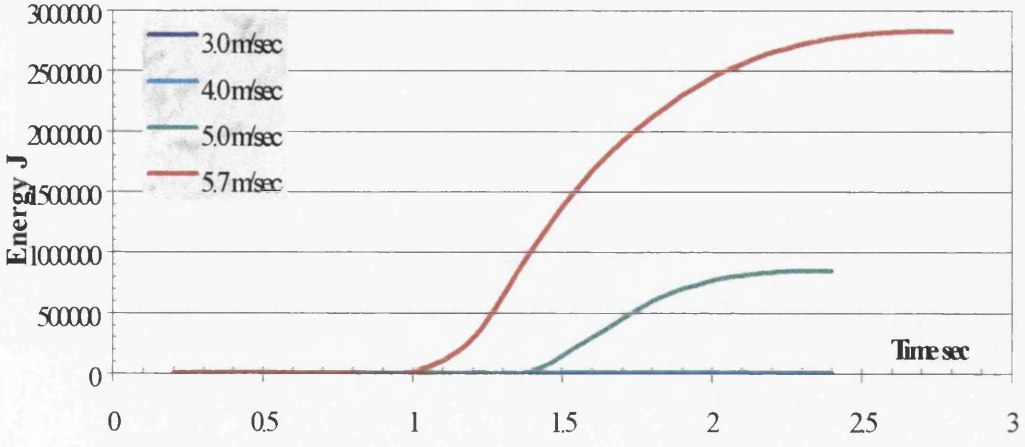


**Figure 3.47** *Total Plastic Energy for Deck3.*

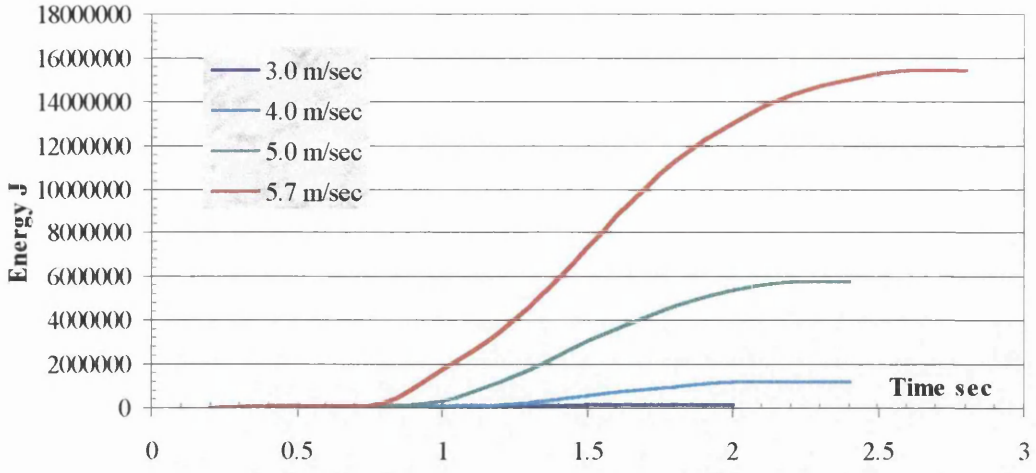


**Figure 3.48** *Total Energy for Deck4.*

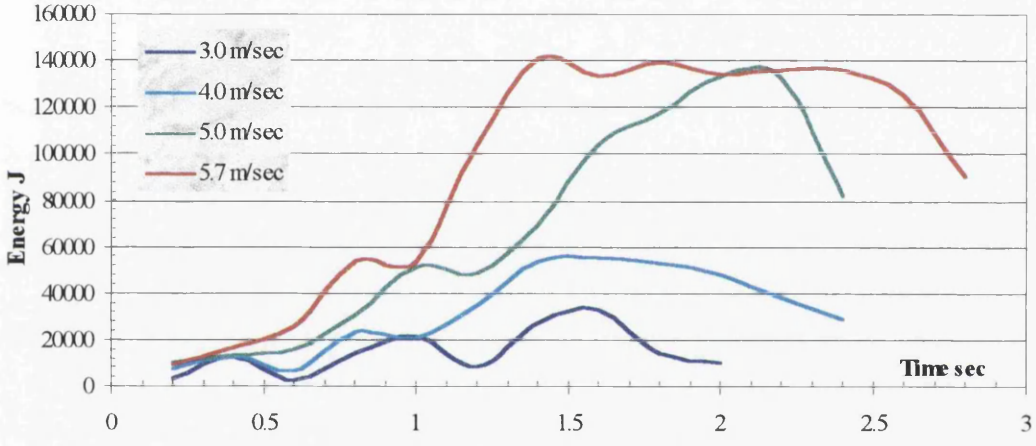


**Figure 3.49** *Total Elastic Energy for Deck4.*

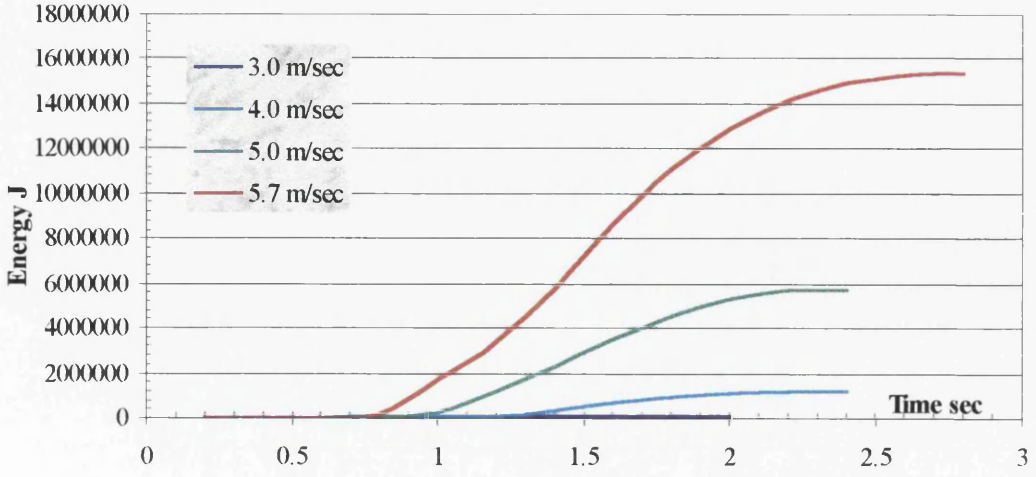


**Figure 3.50** *Total Plastic Energy for Deck4.*

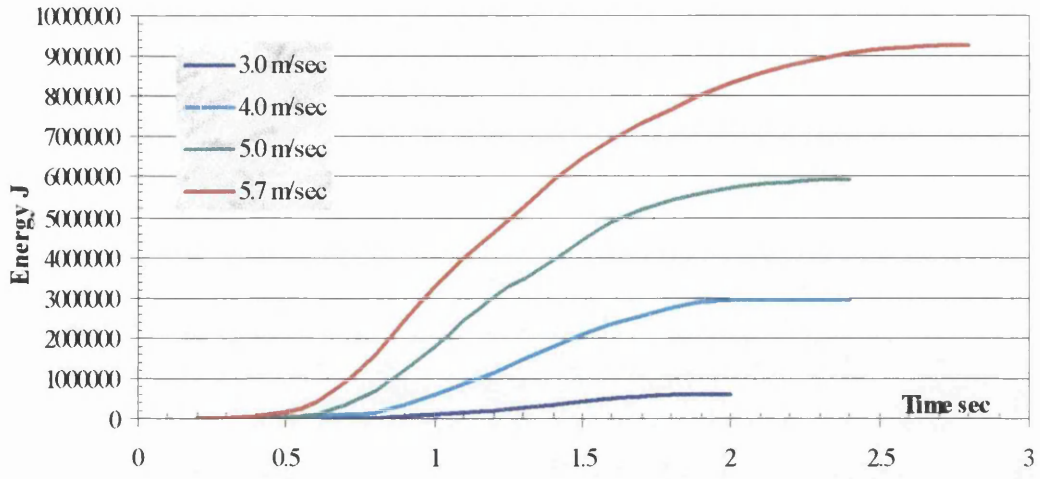


**Figure 3.51** *Total Energy for Deck5.*

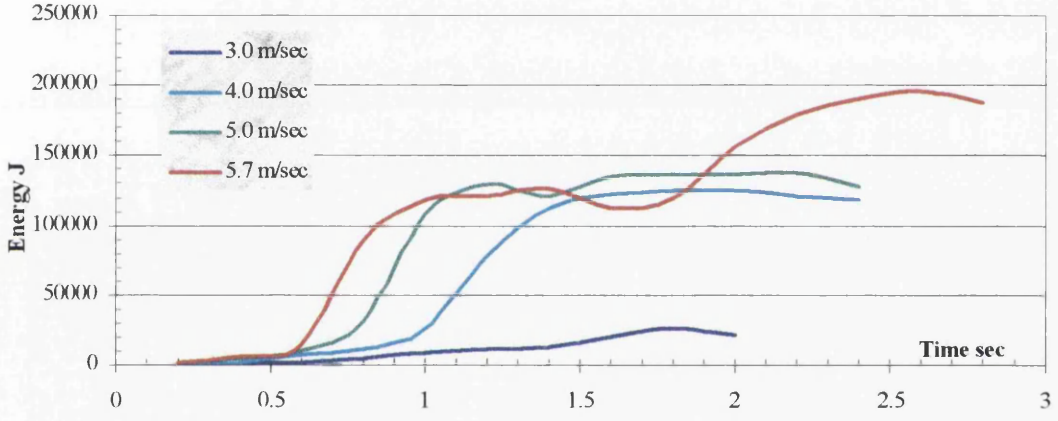


**Figure 3.52** *Total Elastic Energy for Deck5.*

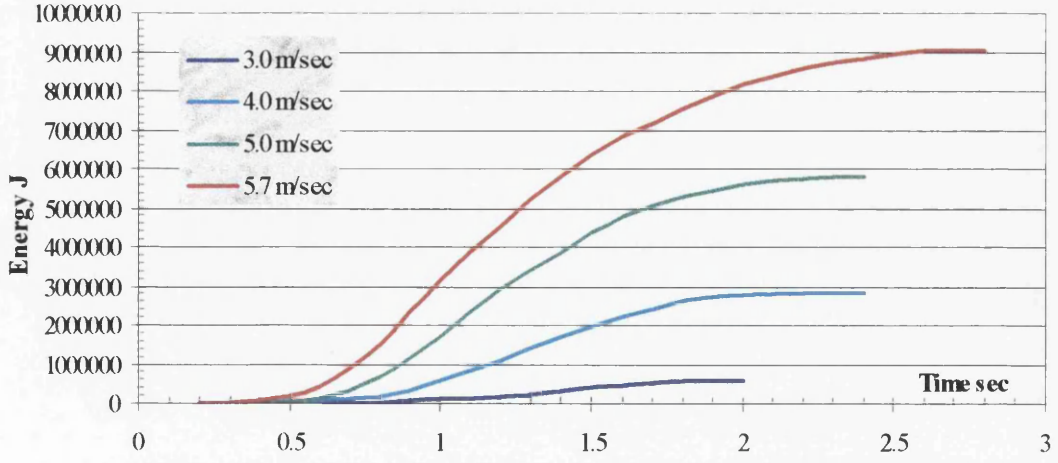


**Figure 3.53** *Total Plastic Energy for Deck5.*

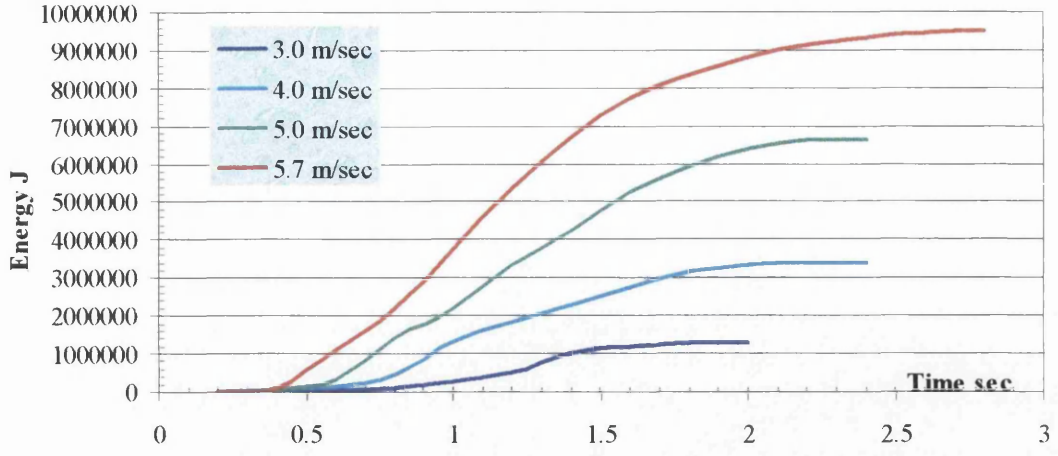


**Figure 3.54** *Total Energy for Deck6.*

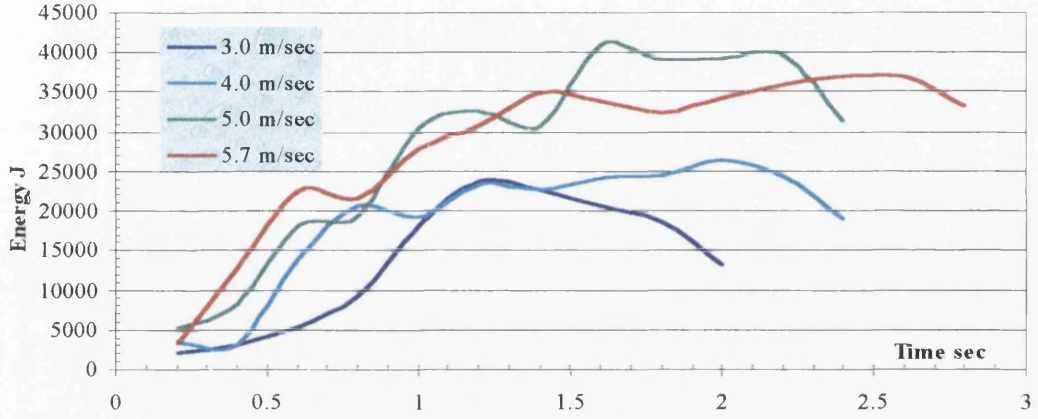


**Figure 3.55** *Total Elastic Energy for Deck6.*

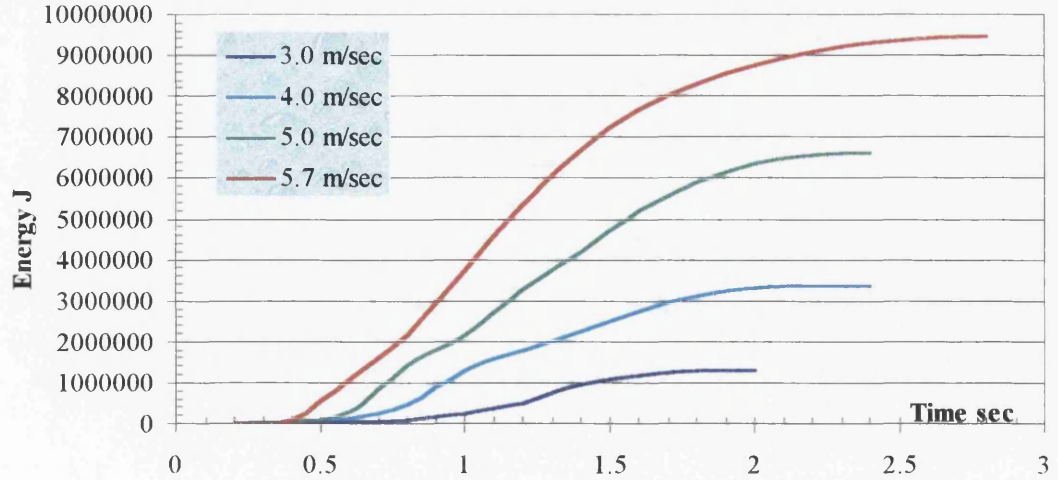


**Figure 3.56** *Total Plastic Energy for Deck6.*

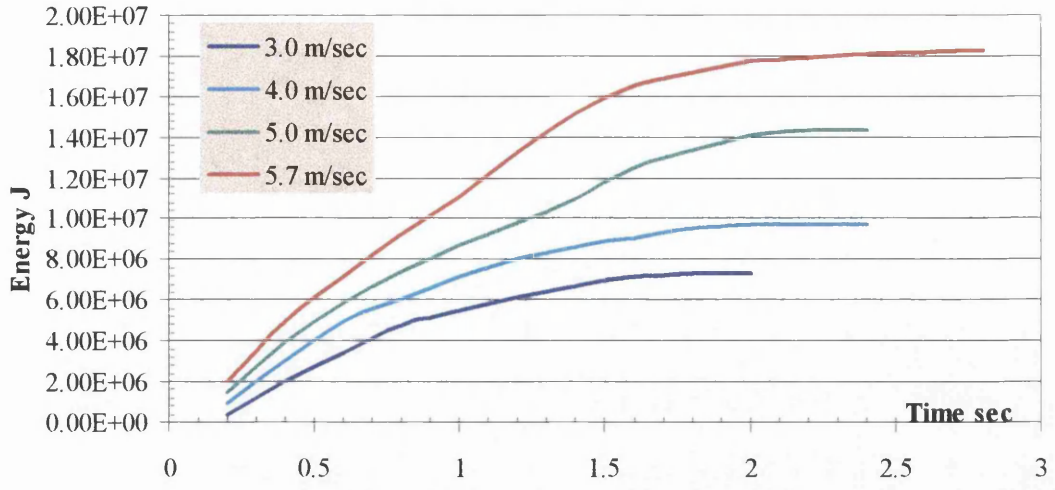


**Figure 3.57** *Total Energy for Deck7.*

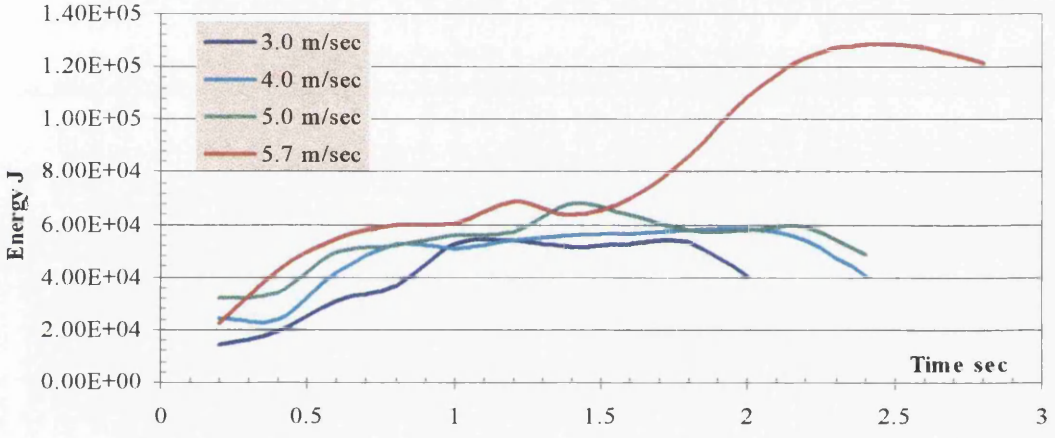


**Figure 3.58** *Total Elastic Energy for Deck7.*

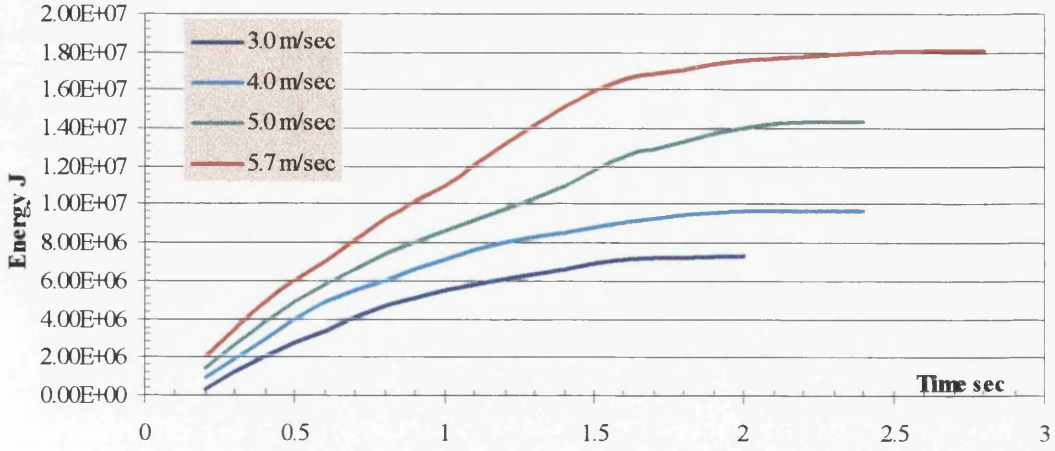


**Figure 3.59** *Total Plastic Energy for Deck7.*

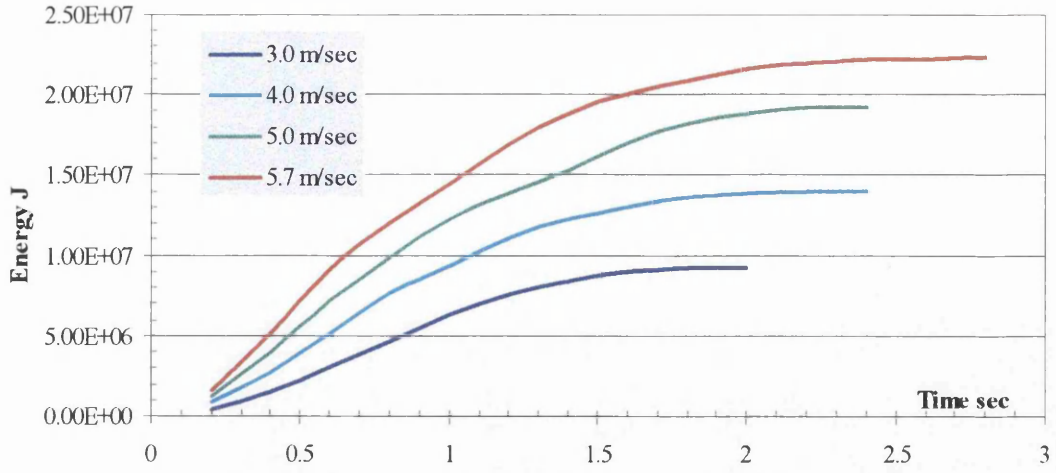


**Figure 3.60** *Total Energy for Deck8.*

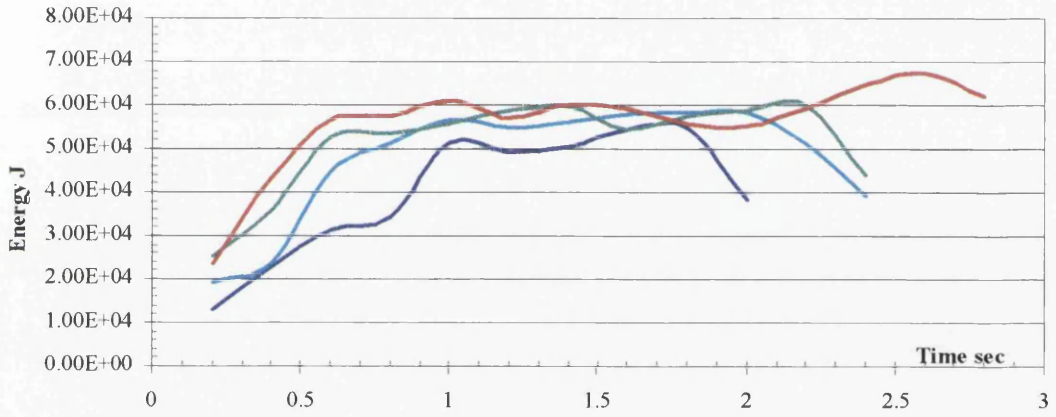


**Figure 3.61** *Total Elastic Energy for Deck8.*

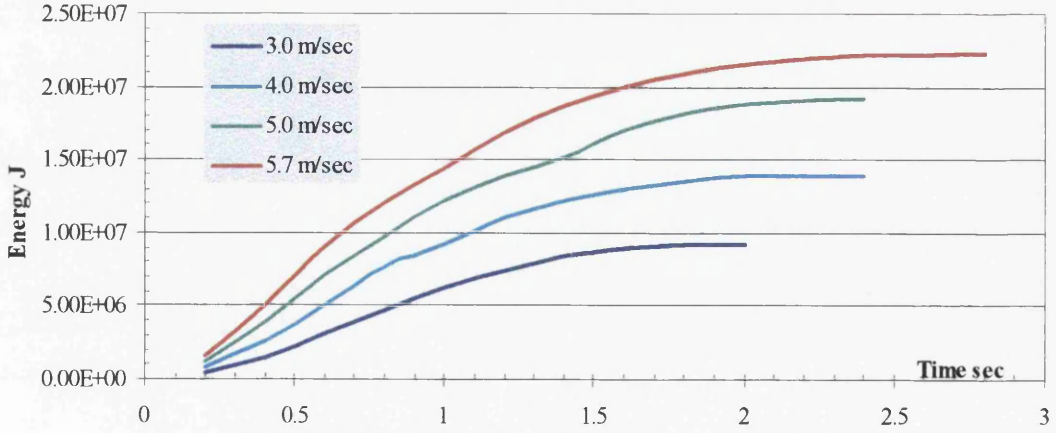


**Figure 3.62** *Total Plastic Energy for Deck8.*

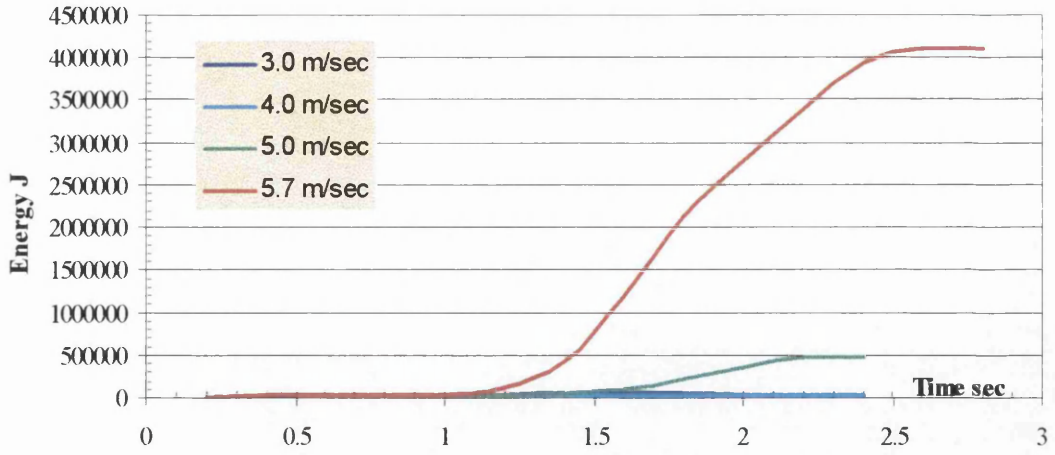


**Figure 3.63** *Total Energy for Deck9.*

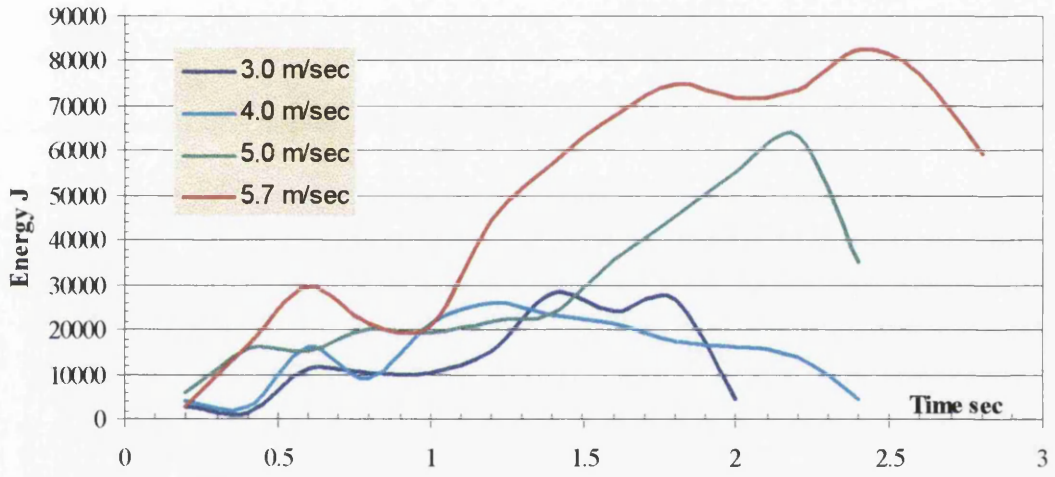


**Figure 3.64** *Total Elastic Energy for Deck9.*

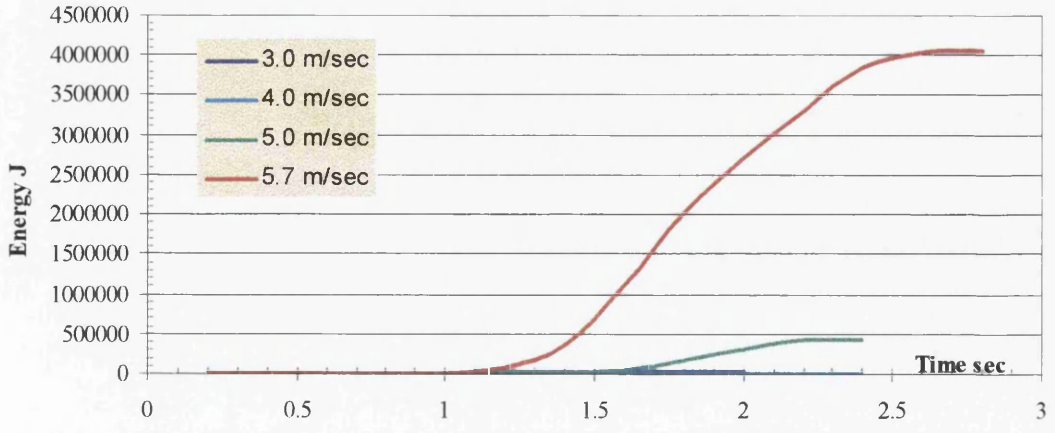


**Figure 3.65** *Total Plastic Energy for Deck9.*

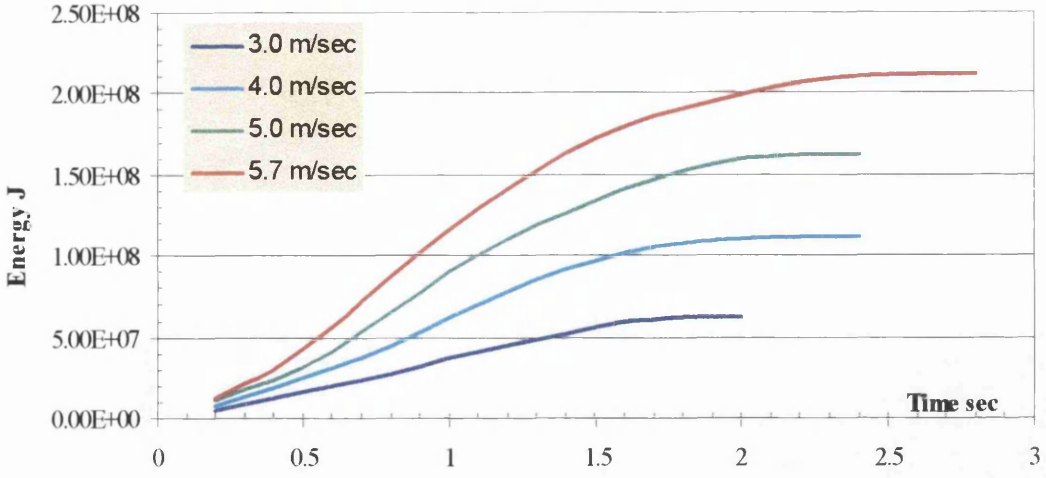


**Figure 3.66** *Total Energy for Shell.*

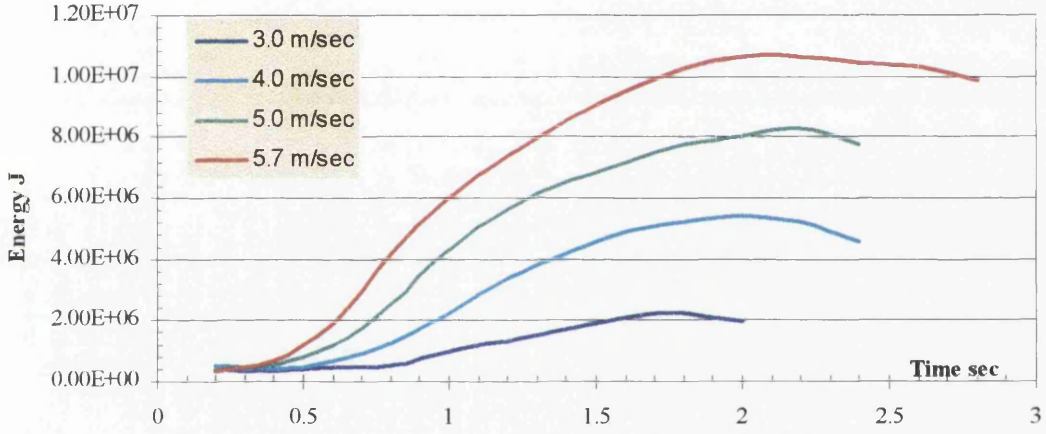


**Figure 3.67** *Total Elastic Energy for Shell.*

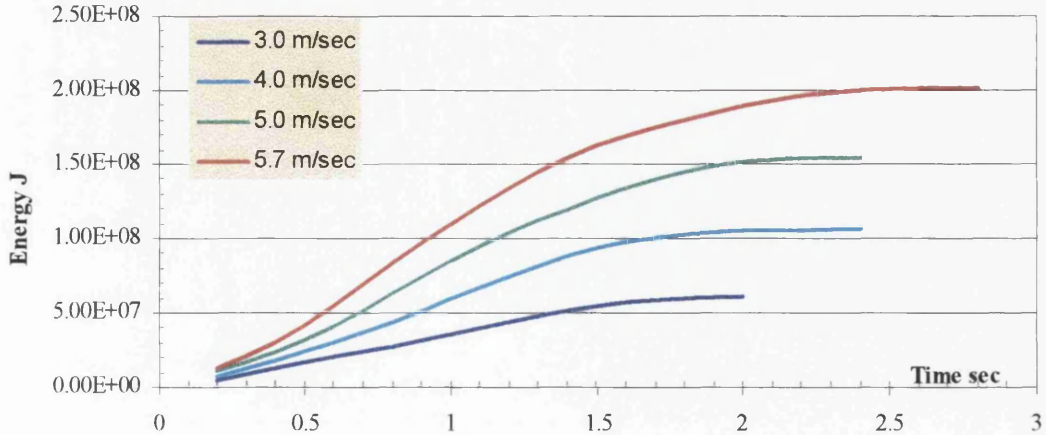


**Figure 3.68** *Total Plastic Energy for Shell.*

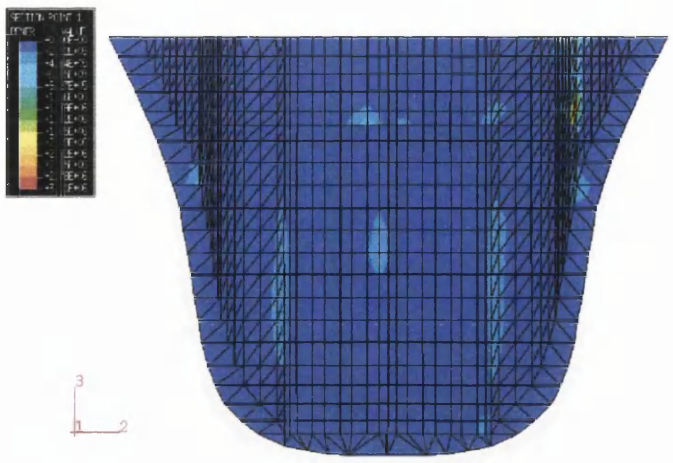

**Figure 3.69** *Plastic Energy on bulkhead 77*

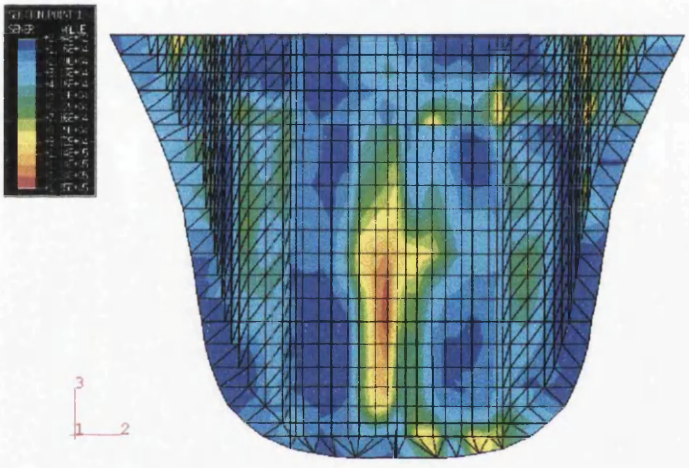

**Figure 3.70** *Elastic Energy on bulkhead 77*

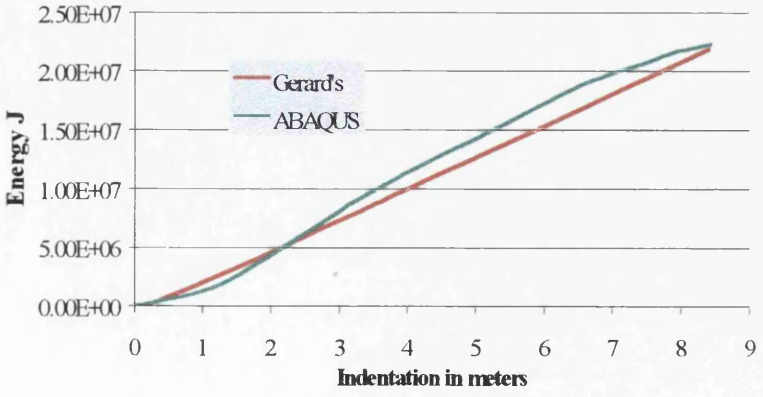


**Figure 3.71** *Comparison of Gerard's and ABAQUS calculations for the total energy dissipated on Deck8.*

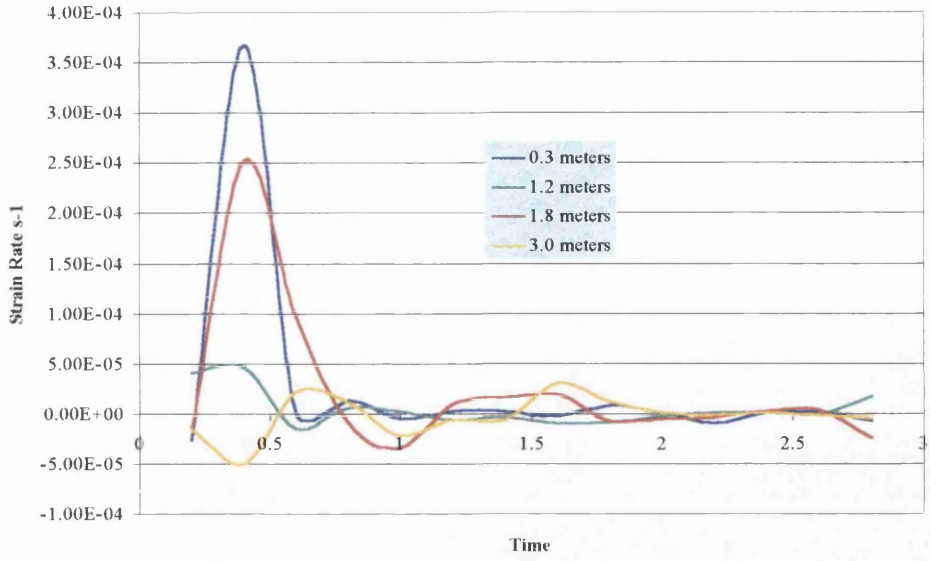


**Figure 3.72** *Strain rates for elements located on Deck8 on various longitudinal locations from 0.3-3.0 meters.*

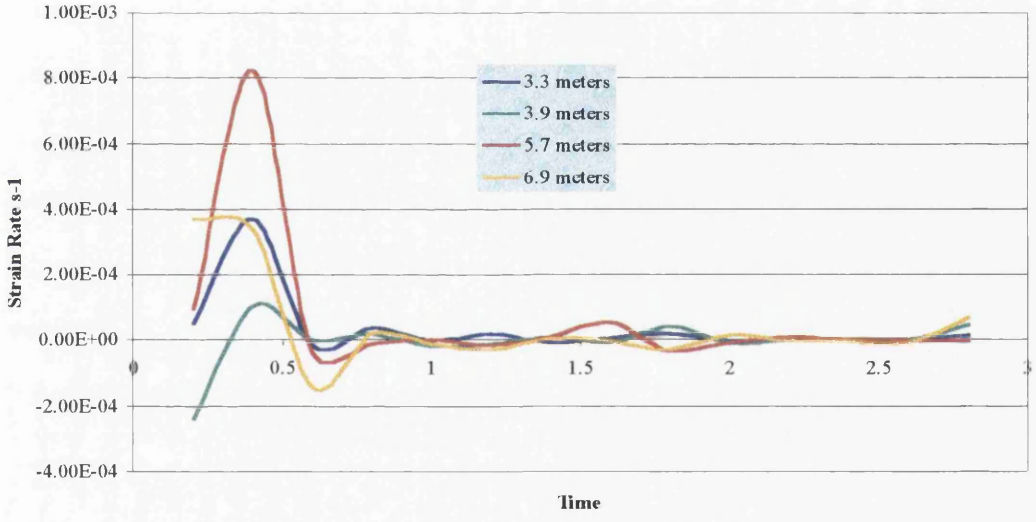


**Figure 3.73** *Strain rates for elements located on Deck8 on various longitudinal locations from 3.3 to 6.9 meters*

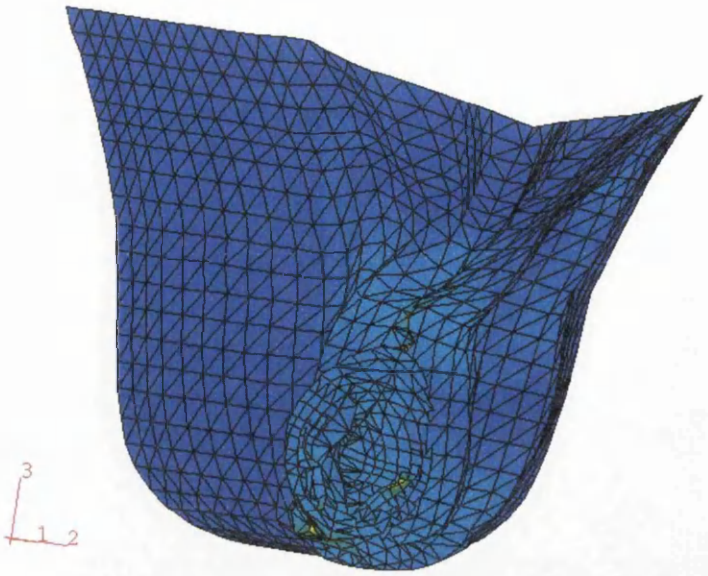


**Figure 3.74** *Plastic energy dissipation for the shell with 5.7 m/sec initial velocity*

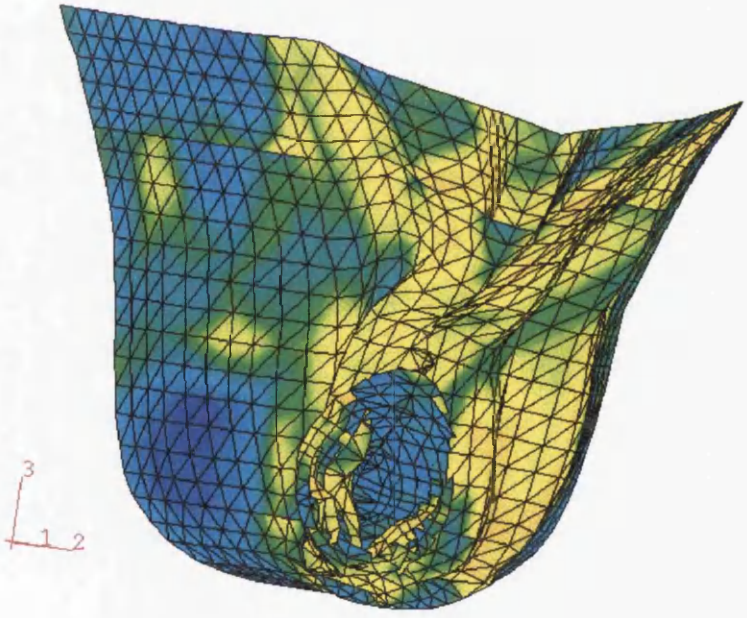


**Figure 3.75** *Elastic energy dissipation for the shell with 5.7 m/sec initial velocity*

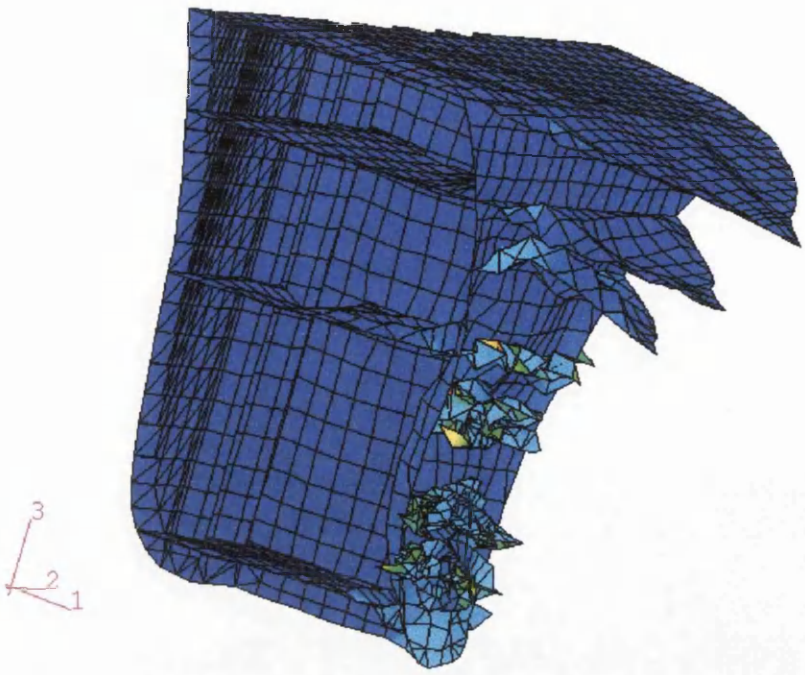


**Figure 3.76** *Plastic energy dissipation for the internal arrangements with 5.7 m/sec initial velocity*

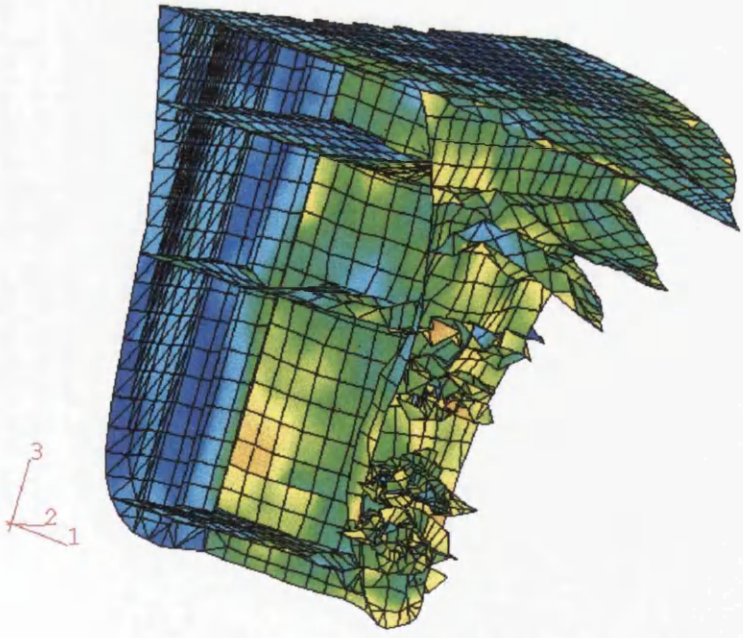


**Figure 3.77** *Elastic energy dissipation for the internal arrangements with 5.7 m/sec initial velocity*

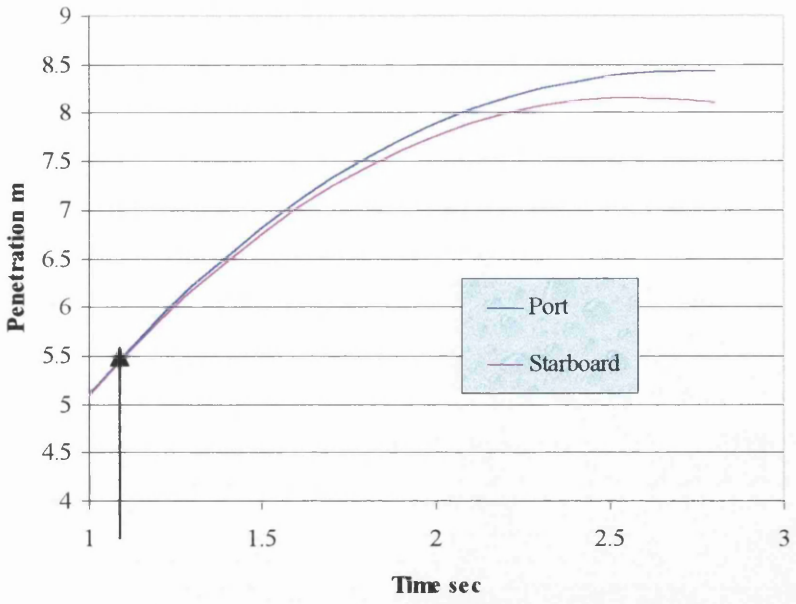


**Figure 3.78** *The horizontal translation in the port and starboard side of the vessel during the collision.*

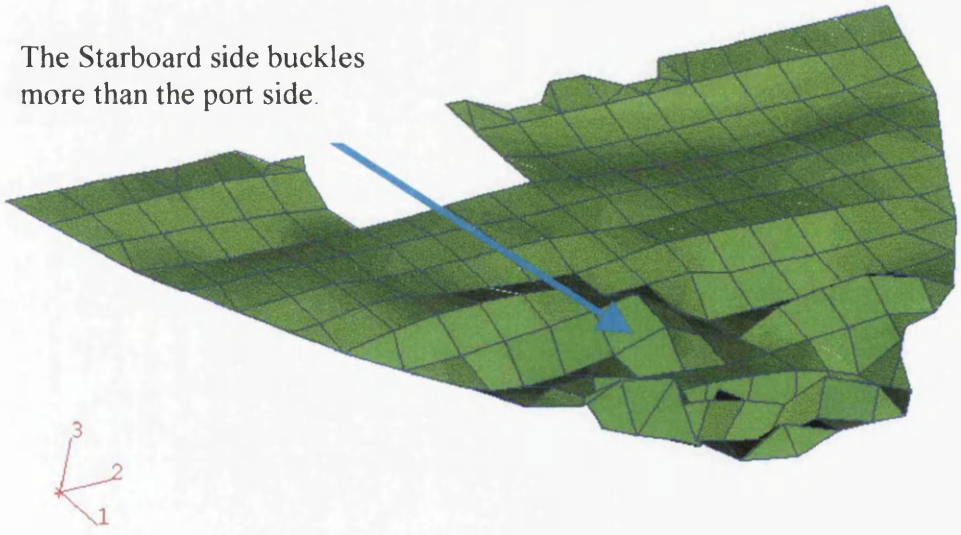


**Figure 3.79** *Deck4 during it's collapse*

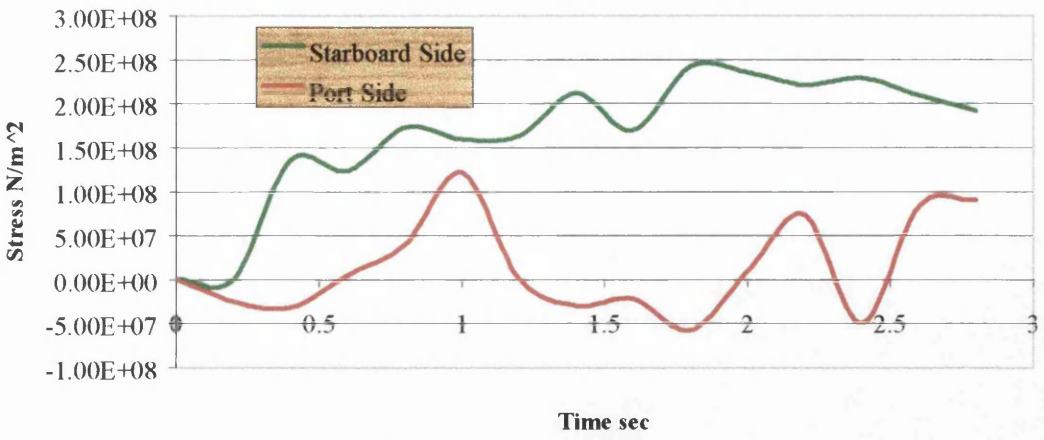


**Figure 3.80** *Stress versus Time for intercostal elements 164, 194 located at the edges of Deck4. For the starboard side at time t=1.8 sec the stress experienced is approaches the yield stress*

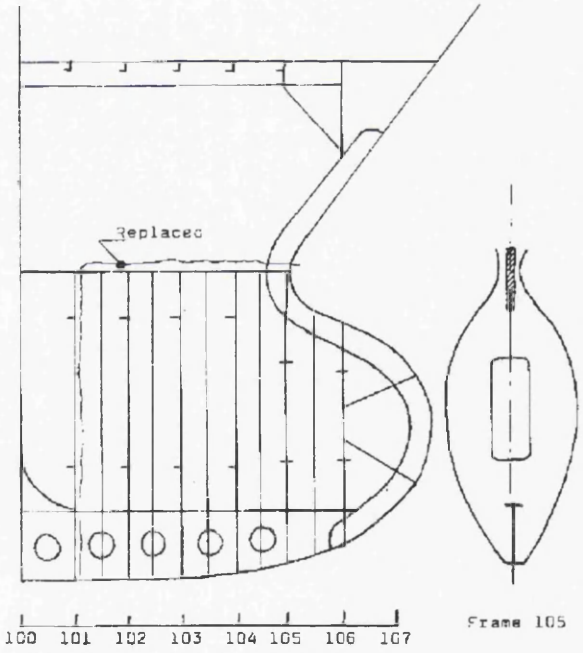


**Figure 3.81** *M/S Fjord grounded in 1983 on Byneset. Only the bulbous section of the bow was damaged Amdahl J. (1983)*

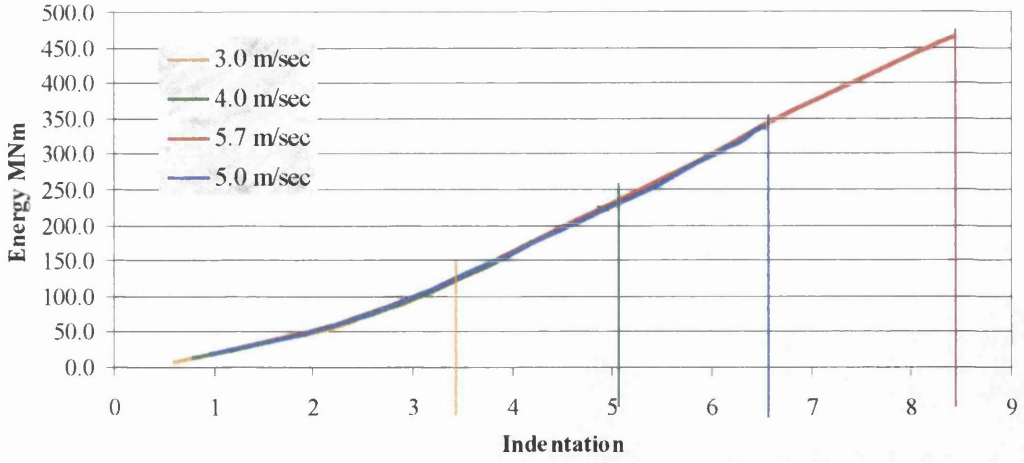


**Figure 3.82** *The energy dissipated on the structure versus the indentation for the four concepts.*

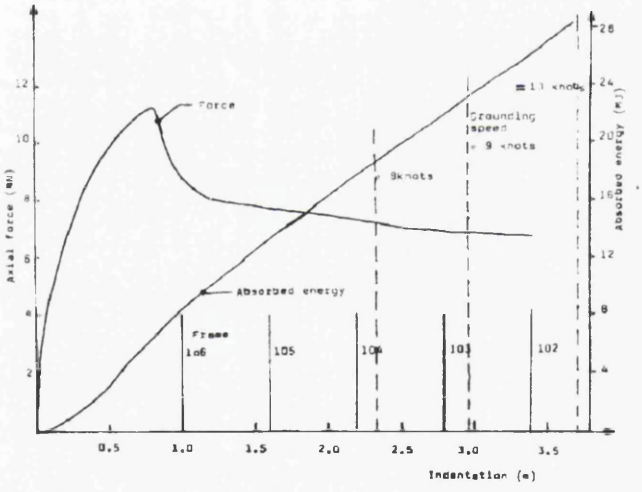


**Figure 3.83** *The energy indentation curve, A shape which has very linear response in respect to the penetration. Amdahl J. (1983)*

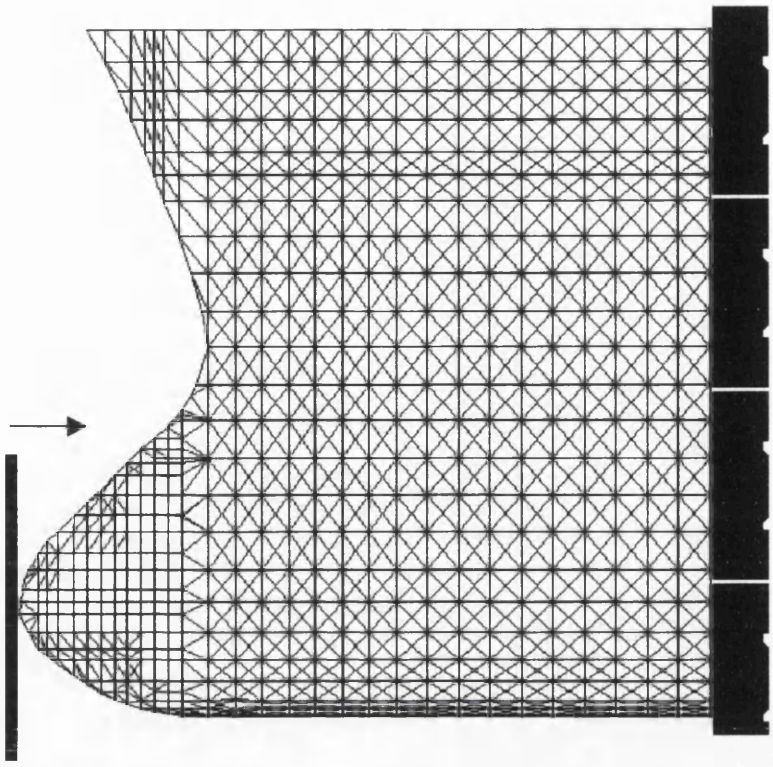

**Figure 3.84** *The static impact scenario. The bow is rigidly fixed at bulkhead 77, while the rigid surface collides with the bow.*

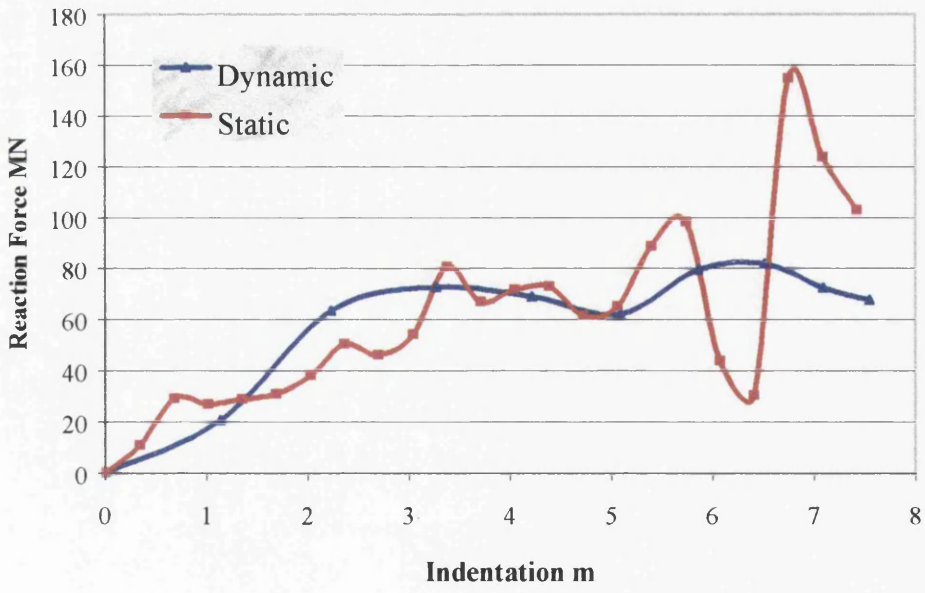


**Figure 3.85** *Reaction Force for the static and dynamic analysis versus the indentation in meters*

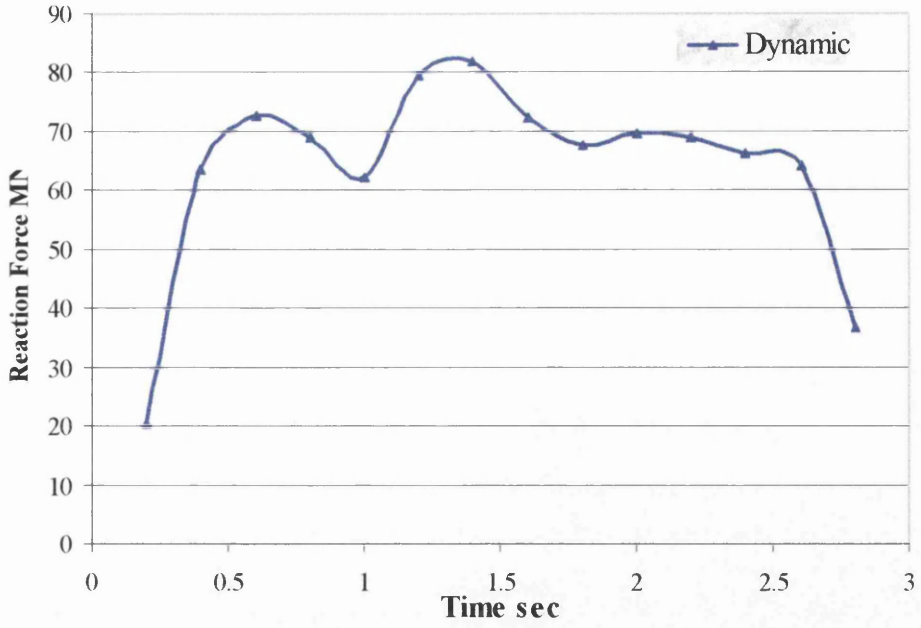


**Figure 3.86** *Reaction Force versus time for the dynamic case. Variation of the reaction force is shown in this case*

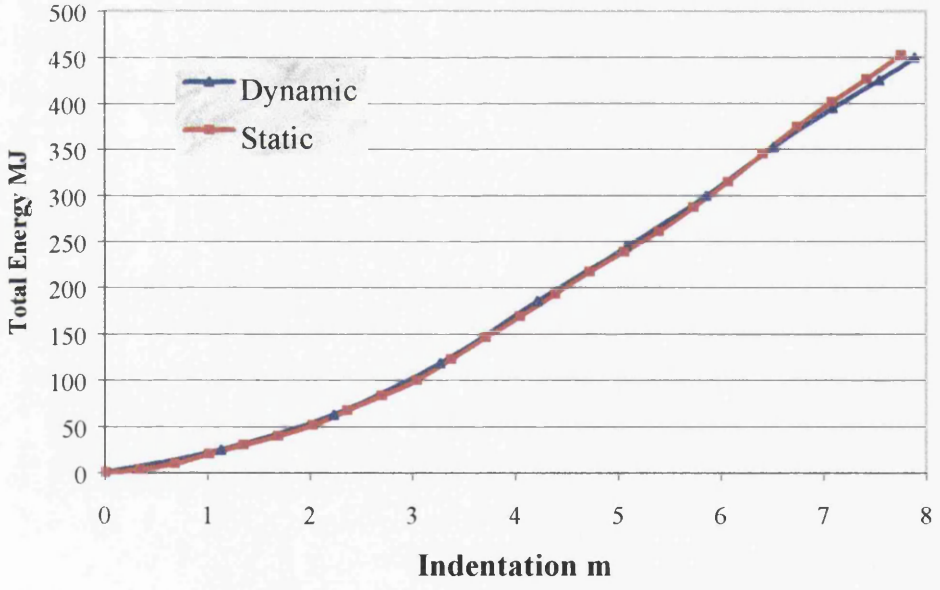


**Figure 3.87** *Total energy dissipated on the structure for the static and dynamic analysis*

# CHAPTER FOUR

# GROUNDING WITH RIGID SURFACE

---

## 4.1 INTRODUCTORY REMARKS

As mentioned previously, grounding analysis has received a great interest with the introduction of double hull construction as a mandatory design in tankers, OPA (90). The approaches developed ever since, yield to simple analytical formulas based on the kinematic relationships of vessels during grounding. However, in the case where a vessel hits a rock, simple formulas have been presented, whereas the forces tearing the bottom structure have been incorporated in the analysis. Simonsen B. C. (1996), Rodd L. (1996)

Neither the maximum allowable bending moment delivered on the structure, during the impact, nor the elasto-plastic energy induced due to local structural deformation of the bow area, have been incorporated to the analytical approaches as these were described in Sections 2.2.1, 2.2.2, and 2.5.2. For example a vessel which grounds on a slide and comes to rest in a position as the one shown in Figures 2.9 or 2.12, may not be capable to withstand the bending moment generated at this condition. Pedersen (1995) in his analytical approach, compares the bending moment derived during the grounding with a slope, to the IACS *maximum wave bending moment.*

In this chapter an numerical approach to the grounding problem takes place which aims to show the contribution of the energy dissipated in the structure due to elasto-plastic deformation. The analytical methods developed until now, neglect this amount of energy, while they are simulating the vessel as a rigid beam. The analytical method is shown here for the scenario of grounding developed and the

bending moment distribution is used in order to ascertain the response of the boundary bulkhead for the finite element model.

## 4.2 MAXIMUM BENDING MOMENT CAPACITY

The maximum bending moment capacity as this is given from Lloyds Rules (1997) is the summation of the Still water Bending moment $M_S$ and the Wave Bending moment $M_W$. Thus we have that

$$M_{MAX} = M_S + M_W \tag{4.1}$$

The still water bending moment is given from the following expression

$$M_S = F_D \cdot \overline{\sigma}_C \cdot Z_D \cdot 10^3 - M_W \tag{4.2}$$

where

$F_D$ is the local scantling reduction factor for hull members above the neutral axis, Part 3, Chapter 4, Section 5.7 Lloyds Rules.

$\overline{\sigma}_C$ is the permissible combined stress, Section 5.6 Lloyds Rules

$Z_D$ Hull midship section module in $m^3$, Section 3,3.4 Lloyds Rules

The wave bending moment follows in expression 4.3;

$$M_W = 0.1 \cdot C_1 \cdot L^2 \cdot B \cdot (c_B + 0.7) \tag{4.3}$$

where L, B are the length and breadth of the ship in [m]

$C_B$ is the block coefficient

$C_1$ is a constant given as $C_1 = 10.75 - \left(\frac{300 - L}{100}\right)^{1.5}$ 4.4

The introduction of equation 4.1 imposes an upper limit solution to the response of a vessel during grounding. Consider Figure 4.1. If φ(t) is the pitching angle of the ship at time t, then the bending moment distribution along the length of the ship is

$$M(x,t) = R \cdot \cos\varphi(t) \cdot x - W \cdot \cos\varphi(t)(x-a) + B\cos\varphi(t)(x-b(t)) \tag{4.5}$$

where a, W, B are given from equation 2.22 and 2.23

$\varphi(t)$ is the pitching angle of the vessel during the grounding. $\varphi(t)<\alpha$, where $\alpha$ is the angle of the slope.

b(t) is the longitudinal distance of the centre of buoyancy at time t. and always b(t)>a

Obtaining reaction R from equation 2.23 where $\nabla$ is given here as W and b as b(t) equation 4.5 yields to

$$M(x,t)=W\left(1-\frac{a}{b(t)}\right)\cdot\cos\varphi(t)\cdot x-W\cdot\cos\varphi(t)\langle x-a\rangle^{x>a}+B\cos\varphi(t)\langle x-b(t)\rangle^{x>b(t)} \quad 4.6$$

The upper bound solution for equation 4.6 is $M_{MAX}$ as this is derived from equation 4.1. If M(x,t) is greater than $M_{MAX}$, then the vessel collapses and theoretically breaks in two parts. However this is not quit true. $M_{MAX}$ is used in conjunction with permissible yield stresses, so reaching $M_{MAX}$ should not cause a failure, just some proportion of final yield. Additionally, the structure is behaving in a ductile way and it will have a plastic capacity greater than the first yield moment. These limitations are valid providing that an earlier failure is not precipitated by either buckling or fracture. This scenario is displayed in Figure 4.2, where $\varphi(t)$ is shown with respect to the time. For each angle of pitching $\varphi(t_i)$ the bending moment is calculated.

When $M(x,t)<M_{max}$ the vessel is still capable to undergo bending load, while when $M(x,t)>M_{max}$, then overall failure is most probable.

The response of the vessel when $M(x,t)>M_{max}$, can not easily predicted since mass and geometry continuity cease, and most possible scenario remains that the vessel will probably break in two. The effects beyond the state $M(x,t)>M_{max}$ are not examined within this chapter.

## 4.3 ARTIFICIAL ISLANDS

In order to avoid endangering bridge integrity by ship impact the piers may be designed to be big enough to be able to sustain a direct ship impact. Another possibility is to surround each bridge pier with a structure, which can absorb the ship impact. This item may either be a very large fendering system of a special structure, an artificial island with sloping beach or a combination of both.

The artificial islands are man made slopes, surrounding the pier to be protected, with a slope varying from 3° to 14°. The construction material of these islands is either earth (dredged materials, sand) or concrete, dependent on the energy absorbing capabilities of an island. A typical artificial island is shown in Figure 4.3. The island around the pier is 300m long and approximately 100m wide. These, protect piers which are 27m wide and 6m breadth.

## 4.4 THE FINITE ELEMENT MODEL DURING THE GROUNDING

Both Minorsky (1983) and Pedersen (1995) in their analytical calculations, for the prediction of the travelling distance of the ship, on a rigid slope, have used simple kinematic relationships. Minorsky in Equation 2.24 estimates that the stopping point may be calculated, if one assumes that the work done by the frictional force F is equal to the energy produced from the initial kinetic energy of the ship. Thus the summation of the work done from the frictional force, $W_F$ and the kinetic energy at a time $t>t_o$, where $t_o$ is the time the grounding commenced, is constant and equal to the initial kinetic energy of the vessel prior to the impact. This is expressed as;

$$W_{Friction} + E^{t_i}_{kinetic} = E^{t_o}_{kinetic} \qquad 4.7$$

Pedersen (1995), introduce the loss of kinetic energy because of potential energy due to change of vertical position of the centre of mass and potential energy due to radial velocity around the centre of flotation. This is shown in equation 2.68.

However both these methods do not account for the loss of kinetic energy due to elasto-plastic energy dissipated on the structure. The examination of how large this

energy is, compared to the friction energy or the potential energy because of change of the centre of mass will be attempted with the use of numerical analysis.

The finite element model as this was described previously, in chapter 3 has been reassembled for the grounding problem. The slope configuration, and the friction coefficient had to be examined, along with the boundary conditions on the collision bulkhead in order to account for the change of the vertical and rotational state of the vessel.

Prior to the modelling an analysis based on equation 4.6 took place in order to get an idea of the magnitude of the reaction force from the ground, as well as the response the vessel is expected to experience during the impact. An energy conservation follows using only the kinematic relationship, and afterwards, these data will be compared to those obtained from the finite element analysis.

### *4.4.1 THE GROUNDING SCENARIO*

The grounding scenario is based on a full loaded condition with draft 9.25 meters and displacement 27,500 metric tons. The vessel is colliding with a rigid surface which has an angle of 19° with the horizontal surface (or a slope 0.34) and a friction coefficient of 0.85. These values were selected after considering the results published from Ottesen H et al. (1994) who showed similar experimental work on a 300 DWT fishing vessel with V-bow. The initial speed of the vessel is 5.766 m/sec (=11.2 knots), which is the service speed of this vessel.

Pedersen (1993) mentions that during the grounding, if the angle of the slope is less than 0.1 rad, or 5.73°, then the kinetic energy lost during the impact, before sliding, is negligible. However if the angle of the slope exceeds the 45°, then the impact results to response similar to the one of the head-on collision of the rigid surface.

The slope selected for this study, aims to show the contribution of the elasto-plastic energy conservation equation, with comparison to the other energy quantities.

The friction coefficient Ottesen (1994) used for his experiments varied from 0.80, 0.85 and 0.95. In this model the 0.85 coefficient was selected which represents an average value.

The ship is taken in full loaded condition since this is the worst credible situation during the impact due to the initial high kinetic energy.

### *4.4.2 THE BOUNDARY CONDITION*

Contrary to the case of impact with a vertical rigid wall, in this case the vessel is expected to move in both the z and x direction. Thus, it is necessary to apply boundary conditions on the collision bulkhead (Bulk77), in order to model the bending moment and shear force generated during the change of the pitching angle of the vessel.

The calculation of these values takes place analytically, by assuming that the vessel is moving as a rigid body, as shown in Figure, 4.1. The z-translation of the contact point is given as

$$Z(t) = X(t) \cdot \tan\alpha \qquad 4.8$$

where $\alpha$ is the slope of the rigid surface. The pitching angle $\varphi(t)$ is calculated from the centre of floatation and is equal to

$$\tan\varphi(t) = \frac{Z(t)}{LCF(t)} \quad \rightarrow \quad \tan\varphi(t) = \frac{X(t) \cdot \tan\alpha}{LCF(t)} \qquad 4.9$$

The reaction R(t) is given from equation 2.23, for a= LCG and b= LCB(t). Therefore, The shear force and bending moment may now be drawn in respect to the indentation or time. Such a graph is shown in Figure A4-1.1, in appendix 1. The values for LCF and LCB were extracted from the hydrostatics of the vessel, and with the help of software AUTOSHIP - AUTOHYDRO. A set of hydrostatics as they

were extracted from the software, for the full loaded condition is included in appendix 2

These prescribed boundary conditions are incorporated in the numerical analysis on the nodes located on the collision bulkhead. Although this way of calculating the boundary conditions is approximate, it is the only method available in this preliminary stage.

In Figure 4.4, the configuration of the grounding scenario is shown from a forward view, at a time prior to the initiation of the impact.

### *4.4.3 ENERGY CONSERVATION IN THE ANALYTICAL SOLUTION*

For a known displacement x of the vessel towards the rigid slope, the time may be calculated through an energy conservation. At each time $t_i$ the equation 2.68 and 2.73 are satisfied. Thus the following equilibrium is valid;

$$E^{t_i}_{kinetic-X} + E^{t_i}_{kinetic-Z} + E^{t_i}_{Rotation} + E^{t_i}_{friction} = E^{t_o} \qquad 4.10$$

These energy quantities are shown in Figure A4-1.2 in appendix 1. The angle of pitching for the displacement values taken is shown in Figure A4-1.5. It can be seen that even for such large displacement the angle is small, less than 5 degrees. Whereas for the impact with a vertical surface the energy is absorbed horizontal along with the energy of the added mass. For this case the heave and pitch added mass may cause additional forces but they should approximately cancel in overall energy terms at least, over the course of the impact. So as an approximation the forces are ignored.

It is interesting to comment on the magnitude of the kinetic energy due to the vertical displacement (E3 in Figure A4-1.2) and due to angular velocity, (E4 in Figure A4-1.2). The former is approximately 1000 times smaller compared to the kinetic, or friction energy and the latter is approximately 9% of the kinetic energy, but comparable to the friction energy for the duration 0 to 5 seconds. This is due to the angular velocity $\omega$, which is relatively high at the initiation of the impact, as it is shown in Figure A4-1.4.

Contrary to these values the friction energy is very high, and this phenomenon, defines the importance of the friction coefficient. Smaller friction coefficient would produce travelling distance much higher than the one calculated here. Indeed, Pedersen (1995), in his study calculated very high travelling distances (30-90 meters, dependent on the slope of the slide) for a friction coefficient $\mu$=0.6 and initial velocity $v_o$=8 m/s for a tanker 60000 DWT.

The following Table displays the friction energy percentage with regard to the initial kinetic energy for the grounding problem examined analytically for the tanker.

| TIME | ENERGY FROM FRICTION in MNm | Percentage to $E_{ko}$ |
|---|---|---|
| 0.2 | 0.95 | 0.20% |
| 0.4 | 4.72 | 0.98% |
| 0.6 | 9.83 | 2.05% |
| 0.8 | 16.68 | 3.47% |
| 1.0 | 27.27 | 5.68% |
| 1.2 | 35.20 | 7.33% |
| 1.4 | 46.66 | 9.72% |
| 1.6 | 59.38 | 12.37% |
| 1.8 | 73.22 | 15.25% |
| 2.0 | 87.96 | 18.33% |
| 2.2 | 103.40 | 21.54% |
| 2.4 | 116.14 | 24.20% |
| 2.6 | 132.38 | 27.58% |
| 2.8 | 145.71 | 30.36% |
| 3.0 | 161.92 | 33.73% |
| 3.27 | 179.10 | 37.31% |
| 4.45 | 252.20 | 52.54% |
| 8.75 | 388.93 | 81.03% |
| 19.46 | 458.24 | 95.47% |

**TABLE 4.1** PERCENTAGES OF THE FRICTION ENERGY WITH REGARD TO THE INITIAL KINETIC ENERGY

Apart from the fact that for a rigid hull, the friction energy is the primary counterbalance to the kinetic energy during the grounding, no other conclusion can be drawn from Table 4.1 yet. The results presented in this Table will, later on, be compared to those, for a deformed hull, from the finite element analysis.

The indentation and final resting time as calculated from the analytical solution are found as;

Indentation = 25.2 meters

Duration = 25.00 seconds

The validity of these results will be discussed when the outcome from the finite element analysis is drawn. As mentioned previously, in the energy conservation described by equation 4.10, the elasto-plastic energy absorbed by the structure is not incorporated in the analysis. This is the question the numerical analysis aims to answer, along with the effects on the global response of the vessel.

### *4.4.4 MAXIMUM BENDING MOMENT CAPACITY*

Evaluation of equation 4.6 regarding the maximum bending moment capacity of the vessel near amidships, follows, using the analytical approach. Figure A4-1.3, in appendix 1, displays the bending moment with regard to the indentation and the time.

According to this analysis beyond time 3.95 seconds, when the indentation is 17.05m, the bending moment exceeds the maximum allowable capacity as this is calculated from equation 4.1. Thus total collapse of the vessel occurs at this stage. The limitation associated to total collapse, as discussed earlier, apply here as well.

Using this ultimate bending moment as a criterion of failure the critical speed prior to the grounding may be defined, using the energy equation 4.10.

For an indentation 21m from Figure A4-1.2, the kinetic energy stored at the system is, 341.2 MNm. Thus the remaining energy to be consumed on the system is

$$\text{Reserved Energy} = (\text{Initial Kinetic Energy})_o - 341.2 \quad [\text{MJoules}]$$

Therefore the required initial kinetic energy is

$$(\text{Initial Kinetic Energy})_1 = (\text{Initial Kinetic Energy})_o - \text{Reserved Energy}$$

or

$$(\text{Initial Kinetic Energy})_1 = 341.2 \quad [\text{MJoules}]$$

Going backwards, with this kinetic energy known the initial velocity is found as;

$$V_{required} = [2 \cdot (\text{Initial Kinetic Energy})_1 / M]^{0.5}$$
$$= 4.98 \text{ m/sec}$$

Hence, if the ship travels with an initial velocity of 4.98 m/sec the maximum bending moment at LCG will not exceed the maximum allowable capacity. This scenario is plotted in Figure 4.5

## 4.5 THE FINITE ELEMENT RESULTS

The structural configuration is the same as described in chapter 3, Section 3.2. The same notation for the bow individual members will be used in this Section. The initial distance of the vessel from the rigid slide is equal to zero. The results will be presented in terms of global and local response separately.

### *4.5.1 GLOBAL RESPONSE*

In this Section, the parameters involved are directly related to the kinematic relationship of the vessel during the impact; they are listed below:

- Energy Conservation
  - *The kinetic energy*
  - *The elastic energy derived on the structure*
  - *The plastic energy dissipated*
  - *The frictional energy*
- The reaction forces on the rigid slope
- The reaction forces and moments on the collision bulkhead
- The angular velocity
- The speed versus time and indentation relation

In the energy conservation the quantities related to the angular velocity energy of the mass around the centre of flotation and the vertical movement of the centre of

gravity will be ignored because they represent a small percentage as discussed previously, in the analytical calculation, Figure A4-1.2.

The four energy quantities are plotted with respect to the time in Figure 4.7, and with respect to the travelling distance in Figure 4.8. It can be seen that the elasto-plastic energy due to deformation of the structure (E2+E3, in Figure 4.7 & 4.8) is a big percentage of the total energy released during the impact. The following Table displays, in detail, the distribution of the energy quantities with regard to the kinetic energy prior to the grounding. The elasto-plastic energy is included as one compound energy quantity.

| Time | Friction Energy From Table 4.1 | Friction Energy From ABAQUS | Elasto-Plastic Energy From ABAQUS |
|---|---|---|---|
| 0.2 | 0.20% | 0.92% | 0.36% |
| 0.4 | 0.98% | 3.83% | 1.48% |
| 0.6 | 2.05% | 8.03% | 3.22% |
| 0.8 | 3.47% | 13.21% | 5.50% |
| 1.0 | 5.68% | 20.41% | 8.60% |
| 1.2 | 7.33% | 28.92% | 11.79% |
| 1.4 | 9.72% | 37.53% | 14.91% |
| 1.6 | 12.37% | 45.19% | 17.46% |
| 1.8 | 15.25% | 52.05% | 19.53% |
| 2.0 | 18.33% | 57.85% | 21.19% |
| 2.2 | 21.54% | 62.64% | 22.56% |
| 2.4 | 24.20% | 66.41% | 23.66% |
| 2.6 | 27.58% | 69.41% | 24.60% |
| 2.8 | 30.36% | 71.57% | 25.41% |
| 3.0 | 33.73% | 73.00% | 25.99% |
| 3.27 | 37.31% | 73.14% | 26.77% |

**TABLE 4.2** PERCENTAGES OF THE FRICTION AND ELASTO-PLASTIC ENERGY QUANTITIES WITH REGARD TO THE INITIAL KINETIC ENERGY

These results show that the elasto-plastic energy is not a negligible amount compared to the initial kinetic energy and its contribution should be incorporated in the analytical calculations for the estimation of the indentation and duration of the grounding.

Comparing the energy derived from the friction force, it can be seen, that values obtained from the finite element analysis are much greater to those from the analytical calculations. Two key points, listed below, should be taken into consideration in this correlation;

1. At the final time shown in Table 4.2, the vessel is still moving towards the rigid surface, in the case of the analytical solution. However at the specified time of 3.27 the vessel is supposed to have come to rest as far as the numerical results are concerned

2. The value of the energy derived from the friction force, in the analytical calculation is based upon consideration of *one* contact point. In the numerical results it is found that *more than one* contact points exist, as shown in Figure 4.6 and additionally the reaction forces are found to be larger than those of the analytical calculations. Thus equation 2.23 should be reconFigured, with the introduction of a distributed load r(x,t) instead of a point load. If a= LCG and b= LCB(t), equation 2.23 becomes

$$\int_0^x r(x,t)dx = \nabla g\left(1-\frac{LCG-x_1(t)}{LCB(t)-x_1(t)}\right) \qquad 4.11$$

where $x_1(t)$ is the distance of the centre of the resultant reaction force from the fore end of the vessel.

Equation 4.11 has been evaluated for triangular and rectangular distributed loads.

Triangular Distribution Figure A4-1.6-a

For a specific time $t_i$ $\int_0^x r(x,t_i)dx = R_{max(i)}\left(1-\frac{x}{h}\right)$

where $R_{max}$ = is the maximum reaction at the fore end

x = distance from the forward end of the vessel

h = The longitudinal extend of the distribution

For this case the reaction force is plotted in Figure 4.9. One may see that the difference obtained from the point load is not more than 20%.

Rectangular Distribution Figure A4-1.6-b

For a specific time $t_i$ $$\int_0^x r(x,t_i)dx = R(x)\cdot h$$

where h = The longitudinal extend of the distribution

For this case the reaction force is plotted in Figure 4.9. One may see that the difference obtained from this case compared to the initial case is almost 50%. Both distributions showed increase in the reaction forces, however this increase was not enough to reach the values acquired from the numerical results.

For the grounding problem, the reaction forces are plotted in Figure 4.9 with regard to the indentation. It is conspicuous that the reaction forces calculated from the numerical analysis are much higher compared to those of the analytical calculation. Although for the static approach, the reaction forces increase linearly throughout the impact, for the dynamic case they increase almost linearly, until penetration reaches 6.60 meters. Thereafter the reaction force remains constant and after 8 meters of penetration decreases.

The difference between the magnitude of the reaction force produced from the numerical and analytical approaches is attributed to the characteristics related to the reaction force described previously, in equation 4.11, as well as the contribution of the mass inertia and the global bending of the bow model.

The variation of the reaction force, in the dynamic case, is related to the progressive deformation of the bottom part of the bow. When the structure collapses, it absorbs energy, which consequently decreases the amount of the reaction force derived from the rigid slope. This variation is also shown in the bending moment developed on the collision bulkhead Figure 4.10.

The crushing of the bow members during the impacted is reflected also in the speed of the vessel. In Figure 4.11 the decrease in the velocity, is shown. Indentation of 6.6 meters corresponds to time equal to 1.2 seconds. At this time the vessel starts decelerating faster, since the slope in the curve of the speed decreases, until the duration becomes 1.75 seconds.

Similar observations are shown in Figures 4.12 and 4.13, where the angle of pitching and the angular velocity are drawn with respect to the duration of the impact. The high reaction forces developed on the structure affect not only the local response but also the global rotation of the model. The angle of pitching regarding the dynamic problem does not represent the angle of the whole vessel, since local bending of the bow model is observed with regard to the collision bulkhead plane, as shown in Figure 4.6. The local bending of the bow commences at time 1.1 seconds, when the slope in the angle increases. One may see in Figure 4.13 that the angular velocity at this time increases rapidly, reaching the maximum value of 4.5 degrees/sec at time 1.8 seconds. Thereafter it decreases, until the vessel comes to rest.

Because of this rotation in the bow area, the outer shell of the model bends inwards in order to respond to this bending mechanism, which results to the appearance of high strains on areas where plasticity develops fast with respect to the time. These areas are shown in Figure 4.14.

It transpires from the numerical results, that there are obvious differences with the analytical calculations. This is mainly attributed to the effect of the elasto-plastic energy dissipated on the structure as well as in the inelastic response of the vessel which produces a local bending effect of the bow model due to the reaction forces derived. The indentation calculated from the numerical approach, is almost half the travelling distance estimated from the static calculation.

### *4.5.2 LOCAL RESPONSE*

The dispersion of this elasto-plastic energy amongst the structural elements of the bow is shown in Figures 4.15-4.27. Similarly to the energy balance that took place in

the case of the head on collision with the vertical surface, one may see that in the case of grounding maximum energy is being absorbed by the shell structure as displayed in Figure 4.27.

Table 4.3 includes the total energy absorbed by the structural members in terms of elastic, plastic and friction energy, only for the shell of the bow since is the only part that comes in contact with the rigid slope.

| Member | Elastic Energy | Plastic Energy | Friction Energy |
|---|---|---|---|
| **Bulk1** | 1.159 | 1.055 | ----- |
| **Bulk2** | 0.214 | 4.870 | ----- |
| **Bulk3** | 0.192 | 8.982 | ----- |
| **Deck1** | 0.155 | 5.158 | ----- |
| **Deck2** | 0.219 | 4.265 | ----- |
| **Deck3** | 0.009 | 0.004 | ----- |
| **Deck4** | 0.120 | 4.950 | ----- |
| **Deck5** | 0.035 | 0.354 | ----- |
| **Deck6** | 0.031 | 1.077 | ----- |
| **Deck7** | 0.067 | 0.938 | ----- |
| **Deck8** | 0.070 | 2.727 | ----- |
| **Deck9** | 0.132 | 3.025 | ----- |
| **Shell** | 3.625 | 60.14 | 374.2 |

**TABLE 4.3** TOTAL ELASTIC AND PLASTIC ENERGY DISSIPATED ON THE STRUCTURAL MEMBERS, THE CODES FOR THE MEMBERS ARE SHOWN IN FIGURE A3-2.3

One may see that the friction energy holds the largest percentage of the released energy, almost 78.3%. From the other members the longitudinal bulkhead Bulk3 contributes a great deal and other members following are Deck1, Deck4, Bulk2 etc. Contrary to the case of the head-on collision, in this situation Decks 7 and 8 do not absorb a lot of energy, since they do not come in contact with the rigid slope.

The deformation of Bulk3 is shown in Figure 4.28. It can be seen that this member is heavily distorted towards the top section where cripples appear at the connection with member Deck1. High tensile stresses appear on the lower right location, at the connection with the collision bulkhead. The local strains at this area exceed the 10% at the final stage of the grounding. One may note a discontinuity on the Von-Mises stresses towards the bottom. This is attributed to the change of thickness on the shell elements as shown previously in Figure A3-2.3.

Similar examination takes place for the outer shell and the rest of the inner scantling of the vessel. In Figure 4.29 a contour of the Von-Mises stresses is shown. High values appear (with red colour) in areas that twist because of the bending mechanism. The bottom part of the structure is folded inwards following the geometric restriction from the rigid slope. The plastic energy dissipated in the shell due to the grounding is concentrated in the bottom part. In Figure 4.31 a contour of the plastic energy density is shown at the time of 3.2 seconds, just prior to the arrest of the vessel.

The deformed inner structure arrangements are shown in Figure 4.30. The contour displays the Von-Mises stresses. Severe damage occurred in the decks, at the aft end, where they are attached to the collision bulkhead (Bulk1) and the longitudinal diaphragm (Bulk3). Deck 1 suffered local buckling along the breadth towards the aft end due to the twisting action during the grounding. Members Deck7 and Deck8 are shown not to have experienced large loads. They have buckled longitudinally (Deck9) and transversely (Deck8) due to the shear load transmitted from the outer shell during to the contact

As mentioned previously the angle of pitching of the bow, Figure 4.12, starts to increase when the indentation is approximately 6 meters. As it can be seen in Figures 4.15 to 4.27 in most members the plastic energy starts increasing from 6 meters onwards. Therefore it is concluded that this bending response of the bow contributes to the plastic energy dissipated on the structure of the bow.

## APPENDIX I

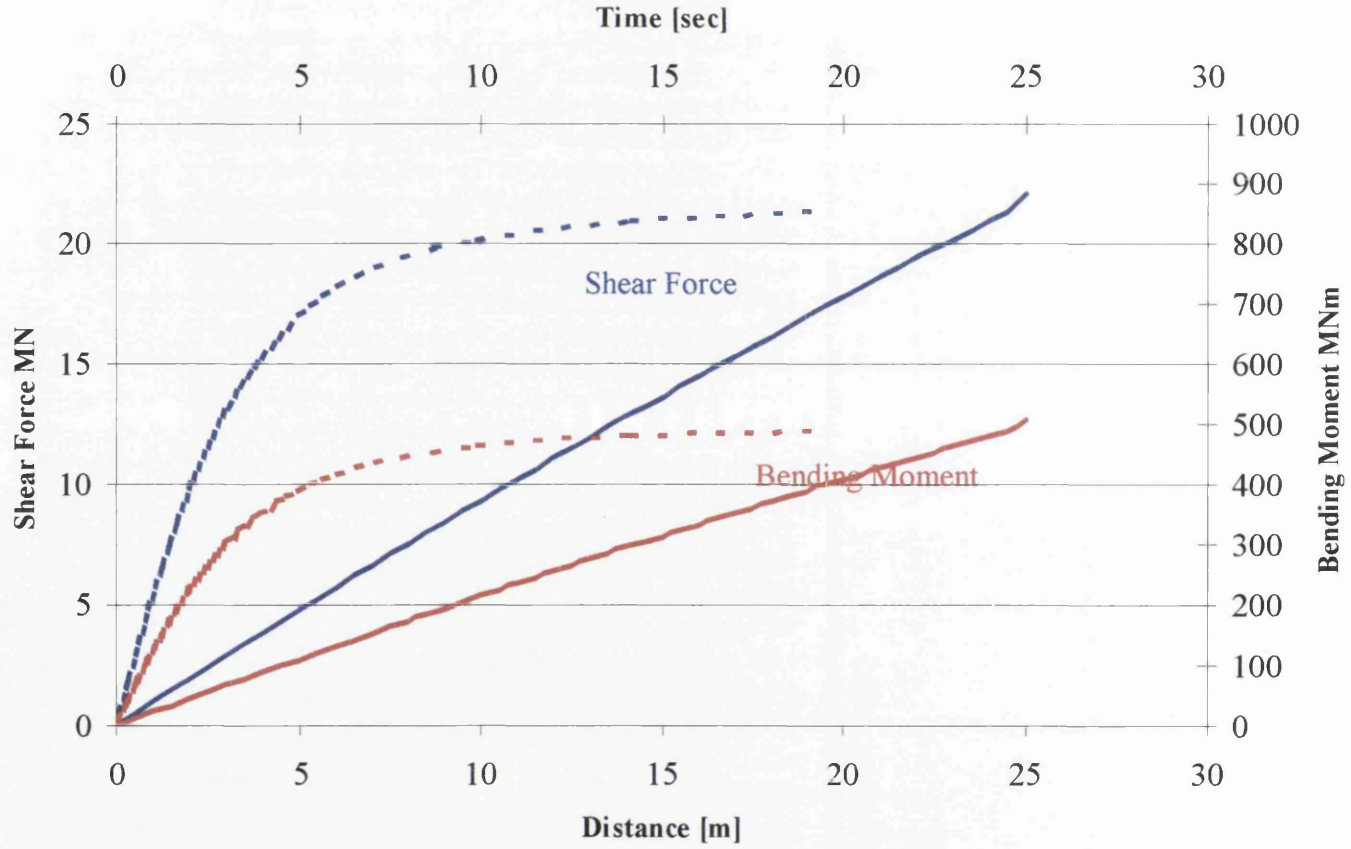


**FIGURE A4-1.1** Bending moment and shear force on the collision bulkhead. The lower X-axis is in respect to the distance (straight lines) while the vessel travel on the slide and the Upper X-axis is in respect to the duration (Dotted lines) of the impact.

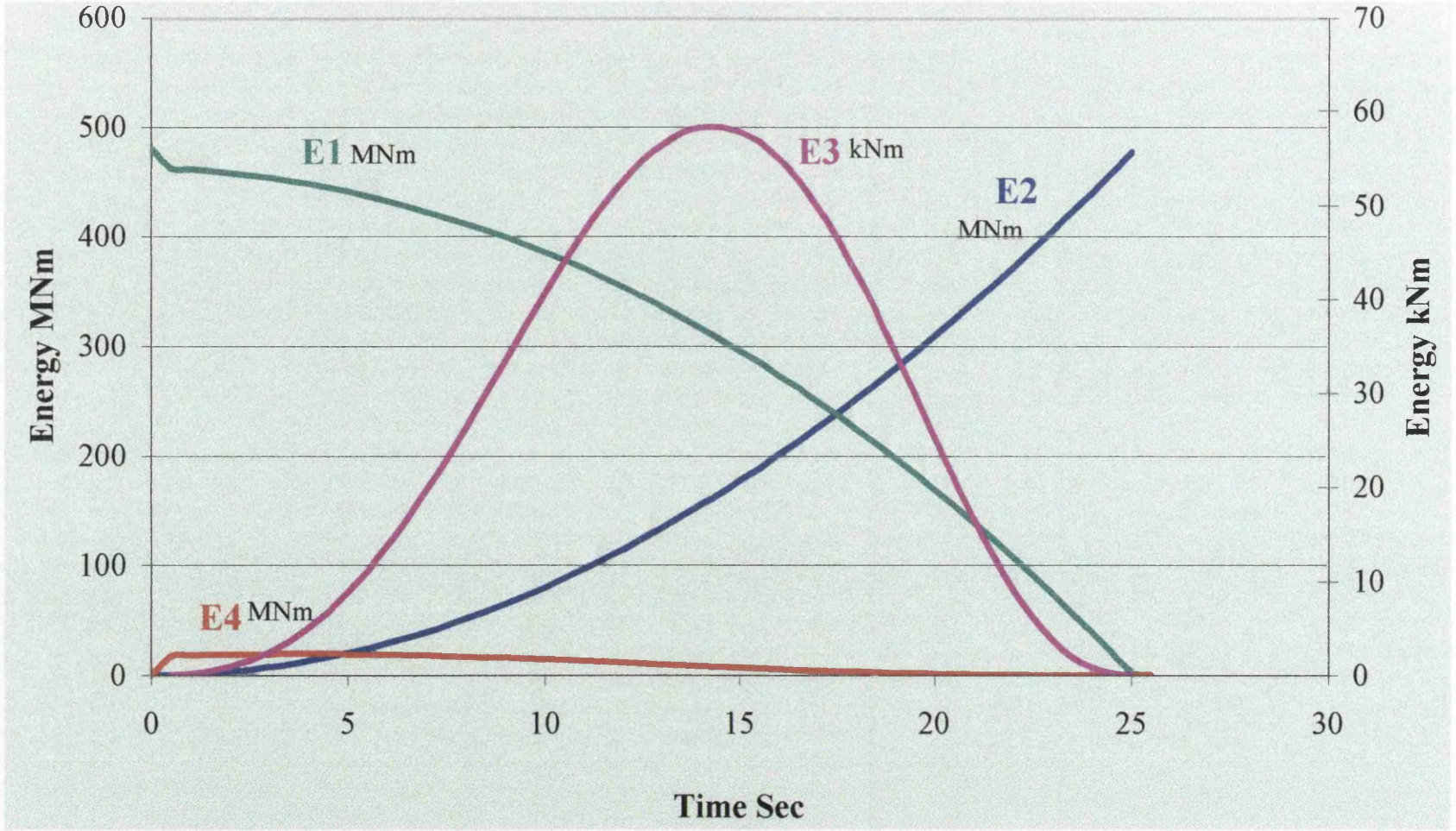


**FIGURE A4-1.2** E1 is the kinetic Energy, E2 is the friction energy, E3 is the kinetic energy due to vertical displacement, Note this energy amount is in kNm, E4 is the energy because of rotation around the Centre of flotation

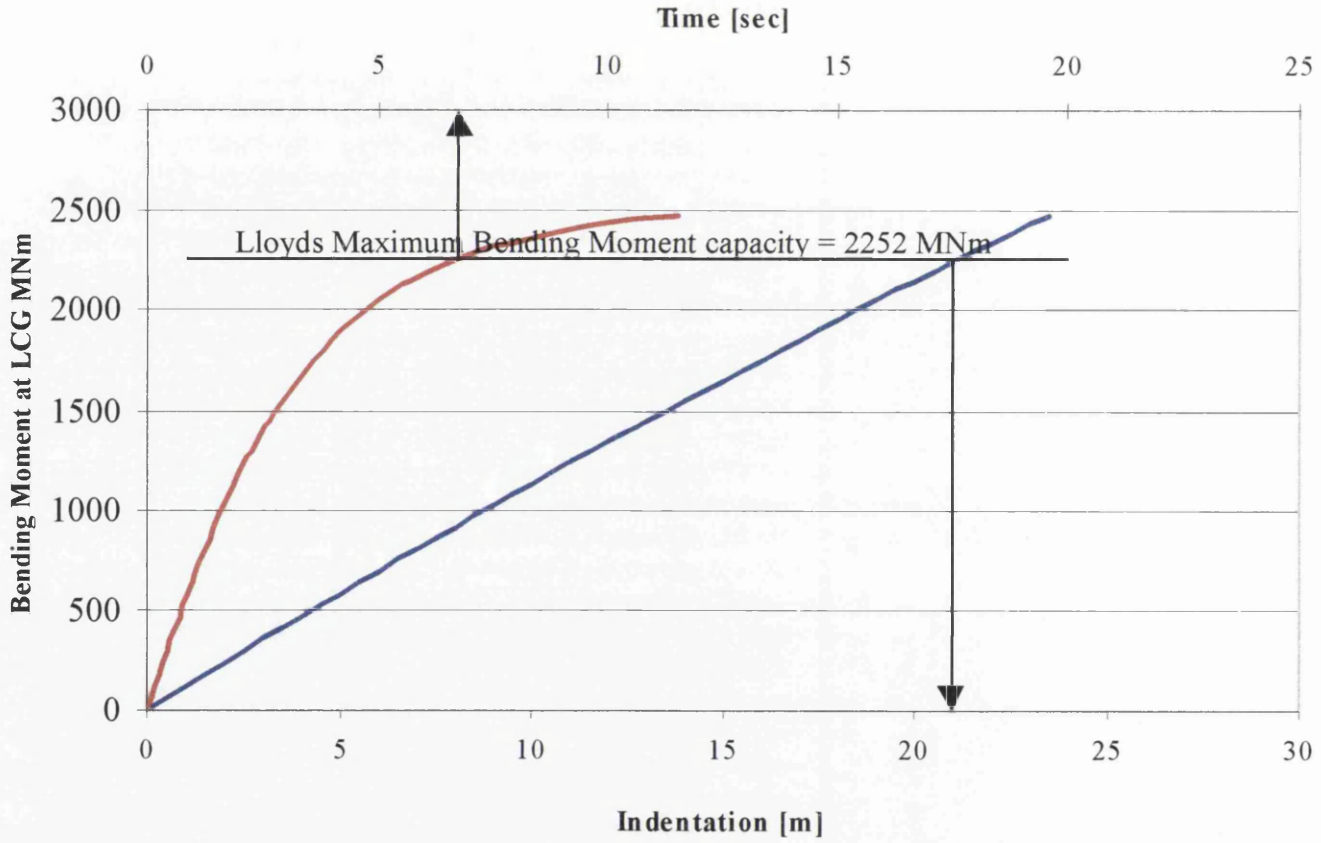


**FIGURE A4-1.3** The bending moment at the centre of gravity is drawn, in respect to the displacement and time during the impact. When it reaches the value of 2252 MNm then probable total collapse of the vessel occur

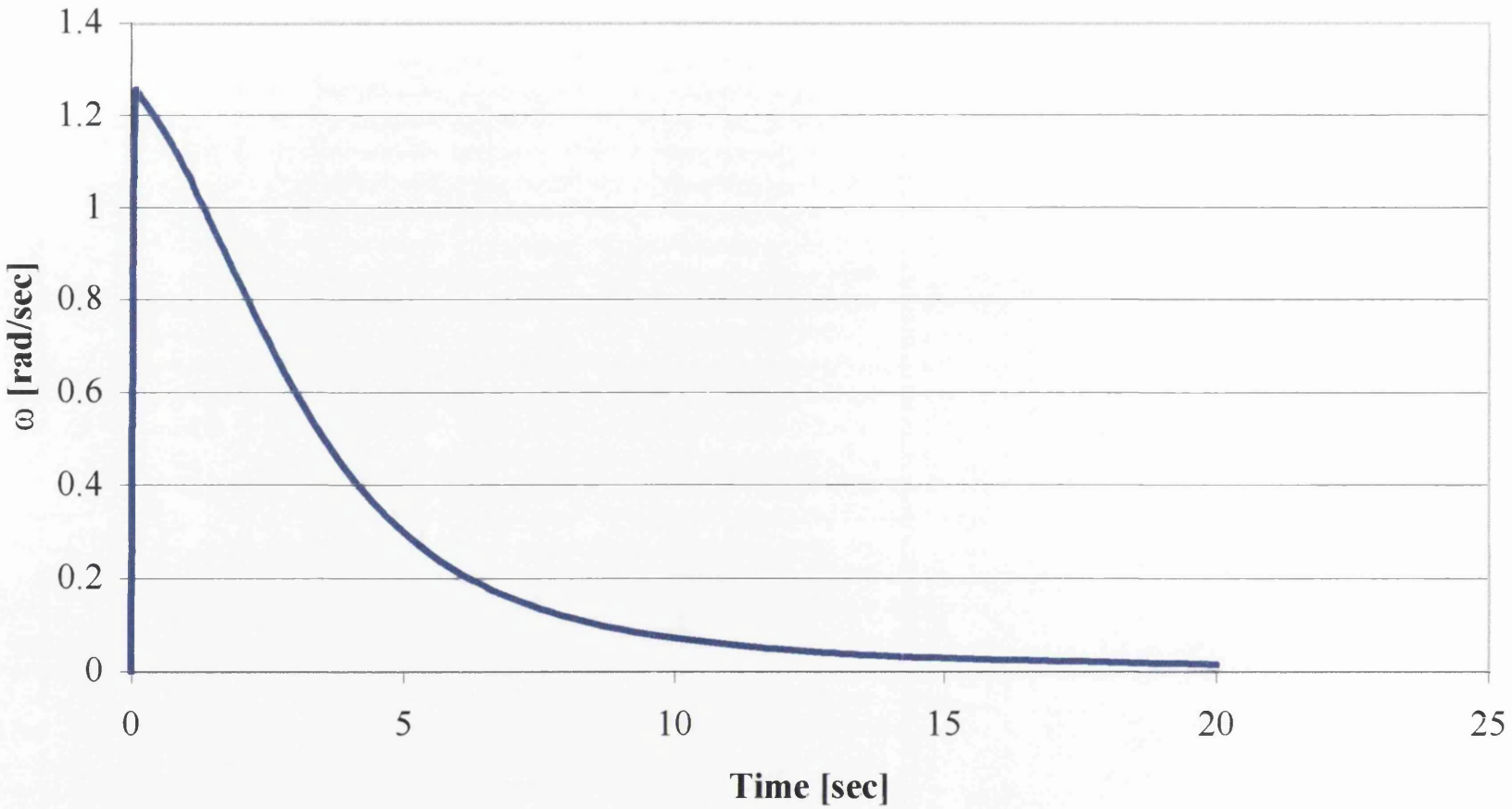


**FIGURE A4-1.4** The angular velocity in respect of the centre of flotation.

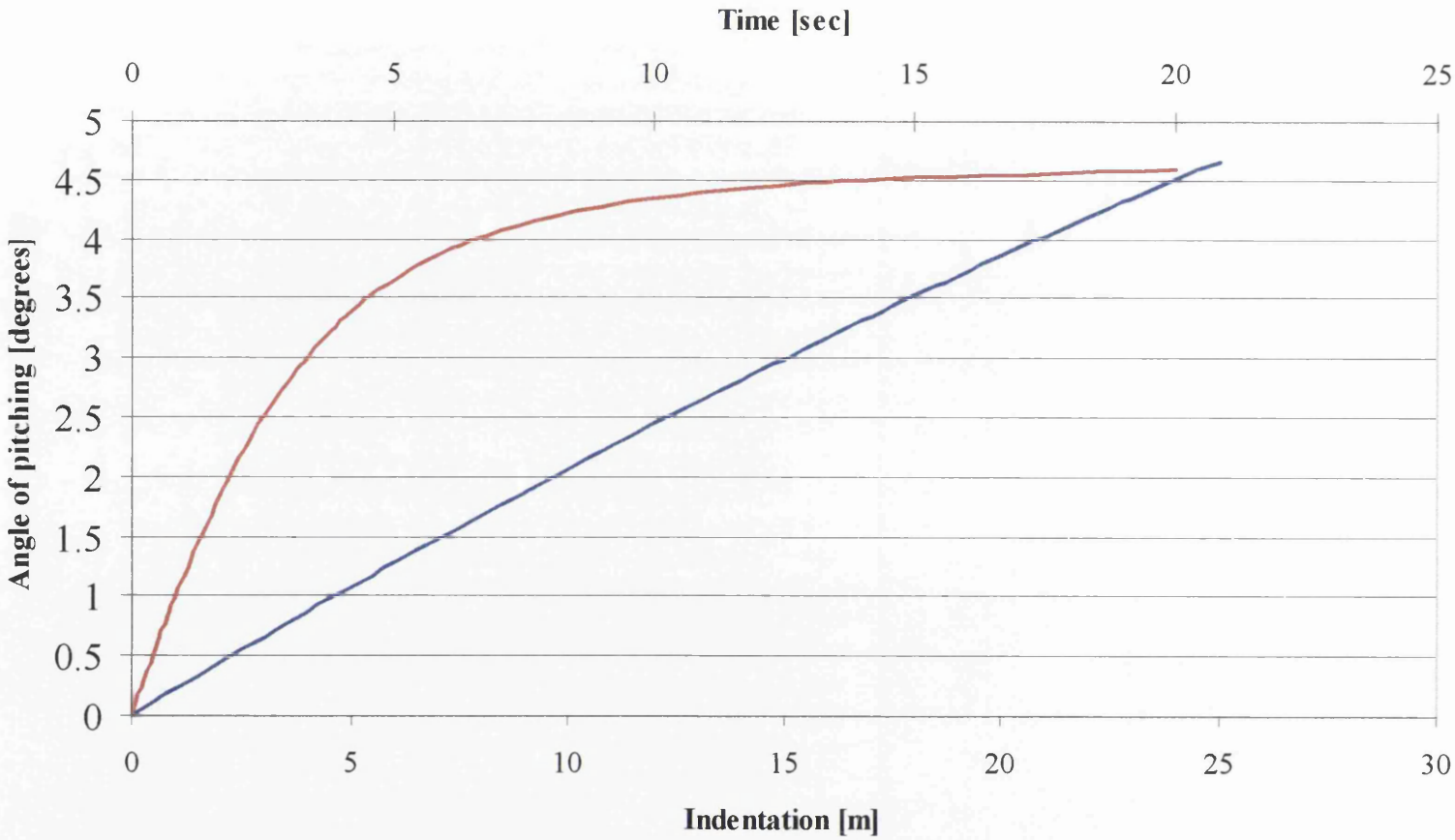


**FIGURE A4-1.5** The angle of pitching with regard to the indentation, (in blue line), and the time (in red line)

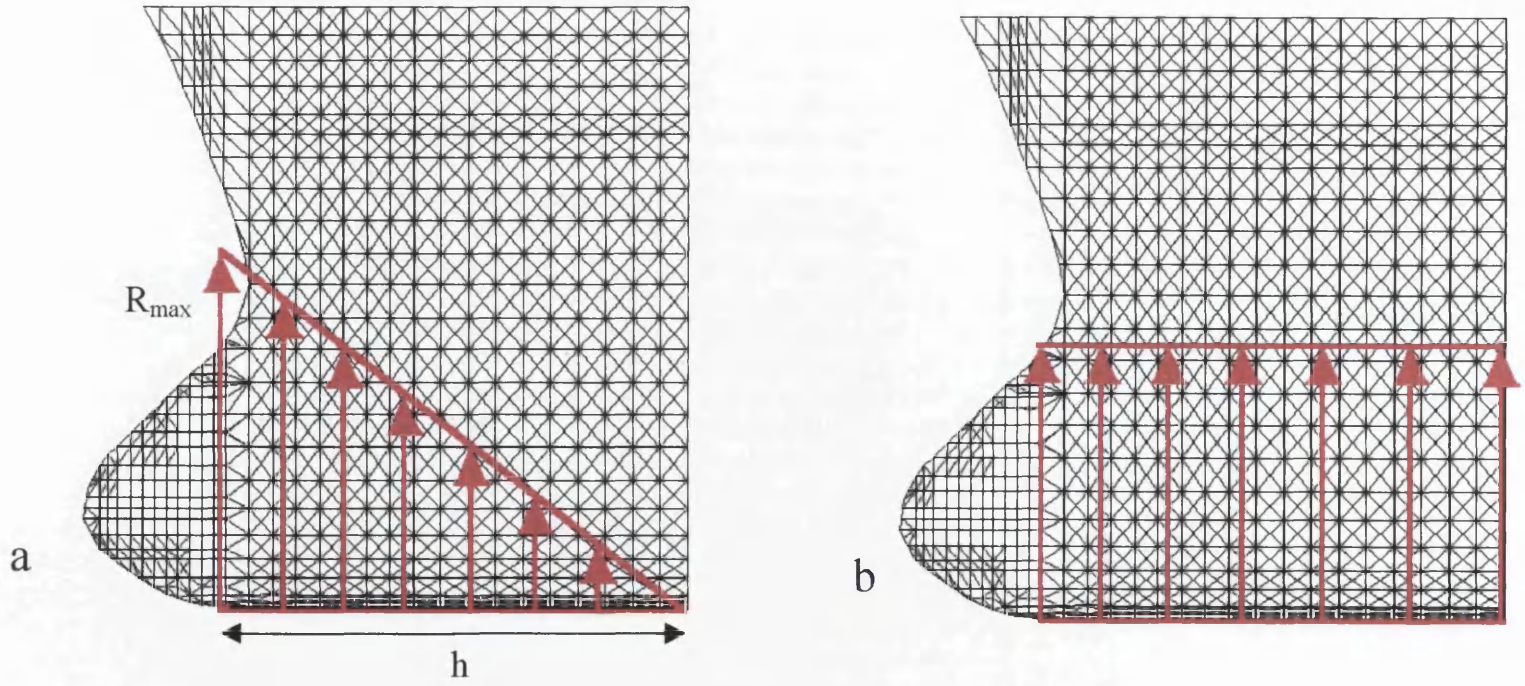


**FIGURE A4-1.6** The load distribution for the reaction during the grounding

# APPENDIX II

Table of Hydrostatics

| Draft | Displacement | LCB | VCB | TPC | LCF | MTC | KML | KMT |
|---|---|---|---|---|---|---|---|---|
| m | Metric Tons | m | m | | m | m-MT | m | m |
| 0 | 0 | | | | | | | |
| 0.2 | 471.56 | 69.914a | 0.102 | 24.54 | 69.928a | 43237 | 5252.81 | 190.454 |
| 0.4 | 973.28 | 69.957a | 0.204 | 25.56 | 70.074a | 46888 | 2759.95 | 99.995 |
| 0.6 | 1492.14 | 70.018a | 0.307 | 26.29 | 70.170a | 49660 | 1906.69 | 69.014 |
| 0.8 | 2023.72 | 70.066a | 0.411 | 26.85 | 70.222a | 51912 | 1469.59 | 53.123 |
| 1 | 2565.4 | 70.108a | 0.514 | 27.31 | 70.295a | 53863 | 1202.86 | 43.363 |
| 1.2 | 3115.37 | 70.148a | 0.618 | 27.68 | 70.374a | 55525 | 1021.08 | 36.708 |
| 1.4 | 3672.03 | 70.188a | 0.721 | 27.98 | 70.446a | 56966 | 888.77 | 31.893 |
| 1.6 | 4234.21 | 70.229a | 0.825 | 28.23 | 70.544a | 58136 | 786.6 | 28.272 |
| 1.8 | 4801.15 | 70.274a | 0.928 | 28.45 | 70.652a | 59186 | 706.23 | 25.463 |
| 2 | 5372.27 | 70.320a | 1.032 | 28.65 | 70.743a | 60155 | 641.49 | 23.21 |
| 2.2 | 5947.19 | 70.366a | 1.135 | 28.83 | 70.817a | 61085 | 588.44 | 21.375 |
| 2.4 | 6525.66 | 70.412a | 1.238 | 29 | 70.898a | 61956 | 543.92 | 19.854 |
| 2.6 | 7107.35 | 70.457a | 1.342 | 29.15 | 70.980a | 62763 | 505.91 | 18.573 |

| Draft | Displacement | LCB | VCB | TPC | LCF | MTC | KML | KMT |
|---|---|---|---|---|---|---|---|---|
| m | Metric Tons | m | m | | m | m-MT | m | m |
| 2.8 | 7691.98 | 70.503a | 1.445 | 29.28 | 71.061a | 63518 | 473.09 | 17.484 |
| 3 | 8279.32 | 70.549a | 1.548 | 29.41 | 71.148a | 64202 | 444.25 | 16.553 |
| 3.2 | 8869.11 | 70.595a | 1.652 | 29.52 | 71.237a | 64822 | 418.72 | 15.744 |
| 3.4 | 9461.13 | 70.642a | 1.755 | 29.63 | 71.321a | 65393 | 395.98 | 15.041 |
| 3.6 | 10055.25 | 70.689a | 1.858 | 29.72 | 71.404a | 65941 | 375.7 | 14.428 |
| 3.8 | 10651.37 | 70.737a | 1.961 | 29.81 | 71.493a | 66455 | 357.44 | 13.89 |
| 4 | 11249.41 | 70.785a | 2.065 | 29.9 | 71.589a | 66958 | 341 | 13.415 |
| 4.2 | 11848.6 | 70.831a | 2.168 | 29.98 | 71.689a | 67410 | 325.94 | 12.991 |
| 4.4 | 12448.94 | 70.874a | 2.271 | 30.05 | 71.793a | 67846 | 312.23 | 12.615 |
| 4.6 | 13050.72 | 70.919a | 2.374 | 30.12 | 71.905a | 68257 | 299.64 | 12.283 |
| 4.8 | 13653.9 | 70.966a | 2.476 | 30.19 | 72.023a | 68661 | 288.09 | 11.986 |
| 5 | 14258.42 | 71.013a | 2.579 | 30.26 | 72.136a | 69051 | 277.45 | 11.722 |
| 5.2 | 14864.22 | 71.061a | 2.682 | 30.32 | 72.251a | 69411 | 267.52 | 11.486 |
| 5.4 | 15471.2 | 71.110a | 2.785 | 30.37 | 72.371a | 69745 | 258.27 | 11.273 |
| 5.6 | 16079.3 | 71.161a | 2.888 | 30.43 | 72.504a | 70112 | 249.81 | 11.083 |
| 5.8 | 16688.69 | 71.213a | 2.991 | 30.5 | 72.655a | 70548 | 242.18 | 10.915 |

| Draft | Displacement | LCB | VCB | TPC | LCF | MTC | KML | KMT |
|---|---|---|---|---|---|---|---|---|
| m | Metric Tons | m | m | | m | m-MT | m | m |
| 6 | 17299.44 | 71.266a | 3.093 | 30.57 | 72.807a | 70990 | 235.1 | 10.766 |
| 6.2 | 17911.58 | 71.322a | 3.196 | 30.64 | 72.960a | 71467 | 228.59 | 10.634 |
| 6.4 | 18525.2 | 71.379a | 3.299 | 30.71 | 73.110a | 71972 | 222.58 | 10.516 |
| 6.6 | 19140.32 | 71.438a | 3.402 | 30.79 | 73.259a | 72498 | 217 | 10.413 |
| 6.8 | 19757.14 | 71.498a | 3.505 | 30.88 | 73.431a | 73139 | 212.08 | 10.323 |
| 7 | 20375.79 | 71.560a | 3.609 | 30.97 | 73.608a | 73777 | 207.44 | 10.246 |
| 7.2 | 20996.37 | 71.624a | 3.712 | 31.07 | 73.794a | 74494 | 203.26 | 10.181 |
| 7.4 | 21619.05 | 71.690a | 3.816 | 31.17 | 73.983a | 75239 | 199.38 | 10.125 |
| 7.6 | 22243.85 | 71.758a | 3.919 | 31.28 | 74.187a | 76065 | 195.91 | 10.078 |
| 7.8 | 22870.81 | 71.827a | 4.023 | 31.41 | 74.398a | 77048 | 193 | 10.039 |
| 8 | 23500.46 | 71.899a | 4.127 | 31.55 | 74.617a | 78090 | 190.37 | 10.01 |
| 8.2 | 24132.87 | 71.974a | 4.231 | 31.69 | 74.837a | 79206 | 188.03 | 9.988 |
| 8.4 | 24768.11 | 72.050a | 4.336 | 31.83 | 75.058a | 80336 | 185.82 | 9.972 |
| 8.6 | 25406.28 | 72.129a | 4.44 | 31.97 | 75.269a | 81457 | 183.68 | 9.962 |
| 8.8 | 26047.29 | 72.209a | 4.545 | 32.12 | 75.475a | 82604 | 181.68 | 9.957 |
| 9 | 26691.05 | 72.290a | 4.65 | 32.26 | 75.666a | 83730 | 179.72 | 9.959 |

| Draft | Displacement | LCB | VCB | TPC | LCF | MTC | KML | KMT |
|---|---|---|---|---|---|---|---|---|
| m | Metric Tons | m | m | | m | m-MT | m | m |
| 9.2 | 27337.61 | 72.372a | 4.756 | 32.4 | 75.852a | 84829 | 177.77 | 9.966 |
| 9.4 | 27986.94 | 72.455a | 4.861 | 32.54 | 76.020a | 85942 | 175.93 | 9.977 |
| 9.6 | 28639.08 | 72.537a | 4.967 | 32.68 | 76.155a | 87071 | 174.18 | 9.992 |
| 9.8 | 29293.98 | 72.620a | 5.072 | 32.81 | 76.285a | 88191 | 172.47 | 10.01 |
| 10 | 29951.62 | 72.702a | 5.178 | 32.95 | 76.406a | 89293 | 170.79 | 10.033 |

# FIGURES

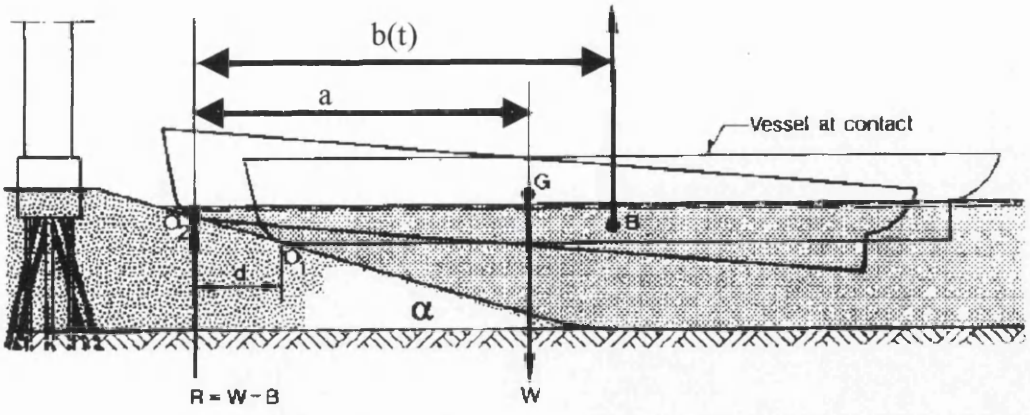


***Figure 4.1*** *Vessel during grounding*

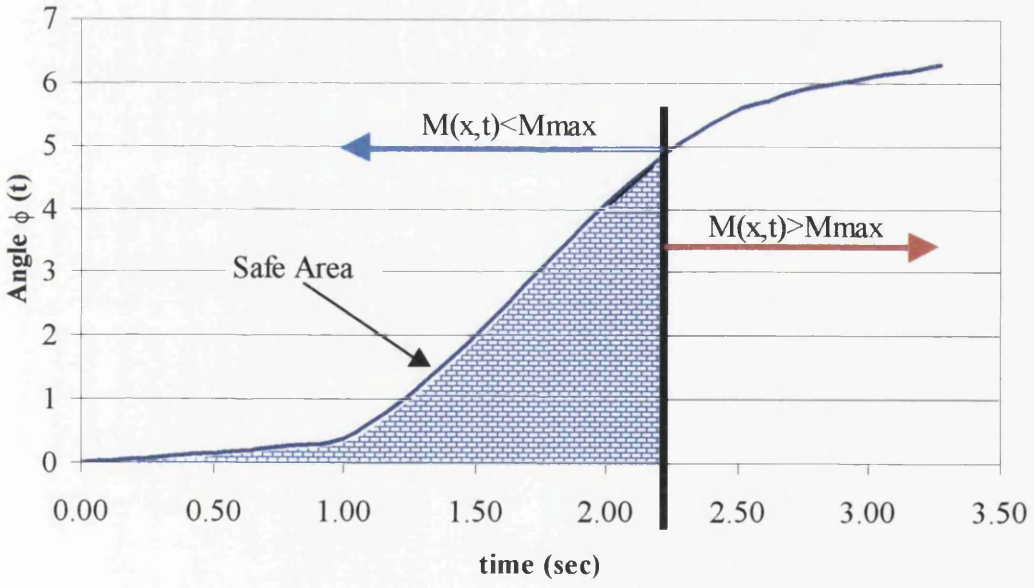


***Figure 4.2*** *The pitching angle of ship during grounding with a surface. The area coloured with blue is the safe zone where the ship is still able to withstand bending.*

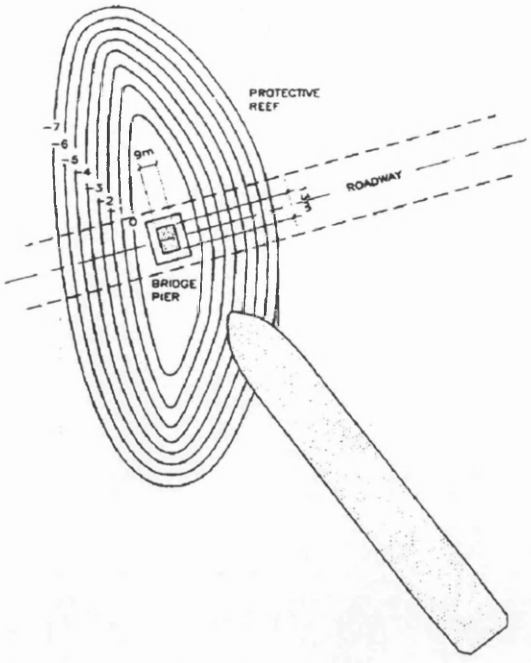


***Figure 4.3*** *Example of Artificial Island*

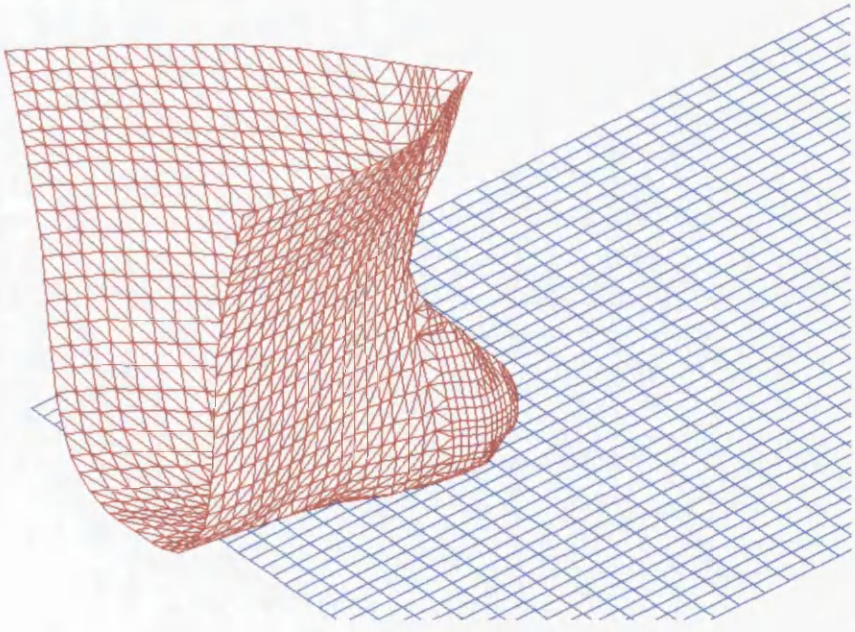

***Figure 4.4*** *The grounding scenario. In this Figure only the shell of the ship is shown*

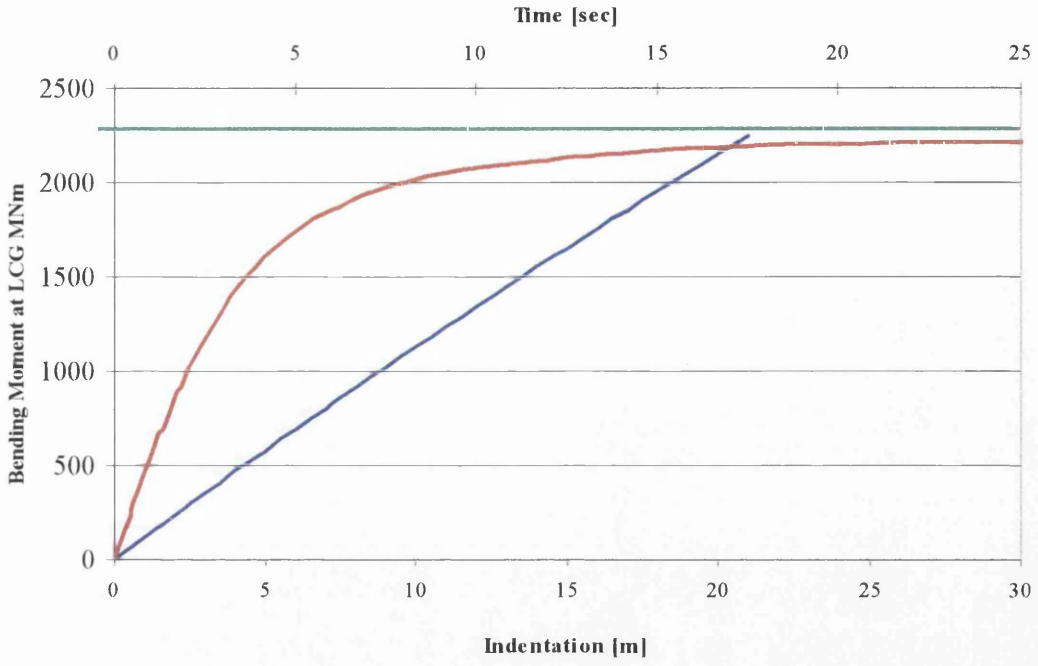


***Figure 4.5*** *Bending Moment at LCG. If the vessel strikes on the slide with an initial velocity of 4.98 m/sec, the bending moment will not exceed the maximum allowable capacity*

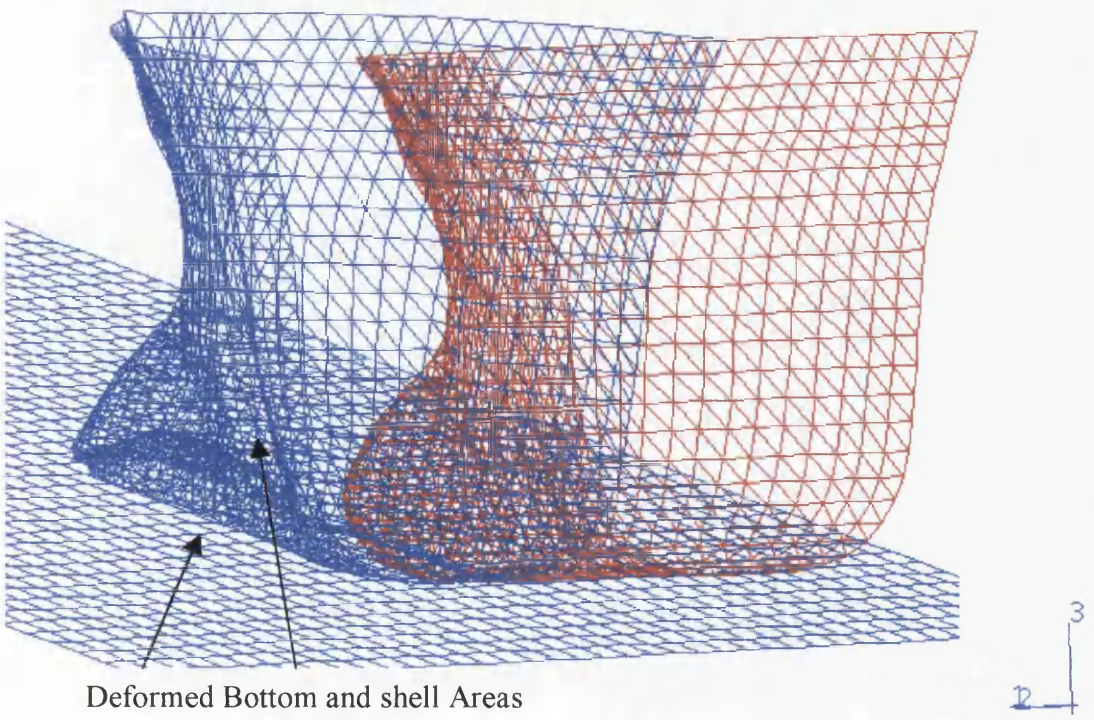


***Figure 4.6*** *The deformed and undeformed mesh of the outer shell during the grounding*

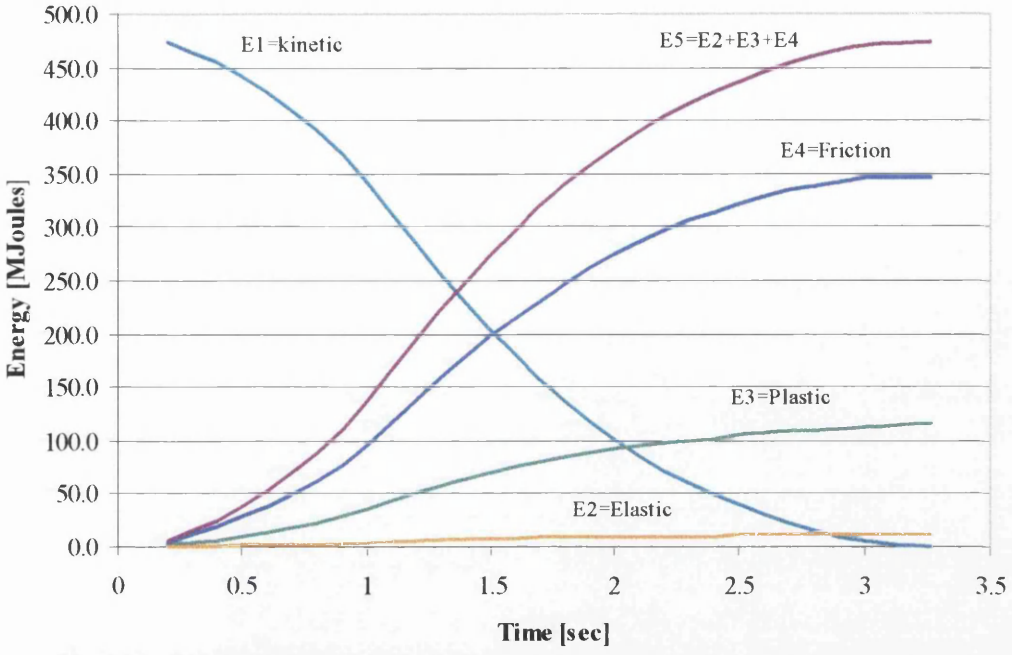


***Figure 4.7*** *Energy Conservation during the grounding, with respect to the duration of the impact. E1 is the kinetic energy, E2 is the elastic energy stored on the deformed structure, E3 is the plastic energy due to plastic deformation and E4 is the energy because of friction. The friction coefficient is 0.85*

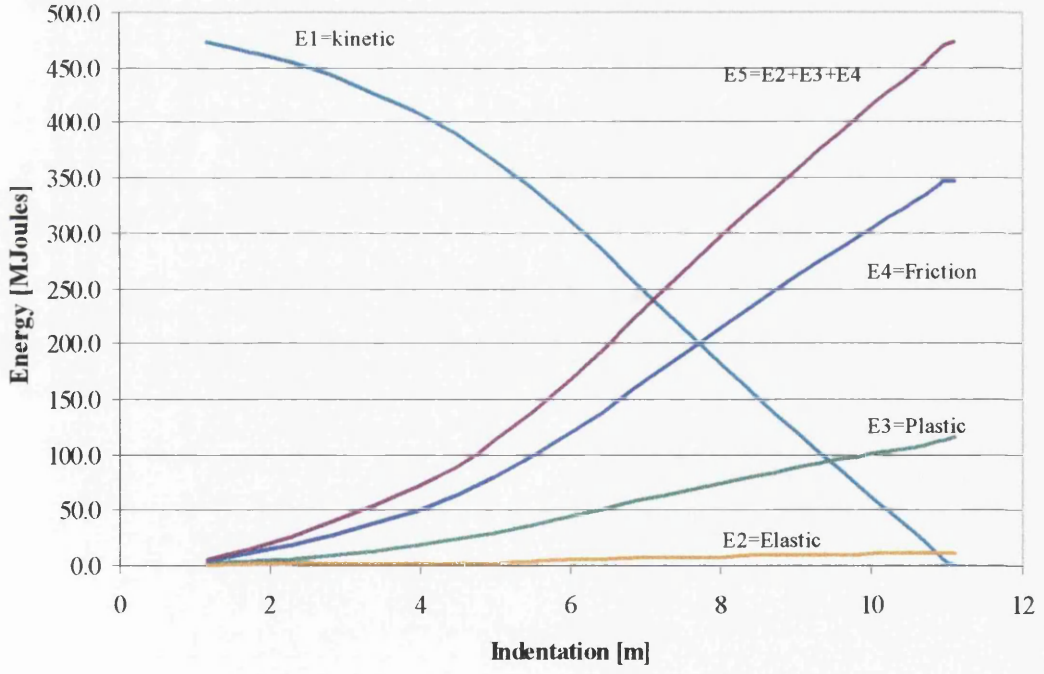


***Figure 4.8*** *Energy Conservation during the grounding, with respect to the duration of the Indentation. Energy quantities are similar to Figure 4.7*

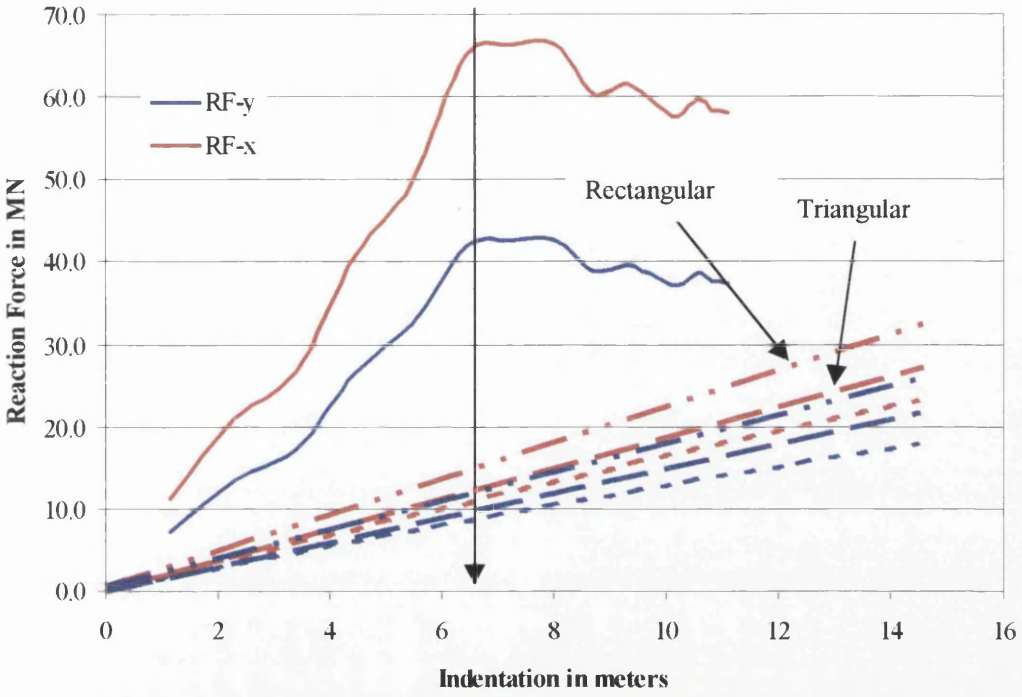


***Figure 4.9*** *Horizontal and vertical reaction forces developed on the rigid slope. The dashed lines represent the static analytical calculations while the continues lines represent the numerical calculation.*

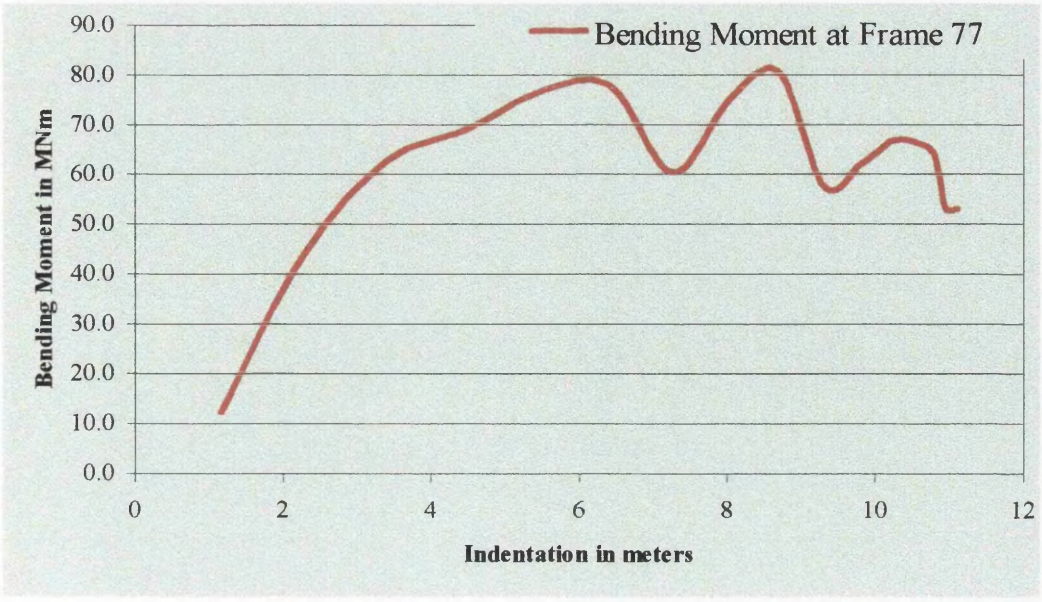


***Figure 4.10*** *Bending Moment on Bulkhead 77.*

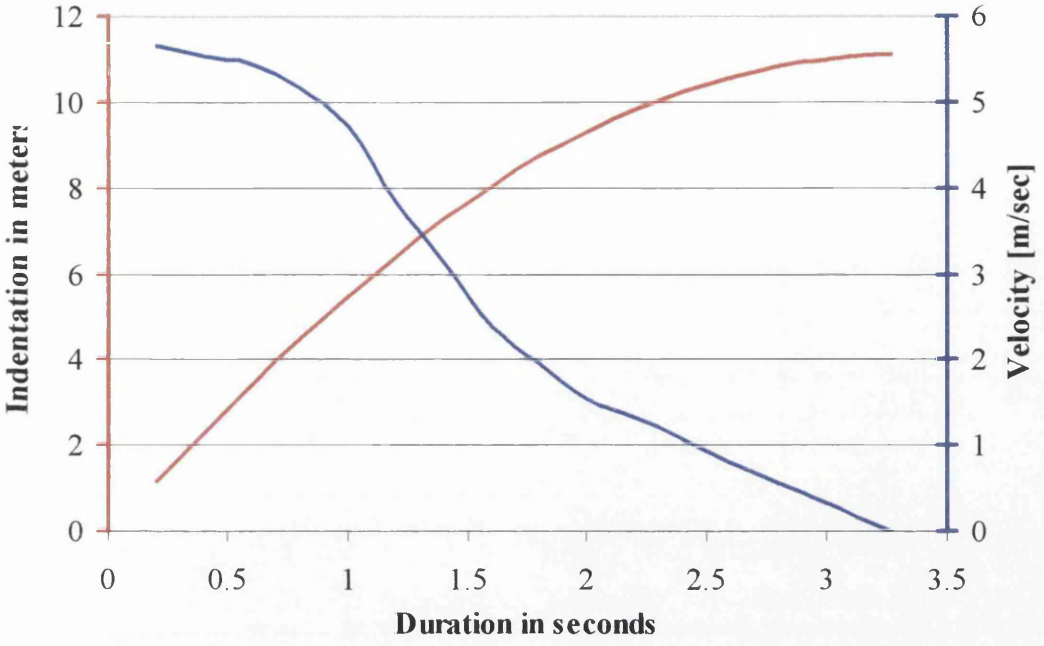


***Figure 4.11*** *The indentation and velocity of the vessel during the grounding.*

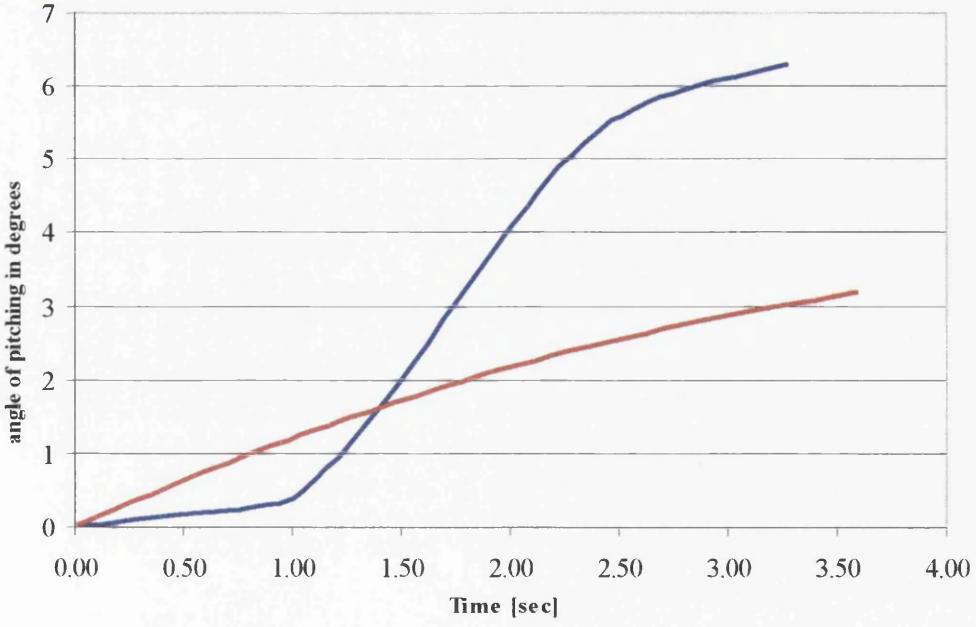


***Figure 4.12*** *Angle of pitching $\varphi(t)$ with regard to the duration of the impact. The red line presents the static solution described in section 4.4.2- and the blue line represents the numerical solution*

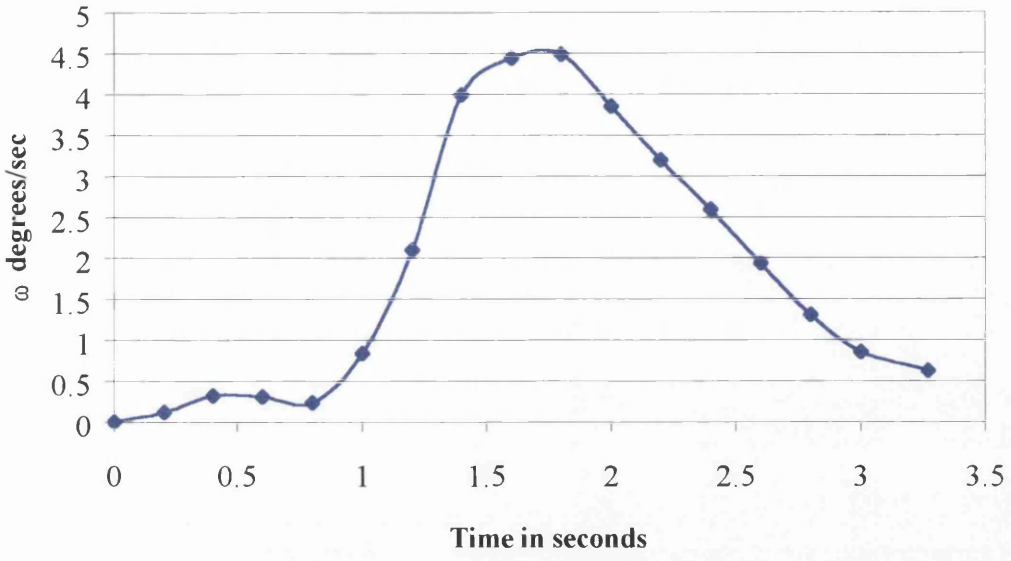


***Figure 4.13*** *The angular velocity of the bow during the grounding.*

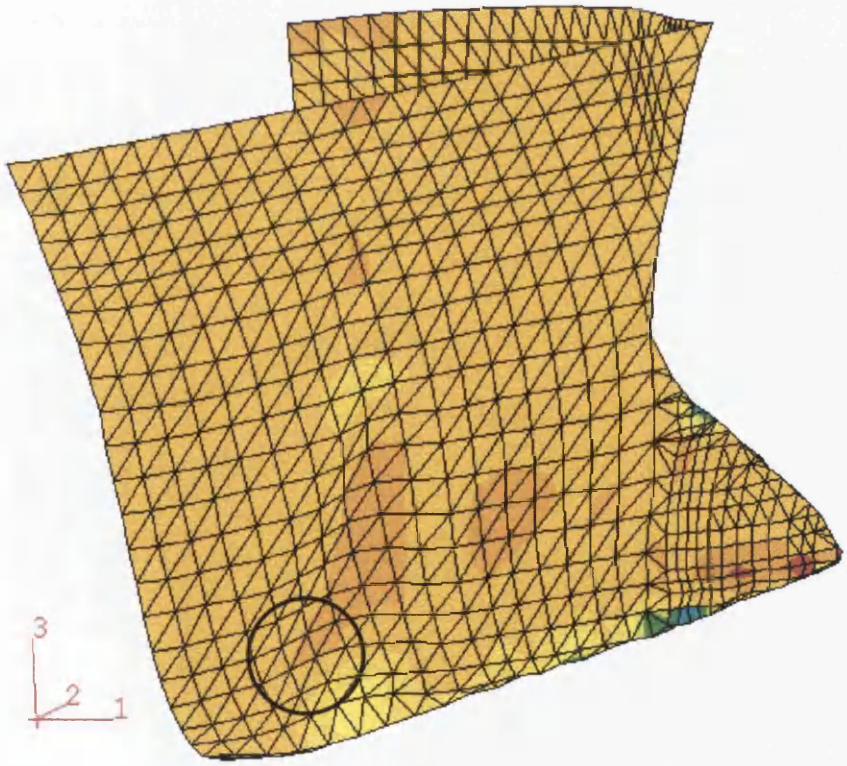


***Figure 4.14*** *Strain contour on the outer shell The circle denotes are with strains that reach the magnitude of 5%*

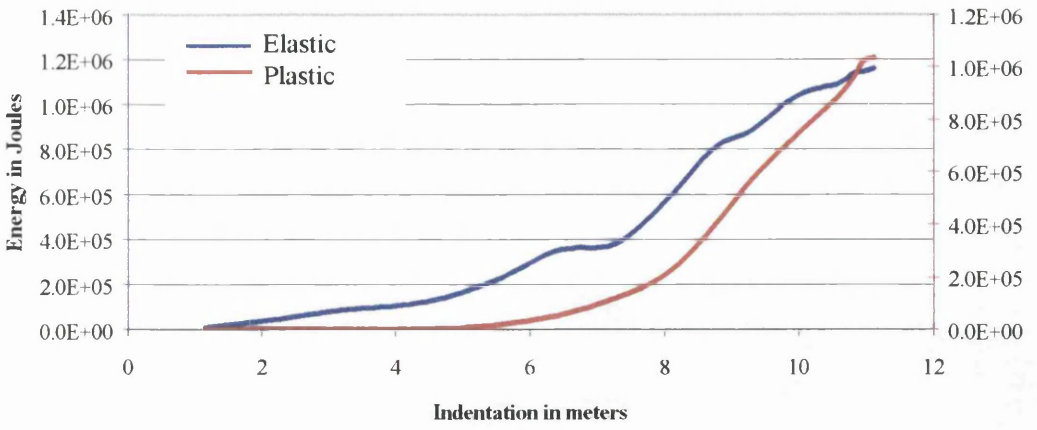


***Figure 4.15*** *Elastic and Plastic Energy dissipated on Bulk1 with regard to the indentation.*

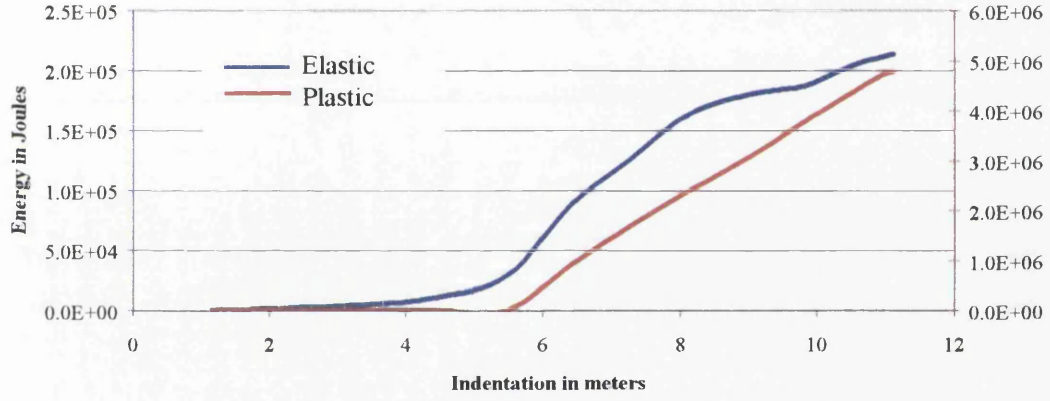


***Figure 4.16*** *Elastic and Plastic Energy dissipated on Bulk2 with regard to the indentation.*

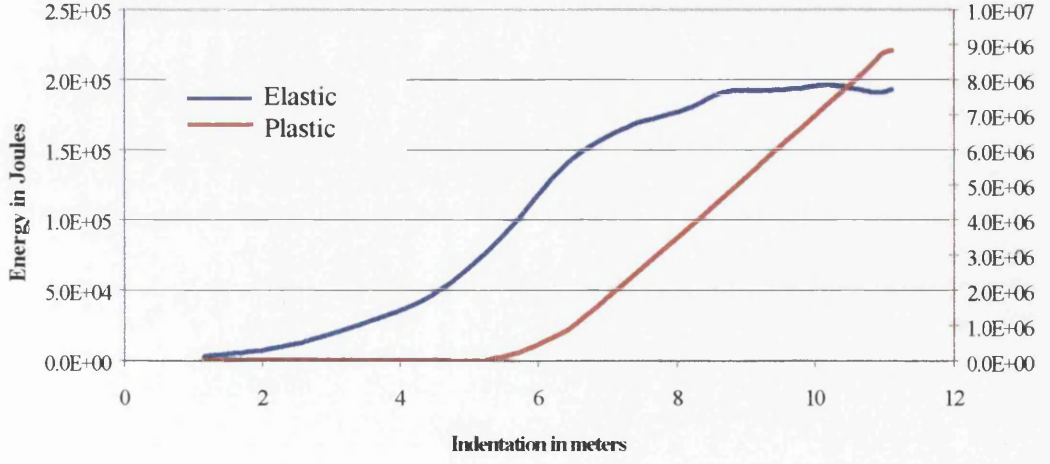


***Figure 4.17*** *Elastic and Plastic Energy dissipated on Bulk3 with regard to the indentation.*

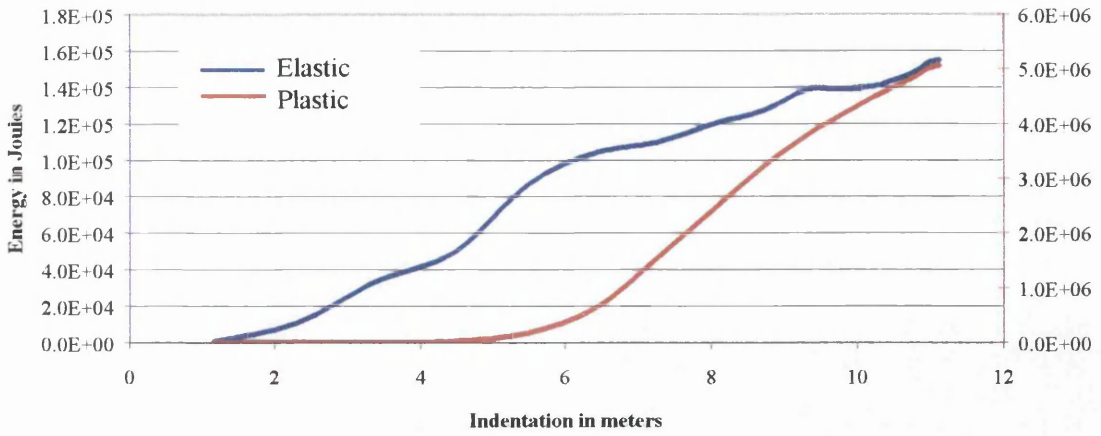


***Figure 4.18*** *Elastic and Plastic Energy dissipated on Deck1 with regard to the indentation.*

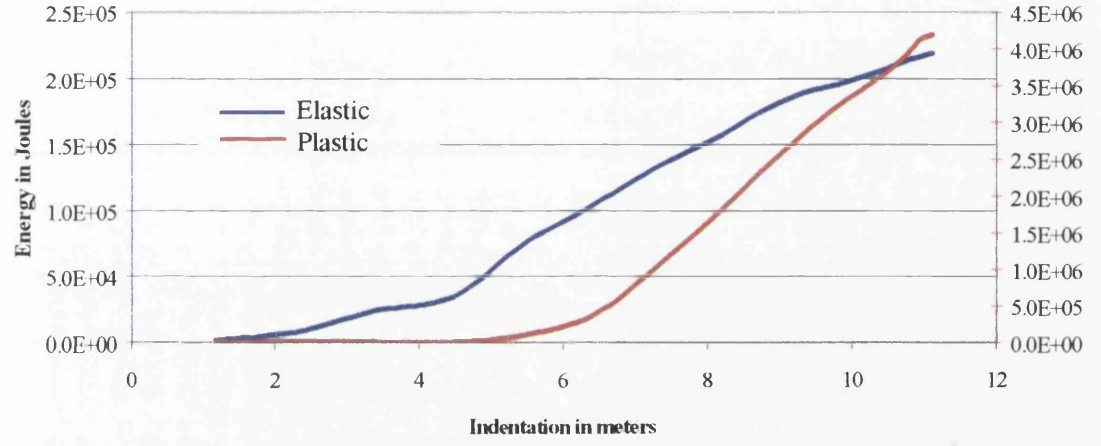


***Figure 4.19*** *Elastic and Plastic Energy dissipated on Deck2 with regard to the indentation.*

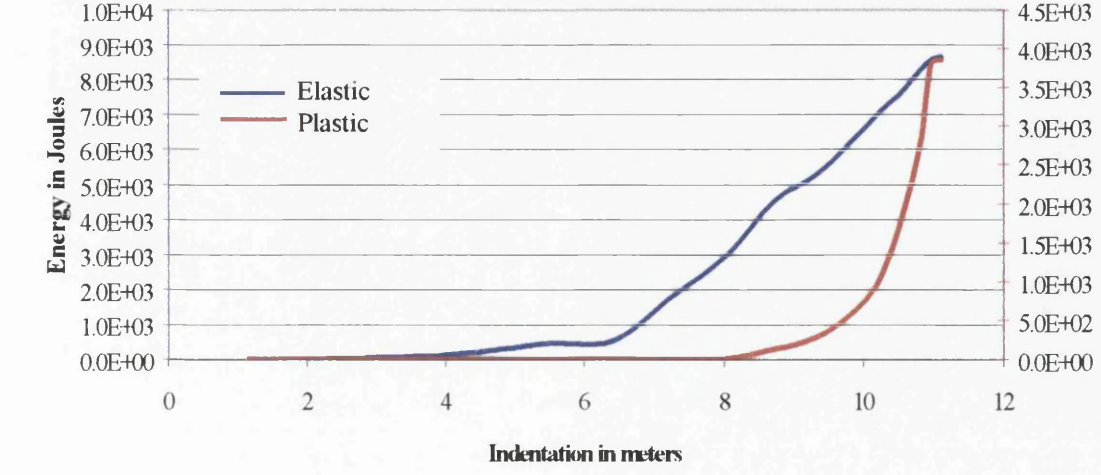


***Figure 4.20*** *Elastic and Plastic Energy dissipated on Deck3 with regard to the indentation.*

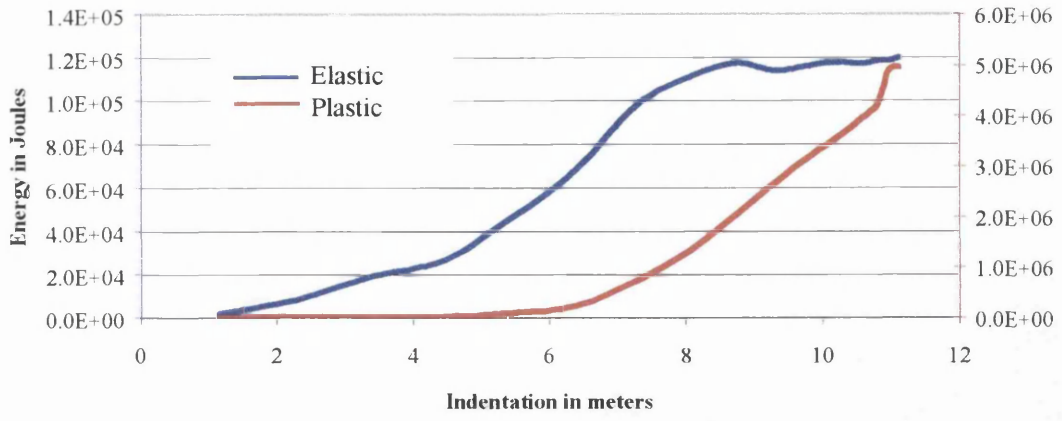


***Figure 4.21*** *Elastic and Plastic Energy dissipated on Deck4 with regard to the indentation.*

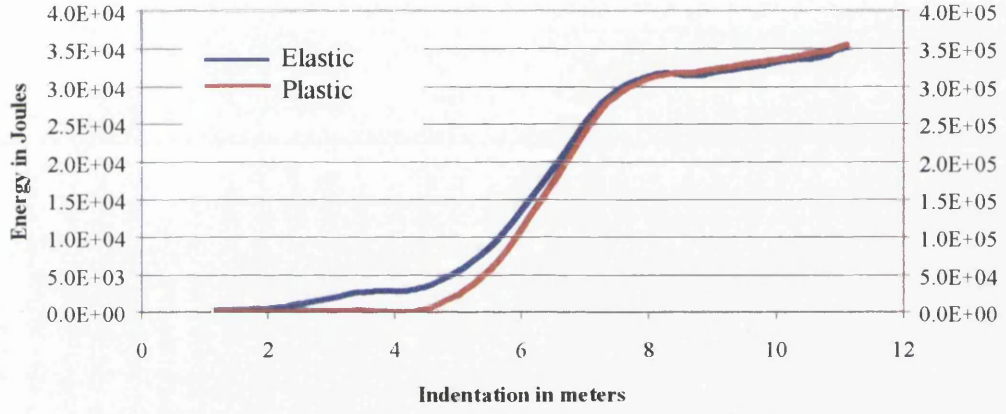


***Figure 4.22*** *Elastic and Plastic Energy dissipated on Deck5 with regard to the indentation.*

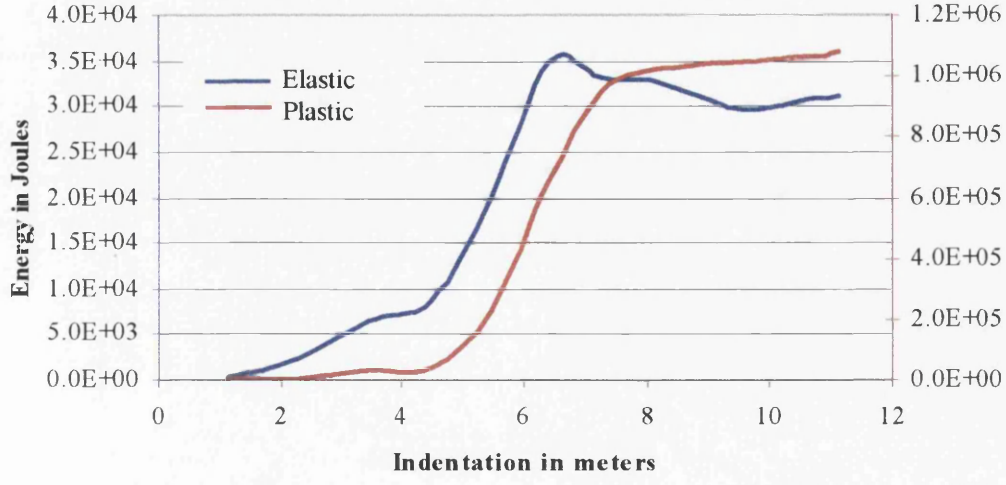


***Figure 4.23*** *Elastic and Plastic Energy dissipated on Deck6 with regard to the indentation.*

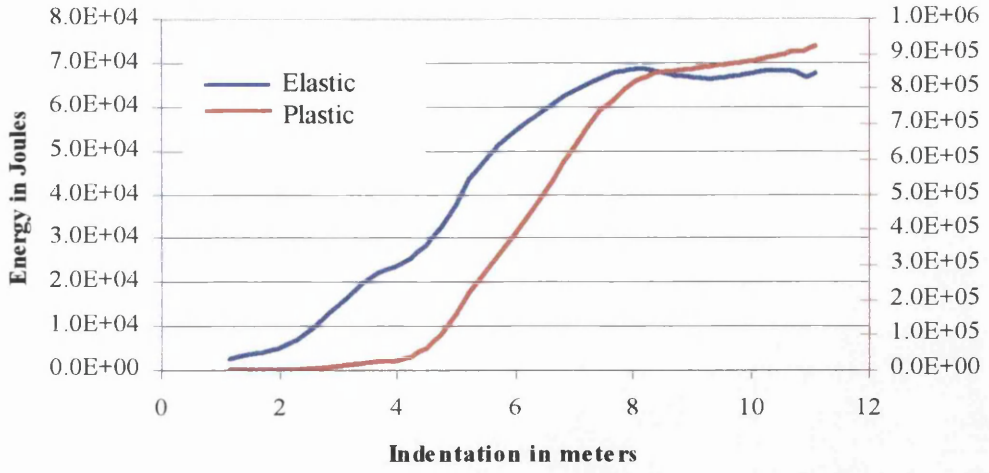


***Figure 4.24*** *Elastic and Plastic Energy dissipated on Deck7 with regard to the indentation.*

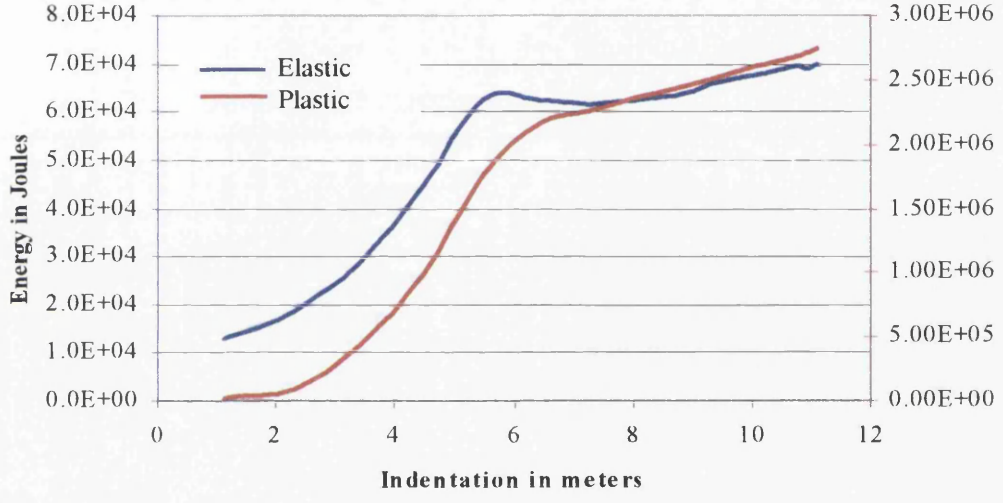


***Figure 4.25*** *Elastic and Plastic Energy dissipated on Deck8 with regard to the indentation.*

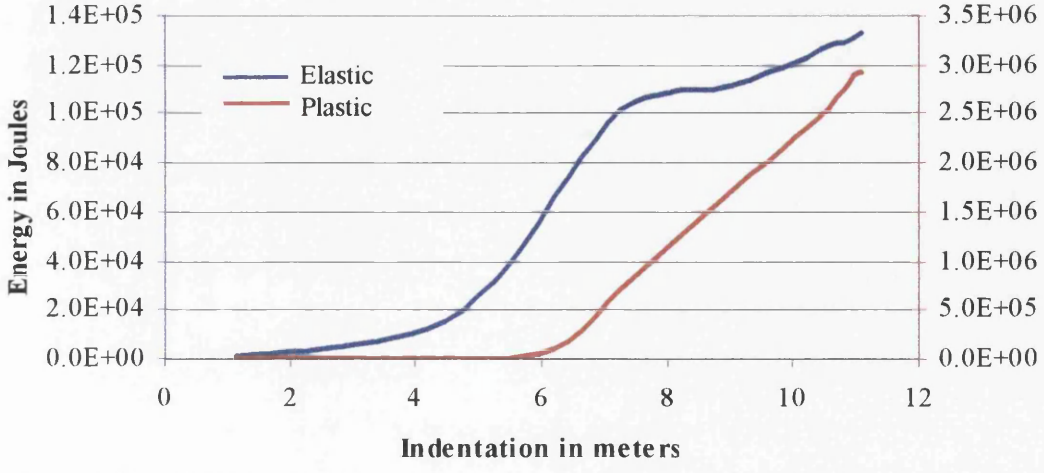


***Figure 4.26*** *Elastic and Plastic Energy dissipated on Deck9 with regard to the indentation.*

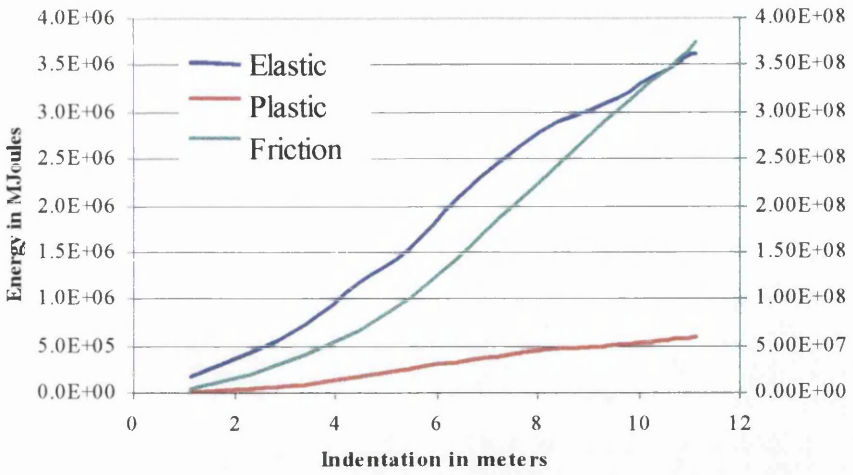


***Figure 4.27*** *Elastic and Plastic Energy dissipated on Shell with regard to the indentation. The red and green line associated with the plastic and friction energy respectively, are linked to the right y-axis.*

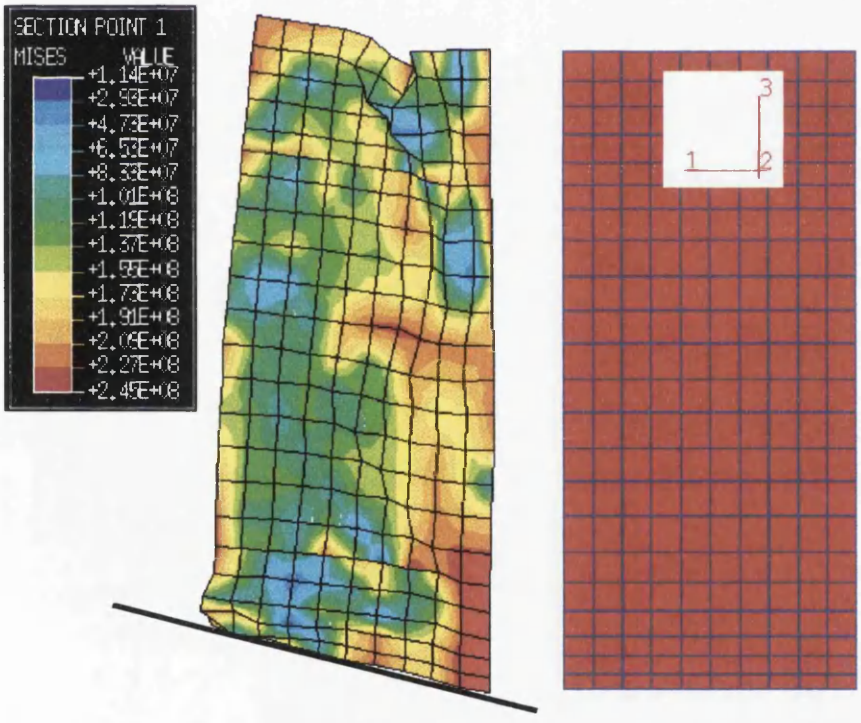


***Figure 4.28*** *Initial and final condition of the longitudinal bulkhead Bulk3. The image on the left displays a contour of the Von-Mises stresses.*

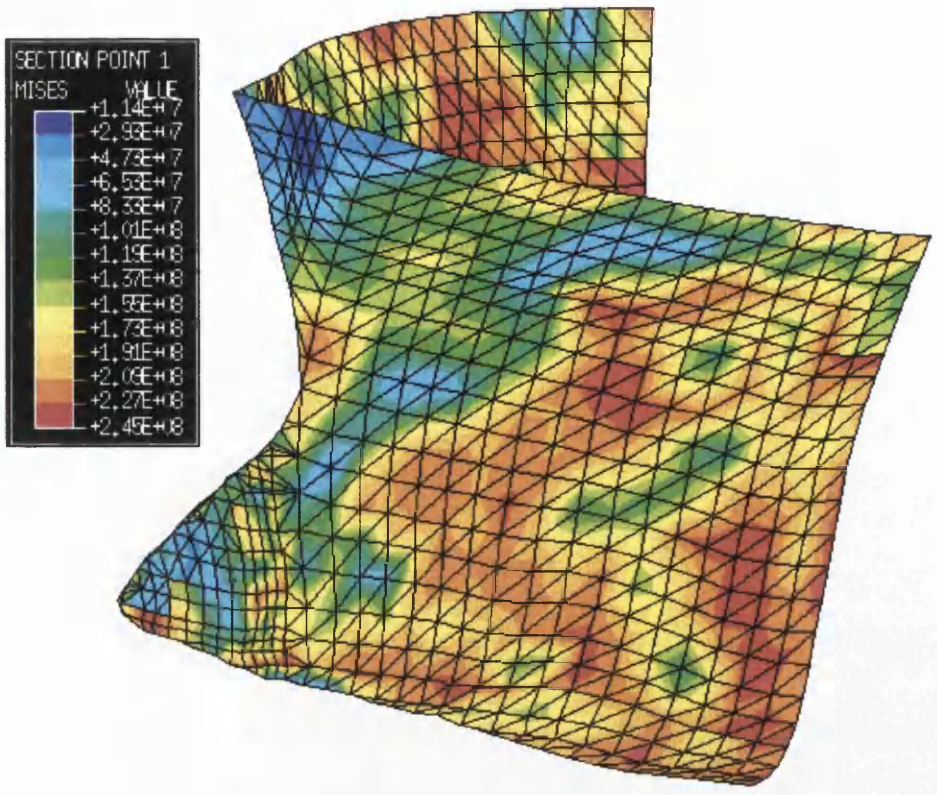


***Figure 4.29*** *Final condition of the shell of the bow model. The contour shown displays the Von Mises stress*

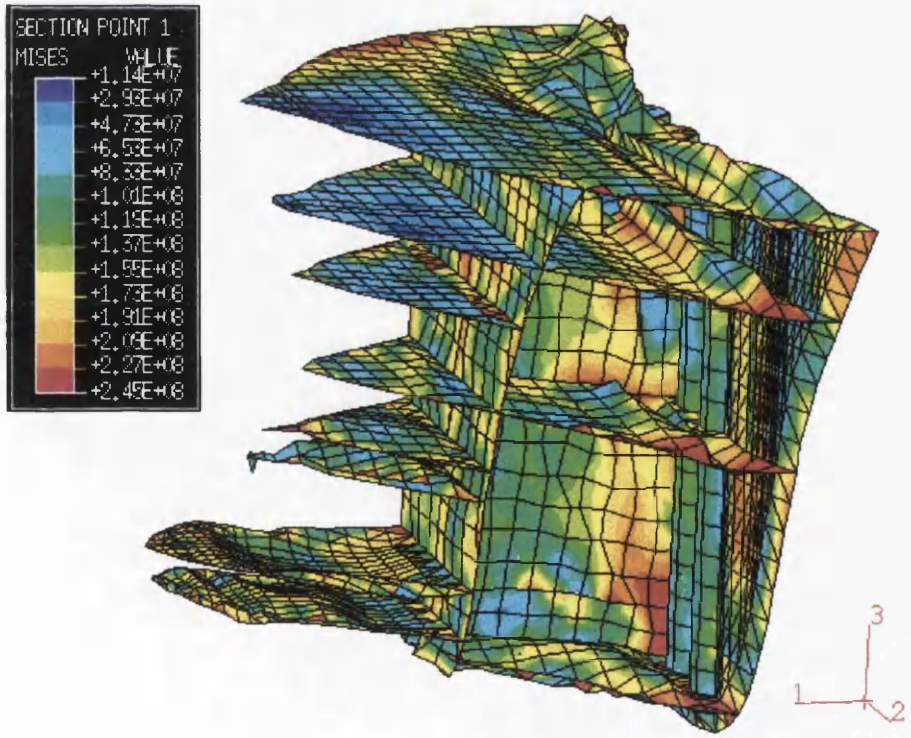


***Figure 4.30*** *Final condition of the structural members of the bow model. The contour shown displays the Von Mises stress.*

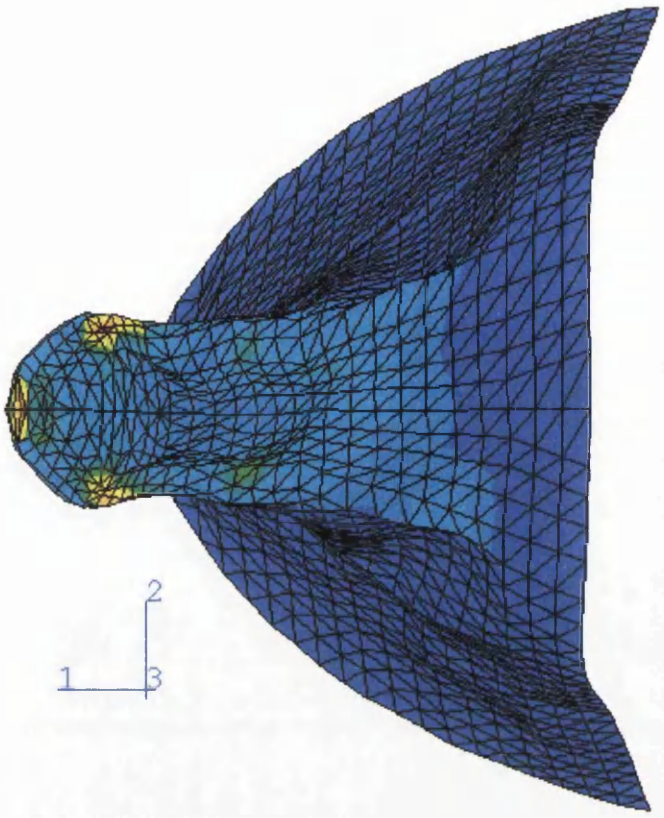


***Figure 4.31*** *Plastic energy dissipated on the bottom part of the shell structure. The dark blue colour represents the area, which has not been plastically affected.*

# CHAPTER FIVE

# FAILURE CRITERIA AND DESIGN APPRAISAL

---

## 5.1 INTRODUCTION

For the assessment of adequacy of the safety level of a structure, it is of great importance to be able to evaluate the response of the structure under accidental loading and also to set criteria for acceptable damage levels caused by an accident i.e. a ship to ship collision or grounding. These criteria may allow, contrary to the case of the normal operating condition, large deflections, large strains and even some limited fracture, depending on the case under examination. In the cases of impact of tanker vessels or other vessels carrying hazardous cargo, the damage is unaccepTable if it results in cargo outflow, something which has a catastrophic consequence on the environment. Thus, the criterion, which a tanker is required to undergo during a collision is the absence of fracture of the skin of the cargo tanks.

It is the object of the work reported herein, to define limit tensile strains and to estimate the energy absorption capacity of a plate up to the initiation of fracture propagation, under uniformly distributed loading, as well as patch loading. Various formulations have been considered for the estimation of the energy absorption capacity of the impact area of the ship hull during a collision. Most of the methods are based on the assumption that the plate is clamped against rotation (clamped) or clamped against rotation and restrained from pulling in (fully clamped). Further, although the collision between vessels is a dynamic phenomenon, the analysis of the structure in the vicinity of the impact could be considered as quasi-static because the inertia forces are applied over a period which is larger to relevant structural periods.

In this Chapter a methodology for the determination of the maximum energy absorption capacity under UDL or Patch load is presented. It is of vital importance to establish the correct prediction of the maximum strains which cause failure and thus to limit the strain at which failure of the plating material occurs.

The energy absorbed is calculated as the integral of the load-deflection curve from the origin until the deflection corresponding to the maximum allowable strain.

$$Energy = \int_{A} \int_{0}^{W_{critical}} (load)(dw)dA$$

The plate response is investigated under the following boundary conditions:

1. In-plane movement and Rotation are restricted {Fully Clamped}
2. In-plane movement is free whilst Rotation is restricted {Clamped}

The load-carrying mechanisms of the laterally loaded plates with various in-plane restraints along the edges differ from each other at the large-deformation stage. The influence of the in-plane and rotational restraints along the edges of a plate on the large-deformation, is studied, in relation to the energy absorbed for each boundary condition.

For this study a non-linear finite element program ABAQUS is used. For the modelling of the plates a Shell Element has been used due to its simple formulation, high accuracy and easy incorporation of the large deformation. The non-linear behaviour is accounted for, with a total Lagrangian formulation in which large deflections and moderate rotations are considered. Through the F.E.A. the deflection/strain relationship of a plate was determined utilising a material-non-linear static solution. For a given plate configuration, a quasi-static load function was used to apply normal pressure loads of increasing magnitude to the plate. Each applied load creates a deformation and a corresponding state of induced strain in the plate. The results of the finite element analysis were used to generate curves relating to the

deformation of the plate to the induced levels of strain in the plate. The geometric and materials parameters of the plates modelled, are as follows:

| | |
|---|---|
| Side length, | a =b = 0.8 m |
| Thickness, | t= 5-12.5 mm |
| Poison's Ratio, | v = 0.3 |
| Elastic Modules, | E = 211 kN/mm$^2$ |
| Yield stress, | $\sigma_y$ = 245 N/mm$^2$ |

**TABLE 5.1 PLATES MODELLED UNDER LATERAL LOADING**

The geometric properties of the plates used were taken from the side shell plates of a 27500 DWT tanker ship, which had transverse frames every 0.8m, and shell thickness 10 mm. The material behaviour used was elastic-fully plastic.

## 5.2 THE FAILURE-FRACTURE CRITERIA

The failure and fracture criteria are based on local strain, average elongation, plastic failure during large deflections and finally fracture propagation. These are:

- Mean strain equal to 5%, Germanisher Lloyd's
- Local Strain equal to 5% in areas where plasticity is predominant, COD, Burdekin, F.M (1971), Jones N. & Wierzbicki T. (1983)
- Rigid Plastic theory as this is described by R.H.Wood (1961)
- Fracture propagation based on $SED_{FM}$ Method, Jennings E. (1991)

Fracture propagation is a failure phenomenon developed in areas of the plate where high strain values are predominant. The critical deflection of the plate is defined as the one above which the failure criteria are not satisfied.

The significant areas of the plate on which our interest is focused are those which produce high strains during the deformation. The utilisation of the above criteria results in the prediction of a critical strain under which the plate fails to resists any further loading. However these criteria produce **limit strains** whose values vary according to the criterion used.

A mean strain equal to 5%, criterion is concerned, this is adopted by Egge & Böckenhauer, Germanisher Lloyds, (1991). Considering a plate panel subjected to lateral loading it is taken that rupture of the panel occurs when the mean strain reaches the 5% level. Within the framework of a research programme "Tanker Safety", Germanischer Lloyd has developed a program system for the evaluation of the absorbed plastic deformation energy in a ship-ship collision. A "critical situation" is defined, for example, rupture of cargo tanks with subsequent spillage of cargo or water ingress into dry cargo holds. They examined the membrane behaviour of the shell using non-linear finite element analysis (ADINA). They demonstrated that the energy absorption evaluated by the non-linear FE. Analysis does not differ substantially from the value obtained on the basis of a simple membrane model of a plate strip. The maximum penetration of a subjected plate strip was calculated on the basis that the elongation when plastic hinges appears is equal to 5%. In Valsgård, S.

and Pettersen, E. (1982) a smaller value of mean strain, approx. 1.5% was used as a rupture strain. The difference in the limit mean strain value is attributed to the boundary conditions used for each analysis.

For welded constructions, using a fracture mechanics approach and the statistics of recorded weld defects, Bokalrud, T. and Karlsen, A (1982) has established a criterion of critical strain rupture. The method of COD (crack opening displacement) developed by Burdekin and Dawes, (1971), gives a design curve, an empirical force, displacement relationship at the tip of a crack. An initiation value for the COD parameter $\delta_i$, defines a crash opening at which crack growth is initiated. The correlation that resulted in the COD design curve is illustrated schematically in Figure 5.1. The critical opening displacement is nondimensionalised by the half crack length, a, of the wide plate and is shown on the ordinate of the graph. The nondimensionalised COD is plotted against the failure strain in the wide plate, normalised by the elastic yield strain $\varepsilon_y$. Based on a plot similar to Figure 5.1 Burdekin and Dawes, (1971), proposed the following relationship.

$$\frac{\delta_c}{2\pi\varepsilon_y\overline{\alpha}_{max}} = \frac{\varepsilon}{\varepsilon_y} - 0.25 \qquad for \qquad \frac{\varepsilon}{\varepsilon_y} \geq 0.5 \qquad 5.1$$

where:

$\delta_c$ is the dynamic critical COD value, estimated to be 0,2 for NVA steel in Valsgård, S. and Pettersen, E. (1982). In Saelter (1980), COD is given in terms of steel quality and test temperature.

$\overline{\alpha}_{max}$ is the equivalent half through-thickness crack dimension corresponding for rupture

$\varepsilon_y$ is the elastic yield strain

Jones, Wierzbicki (1983) state that for the behaviour of brittle material the crack becomes unstable and extends instantaneously with no further input of energy. This corresponds to a critical value of opening parameter, $\delta_c$. Such conditions can prevail in normally ductile materials as a result of high loading (strain) rate, low temperature or large thickness. During ductile behaviour, however, more energy is necessary to

extend the crack. A measure of the resistance to fracture during slow, stable crack extension is offered by the R-curves {Rolfe and Barsom (1977) and in Harrison et al. (1979)} in the form of a plot of stress intensity factor, $K_R$ versus crack extension, $\Delta\alpha$. For $K_R=K_{CRITICAL}$ is the stress intensity fracture toughness which corresponds to the theoretical COD value and is dependent on thickness, temperature and strain rate hardening i.e. the loading rate.

Based on the statistics of internal defects in materials used for welded ship plates reported in Bokalrud and Karlsen (1982), the average value for internal defects with size $2\alpha$ is taken to be 3.5 mm. An equivalent through-thickness crack can be derived from PD 6493 (1980) as $\bar{\alpha}/B=0.11$ (infinitely long crack). With a plate thickness B of 17 mm this yields $\bar{\alpha}=1.87$ mm and $\bar{\alpha}_{max}=0.62$ mm.

In Jones, Wierzbicki (1983) equation 5.1 is plotted for various sizes of internal defects for normal, ship yard, mild steel (NVA) in Figure 5.2. Using the above values these Figures yield an equivalent rupture strain equal to 45 times the yield strain or approximately 5% for the plate panels in question. It should emphasised that this 5% strain applies to the local strain near defects.

The Plastic failure criterion is developed for elasto-plastic laterally loaded plates with different boundary conditions. Because of the complexity of large deflection theory, there is no direct analytical method, which is able to yield accurate results for realistic cases. Large deflection theory has the following sources of nonlinearities as mentioned in Owen Hughes (1983):

- Yielding
- Large deflections (the membrane effect)
- Non linear boundary conditions produced from the restraining for edge pull-in, which appears and becomes significant as deflections become very large

There is, however, one empirical approach presented by Wood (1961), which produce simple load-deflection formulas for plates under lateral loading. This is the rigid-plastic hinge-line method originally developed in civil engineering for the

design of concrete slabs. Sawczuk (1964) extended the basic approach to large deflection. The principal features of the method, as applied to rectangular plates, are as follows;

- The edges are assumed to be completely restrained from pulling in, so that the large defections membrane stresses are dominant
- Elastic deflections are ignored, and the material is assumed to be rigid-perfectly plastic, that is, zero strain until $\sigma=\sigma_{yield}$, then unlimited strain with $\sigma=\sigma_{yield}$
- The plate is divided into four rigid regions separated by straight line hinges so as to form a kinematically admissible collapse mechanism, as shown in Figure 5.3

This consideration concerns rectangular plate elements, e.g. the plate elements between transverse webs. For plate configurations with pinned and free to pull-in boundaries, the collapse load is

$$P_C = \frac{24M_P}{b^2\left(\sqrt{3+\frac{b^2}{a^2}}-\frac{b}{a}\right)^2} \qquad where \quad a/b \geq 1 \qquad 5.2$$

where a, b are the plate edges and

$M_P$ is the plastic moment capacity per unit length and is equal to

$$M_P = \sigma_{yield}\frac{t^2}{4} \qquad \left[Nmm/mm\right]$$

In case of a clamped, horizontally free plate the mechanism model has to be supplied with plastic zones along the plate edges. The kinematic relations remain unchanged. Thus the external work has to be supplied with the work along the edges. From this simplified calculation shown in Woods (1961) the collapse pressure comes out as

$$P_C = \frac{48M_P}{b^2\left(\sqrt{3+\frac{b^2}{a^2}}-\frac{b}{a}\right)^2} \qquad where \quad a/b \geq 1 \qquad 5.3$$

The principal limitation of rigid-plastic theory is the assumption that membrane effects are dominant. There are two ways this may occur;

- Either the plates edges are restrained from pulling in or
- The deflections have become so large that the in-plane restraint arises from the non-uniform distribution of in-plane strain due to the non-uniform lateral deflection, such that partitions of plating with less deflection provide some restraint to partitions with greater deflection.

The amount of deflection, and therefore the in-plane restraint depends entirely on the slenderness $\beta$. For slender plates ($\beta$>2.4) the lateral deflection grows quickly with load, and consequently some in-plane self restraint arises in the plating. Hence it can be expected that rigid plastic theory will give better results for slender plating.

Hooke and Rawlings (1969) have presented experimental results for laterally loaded plating in which the plate edges were rigidly bolted to a non-deflecting frame. From these results Jones and Walters (1971) have shown that if there is such complete or near complete restraint, and if the plate is truly slender ($\beta$>2.4) then the rigid plastic theory gives very good results.

## 5.3 FRACTURE PROPAGATION

Fracture propagation is a criterion introduced herein, which is based on Griffith's Fracture Mechanics and relates to plates that have already developed crack throughout the thickness of the plate. The maximum allowable strain is calculated on the basis that the elastic energy released during a crack growth, as calculated by Griffith's theory, (1920), equals the plastic energy capacity absorbed by the plate material in the vicinity of the crack. ***Thus when the plastic energy is less than the energy released by the crack growth, unstable augmentation of the already existing crack, occurs, Jennings E. (1991) shown in Figure 5.4.*** *{Reference of the source is included in Appendix 2}*

The fracture criterion, which has been utilised in this project, is based on the plastic energy capacity absorbed by the material at a certain mass volume where the true strains are ultimate. It is assumed that if this plastic deformation energy is greater than a critical value, then the material will initiate cracking in that area. The critical value of this plastic energy is defined through Griffith's (1920), fracture criterion. A theoretical crack with length c (c is the length for the half crack) is assumed to exist in the critical area of the material, and this only indicates the size of the crack which could be created under the specific loading conditions.

The plastic energy absorbed by the material is calculated through the FE Analysis results for certain points of the plate where yield occurs first and therefore these are the points where cracks will first initiate.

### *5.3.1 THE ENERGY BALANCE AROUND THE CRACK PERIPHERY*

Referring to Figure 5.5, the damage zone is nested inside the zone of uniform plastic yielding, where the metal is stressed above it's yield point but below ultimate strength (UTS). In this region, plastic deformation is fairly well understood. The metals volume and Poisson's ratio is constant.

The inner zone, the damage zone, corresponds to the region of the engineering stress-strain curve where necking occurs. This region is not accurately described by

plasticity models. Void growth can cause a variable density and Poisson's ratio. The strain hardening coefficient is not constant.

The two plastic zones correspond to different locations on the true-stress true-strain curves as shown in Figure 5.6, where the different strain energy densities are illustrated relative to their location on the engineering and on the true-stress true-strain curve. Examining the true-stress true-strain curve of Figure 5.6, shows that typically the majority of the plastic strain energy density is under the stress-strain curve after necking occurs to UTS.

Therefore, two analytically different plastic zones exist;

- The uniform plastic deformation zone and the
- The damage zone.

The plastic strain energy absorbed at the crack tip is then the sum of the two zones.

The plastic Energy absorbed in the uniform zone, $U_u$, during crack growth is evaluated by determining the local strain energy density absorbed in an elemental volume and integrating around the crack tip where the stress is between yield stress and ultimate stress. The Plastic Energy absorbed in the damage zone, $U_f$, during crack growth has been empirically related to the strain energy density from ultimate stress to fracture.

In considering Griffith's theory for equilibrium cracks, Sanders (1960) pointed out that the region for which the energy balance holds can be any portion of the body enclosed within a simple closed curve L surrounding the crack tip where the energy is being dissipated Figure 5.7. In three dimensional cases this curve may be the profile of a toroidal region surrounding the crack periphery. Thus, the Griffith criterion may be stated as "the rate at which work is being done by forces acting across L equals the rate of increases of strain energy stored in the material inside L plus the rate at which energy is dissipated by the growing crack" Sanders (1960), the rate being with respect to some parameter which increases with the expanding crack periphery.

An approach to the energy release rate can be derived through the following equation relating the elastic energy stored in a unit volume of material just ahead of the crack with the stress at infinity and the size of the crack;

$$U_e = \frac{\pi c^2 \sigma^2}{E} \qquad 5.4$$

where Ue is the elastic energy stored in a unit volume of a plate of unit thickness, E is the Young's modules, and the other terms are the same as before. Incidentally, the solution for a surface crack of depth c is approximately the same. This expression is valid only for thin plates where the thickness direction stress is zero, a condition called plane stress. For thick plates, wherein thickness-direction stresses develop as a consequence of non uniform Poisson's ratio contraction near the apex of the notch, the thickness-direction strain is considered to be equal to zero. This state is "plane strain", and the strain energy per unit of volume is given for a unit thickness by

$$U_e = \frac{\pi c^2 \sigma^2 (1-\nu^2)}{E} \qquad 5.5$$

where v is the Poisson's ratio. The surface energy per unit of thickness of a crack 2c in length is given by:

$$U_S = 4a \cdot c$$

where a is the surface energy per unit area. A crack will *become unstable when the stored elastic energy is equal to or greater than the energy needed to create the new crack surface formed when the crack extends, as shown in Figure 5.4.* Thus, for the plane stress case

$$\frac{d}{dc}(U_e - U_S) = \frac{d}{dc}\left(\frac{\pi c^2 \sigma^2}{E} - 4ac\right) = 0 \qquad 5.6$$

or

$$\frac{2\pi c \sigma^2}{E} = 4a \qquad 5.7$$

which leads to the Griffith relation

$$\sigma^2 = \frac{2aE}{\pi c} \qquad 5.8$$

The appropriate expression for thick plates (plane strain case) is

$$\sigma^2 = \frac{2aE}{\pi c(1-\nu^2)} \qquad 5.9$$

The terms $\pi c\sigma^2/E$ and 2a are "energy release rate" terms, denoted by G in current terminology. Thus we have:

$$G = 2a = \frac{\pi c\sigma^2}{E} \quad \text{for plane stress} \qquad 5.10$$

and

$$G_I = \frac{\pi c\sigma^2(1-\nu^2)}{E} \quad \text{for plane strain} \qquad 5.11$$

The subscript I is used to distinguish the plane strain case.

For plates having finite dimensions, these equations must be modified. Irwin (1963), using a method developed by Westergaard (1939), derived the following modified relationship

$$G = \frac{\sigma^2 W}{E}\tan\left(\frac{\pi c}{W}\right) \quad \text{for plane stress} \qquad 5.12$$

and

$$G = \frac{\sigma^2 W(1-\nu^2)}{E}\tan\left(\frac{\pi c}{W}\right) \quad \text{for plane strain} \qquad 5.13$$

where W is the specimen width.

When W→∞ then $W\tan\left(\frac{\pi c}{W}\right)\rightarrow \pi c$. Diagrams No. 1, 2, 3, 4, show the correlation between equations 5.10 and 5.12 in Appendix 1.

***Unstable crack growth occurs when the total plastic energy absorbed in the two zones is less than the elastic energy released rate during crack growth, Ue.*** *{Reference of the source is included in Appendix 2}*

Thus from equation 5.10 we have:

$$U_e = \frac{\pi\sigma^2 c}{E} \geq U_f + U_u \qquad 5.14$$

Solving for half crack length:

$$c = \frac{E(U_f + U_u)}{\pi\sigma^2} \qquad 5.15$$

Equation 5.12 produces

$$c = \frac{W}{\pi}\tan^{-1}\left(\frac{E(U_f + U_u)}{\sigma^2 W}\right) \qquad 5.16$$

The sum $U_f + U_u$ is the total plastic energy and therefore it will be defined as $U_p$. For the metric system, the second term of equations 5.15 and 5.16 should be multiplied by the factor 0.175.

Solving equation 5.15 and 5.16 with respect to $U_p=U_u+U_f$ we have:

$$U_P = \frac{W\sigma^2}{E}\tan\left(\frac{c\pi}{0.175\cdot W}\right) \text{ for a finite plate} \qquad 5.17$$

$$U_P = \frac{c\pi\sigma^2}{0.175\cdot E} \text{ for an infinite plate} \qquad 5.18$$

The Energy released, as calculated from formulas 5.17 and 5.18 is energy per unit area. This area is the projected area of the crack vertical to the load. Hence for a crack of length 2c and depth t, the projected area, vertical to the load axis is:

$$Area = [c \cdot t]$$

Thus equation 5.18 yields to:

$$U_P = \frac{t \cdot c^2 \pi \sigma^2}{0.175 \cdot E} \qquad 5.19$$

For a certain nodal point of the plate, where the crack is assumed to propagate the integration of the true stress-strain curve produces an amount of energy per unit volume. This volume is considered to be the volume of the plastic zone around the end of the crack, which was clearly calculated by Irwin (1961), as a function of the geometric characteristics of the crack, Figure 5.8. Irwin's formula presents the radius of the plastic zone as

$$r_y = \frac{1}{2\pi}\left(\frac{K}{\sigma_{yield}}\right)^2 \qquad 5.20$$

where:

| | |
|---|---|
| K | is the stress intensity factor and it is equal to $\sigma(\pi c)^{0.5}$ |
| $\sigma_{yield}$ | is the yield stress of the material and it is equal to 245 N/mm$^2$ |
| $r_y$ | is the radius of the plastic zone. |

This expression is only an approximation to the size of the plastic zone, but is nevertheless a useful estimation.

Thus the volume of the material at the tip of the crack, which refers to the plastic zone of the material is

$$Volume = \frac{(\pi \cdot r_y^2) \cdot t}{2} \qquad 5.21$$

The direction of the propagation of a crack and the position where it will first initiate is a function of the following factors:

1. Microscopic flaws as a result of the material process
2. Position of the load
3. Type of the load
4. The existence of already developed crack

Factor No. 1 is dependent on the material quality and therefore on the non-destructive method under which the material was tested in order to determine flaws which could lead the material to failure.

In this project the material is supposed to have perfect internal construction or the distribution of the existing flaws is such that it does not affect the results.

Factor No. 4 is neglected. F.E. Analyses which would consider the existence of any cracks inside the material construction would create F.E. models whose mesh size would be big enough, compared to the size of the commercial hardware computing systems provided nowadays. For example, an attempt to estimate the size of the memory needed for the parametric F.E. analyses of a square plate, in which already exists a crack inside the material, with a ratio (Plate edge length/crack main axis length)=1/2000, would create a plate mesh which should be divided into 2000x2000 elements, number which leads to an enormous size of required equations. If the element has 4 nodes and 6 degrees of freedom, the number of the equations is $96 \cdot 10^6$, which is huge! The hard disk space needed for such a problem is estimated through the F.E. Lusas, FEA (1995) as a result of the following formula:

$$\frac{Mbytes}{Element} = Const \cdot (No.elements) \cdot \left(1 + \frac{No.loadcases}{5}\right) \qquad 5.22$$

where Cons. $=9.2 \cdot 10^{-3}$ for element QSL8

No. elements $=4 \cdot 10^6$

No. load cases $=35$

For these inputs the estimated required number of hard disk memory is 0.3Gb./element. Considering that a conventional Computer has no more that 10Gb available it is obvious that it is not applicable to this type of modelling.

There have been finite element models where crack problems were involved. In these problems the main object of the analysis was the behaviour and the modelling of a crack with specific geometric properties. The problem was localised on the crack vicinity and therefore the number of elements required was finite and did not exceeded a normal number for the existing computing standards.

### *5.3.2 METHODOLOGY FOR ASSESSING THE CRITICAL PLATE DEFLECTION*

Griffith's fracture criterion is utilised for this project according to the following methodology for assessing the critical plate deflection.

a. We plot the contour for the equivalent strains for the top and the bottom surfaces of the plate. Assuming that the crack will initiate on the plane which is under tension stresses. From these Figures we decide which node of the plate has the greater tensile strains and therefore this is the critical point where the assuming crack will initiate.

b. A critical crack length is assumed to exist on the plate where the material yields first while the lateral UDL load increases. The yield point on the plate can be easily found through the FE Analysis.

c. We define the stress $\sigma$ on the edge of the plate, from the FE analysis, when the assumed crack is supposed to initiate on the boundary of the plate. When the crack is assumed to initiate in a place of the plate elsewhere than the boundary, then after we define the way the crack initiates we calculate the true stress-strain curve in that point for the biaxial loading

d. For a given crack length c and a plate width W we calculate, as shown on diagrams No.3-6 the tolerance between equation 5.10 and equation 5.12 and therefore we decide which one formula represents our problem.

e. With a known $U_p$ critical we calculate from the true stress, true strain curve, as an output from the FE Analysis, Figure 5.9, the appropriate strain so that the included plastic energy under the curve is equal to the $U_p$ critical. Therefore we are able to define the lateral load increment, under which we have the fracture of the plate.

f. Since the load increment in any case is known it is possible now to calculate;

- the Total Plastic Energy which was absorbed by the plate through the Load-Deflection Curve and
- the displacement contour of the plate.

## 5.4 RESULTS

Results of the Finite Element Analysis of the plates are presented in terms of bending and membrane strain and stress fields. The spread of plasticity during the incident is also presented and discussed. Comparisons among the strain fields under various boundary conditions indicate, that the boundary conditions influence the mode of response, i.e. the development of bending or membrane stress fields, and consequently their effect on the energy absorption capacity. Also the reduction of the strength capacity of the plate with an existing crack throughout the thickness is discussed and the effect of the UDL and patch loading is shown.

### *5.4.1 UNIFORMLY DISTRIBUTED LOAD.*

The effect of the membrane forces developed to the plate while bending occurred has been examined, using different boundary conditions as well as different plate thickness. Tables 5.2, 5.3, which follow show the variation of the membrane stresses and strains in terms of plate bending, respectively.

| Boundary Condition | w/t=0.5 | w/t=1 | w/t=3 | w/t=5 |
|---|---|---|---|---|
| Fully clamped | 2.97 | 2.77 | 3.82 | 31.25 |
| Clamped | 1.12 | 1.85 | 3.12 | 30.62 |

**TABLE 5.2 MEMBRANE STRESSES IN N/MM$^2$**

| Boundary Condition | w/t=0.5 | w/t=1 | w/t=3 | w/t=5 |
|---|---|---|---|---|
| Fully clamped | 0.0012 | 0.0044 | 0.0072 | 0.0598 |
| Clamped | 0.0005 | 0.0008 | 0.0050 | 0.0536 |

**TABLE 5.3 MEMBRANE STRAIN %**

From these Tables it can be seen that both membrane stresses and strains do not become significant for these deflections. The ratio a/t for this plate is not big enough to produce significant membrane effects in the plate at deflections less than w/t<5.

Table 4 shows the energy absorbed by the plate, when adapting any of the failure criteria described in the previous Section. The calculations were performed for both fully clamped and clamped plates.

| Boundary conditions | Fracture Criterion [J] | Local strain Criterion [J] | Collapse load Criterion [J] | Mean strain Criterion [J] |
|---|---|---|---|---|
| Fully clamped | 409.25 | 5910.90 | 4582.40 | ---- |
| Clamped | 420.40 | 3251.10 | 4139.30 | ----- |

**TABLE 5.4 ENERGY ABSORBED VS. FAILURE CRITERIA**

As it can be seen from the Table, the energy absorption capacity of the plate increases considerably when in-plane restrictions are imposed in the boundaries in **combination** with the local strain and the collapse load criteria. The mean strain criterion did not yield any results because the execution of the program ceased long before the mean strain reached the value of 5% - for a 5% mean strain the deflection expected is equal to 128 mm or otherwise the w/t ratio equals to 12.8. When the fracture criterion is applied the energy absorbed did not differ significantly when the in-plane boundary conditions changed. This is attributed to the fact that the energy absorption capacity exhausted at low values of deflection over plate thickness ratios. I.e. at w/t equal to 0,633 for fully clamped and equal to 0,878 for clamped boundaries, as it can be seen in Table 5.5.

| Boundary conditions | Critical w/t | Critical Energy for propagation [J] | mean strain % |
|---|---|---|---|
| Fully clamped | 0.633 | 5.154 | 0.013 |
| Clamped | 0.878 | 3.862 | 0.024 |

**TABLE 5.5 PLASTIC ENERGY AT THE TIP OF THE CRACK VS. BOUNDARY CONDITIONS**

The small difference in the energy absorption capacity may be explained as a result of the magnitude of the plasticity, which develops in the plate while bending. A fully

clamped plate develops faster plastic hinges and therefore the crack propagates faster, since the plastic energy is released faster. The plastic energy released at the tip of the crack when the propagation of the crack commenced is shown in Table 5.5.

### *5.4.2 EFFECT OF PLATE THICKNESS*

The effect of the plate thickness has been investigated using only clamped boundary conditions, since this gives a good description of a welded side shell plate, Hughes (1983), for thickness from 5 mm to 12.5 mm with step 2.5 mm.

The energy absorbed while the plate was deformed is illustrated in Table 5.6, using all the failure criteria, except the mean strain criterion.

| Thickness mm | Fracture Criterion [J] | Local strain Criterion [J] | Collapse load Criterion [J] |
|---|---|---|---|
| 5 | 468.07 | 2065.20 | 1179.10 |
| 7.5 | 453.62 | 2447.20 | 2128.40 |
| 10 | 420.40 | 3251.10 | 4139.30 |
| 12.5 | 427.21 | 4273.20 | 8037.30 |

**TABLE 5.6 ENERGY ABSORBED VS. PLATE THICKNESS**

The obvious difference in the energy values appearing in that Table is a result of the different failure criteria used. The fracture criterion considers an already existing crack whose propagation is an outcome of the plastic energy concentrated on the crack tip and therefore this defect reduces the strength of the plate. When this energy becomes greater than the energy required for the crack augmentation then failure occurs. This energy is depicted on Table 5.7, for the 4 different plate thickness, as well as the ratio w/t. Although the plate thickness and the critical Plastic Energy increases the w/t decreases. This leads to the conclusion that the plate with the smaller thickness is less vulnerable to crack propagation since this phenomenon is depended on the bending strains developed on the plate surface.

| Plate Thickness mm | Critical w/t | Critical Plastic Energy [J] | Mean Strain % |
|---|---|---|---|
| 5 | 4.63 | 2.643 | 0.160 |
| 7.5 | 1.40 | 3.703 | 0.030 |
| 10 | 0.88 | 3.862 | 0.024 |
| 12.5 | 0.32 | 6.561 | 0.005 |

**TABLE 5.7 PLASTIC ENERGY AT THE CRACK TIP, MEAN STRAIN AND W/T VS. PLATE THICKNESS.**

As a result, the thicker plate produces high bending strains while the deflection remains small and therefore the propagation commences with lower w/t ratios than in the plates with smaller thickness. All the same, it can be seen in Table 5.6 that this phenomenon is reversed in the case of the 12 mm plate since the energy absorbed in that case is higher than in the plate with 10 mm thickness. This is explained as a result of the geometric properties of the plate, which becomes larger as the thickness increases.

Table 5.8, shows the w/t ratio in relation to the thickness of the plate.

| Thickness mm | Fracture Criterion | Local strain Criterion | Collapse load Criterion |
|---|---|---|---|
| 5 | 4.63 | 15.77 | 10.99 |
| 7.5 | 1.40 | 5.98 | 5.42 |
| 10 | 0.88 | 3.52 | 4.21 |
| 12.5 | 0.32 | 2.40 | 3.93 |

**TABLE 5.8 W/T RATIO VS. PLATE THICKNESS AND FAILURE CRITERION**

The maximum allowable deflection decreases while the thickness of the plate increases in both the local strain and the collapse load criterion as well. This can be explained by the effect of bending and membrane stresses developed by the plates since this phenomenon is dependent on the ratio a/t which varies from 160 for the plate of 5 mm thickness to 64 for the plate of 12.5 mm. Table 5.9, depicts the

membrane stresses and Table 5.10 depicts the bending stresses in $N/mm^2$ for several deflections for the four plates.

| | Deflection | | | |
|---|---|---|---|---|
| Thickness | 10 mm | 20 mm | 30 mm | 40 mm |
| 5 mm | 5.75 | 12.45 | 22.56 | 115.25 |
| 7.5 mm | 2.25 | 3.56 | 5.78 | 56.38 |
| 10 mm | 1.85 | 2.15 | 3.12 | 25.68 |
| 12.5 mm | 1.15 | 1.75 | 3.05 | 24.75 |

**TABLE 5.9 MEMBRANE STRESSES IN $N/MM^2$ VS. DEFLECTION AND PLATE THICKNESS**

| | Deflection | | | |
|---|---|---|---|---|
| Thickness | 10 mm | 20 mm | 30 mm | 40 mm |
| 5 mm | 258.13 | 257.20 | 236.44 | 147.49 |
| 7.5 mm | 258.38 | 300.70 | 295.22 | 265.07 |
| 10 mm | 292.15 | 301.39 | 304.57 | 283.07 |
| 12.5 mm | 294.85 | 308.45 | 313.05 | 296.45 |

**TABLE 5.10 BENDING STRESSES IN $N/MM^2$ VS. DEFLECTION AND PLATE THICKNESS**

The bending stresses are much higher in the 12.5 mm plate than the 5 mm plate and therefore the contribution of bending to the response of the plate, results in the difference of the critical deflections, calculated previously.

Although the energy absorbed by the plate increases where the local strain and collapse load criteria are concerned, Table 5.6, it can be seen that in the case of the 10 mm and 12 mm plate thickness there is a great difference in the results. The collapse load takes into consideration the plastic moment capacity $M_p$, which is proportional to $t^2$. Therefore the energy absorbed becomes greater, almost double, as the thickness increases. On the contrary, with the local strain criterion, although it takes into consideration the growth of the thickness, the energy absorbed does not increase rapidly.

### *5.4.3 PATCH LOADED PLATES*

In this case the phenomenon of plasticity is mostly concentrated in the area of the load Figure 5.10. The boundary of the plate had only the rotation restricted since the response of the fully clamped plates had no major difference in the amount of energy absorbed. Table 5.11 includes the results obtained for the energy from the problem case where the load was partially imposed onto the plate surface.

In the first case the load was covering the 4.68% (Patch load 1) of the area of the plate around the centre of the plate and on the second case the 11.7% (patch load 2). In both cases the total amount of the load was equal.

| Case | Fracture Criterion [J] | Local strain Criterion [J] | Collapse load Criterion [J] | Mean strain Criterion [J] |
|---|---|---|---|---|
| Patch load 1 | 84.97 | 3551.79 | 6134.41 | --------- |
| Patch load 2 | 88.54 | 3874.42 | 6254.15 | --------- |

**TABLE 5.11 ENERGY ABSORBED FOR THE PATCH LOADED PLATE VS. THE FAILURE CRITERIA.**

It can be seen that in this case the fracture criterion produce results with great difference compared to those of the uniformly distributed plate in Table 5.4. This yields to the conclusion that the fracture criterion is not only dependent on the crack existence but also on the area where high plasticity is predominant although the deflection of the plate is not big enough. The mean strain criterion does not produce any results in this case since the plates that were modelled failed to reach such a large deflection.

Plates with different thickness have also been modelled for patch load covering 4.68% of the area of the plate and the results for the energy absorbed during the bending, using the failure criteria, follow in Table 5.12.

| Thickness mm | Fracture Criterion [J] | Local strain Criterion [J] | Collapse load Criterion [J] |
|---|---|---|---|
| 5 | 153.18 | --------- | 1096.85 |
| 7.5 | 67.80 | 4384.76 | 2297.22 |
| 10 | 84.97 | 3551.79 | 6134.41 |
| 12.5 | 280.43 | 4698.01 | 7912.36 |

**TABLE 5.12 ENERGY ABSORBED VS. PLATE THICKNESS**

In this case although the energy absorbed, as far as the fracture criterion is concerned, decreases from the 5 mm to 7.5 mm plate, it increases from the 10 mm to 12.5 mm plate. The phenomenon of the increase of the bending stiffness as well as the magnitude of the bending stresses in relation to the thickness of the plate is clearer in this case since it does not appear only to the 12.5 mm plate as it was in Table 5.6.

Table 5.13 shows the critical w/t ratio and the critical plastic energy absorbed at the tip of the crack in relation to the several plate thickness.

| Plate Thickness mm | Critical w/t | Critical Plastic Energy [J] | Mean Strain % |
|---|---|---|---|
| 5 | 2.56 | 4.831 | 0.051 |
| 7.5 | 0.57 | 7.281 | 0.005 |
| 10 | 0.37 | 9.202 | 0.004 |
| 12.5 | 0.27 | 12.229 | 0.003 |

**TABLE 5.13 W/T RATIO, PLASTIC ENERGY ABSORBED IN THE TIP OF THE CRACK VS. THICKNESS**

Comparing these results to those of Table 5.7 one can see the great tolerance on the critical plastic energy on the tip of the crack. This explains very clearly the effect of the patch load since we get high plasticity in the area of the load although the deflection of the plate is not as high as those shown in Table 5.7

Relevant to Table 5.8, Table 5.14., is formed to compare the w/t ratios among the other criteria used.

| Thickness mm | Fracture Criterion | Local strain Criterion | Collapse load Criterion |
|---|---|---|---|
| 5 | 2.56 | --------- | 5.51 |
| 7.5 | 0.57 | 5.42 | 3.91 |
| 10 | 0.37 | 2.50 | 3.23 |
| 12.5 | 0.27 | 1.30 | 2.15 |

**TABLE 5.14 W/T RATIOS FOR THE PATCH LOADED PLATES**

One can see that the deflections derived are smaller than the ones in the case of the uniformly distributed load, therefore the patch-loaded plate is more vulnerable than the Uniformly distributed plate.

Tables 5.15, 5.16, illustrate the mean elongation/strain on the plates developed in this Chapter for the two different loading conditions.

| Thickness mm | Fracture Criterion | Local strain Criterion | Collapse load Criterion |
|---|---|---|---|
| 5 | 0.167 | 1.920 | 0.939 |
| 7.5 | 0.034 | 0.627 | 0.515 |
| 10 | 0.012 | 0.384 | 0.550 |
| 12.5 | 0.005 | 0.288 | 0.750 |

**TABLE 5.15 MEAN STRAIN FOR THE UNIFORMLY DISTRIBUTED LOADED PLATES IN %**

It can be seen that although the plates are satisfying the failure as well as the fracture criteria, the mean elongation is still very small. The highest mean strain is observed in the case of the local strain criterion.

| Thickness mm | Fracture Criterion [J] | Local strain Criterion [J] | Collapse load Criterion [J] |
|---|---|---|---|
| 5 | 0.051 | --------- | 0.236 |
| 7.5 | 0.005 | 0.520 | 0.268 |
| 10 | 0.004 | 0.200 | 0.325 |
| 12.5 | 0.003 | 0.082 | 0.225 |

**TABLE 5.16 MEAN STRAIN FOR THE PATCH LOADED PLATES IN %**

## 5.5 DISCUSSION OF THE FRACTURE CRITERION

This Chapter presents the determination of the energy absorption capacity of steel plates under uniformly distributed and patch load. The analysis is performed in three phases. Initially a load-deflection curve is determined for the plate, using a Finite Element code, which in the present case was the code ABAQUS. The second phase consists in the determination of a failure criterion, i.e. the determination of an ultimate point in the load-deflection curve, which is assumed to represent the point beyond which the plate has exhausted its energy absorption capacity. This ultimate point is equivalent to the definition of a critical deflection. The last phase is the calculation of the energy absorption capacity of the plate, which is represented by the area under the load-deflection curve, from the origin to the above mentioned ultimate point.

The Chapter focuses in the determination of the ultimate point on the load-deflection curve.

Four criteria have been used therefore:

- The mean strain criterion, according to which the mean strain along the length of the plate should not exceed 5%. However this criterion did not yield any result, because the execution of the finite element code ceased long before the mean strain reached the value of 5%.
- The ultimate load criterion. In accordance therewith the plate ceases to absorb energy when the load reaches the collapse load of the plate.
- The third criterion imposes a limit of 5% to the local strains.
- Finally the applicability of the fracture criterion in accordance with Griffith's theory has been extensively investigated.

The following conclusions are drawn from the work:

When the fracture criterion is applied, the ultimate deflection and the corresponding strain are much lower than values obtained from the other criteria. In this case the

effect of the in-plane boundary conditions of the plate is not of vital importance, because of the low value of the ratio of the deflection over plate thickness.

The results presented revealed that membrane response is of importance for breadth over plate thickness ratios greater that 150, a value, which is considered to be high for ship plating.

In accordance with the fracture criterion, the mean strain does not exceed the value of 2%, when the ultimate point is reached.

Local strains are considerably higher than mean strains, in particular under patch load. In this case the application of a criterion based on a maximum mean strain is considered inappropriate.

The determination of the energy absorption capacity of plates are of importance, in particular when designing plating against accidental loading, such as designing ship plating against collision or grounding. The Chapter presents an integrated method and a parametric study relevant to ship plating. The extension of the study to cover a wide range of aspect ratios of ship plating is planned for the near future. Finally the method will be applied for the analysis of the plating of double hull tankers as well as of equivalent designs.

In this fracture criterion the stress intensity factor (K) for mode I cracks has been utilised as it was described in Griffith's fracture mechanics. In mode I case the stress on the tip of the crack is uniformly distributed throughout the thickness. On the contrary, in the present case the distribution is a combination both of bending and membrane stresses. Therefore there is not a uniform distribution, on the contrary the crack is subjected both to tension and compression throughout the thickness. Hence the propagation of the crack doesn't start at both surfaces at the same time but there is an undefined time lag between the tip, which is under compression and the tip which is under tension. All the same the critical propagation of the crack is taken to commence on the tension surface of the plate and in this stage the plate is considered to have failed.

The fracture criterion described above is relevant to the experimental J-integral fracture method ASTM (E813-88) which measures the load-line displacement in order to calculate the work (Force x Distance) performed on a test coupon up to the point of crack instability. The plane strain fracture toughness ($K_{Ic}$) ASTM (E399) can be estimated from the critical elastic-plastic energy release rate, $J_{Ic}$ using the following relationship:

$$K_{Ic} = \sqrt{J_{Ic} E}$$

The plain strain fracture toughness $K_{Ic}$ is considered to be an invariant property of the material, similar to the yield strength of tensile strength. The J-integral method does not provide an analytical approach for estimating "residual toughness" under plane stress (inelastic) conditions. The J-integral is an experimental method of estimating $K_{Ic}$ and is not analytically related to a "critical" strain limit Jennings et al., 1991.

# 5.6 APPLICATION OF FAILURE AND FRACTURE CRITERIA ON THE HEAD ON COLLISION

### *5.6.1 INTRODUCTORY REMARKS*

In this Section an attempt at applying the failure criteria in the head on collision with the rigid body, is carried out. It is of great importance to be able to evaluate limit strains during the impact in areas of considerable interest, in order to ascertain the state of the structural integrity, as well as retaining an intact condition.

During the impact there are numerous areas bearing high strains. Especially those located in the bulbous bow, which fail under catastrophic buckling loads. The interest of the analysis is not concentrated in these areas owing to the fact that failure is inevitable during the impact. However, there are areas such as the transverse diaphragm, Bulk2, (reference in Figure A3-2.3) at frame 87 whose integrity affects the deep tank located from frames 77 to frames 87, Figure A3-2.1. Progressive flooding of the deep tank along with the fore peak volumes, will contribute negatively in the stability of the vessel after the impact. In cases where the deep tank is partially full, fluid outflow will take place. Similarly, the shell exhibits high strains in several parts but the highest are located in those parts of the shell which contribute to the bending of the upper part of the bow.

The wisdom of relying entirely on resistance to crack initiation in a large complex welded structure is, of course, debatable. It is always possible to argue that a running crack may emerge from a weld or a heat affected zone, where the toughness quality is not entirely controllable. Thus the areas selected for examination in this analysis are located close to welded joint members. Whether the propagation is brittle or ductile is not examined within this thesis. It has been referenced in Shuji et al. (1994) that welded zones are more likely local brittle zones LBZ because of the microscopic flaws, as well as the heat affected zones HAZ.

For the fracture propagation criterion the crack length assumed is 1.5 mm. In Lloyds rules LR Rules (1996) in transverse bend test Section it is noted that specimens, after

bending, there is to be no crack or defect exceeding 1,5 mm measured across the specimen.

The areas where failure will be examined are divided in four categories depending on each location. For the transverse diaphragm Bulk2, there are 3 areas that reveal high strain concentration. These are shown in Figures 5.10, 5.11. For the shell, the maximum strains are in Area 4 as this is displayed in Figure 5.12, 5.13. Four different areas have been selected for examination of the failure criteria. One could utilise more areas since there are plenty in which high strain concentration is shown. The aim of this practice is to show and prove the applicability and validity of the method of the fracture propagation criterion.

These zones of interest have been located in the finite element model through the strain contours. Moreover they were individually modelled using a more dense mesh due to the requirement of higher accuracy in the results for better applicability of the fracture criterion. The loading of the resulting discreet mesh was based on prescribed displacements as they were taken from the global model. For the additional boundary nodes linear interpolation was used in order to define the displacements with respect to position and time.

The stress and strain results for the dense meshes came out very similar to the initial reaction, but the contours derived are better detailed. For comparison one can see the difference in the contours shown in Figure 5.26 A & B

All the criteria mentioned in the previous Sections will be used for the bow model except the plastic failure criterion Wood (1961). This criterion is developed on the basis of fixed boundary conditions and the resulting deflections are attributed only to lateral loading. In the case of the side ship impact, failure of the shell plates, located between webs, is being modelled using this criteria, Hughes (1983). However, as far as the head-on ship impact is concerned, the loading in local areas with high strains can not be described as lateral since it is a combination of stresses in the three directions of a fixed Cartesian system.

The material used in this analysis is supposed to be ordinary shipbuilding mild steel with no certified toughness. Others may use different steel grades such as Grade D conformed to the recommendations regarding brittle fracture made from Hodgson and Boyd (1958) with a Charpy energy of 47 J at 0°C, or alternatively Grade E with a specified Charpy energy of 61 J at –10°C, Sumpter et al. (1988).

### 5.6.2 EXAMINATION OF AREA 1.

Area 1 is located on the lower part of the transverse diaphragm bulkhead, which is located longitudinally at frame 87. The Von-Mises contour is shown in Figures 5.10 and 5.11 in different views. In Figure 5.10 the longitudinal bulkhead, Bulk3, is shown in a separated view for better understanding. It can be seen that the largest deflections in bulkhead 87 occur in the lower part due to the fact that the transition of the forces from the forward members are carried through this area.

The members of Area 1 are separated and modelled in a different file using more dense mesh. The modelling is done using prescribed displacements on the available nodes from the coarse mesh. The output strain contours for this area is shown in Figure 5.14.

Two partitions in Area 1 are found with high strain concentration. These are identified by sector 1 and sector 2 labels. The failure criteria are developed for both these areas.

#### 5.6.2.1 FAILURE CRITERIA ON SECTOR 1

The application of the fracture criterion in this sector, yields Figure 5.15. The Critical energy released during a crack propagation is calculated with reference to equation 5.19. The energy absorbed from the crack tip is displayed, and the correlation of these two curves produces the critical point where propagation of the crack takes place. This is shown to occur at time 1.49 sec, when the local strain is 1%. In relation to Figure 3.25 the indentation at this time is 6.75m and the energy absorbed from the vessel is taken from Figure 3.82 equal to 355 MJoules. The plastic energy dissipated at this stage on collision bulkhead 87, Bulk 2, is taken from Figure 3.33 equal to 6.5 MJoules.

The local strain at this stage is 1% as shown in Figure 5.15 from the black line. It can be seen that the local strain criterion (equal to 5%) is not valid for this region since the local strain does not exceed the 1.4 %. However, the mean strain, shown in

Figure 5.16, at the time when the fracture starts the propagation, is only 1%. This value was expected to be smaller than the local strain and as shown in the models of the rectangular plates, in Table 5.13, the mean elongation is by far smaller than the local strains.

In this case, in sector 1, the mean strain is 1% only because the boundaries of the plate segment under consideration are free to move along the axis of the collision. The maximum values that the mean strain reached do not exceed the 2%, which occur at the final stage of the collision. Therefore it is shown that the 5% mean strain criterion is not valid for this model.

#### *5.6.2.2 FAILURE CRITERIA ON SECTOR 2*

This sector is located on the lower part of Area 1, Figure 5.14. This sector consists of more thickness in the plate material. It is located in the centre area where the longitudinal bulkhead Bulk3 is attached, beyond Bulk2. Thus it is expected to undergo much higher strains and material thinning owing to Bulk3. The fracture criterion produced considerably higher energy release for the crack propagation as shown in Figure 5.17. At time 1.0 sec. the energy release $U_p$ reached locally high values due to the stress magnitude although the energy absorbed by the material at this vicinity is shown to be notably smaller, therefore fracture propagation does not occur. However, at time 1.6 seconds the energy absorbed by the material becomes greater than the energy required for the fracture propagation and failure occurs.

The local strain at this point is 2.9%, while the mean strain is 0.4%, Figure 5.18. In this case where there is a restriction in the X-translation, i.e. a "fixed" boundary condition exists, the mean strain is much smaller than the in sector 1.

At time 1.6 seconds, the indentation is 7.2 meters and the total energy absorbed from the vessel at this time is 380 MJoules, while the total energy absorbed from Bulk2 is 4.9 MJoules.

From Figure 5.17 one can see that the 5% local strain criterion occurs at a time 1.70 seconds when the indentation is 7.4 meters, the total energy absorbed from the ship is 400 MJoules and the energy absorbed from the transverse bulkhead is 6.0 MJoules. The mean strain at this time is 0.7.

The data are summarised in Table 5.16 where the results from all the areas under examination are discussed. The data on the $7^{th}$ column show the critical speed of the vessel before the commencement of the impact so that the criteria are marginally satisfied.

### *5.6.3 EXAMINATION OF AREA 2.*

This area is located below Area 1 on bulkhead 87, or Bulk2 as shown in Figure 5.11. It is of great importance to examine the failure in this area since it belongs in the lower connection of Bulk2 and the outer shell of the ship. As it can be seen on Figure 5.11, it appears that in this area high stress concentration is predominant.

The strain contour of the dense mesh of this area is shown in Figure 5.19. The light blue area as displayed within the rectangle denotes a zone with high tensile strains. The fracture criteria application is described in Figure 5.20, where the limit time when fracture propagates is calculated at 1.24 seconds. The indentation of the vessel at this time is taken from Figure 3.25 equal to 6.00 meters. The Energy absorbed from the vessel at this stage is 300 MJoules and the energy of bulkhead 87 is shown to be equal to 1 MJoule.

The 5% local strain criterion for Area 2 estimates a limit time at 1.81 seconds, when the indentation is 7.6 meters. The total energy derived on the vessel is 410 MJoules and the energy derived on the bulkhead is 7.1 MJoules. The mean strain at this stage is 2%.

The 5% mean strain criterion defines a limit time at 2 seconds, with indentation equal to 7.8 meters. The global energy comes to 440 MJoules while the energy derived on

the bulkhead is 8.7 MJoules. The local strain is 8.8 %. The maximum value the mean strain criterion shown is 14 % which is practically, a very large value.

In this case the mean strain criterion showed high values but it is not realistic. Since this area consists of less elements than Area 1, and considering that the location is similar with regard to the longitudinal bulkhead extended beyond frame 87, it should not yield 5% mean strain. The only explanation provided is the fact that Area 2 is located on the boundary of the transverse bulkhead zone highly vulnerable to bending and membrane stresses as can be seen in Figure 5.10. As a result these stresses elongate the material, far beyond the elastic limit in high plasticity values with viscous effects.

The fracture criterion, because it is dependent on energy quantities and not strain values, is very predictable as far as the stress and strain rates are concerned. As a result, it is shown that the time the fracture propagates is limited to 1.24 seconds (<<2.00 seconds). Exactly the same phenomenon appeared in the rectangular plates in previous Sections, where the fracture criterion was dependent on the bending stresses. It was shown, Table 5.13, that the deflection calculated for the 10 mm plate was smaller compared to the deflection calculated from the 7.5 mm plate. And this phenomenon was attributed to the existence of higher tensile bending stresses on the surface of the plates.

### *5.6.4 EXAMINATION OF AREA 3.*

This Section is also located on the transverse diaphragm Bulk2, as shown in Figure 5.11. Rearrangement of the elements produces a more dense mesh, which creates the strain contour shown in Figure 5.22.

The blue area inside the rectangle consists of the highest strains. Following the same route, relative to the previous areas, the fracture criterion defines a time equal to 2.35 seconds as the time at which the crack starts the propagation, Figure 5.23. The indentation at this time is found to be 8.3 meters, the global energy is 460 MJoules

while the energy of bulkhead 87 is 10.5. The local strain is 11.25 % and the mean strain is only 0.09% as shown in Figure 5.24.

One may see that in this case the fracture criterion coincides with high local strains, while the mean strain remains very small. The phenomenon of the local high bending stresses is repeated once more. This zone, Area 3, is positioned on the upper part of bulkhead 87, (Bulk2) where it meets with the shell and the top deck (Deck1). These boundary conditions protect Area 3 from high deflections, normal to its plane, but in the local vicinity near the attachment with the shell, the strain concentration is high enough to propagate a flaw located.

The 5% local strain criterion defines a limit time equal to 1.82 seconds, similar to Area 2. Hence the indentation is 7.61 meters, the global energy 411 MJoules, the energy derived on bulkhead 87 is 7.2 MJoules, and finally, the mean strain at this time is 0.01 %, taken from Figure 5.24.

The fact that the 5% local strain criterion agrees with the results from Area 2, is not however consistent with the result showing that the energy derived from the elements in area 2 is much greater than those from area 3. This is shown in Figure 5.25 where at time 1.82 seconds the energy for area 2 is almost 60 times greater than the one of area 3. Applying this argument the accuracy of the 5% local strain criterion must be debatable.

### *5.6.5 EXAMINATION OF AREA 4.*

Area 4 is located in the shell, as one may see in Figures 5.12 and 5.13. It is located in the area that contributes to the change of the vertical displacement of the upper part of the bow. At the inner part of the shell at this location there is the deck, Deck 3, (refer to Figure A3-2.3) is attached.

Figure 5.26 displays Area 4 in 2 forms. Form A is the Von-Mises contour, as it was isolated from the global model, while form B is the contour for the remodelled dense

mesh. Figure 5.27 displays the strain contour of the fine mesh. Here, again the blue area shows the maximum tensile strains.

The fracture criterion yields a time of propagation for the crack equal to 1.06 seconds, Figure 5.28. The indentation of the vessel at this time is 5.2 meters. The global energy is equal to 25 MJoules, while the energy dissipated on bulkhead 87 (Bulk2) is 0.2 MJoules. The local strain is 8.08% and the mean strain as shown in Figure 5.29 in nearly 0.

The 5% local strain criterion predicts a time of failure at time 0.98 seconds, when the indentation is 5.0 meters. The Vessel energy is 20 MJoules, when the Bulk2 energy is 0.1 MJoules. The mean strain is very small in this case as well, almost equal to 0.

In this case we see a good correlation between the results from both the criteria. This is attributed to the high stresses developed, because of the connection with Deck3. The mean strain as shown from Figure 5.29 is very small because of the contribution of the beam elements attached on the shell. The transition of the forces in this area is in the vertical direction, thus the frame stiffening is subjected to tensile loading, event that makes the structure quite strong in this direction. It proves to be strong enough to deform Deck1 and Deck2 downwards.

### *5.6.6 DISCUSSION AND DESIGN APPRAISAL*

The following Table summarises the data extracted from Areas 1-4 using the 3 failure criteria.

| *Failure Criterion* | Time Sec | Indent. m | Vessel Pot. energy MJoules | Bulkhead Pot. energy MJoules | Local Strain % | Initial Velocity m/sec | ***Mean Strain %*** |
|---|---|---|---|---|---|---|---|
| **AREA 1** | | | | | | | |
| **Fracture Criterion Sector I** | 1.49 | 6.75 | 355 | 3.6 | 1.0 | 4.96 | 1.0 |
| **Fracture Criterion Sector II** | 1.60 | 7.20 | 380 | 4.9 | 2.9 | 5.13 | 0.4 |
| ***5% local Strain*** | 1.70 | 7.4 | 400 | 6.0 | **5.0** | 5.26 | 0.7 |
| **AREA 2** | | | | | | | |
| ***Fracture Criterion*** | 1.24 | 6.00 | 300 | 1.0 | 0.5 | 4.56 | 005 |
| ***5% local Strain*** | 1.81 | 7.60 | 410 | 7.1 | **5.0** | 5.33 | 2.0 |
| ***5% mean Strain*** | 2.00 | 7.80 | 440 | 8.7 | 8.8 | 5.52 | **5.0** |
| **AREA 3** | | | | | | | |
| ***Fracture Criterion*** | 2.35 | 8.3 | 460 | 10.5 | 11.3 | 5.64 | **0.09** |
| ***5% local Strain*** | 1.82 | 7.61 | 411 | 7.2 | 5.0 | 5.33 | **0.01** |
| **AREA 4** | | | | | | | |
| ***Fracture Criterion*** | 1.06 | 5.2 | 25 | 0.2 | 8.1 | 1.73 | **≈0.001** |
| ***5% local Strain*** | 0.98 | 5.0 | 20 | 0.1 | 5.0 | 1.39 | **≈0.001** |

**TABLE 5.17 APPLICATION OF THE FAILURE CRITERIA ON AREAS 1-2-3-4**

The following conclusions are drawn from this analysis;

- The fracture propagation criterion is dependent on the energy dissipated on the structural members of the structure. The failure of these members follows the pattern of the energy dissipation. Therefore the area which absorbed energy faster, enough to propagate a prescribed crack, will fail first. According to this scenario fracture propagates faster in Area 4, then Area 2, then Area 1-I, Area 1-II follows, and finally Area 3.

  Following the same design line, the 5% local strain criterion describes the failure pattern with Area 4 failing first, then Area 1 follows and Area 2 with Area 3 at the end. Although local strains reach the 5% this scenario does not follow the pattern of the fracture criterion.

  The mean strain criterion is not describing this failure pattern, since the elongation of the plate zones does not exceed the 1% in most cases, except in area 2 where it's values are quit high.

- The Indentation with regard to the failure criteria can be used as an accepted design limit of the bow structure in order to undergo collision forces avoiding the appearance of fracture at the shell or any other member comprising the bow. From the Energy-Indentation acceptable limit speeds for the head on collision can be extracted. Using the fracture criteria the following critical speeds are found;

| **Fracture Criterion** | |
|---|---|
| Area | Critical Speed in m/s-knots |
| Area 4 | 1.73 – 3.36 |
| Area 2 | 4.56 – 8.86 |
| Area 1-I | 4.96 – 9.64 |
| Area 1-II | 5.13 – 9.97 |
| Area 3 | 5.64 – 10.96 |

**TABLE 5.18 CRITICAL SPEEDS DERIVED FROM THE FRACTURE CRITERION**

Considering the 5% local strain criterion the following critical speeds are found;

| **5% local strain Criterion** | |
|---|---|
| Area | Critical Speed in m/s-knots |
| Area 4 | 1.39 – 2.70 |
| Area 1-II | 5.26 – 10.22 |
| Area 2 | 5.33 – 10.36 |
| Area 3 | 5.33 – 10.36 |

**TABLE 5.19 CRITICAL SPEEDS DERIVED FROM THE 5% MEAN STRAIN CRITERION**

It can be seen that the later criterion creates higher critical speeds, for the areas where it is applicable. For Area I the criterion is not valid

- The conjecture from the fracture criterion is that areas with high-energy concentration during tensile response under various loading will eventually propagate a crack. The global failure is defined when either the structure does not take any further loading or when the response has exceeded acceptable design criteria, such as intact stability criteria, or change of equilibrium state due to liquid ingress in void spaces and resultant loss of buoyancy. The limit values have to be considered and evaluated by the designer and the relative rules for controllable operation at sea.

- The 5% local strain criterion may not however locate accurately the areas of probable failure. It proposes values very similar to the fracture criterion notwithstanding the fact that it fails to acknowledge the idiosyncrasy of the strains appearing in areas close to a fixed boundary. Similarly it does not distinguish the difference between high bending stresses developed in thicker material. Therefore this criterion should be very carefully used and always in relation to the plate thickness and the boundary conditions.

- The mean strain equal to 5% should be reconsidered since in neither of the plate models used, under UDL or Patch load, nor in the bow model is it valid. This 5%

elongation is by far too large, and it is shown that in most case it just about exceeds the 2%.

## 5.7 APPENDIX I

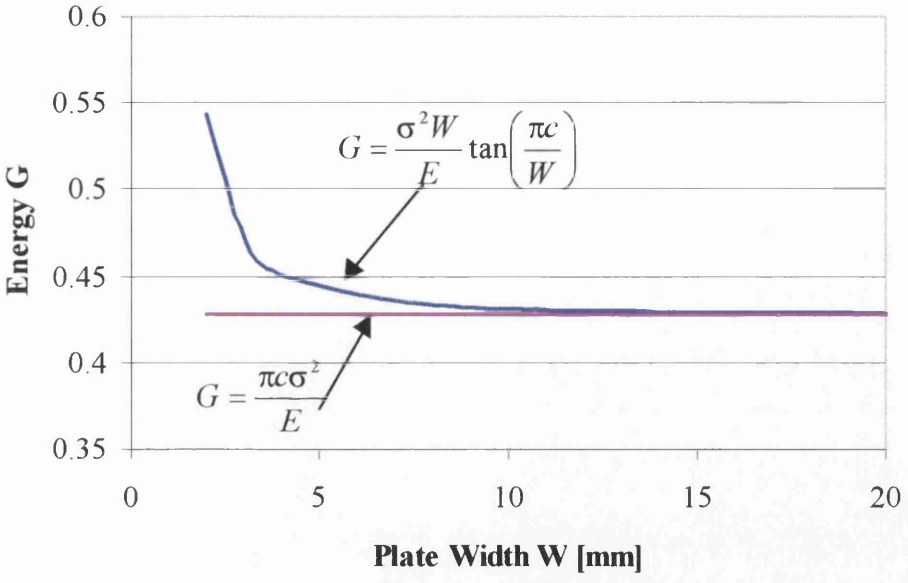


**Diagram 1** **Comparison of formulas 5.10 and 5.12 for a crack length 5 mm**

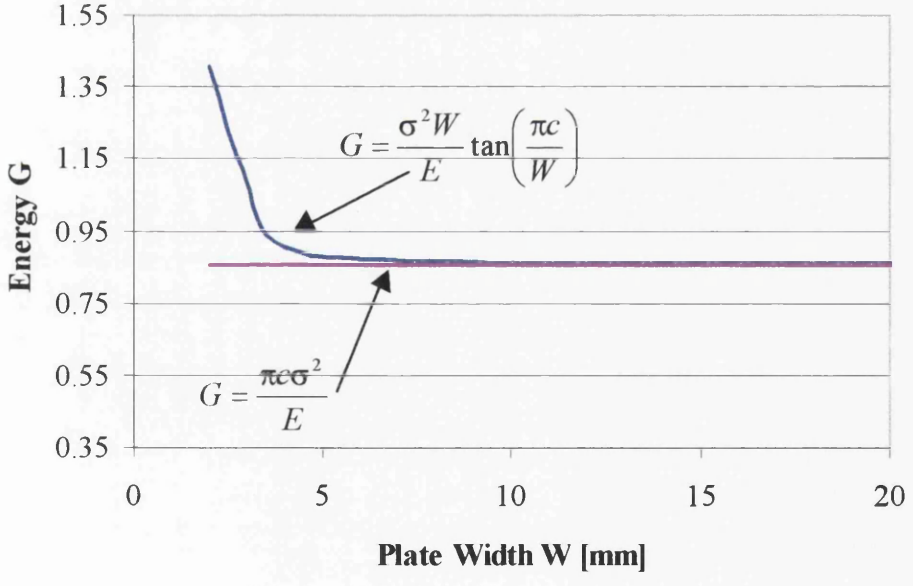


**Diagram 2** **Comparison of formulas 5.10 and 5.12 for a crack length 10 mm**

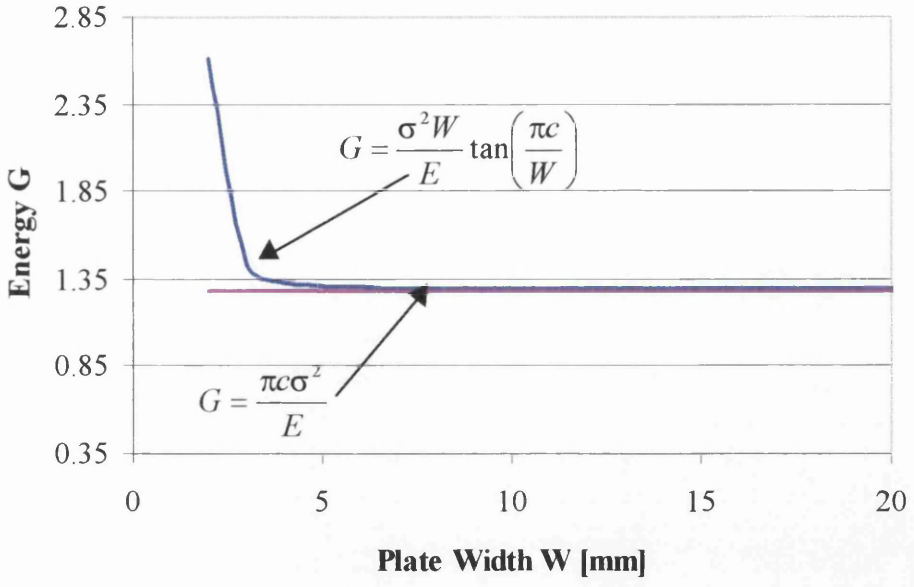


**Diagram 3** **Comparison of formulas 5.10 and 5.12 for a crack length 15 mm**

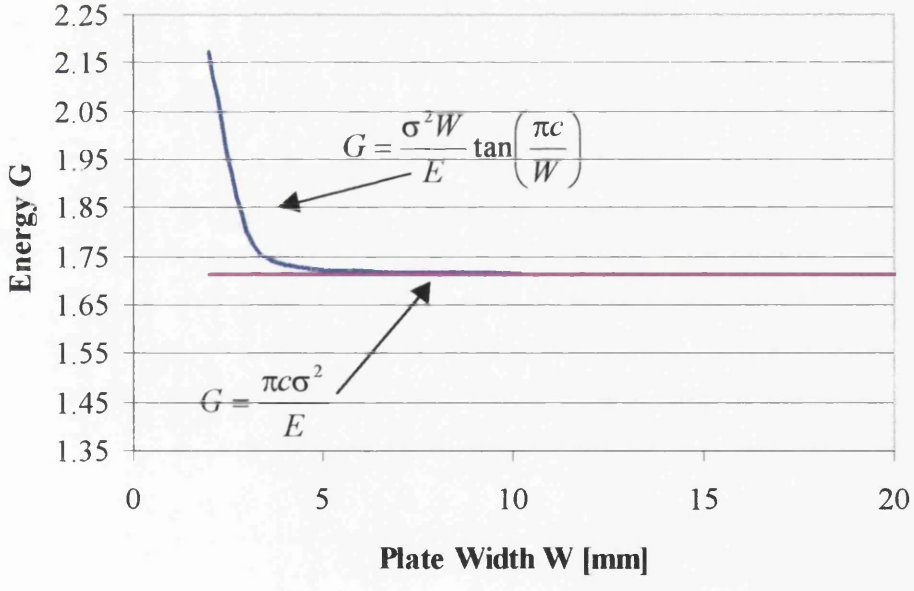


**Diagram 4** **Comparison of formulas 5.10 and 5.12 for a crack length 20 mm**

## 5.8 APPENDIX II

### STRAIN ENERGY DENSITY FRACTURE MECHANICS ($SED_{FM}$) MODEL

### Ship structure Committee Report SSC-364

Tensile testing is by far the most routine, inexpensive test mechanical method, sort of impact testing, and is currently used by a large number of test laboratories. Ductility ratio based on %RA is a commonly used toughness parameter, but it has limited applicability. Only stress intensity operating service that will confidently assure life is a specified environment. Estimating a stress intensity parameter from a tensile test has obvious advantages and many models are available for estimating $K_{IC}$. From tensile data but they empirical and therefore restricted in use to a particular material or strength level. The model that was found to be most adaptable to handling a variety of materials over a wide range of strength is that proposed by Bockrath and Glasco (1980).

The difference between the proposed model and conventional J-integral analysis is;

1. the estimation of the size of a damage zone at the tip of a crack, and
2. the use of the strain energy density from UTS to the fracture strength to calculate the total energy at the crack tip.

This zone is characterised by localised plastic deformation that includes micro-void coalescence (MVC) and it therefore not necessarily a constant volume process.

Referring to Figure 5.5, the damage is nested inside the zone of uniform plastic yielding, where the metal is stressed above the yield point but below UTS. In this region, plastic deformation is fairly well understood. The metals volume and Poisson's ratio is constant.

Its flaw behaviour is accurately described by an exponential function with a constant strain hardening coefficient, and the octahedral sear stress accurately translates uniaxial deformation in biaxial and tri-axial deformation. This makes the metals behaviour in this zone amenable to analysis.

The inner zone, the damage zone, corresponds to the region of the stress-strain curve where necking occurs. Plasticity models do not accurately describe this region. Void growth can cause a valuable density and Poisson's ratio. The strain-hardening coefficient is not constant and the octahedral shear stress does not accurately describe deformation.

The two plastic zones correspond to different locations on the true stress true strain curves as shown in Figure 5.6, where the different strain energy densities are illustrated relative to there location on the engineering true stress true strain curve. Examining this curve of Figure 5.6 shows that typically the majority of the plastic strain energy density is under the stress strain curve after necking occurs to UTS.

Therefore, two analytically different plastic zones exist;

1. Uniform plastic deformation zone and
2. Damage zone

The plastic strain energy absorbed at the cracked tip is then the sum of the two zones.

The plastic energy absorbed in the uniform zone, $U_U$, during crack growth is evaluated by determining the local strain energy density absorbed in an elemental volume and integrating around the crack tip where the stress is between yield stress and ultimate stress. The plastic energy absorbed in the damaged zone, $U_f$, during crack growth has been empirically related to the strain energy density from ultimate stress to fracture. Unstable crack growth occurs when the total plastic energy absorbed in the two zones is less than the elastic energy released during the crack growth $U_e$, equation 5.14.

Solving for half crack length yields equation 5.15.

# FIGURES

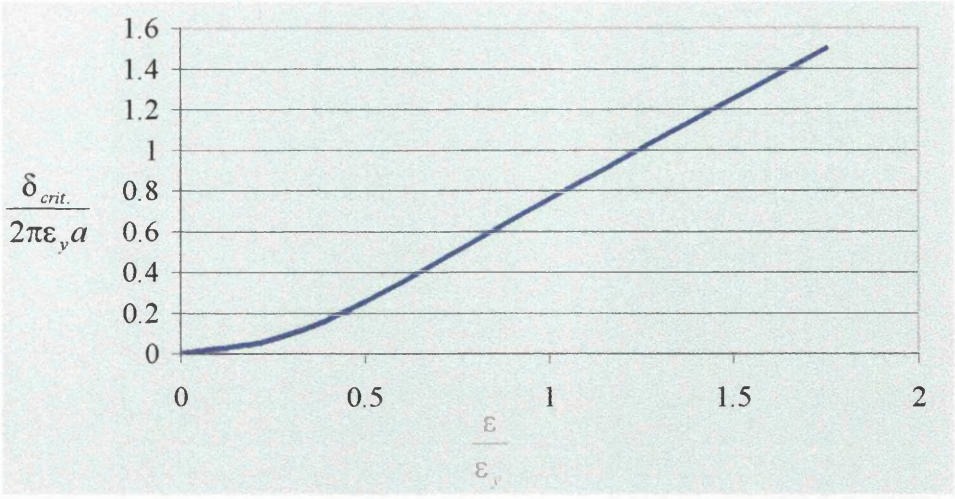


**Figure 5.1** *The semi-empirical COD design curve*

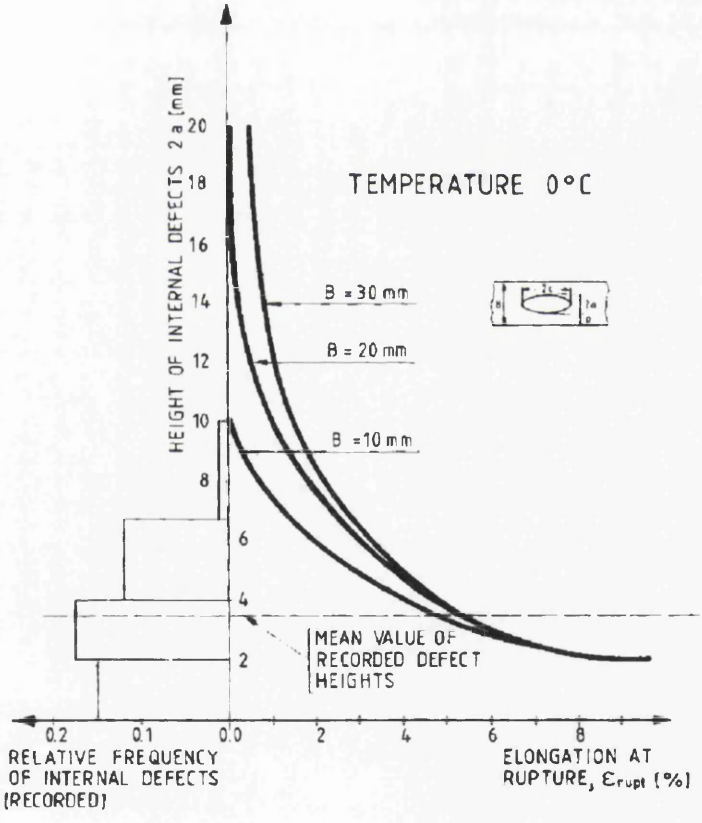


**Figure 5.2** *Critical rupture strain as function of internal defect size*

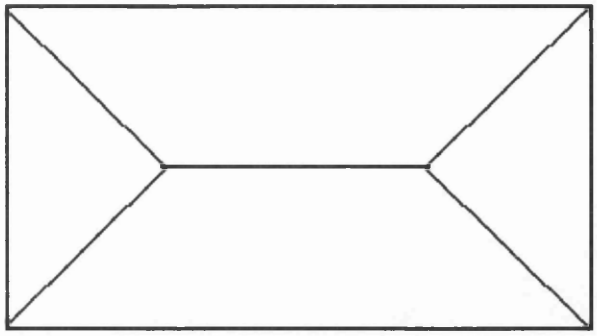

**Figure 5.3** *Collapse mechanism for lateral loaded plates*

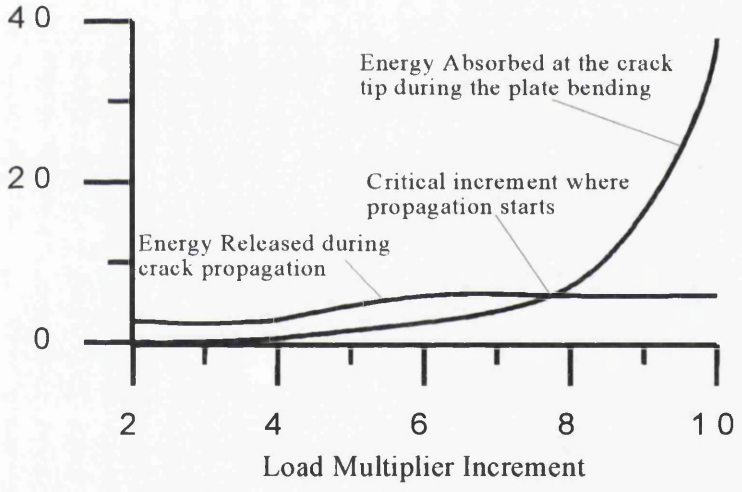


**Figure 5.4** *The critical load multiplier increment is determined through the comparison of the Plastic energy absorbed at the tip of the crack and the energy required for the crack propagation*

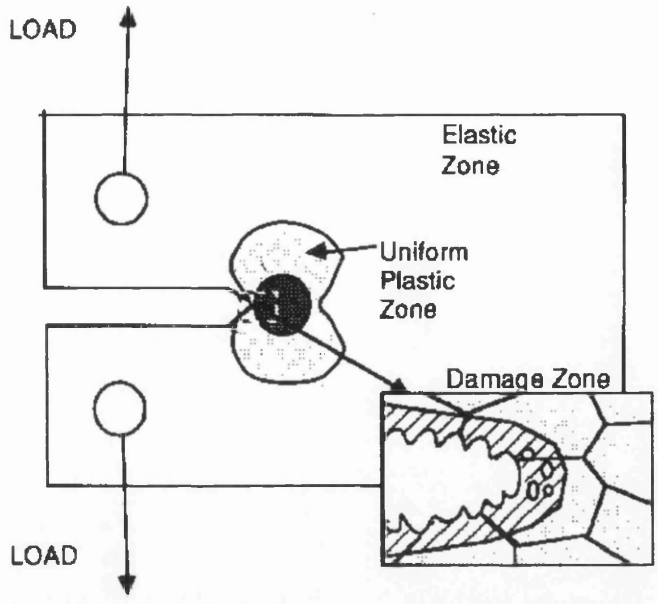


**Figure 5.5** *Characterisation of the stress-strain field in front of a crack showing the elastic, Uniform Plastic, and Damage Zone as related to true-stress-strain curve in Figure 5.6*

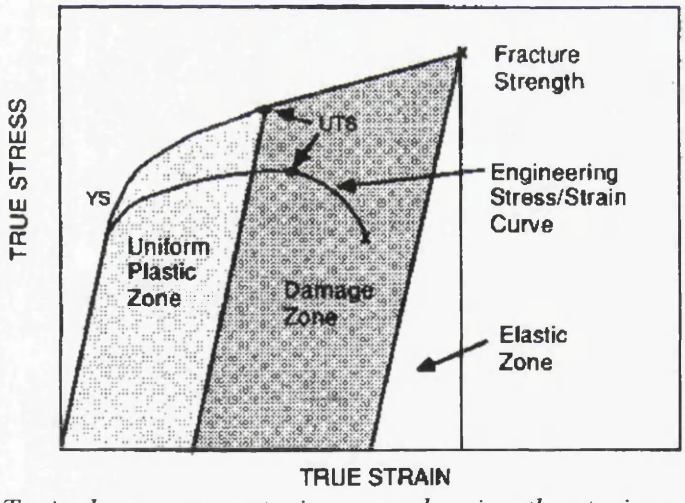


**Figure 5.6** *Typical true stress-strain curve showing the strain energy density under the curve, and the zones relating to the strain field in front of a crack tip as shown in Figure 5.5*

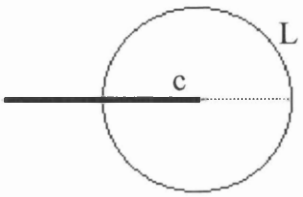


**Figure 5.7** *Sanders (1960) Pointed out that the region around the crack periphery where the energy balance holds can be any portion of the body enclosed within a simple closed curve L*

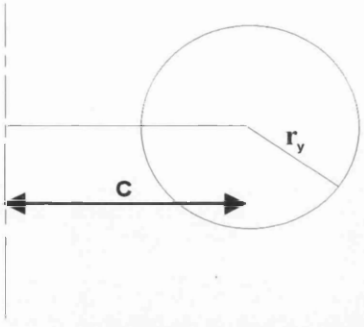


**Figure 5.8** *The radius of the plastic zone around the tip of the crack as was defined by Irwin, (1961)*

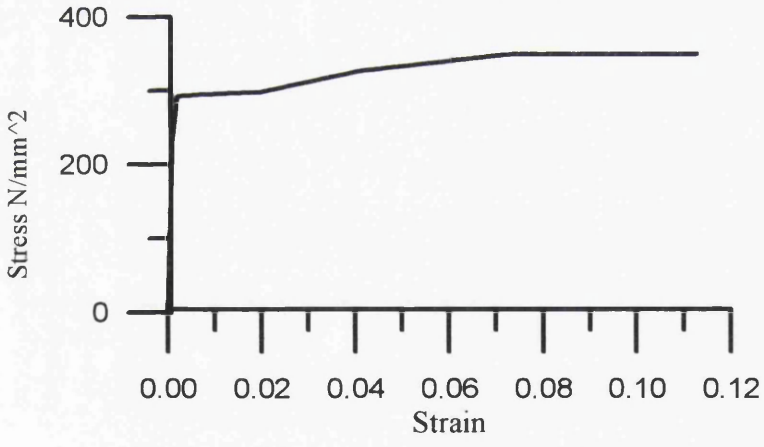


**Figure 5.9** *Typical Stress-Strain curve at the tip of the crack*

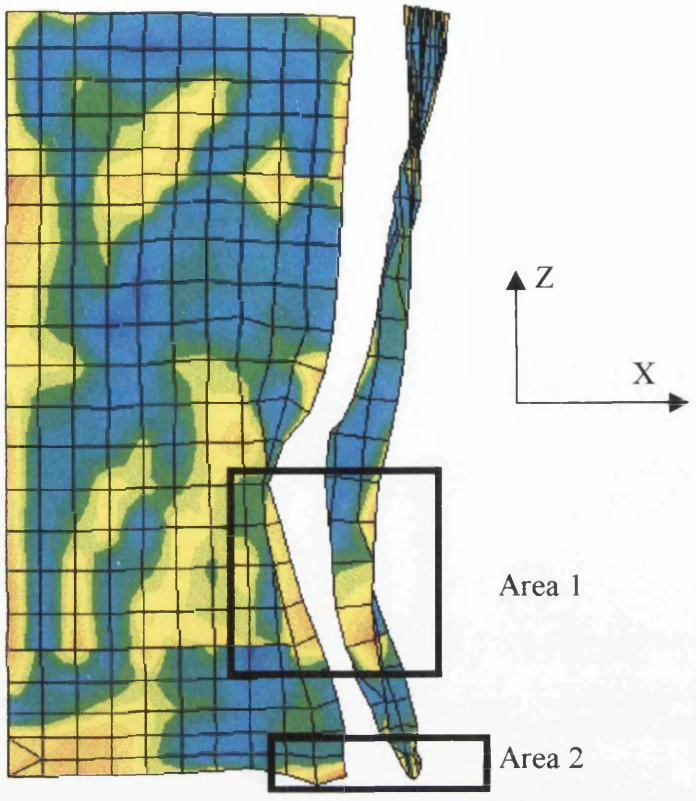


**Figure 5.10** *Bulk2 and Bulk3 with the critical areas where failure is examined*

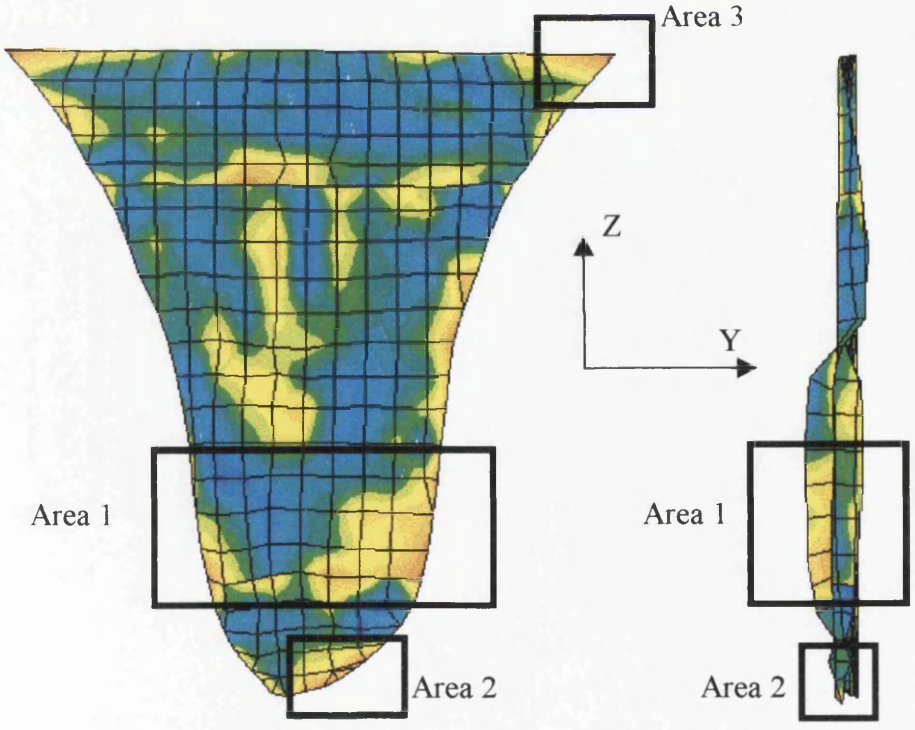


**Figure 5.11** *Bulk2 and Bulk3 with the critical areas where failure is examined*

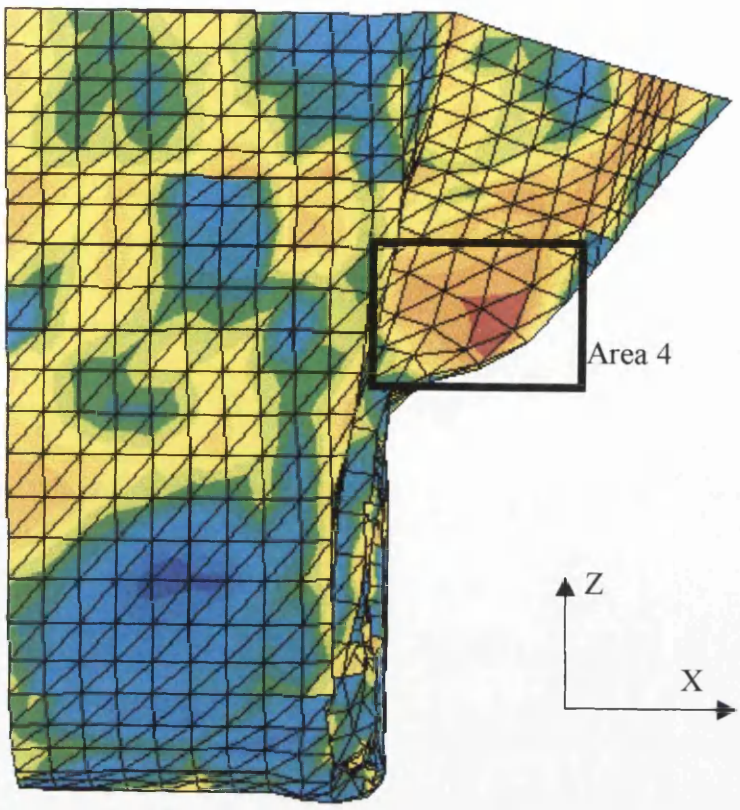


**Figure 5.12** *The shell with the critical areas where failure is examined*

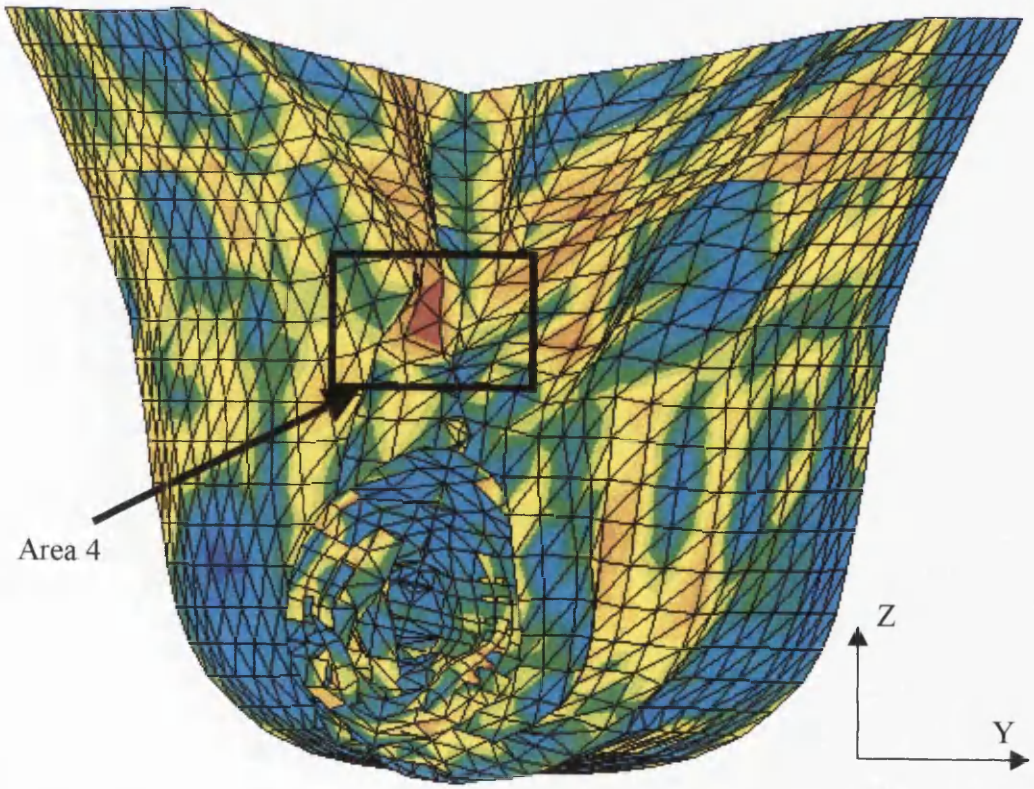


**Figure 5.13** *The shell with the critical areas where failure is examined*

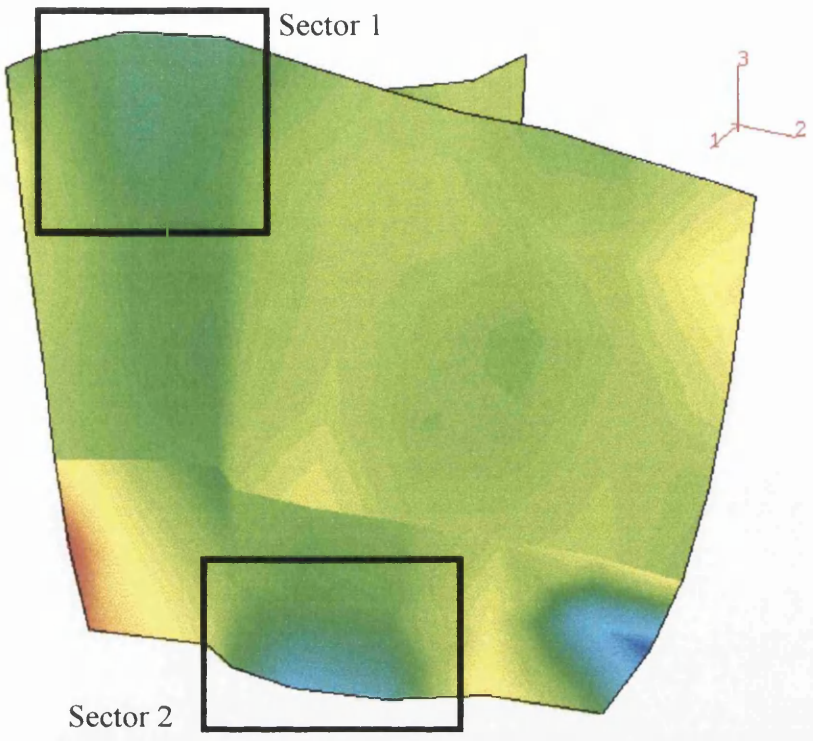


**Figure 5.14** *Area 1, Strain contour. The rectangular divisions denote sectors with high tensile strains*

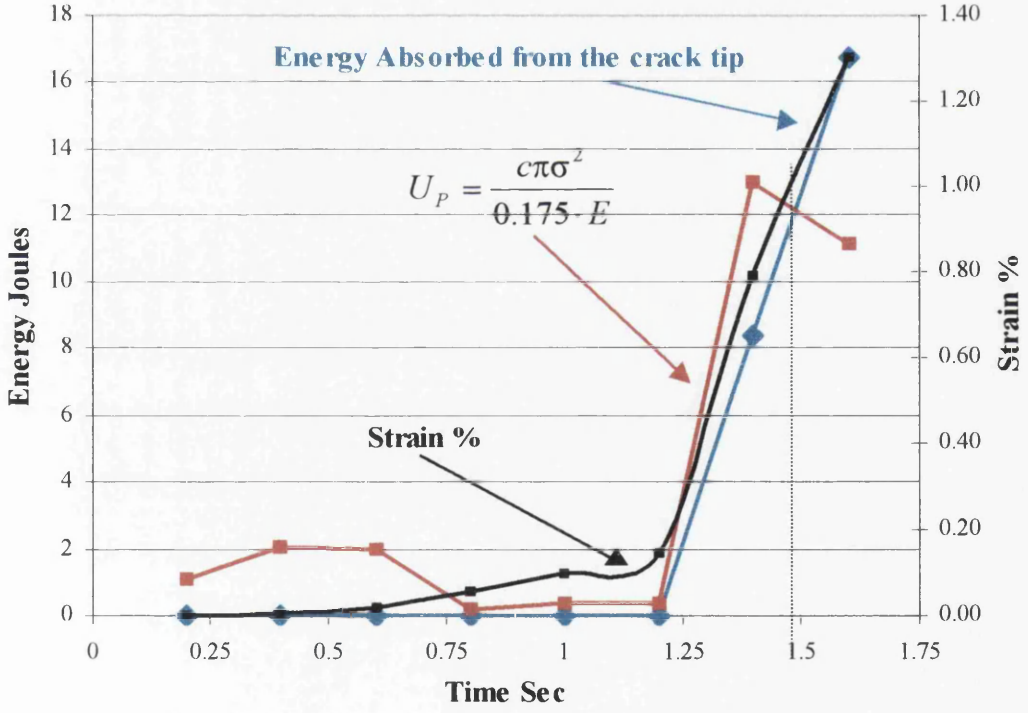


**Figure 5.15** *Fracture propagation Criterion for Area-1, Sector 1. As indicated Crack propagates at time 1.49 seconds, when the strain is 1.03 %.*

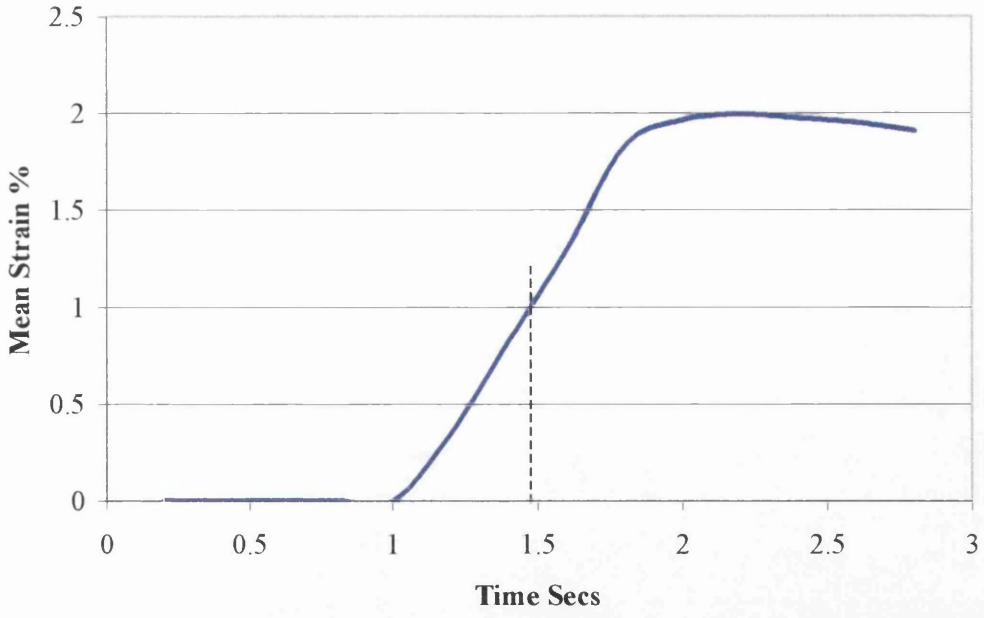


**Figure 5.16** *Mean strain for Sector 1. The 5% mean strain criteria produce collision time equal to 1.25 sec*

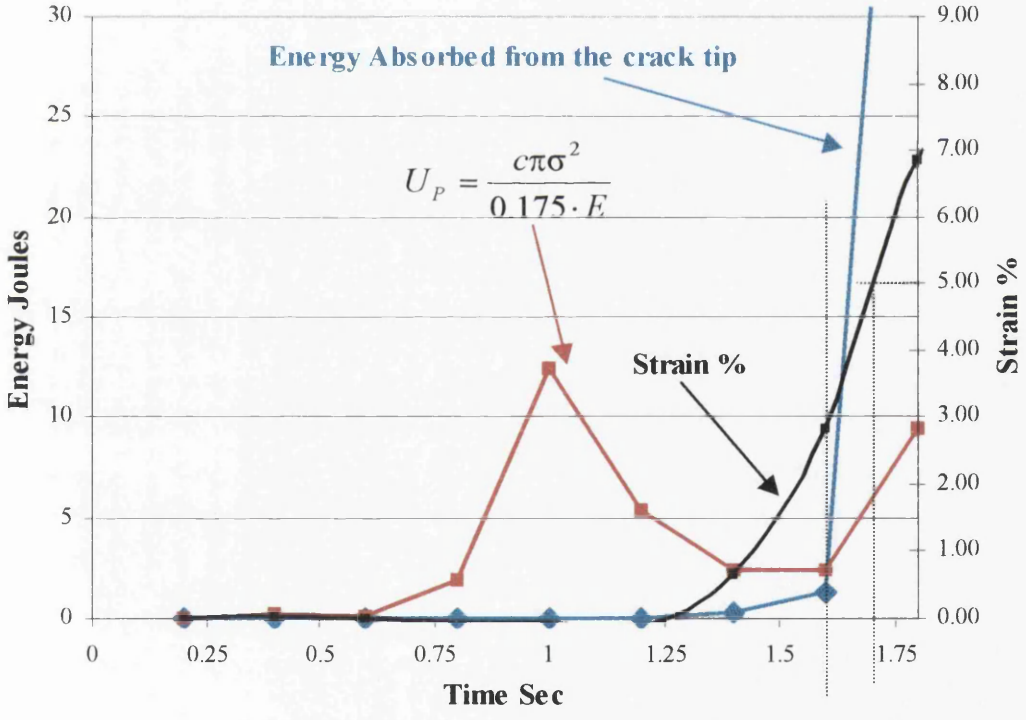


**Figure 5.17** *Fracture propagation Criterion for Area-1 Sector 2. As indicated Crack propagates at time 1.60 seconds, when the strain is 2.90 %. The 5% local strain criterion produce failure at 1.70 seconds*

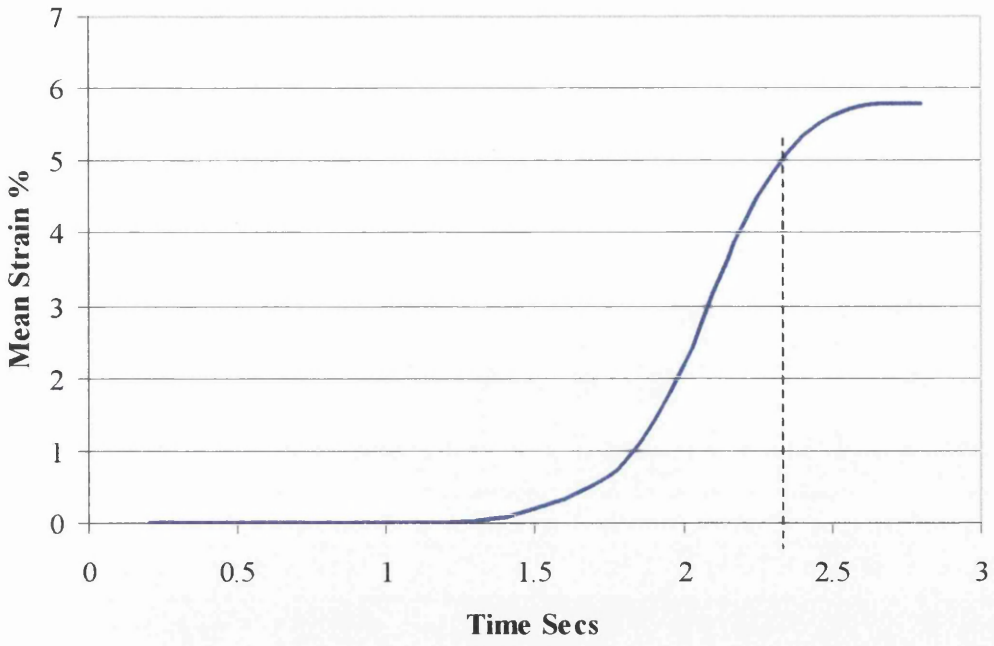


**Figure 5.18** *Mean strain for Sector 2, in Area 1. The 5% mean strain criteria produce collision time equal to 2.34 sec*

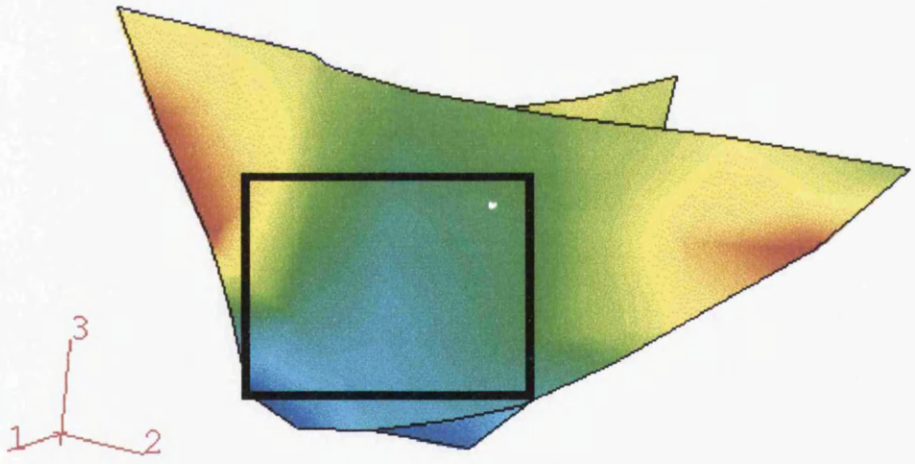


**Figure 5.19** *Area 2, Strain contour. The rectangular division denote the zone with high tensile strains*

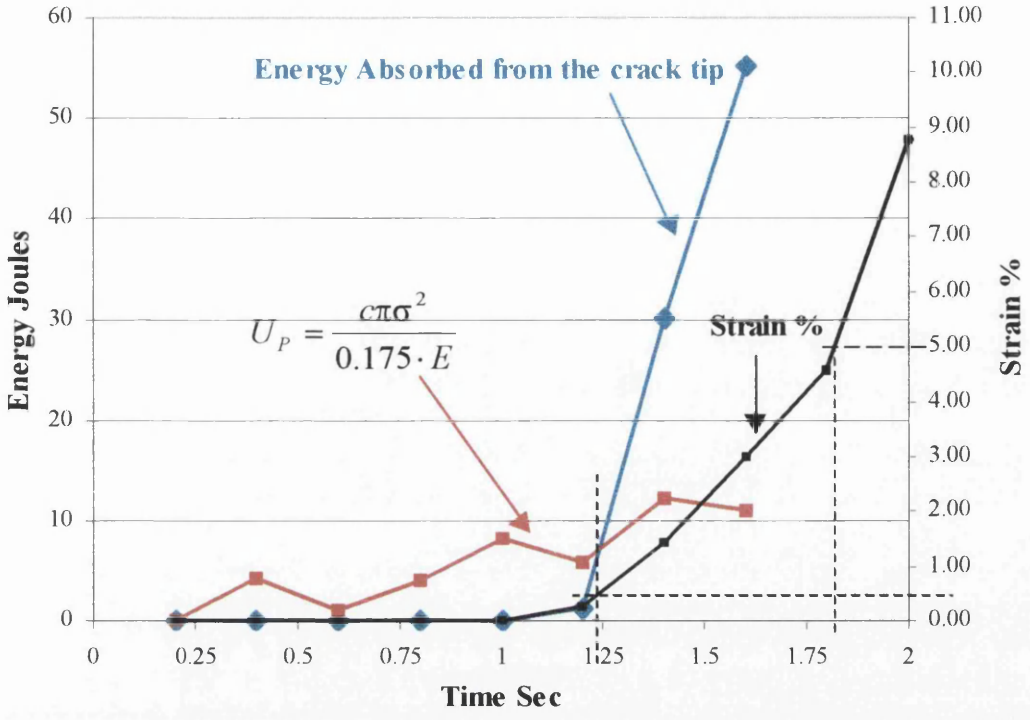


**Figure 5.20** *Fracture propagation Criterion for Area-2. As indicated Crack propagates at time 1.24 seconds, when the local strain is 0.50 %. The 5% local strain criterion produce failure at 1.81 seconds*

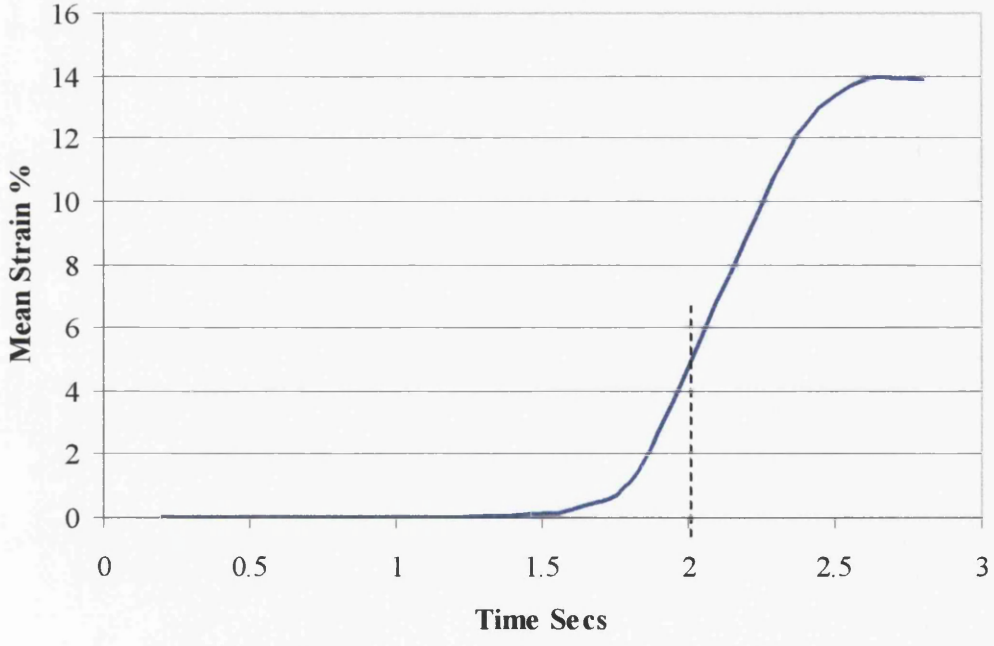


**Figure 5.21** *Mean strain for Area 2. The 5% mean strain criteria produce collision time equal to 2.00 sec*

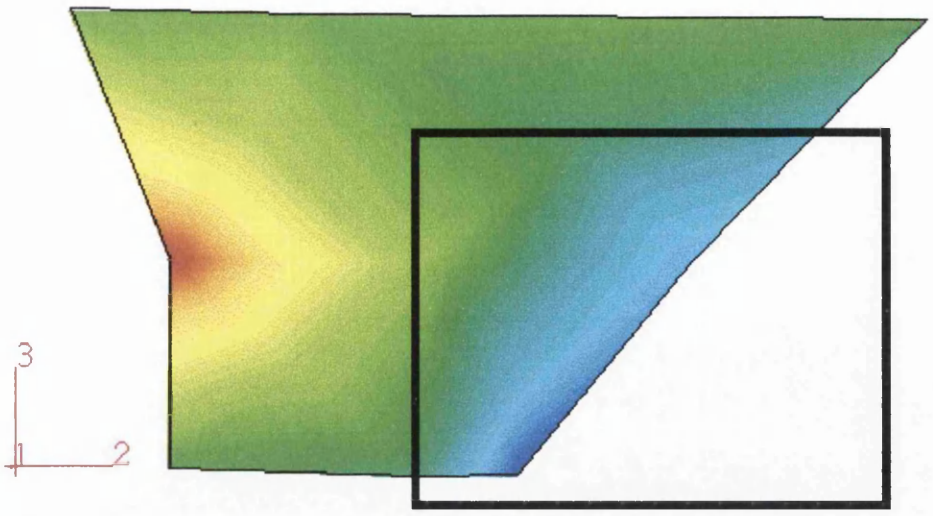


**Figure 5.22** *Area 3, Strain contour. The rectangular division denote the zone with high tensile strains*

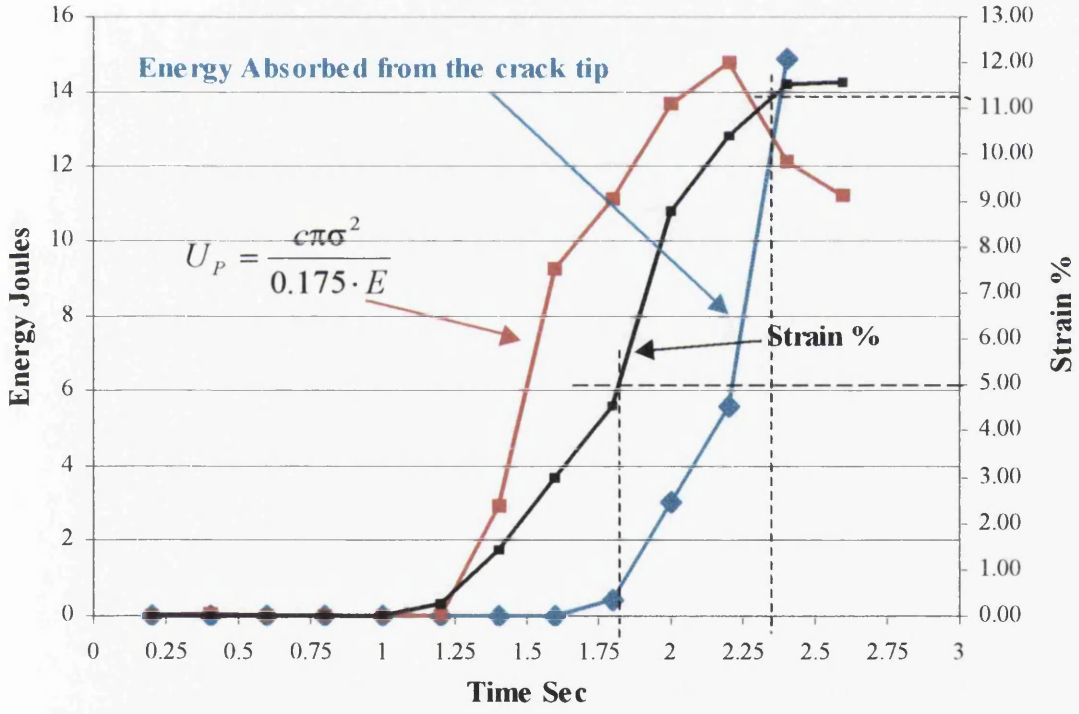


**Figure 5.23** *Fracture propagation Criterion for Area-3. As indicated Crack propagates at time 2.35 seconds, when the local strain is 11.25 %. The 5% local strain criterion produce failure at 1.82 seconds*

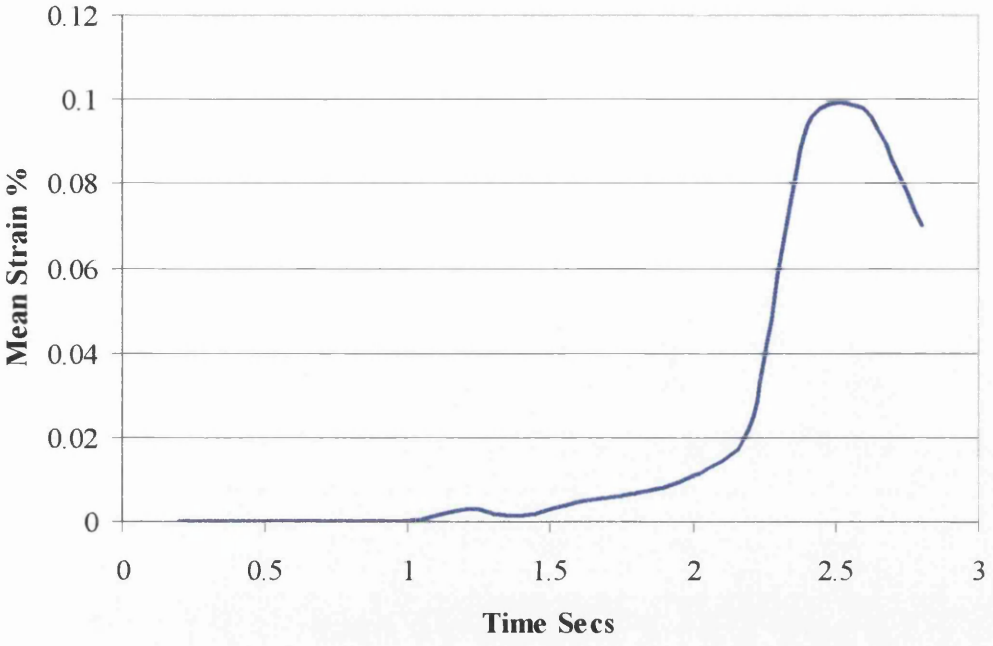


**Figure 5.24** *Mean strain for Area 3. The 5% mean strain is not valid in this case since the maximum mean strain is only 0.1% due to the boundary restriction of this area.*

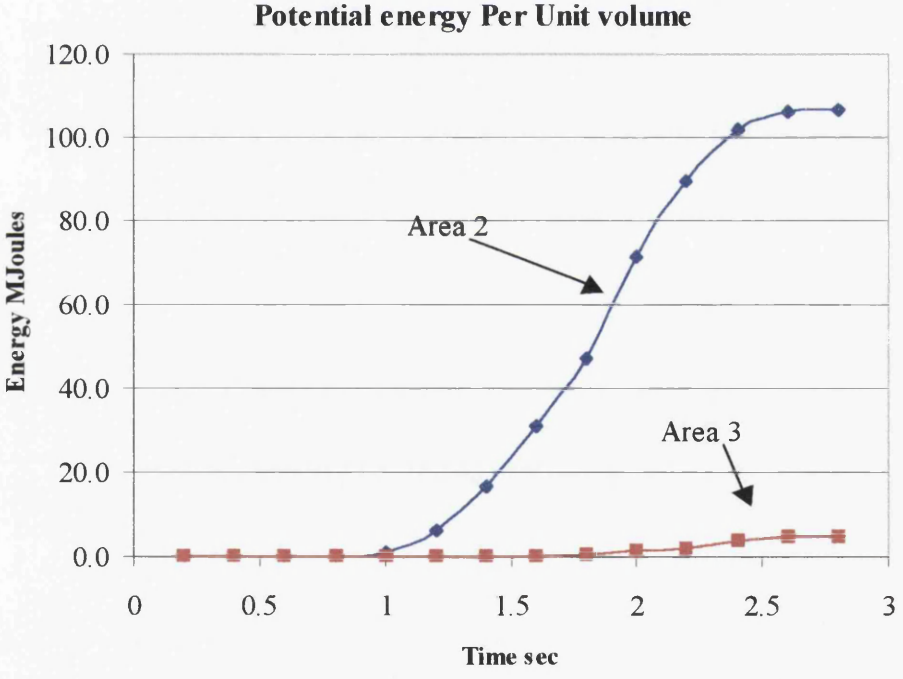


**Figure 5.25** *Energy per unit volume for areas 2 and 3.*

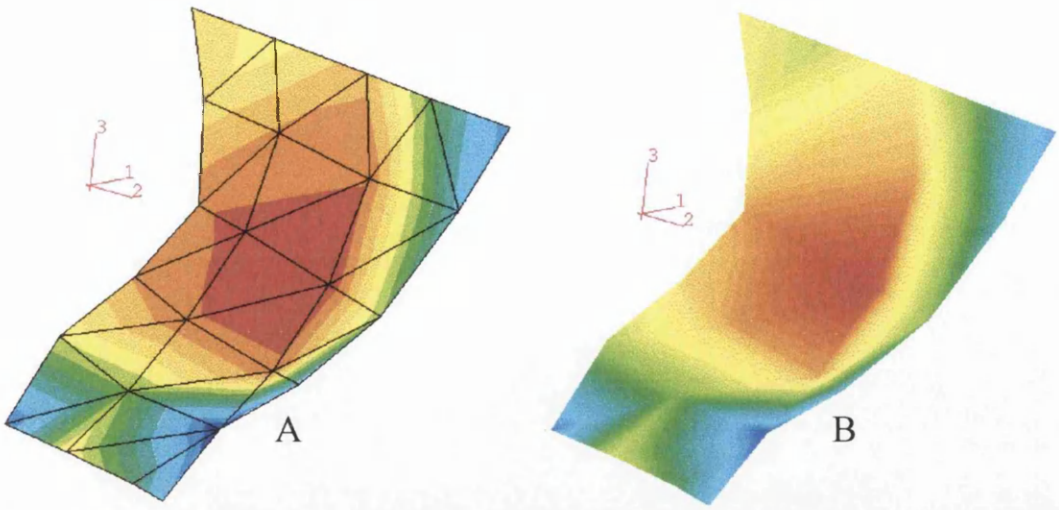


**Figure 5.26** *Contours of Mises stress from Area 4 of the shell. If one correlate part A with Figure 5.12 or 5.13, then orientation will be established. Part B is the same contour output, using a more dense mesh with prescribed displacements on the boundary as they were derived from part A.*

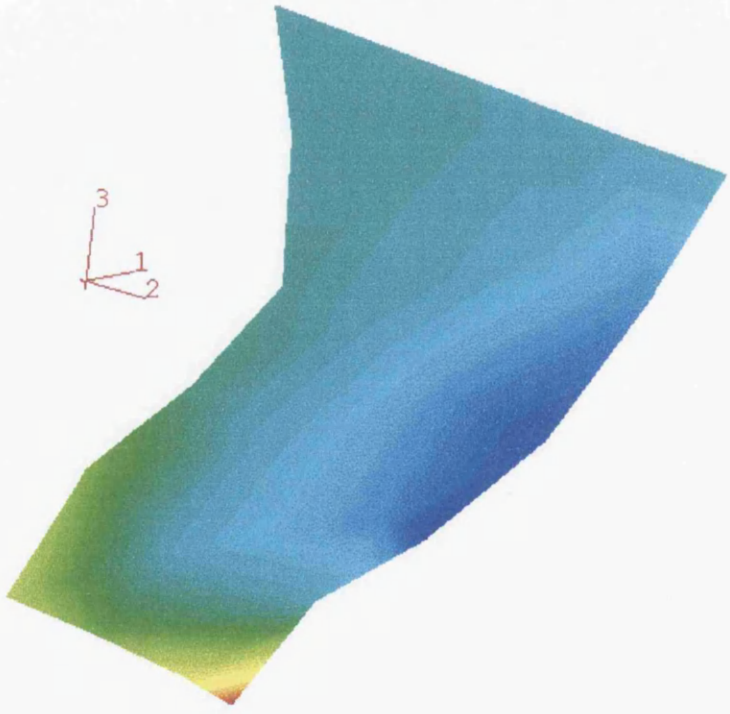


**Figure 5.27** *Contour of strain in Area 4. The Dark blue denotes area with high tensile strain concentration.*

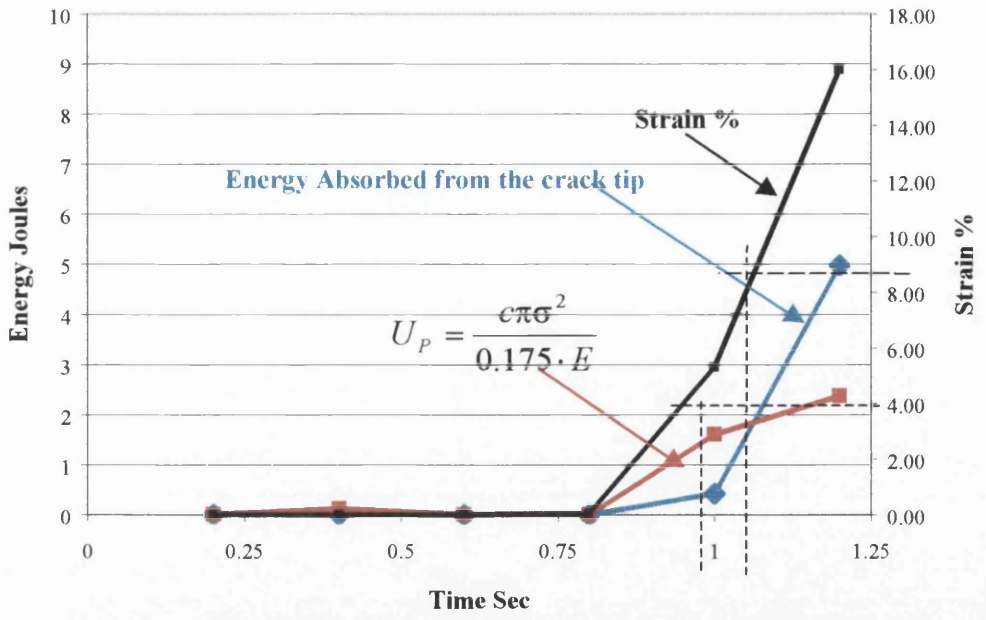


**Figure 5.28** *Fracture propagation Criterion for Area-4. As indicated Crack propagates at time 1.06 seconds, when the local strain is 8.08 %. The 5% local strain criterion produce failure at 0.98 seconds*

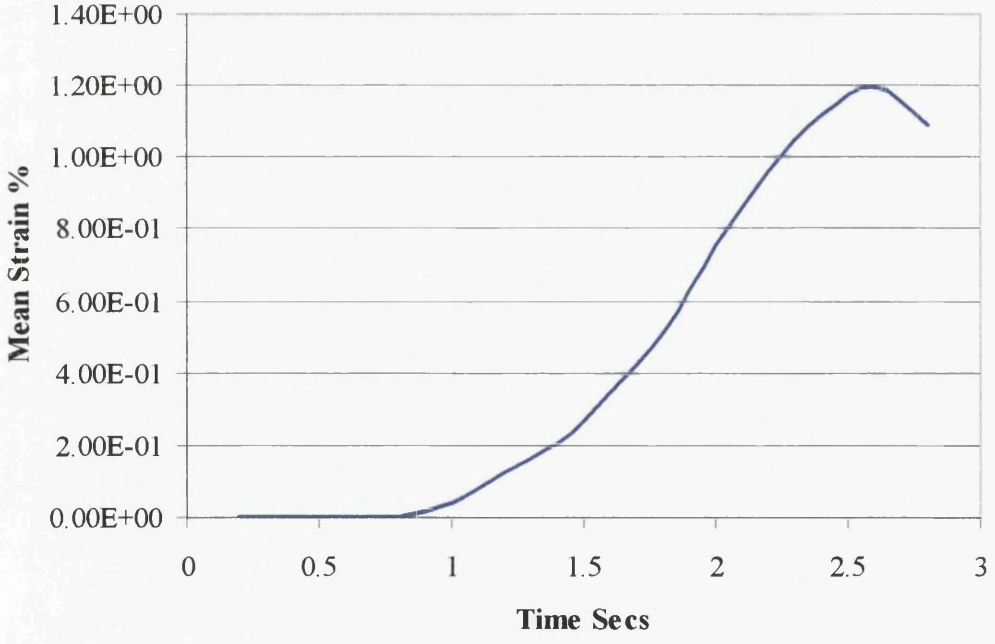


**Figure 5.29** *Mean strain for Area 4. The 5% mean strain is not valid in this case since the maximum mean strain is only 1.4%.*

# CHAPTER SIX

# CONCLUSIONS AND PROPOSALS FOR FUTURE WORK

---

## 6.1 CONCLUSIONS AND RECOMMENDATIONS

In this Thesis a numerical analysis is presented, of the head-on collision and grounding of a tanker vessel, using the Finite Element Package ABAQUS. The numerical results are compared with analytical and empirical approaches. The energy dissipation characteristics of the structural members of a tanker bow model, are introduced and the energy conservation during the collision is examined, including the energy quantities produced from the kinematic response as well as the energy quantities resulting from the elasto-plastic behaviour of the structure. A fracture criterion is developed on the basis of the energy released which is calculated from Griffith's Fracture Mechanics. Application of the fracture criterion is adopted on the head-on collision and is compared with three other fracture criteria.

### *6.1.1 HEAD-ON COLLISION WITH A RIGID SURFACE*

Four empirical approaches have been considered for the evaluation of the maximum indentation and energy absorption during a head-on collision. The total energy absorbed by the structure, as this was calculated using Gerard's method, and Aldwinckle's statistical approach, produced results similar to those extracted from the numerical analysis. However, the maximum indentation result from the theoretical approaches does not agree with the numerical outcome since the collapse mode due to buckling loads developed is conservative. This is explained in Sections 3.1 and 3.3.2 and correction for the indentation is proposed with the introduction of equation 3.33 and 3.34.

The dissipation of the elasto-plastic energy on the entire model is presented with regard to the energy spread on the individual members of the structure. Energy conservation takes place and the comparison with the available energy prior to the collision yields results with very good correlation. The elastic energy dissipated on the structural members is much smaller than the plastic energy, except in the case of the collision bulkhead.

The shell structure appears to consume the largest amount of energy amongst the other members. Decks 7 and 8 follow since they directly come in contact with the rigid surface.

Gerard's approach estimates the crippling forces derived on the longitudinal structural elements of the model. A correlation with the results produced from the numerical and the empirical methods reveals that ABAQUS calculates slightly higher quantities, somewhat 10% higher as far as the total energy is concerned. This tolerance is within acceptable limits since similar difference were shown from Minorsky (1984) and Pedersen (1995)

The relation of energy with regard to the indentation yields to an important conclusion since it is not affected by the speed prior to the collision. Provided that the final energy absorbed is known for at least one collision scenario of the same vessel, it is possible to predict the energy dissipated on the structural members, until the vessel comes to rest, for any initial speed.

Using regression analysis it was possible to derive a relationship between the speed of the vessel during the collision and the speed prior to collision. Similar relationships have been derived between the indentation, and the collision time and the loss of kinetic energy with regard to the indentation. Therefore, one may numerically model the collision scenario using one initial speed value and be able to detect the indentation, velocity and loss of kinetic energy (or energy absorbed) for any initial speed.

The dynamic factors of mass inertia and strain rate appear not to contribute in the reaction of the vessel during the impact; their effects are negligible. This phenomenon indicates that the collision could have been examined as a quasi-static problem for this particular ship, for energy consideration. Such a static model was presented in this work and a comparison among the energy-indentation (E-I) curve with relation to the E-I curve produced from the dynamic problem yielded almost identical results. Therefore it is concluded that the head-on collision problem can be examined as quasi-static. This advantage is that the compile run-times are much lower.

Symmetry conditions during the modelling of the structure could not be used since the structure itself was not symmetric. The loss of symmetry was examined during the head-on collision and it was found that there are two reasons for this reaction. The progressive asymmetrical development of boundary reactions which appeared on those members that came into contact with the rigid surface, and the existence of a hatch opening on the starboard side of Deck4 as shown in figure 3.11 are the possible explanations.

The loss of symmetry during impact results in non-uniform loading on the collision bulkhead. This observation leads to the conclusion that the collision bulkhead should not be designed primarily to withstand symmetrical loads in case of a collision. Should there exist any asymmetry in the structure, this should be taken under consideration.

The applied procedure of adding up the load contributions of the bulb and bow will not always be correct. For a bulb/bow structure with a heavily-reinforced forward part followed by a weaker rear part, it was shown that the deformations may start in the rear part of this structure as well as in the forward part. The finite element analysis showed that the collapse mechanism of such a deck segment affects the elements, which are connected together and have not come in contact with the rigid surface.

The 90° head-on collisions could be used for design appraisal of the bow structure with regard to the indentation and loss of watertightness. The calculation of the indentation during the impact predicts whether penetration of the collision bulkhead will take place when the ship comes to rest, or even before. The collapse behaviour of longitudinal or transverse diaphragms, located in the bow, may result to the loss of watertightness and consequently oil outflow from the fuel tank, usually located in front of the collision bulkhead.

During design stage the global stiffness of the bow should be investigated in conjunction to the stiffness of the structural members located behind the collision bulkhead. For example, the designing of the bow to be able to withstand dynamic slamming loads produce highly strengthened members. During collision, these members, being able to withstand impact loads transmits most of the energy in the structure located behind the collision bulkhead, with resultant loss of watertightness in rear parts of the ship. Similar effects related to the strengthening of the bow are highly recommended, to be taken under consideration during assessment of collision damages in preliminary design.

### *6.1.2 GROUNDING WITH A RIGID SLIDE*

The grounding response of a tanker vessel was examined in order to ascertain the loss of kinetic energy due to elasto-plastic deformation of the bow structure. The bow model used for this analysis hits a rigid slide with a high frictional coefficient. The boundary conditions for the aft end of the bow model were derived from a static analysis, with the assumption that the vessel responds as a rigid beam.

It was found that the energy conservation in the case of grounding is primarily dependent on the kinetic energy lost due to friction and the elasto-plastic deformation of the bow structure. Until now, analytical approaches to this case have not incorporated any loss of kinetic energy due to local crippling of the structure.

The slope of the slide is a very important component since high slopes increase the elasto-plastic deformation of the bow, while low slopes increase the travelling

distance during the grounding and hence the friction energy. For the slope selected in this analysis it was shown that the elasto-plastic energy dissipated on the structure is almost 27% of the initial kinetic energy.

Other energy quantities, associated to the kinematics of the vessel during grounding, such as energy due to radial velocity and energy due to vertical displacement, have been examined. It was concluded that their contribution is negligible compared to the other two factors. It was found that the kinetic energy loss because of the radial velocity is at average less than 2% of the initial kinetic energy and the loss because of vertical displacement is almost 0.001% of the initial kinetic energy. The later value is small because of the small angle of pitching and the relative position of LCG with regard to the LCF.

The maximum bending moment capacity of the vessel should be incorporated in the grounding analysis since it is a factor that limits the global response of the vessel during the collision. Using the analytical solutions, an upper limit for angles was found, that is approximately, four degrees. Under this trimming angle the vessel under examination exceeds the design bending moment capacity. Beyond this limit, overall failure is considered to take place.

### *6.1.3 FAILURE CRITERIA*

In this thesis a Fracture Criterion has been introduced on the basis of the energy released at the tip of a crack during propagation. The energy needed to commence the propagation has been theoretically calculated using Griffith's (1920) fracture mechanics and considerations of Irwin's (1961) regarding the plastic zone around the tip of the crack.

The fracture criterion was developed during a study involving the evaluation of maximum energy absorption capacity of steel plates under lateral loading. The results were compared with three other empirical failure criteria from which two were associated with the magnitude of the local and mean strain. All criteria were used for the determination of an upper limit on the load deflection curve. It was

shown that the fracture criterion is very much dependent on the energy dissipated on the plate, during bending, in areas where plasticity is predominant.

When the fracture criterion is applied, the ultimate deflection and the corresponding strain are much lower than values obtained from the other criteria. In this case the effect of the in-plane boundary conditions of the plate is not of vital importance, because of the low value of the ratio of the deflection over plate thickness.

The study revealed that membrane response is of importance for breadth over plate thickness ratios greater than 150, a value which is considered to be high for ship plating.

In accordance with the fracture criterion, the mean strain does not exceed the value of 2%, when the ultimate point is reached.

Local strains are considerably higher than mean strains, in particular under patch loading. In this case the application of a criterion based on a maximum mean strain is considered inappropriate.

The fracture criterion was applied in the bow model during the head-on collision in areas where strains exceeded the plastic limit. It was possible to identify four areas with particular interest to the structural integrity of the structure.

The energy absorption characteristics of the bow model with regard to the fracture criterion were possible to be determined. Critical values for the initial speed yielded along with the minimum indentation required.

The 5% mean strain criterion did not prove to be applicable since the maximum elongation did not exceed 1% in most cases.

The 5% local strain criterion proposes values very similar to the fracture criterion. However, the strains calculated from the 5% criterion are less likely to identify a fracture in areas close to a fixed boundary.

## 6.2 PROPOSALS FOR FUTURE WORK

The work developed in this thesis proposes a methodology for the determination of the response of a tanker vessel during the head-on collision and grounding. The evaluation of the energy absorption characteristics and the behaviour of the structural members have been successfully carried out with the use of finite element code ABAQUS. For future research, the following work is proposed in this area.

- Modelling of the same head-on collision scenario, using several representative bow shapes in order to build a set of curves related to the Energy-Indentation relation and the Initial Speed-Indentation. This analysis will broaden the use of this method, and will positively identify the correction factors needed for the calculation of the indentation.

- It is proposed that examination of the crippling response of stiffened plates under dynamic axial loading with boundary constrains on edges should take place. This examination is very significant since evaluation of the energy-indentation relationship of a vessel during a head-on collision is depended upon the response of individual decks.

- The introduction of a parametric analysis in the grounding scenario, is suggested, using the slope of the slide, the friction coefficient, the initial speed of the vessel and the maximum bending moment capacity as parameters. Several representative vessels could be used in this case as well. With this analysis it will be feasible to evaluate the contribution of the elasto-plastic energy with respect to these parameters.

- Evaluation of the fracture criterion through experimental work. Plates with through thickness cracks could be modelled with various boundary conditions subjected to uniformly distributed and patch loading. Amplification factors could be introduced for these plates in order to represent similar plates with internal

flaws due to manufacturing or residual stresses rather than through thickness crack.

## 6.3 EPILOGUE

The results and conclusions presented in this thesis provide a better understanding of the energy dissipation during a head-on collision or grounding with a rigid surface. The analysis was performed with the use of powerful numerical tools and state of the art computer hardware. As mentioned previously, in the preface, this work is a step forward in the effort of mankind to answer to the question "*how does it work*?". It is also hoped that the work will also allow better design so that it will contribute to "how do we make it work better".

Apart from a better understanding in reliable designs there are other issues which have to be addressed towards an improved operation of vessels that sail in areas with high risk of collision.

It should be mentioned that ships are designed to undergo accidental loading on the basis of hazards and risks involved in marine operations. Systematic methods for hazard identification, quantitative risk assessment and cost benefit analysis have been developed, Cazzulo (1995), in order to minimise the human error influence in marine accidents.

Both prevention and mitigation is the solution to the problem. Controllable manufacturing, optimised repairing along with the appropriate feedback from responsible operation and efficient guidance for seamen are key points, which have to be introduced in order to re-evaluate the importance in shipping transport.

# REFERENCES


Akita Y., Kitamura K., A study on collision by an elastic stem to a side structure of ships, Transaction, Society Of Naval Architects Of Japan, vol. 131/307/, 1972

Akita Y., Ando N., Fujita Y., And Kitamura K., Studies on collision protective structures in nuclear powered ships, Nuclear Engineering And Design, vol. 19/365, 1972

Akita Y., Ando N., Fujita Y., Kitamura K., Studies on collision-protective structures in nuclear powered ships, Nuclear Engineering and Design, Vol. 19, pp. 365-401, 1972

Aldwinckle D. S., Lock J. E., Statistical analysis of classification records for oil tanker collisions and groundings, RINA, International Conference on Tankers and Bulk Carriers, The Way Ahead, 10-11 December, London 1992

Aldwinckle D. S, Lewis K. J., Prediction of structural damage penetration and cargo spillage due to ship collisions with icebergs, Report SSC-345, ICETECH-84 SNAME, ARTIC SECTION, April 1984

Amdahl J., Kavlie D., Analysis and design of ship structures for grounding collision, Practical Design of ships and Mobile Units, Caldwell & Ward Edition, 1992

Amdahl J., Mechanics of ship-ship collisions, basic crushing mechanics, Accidental Loadings on Marine Structures, Risk and Response, WEMT-95, Copenhagen. April-1995

Amdahl J., Energy absorption in ship platform impacts. Division of Marine Structures. The Norwegian Institute of Technology. report. no. UR-83-34. September 1983

Anderson T. C., Elastic plastic fracture mechanics-Marine structural applications, Ship Structures Committee, report SSC-345, April 1990

Anderson T. L., Elasto-plastic fracture mechanics-A critical review, Ship Structure Committee, Report SSC-345. Part 1 & 2, April 1990

Ando N., Arita K., A Study on the strength of double hall structures in collision trays, Society Of Naval Architects In Japan, /139/, 1976

Bates J. M., Impact of safety requirements on the design of ships, Oslo May 1975.

Bishop R., Burcher R. K., Price W. G, The use of functional analysis in ship dynamics, Proceedings. Of the Royal Society of London, Series A, Vol. 332, pp. 23-35, 1973

Bockrath G. E., Glassco J. B., A method of calculating R-curves from uniaxial tensile stress-strain curves, Presented at American Society of Testing and Materials, Report ASTM E-24, Louisville, Kentucky, March 18, 1980

Bokalrud T., Karlsen A., Control on fatigue failure in ship hulls by ultrasonic inspection, Norwegian Maritime Research, 10 (1), 9, 1982

Bonder S. R., Symonds P.S., Plastic deformation in impact and impulsive loading of beams, In Plasticity Proceedings. of the 2nd Symposium of Naval structural mechanics, Pergamon Press, 1960.

British Standard Institution. Guidance on some methods for the derivation of acceptance levels for defects in Fusion Welded Joints, Published Document, PD 6493, 1980

Broberg K. B., Fracture mechanics, Arkiv Fysik 18. 159, 1960

Burdekin F. M., Dawes M. G., Practical use of linear elastic and yielding fracture mechanics with particular reference to pressure vessels, Proceedings of the Institute of Mechanical Engineers, Conference, London, pp.28, May 1971

Burness, Corlett & Partners (IOM) Ltd. Glasgow, Forth Road Bridge Collision Assessment, Report NAOE-95-22, 12 July 1995

Cazzulo R. P., Maritime safety and risk acceptance criteria, 22nd WEGEMT Graduate School, Accidental Loading on Marine Structures, Risk and Response, Technical University of Denmark 24th-29th April 1995

Chapelle H. I., Late Senior Historian, Museum of History and Technology, Smithsonian Institution, Author of Boat building, A Complete Handbook and Yacht Designing and Planning, 1998

Corbett G. G., Reid S. R., Quasi-Static and dynamic local loading of monolithic simply-supported steel plate, International Journal of Impact Engineering Vol. 13, No. 3, pp. 423-441, 1993

Cowper G. R., Symonds P. S., Strain hardening and strain rate effects in the impact loading of cantilever beams, Technical Report No. 28 from Brow University Rhode Island, 1957

Craggs, L. W., In fracture of solids, D. C Drucker and J.J. Gilman, editors. Wiley, New York, 1963

Crisfield M. A., Full-range analysis of steel plates and stiffened plating under uniaxial compression, Proceedings of the Institution of Civil Engineers. Part 2, 59, pp. 595-624, December 1975

Cummins, W. E., The impulse response function and ship motions, Schiffstechnik, Heft 47, (9 Band), pp 101-109, June 1962

Daidola J., Tanker structures behavior during collision and grounding. Marine Technology, vol. 32, No. 1, pp. 20-32, January 1995

Dan E., Aldstedt E., Design of offshore concrete structure based on post processing of results from finite element analysis (FEA), Methods Limitations and Accuracy, International Offshore and Polar Engineering Conference-94, vol. IV April 10-15 1994

Das P.K., Glykas A., Faulkner D., Forth road bridge ship collision assessment, Department of Naval Architecture and Ocean Engineering, Technical Report, NAOE- 95- 22, July 1995

Duffey T. A., Scaling laws for fuel capsules subjected to blast, impact and thermal loading, Proceedings Intersociety Energy Conversion Conference., Paper S.A.E. 719107, 1971

Egge E. D., M. Böckenhauer, Calculation of the collision Resistance of ships and its assessment for classification purposes. Germanischer Lloyd, Marine Structures, Elsevier Science Publishers Ltd. Pp. 35-56, August 1991

Fan Z., Load-carrying mechanism of restrained plates at large deflections, Journal of Engineering Mechanics, vol. 120, No 6, June 1994

Faulkner D., Compression tests on welded eccentrically stiffened plate panels, in steel plated structures, Crosby Lockwood Staples, London, pp. 130-139, 1977

Finite Element Analysis Ltd, Lusas (Finite Element Code) theory manual version 11, FEA Ltd. Forge house, 66 high street, Kingston, Upon Thames, Surrey, KT1 HN, UK, 1995

Frieze P. A., Dowling P. J. and Hobbs R. H., Ultimate load behaviour of plates in compression, in steel plated structures, Crosby Lockwood staples, London, pp. 24-50, 1977

Gerard G., The crippling strength of compression elements, Journal of the Aeronautical Sciences, 1958

Glykas A., Das P.K., Energy conservation during a tanker collision, Journal of Ocean Engineering, Accepted for Publication, March 1998

Glykas A., Das P.K., Failure criteria assessment during a tanker collision, Under preparation, Journal of Ocean Engineering, April 1998

Glykas A., Samouelides E., Das P. K., Energy absorption capacity of plates under lateral loading, Proceedings of the 6$^{th}$ International Conference Of Offshore and Polar engineers, Los Angeles-96, vol. IV pp. 502-509, May 1996

Griffith A., The Phenomena of rupture and flow in solids, Philosophical Transactions, Series A, Vol. 221, pp. 163-198, 1920

Harding J. E., Hobbs R. E. and Neal B. G., The elasto-plastic analysis of imperfect square plates under in-plane loading, Proceeding of the Institution of Civil Engineers, Part 2, vol. 63, pp. 137-158, 1977

Harima T., Research on the collision-resisting construction of the sides of a nuclear powered ship, Mitsubishi Nippon Industries Technical Review, 1962

Harrison J. D., Davies M.G., Archert G. L., Kamath M. S., The COD approach and it's application to welded structures, Elastic Plastic Fracture, American Society of Testing and Materials Technical Publication No. 668, pp. 606 1979

Haywood J. H., A note for collision estimate for LNG carriers, NCRE, Dunfermline, Fife, Report G27 1a/110l,1971

Hegazy E. H., Assessment of collision resistance of Ships - A survey of the state of the art and new methodology, Newcastle upon Tyne. October 1980.

Hibbit, Karlsoon & Sorensen, ABAQUS Theory Manual, Version 5.5, January 1995

Hudson J., Boyd G. M., Brittle fracture in welded ships-An empirical approach from recent experience. Institution of Naval Architects, Vol. 100, No. 3, pp.141, July 1958

Hooke R., Rawlings B., An experimental investigation of the behaviour of clamped rectangular mild steel plates subjected to uniform transverse pressure, Proceedings of the Institute of Civil Engineers, 42, pp. 75-103, 1969

Horne M. R., Narayanan R., Ultimate capacity of stiffened plates used in girders, Proceedings of the Institution of Civil Engineers, Vol. 61, pp. 253-280, 1976

Horne M. R., Montague P., Narayanan R., Influence on strength of compression panels of stiffener section-Spacing and welded connection, Proceedings of the Institution Of Civil Engineers, Vol. 63, Part 2, pp.1-20, 1977

Hughes Owen F., Ship structural design-A rationally-based, computer based optimisation approach, John Wiley Sons, Interscience Publications, 1983.

Irwin G. R., Materials for missiles and spacecraft, Mc Graw-Hill, New York, 1963

Irwin G. R., Plastic zone near a crack and fracture toughness, Sagamore Research Conference Proceedings, Vol. 4, 1961

Ito H., Kondo K., Yoshimura N., Kawashima M., Yamamoto S, A simplified method to analyse the strength of double hulled structures in collisions (1st report ). Read at the autumn meeting of The Society Of Naval Architecture Of Japan, Journal Of The Society Of Naval Architects Of Japan, vol. 156/283/, 1984

Ito H, Kondo Yoshimura N, Kawashima M And Yamamoto S, A simplified method to analyse the strength of double hulled structures in collisions (2nd report ). Read at the autumn meeting of The Society Of Naval Architecture Of Japan, Journal Of The Society Of Naval Architects Of Japan, vol. 158/543/, 1985

Jennings P. E., Kim G. Luis R., Inelastic deformation of plate panels, Ship Structure Committee, SSC-364, January 1991.

Jones N., Walters R.M., Large deflection of rectangular plates, Journal of Ship Research, 15(2), pp. 164-171, June 1971

Jones N., Some remarks on the strain rate behaviour of shells in problems of plasticity, Edited, A Sawczuk, Leyden, pp. 403-407, 1972

Jones N., Slamming damage, Journal of Ship Research, Vol. 17, pp. 80-86, 1973

Jones N., Plastic behaviour of ship structures, Transactions, SNAME, vol. 84, p. 115, 1976

Jones N., Literature survey on the collision and grounding protection of ships, SSC 283, U.S. Coastguard, Washington, 1979

Jones N., Wierzbicki T., Structural crashworthiness, Butterworth & Co Publishers Ltd, 1983

Jones N., Jouri W. S., Birth R. S, On the scaling of ship collision damage, In Proceedings, 3rd International Marine Technology, Athens, International Maritime Association Of East Mediterranean Phivos Publishing co., pp 287-294 1984

Jones N., Scaling of inelastic structures loaded dynamically, in structural impact & crashworthiness, vol. 1, G.A.O Davies Ed, Elsevier applied science Publishers, pp 45-74, 1984

Jones N., Jouri W. S., Study of plate tearing for ship collision and grounding damage, Journal of Ship Research, vol. 31, No. 4, pp. 253-268, December 1987

Jones N., Liu T. G., Zheng, Shen W. Q., Clamped beam grillages struck transversely by a mass at the center, International Journal of Impact Engineer. 11(3), pp. 379-399, 1991

Hagiwara K., Takanabe H., Kawano H., A proposed method of predicting Ship collision damage. Ship strength laboratory, Nagasaki Technical Institute, Japan, 1982

Kisielewicz L. T., Ando K., Petitjean A., Numerical simulation of a ship colliding against a pier structure, ESI ASIA, Tokyo, Japan, International Offshore and Polar Engineering Conference, 93 Singapore, 6-11, vol. IV, pp. 677-684, June 1993

Kitamura O., Comparative study on collision resistance of side structure, Nagasaki, R & D center, Mitsubishi Heavy Industries, 1997

Köhler P. E., Potential oil spills from tankers in case of collision and grounding, DNVC Report, 90-0074, Det Norske Veritas, Oslo, 1990

Kuroiwa T., Nakamura T., Kawamoto Y., Study on structural damage of ships due to collision and grounding, International Offshore and Polar Engineering Conference-94, VOL. IV April 10-15 1994

Liang W. J., Dynamic analysis of ship-ship collision, International Symposium on Marine Structures [ISMS]-91, Shanghai CHINA, September 13-14, 1991

Little G. H., Stiffened steel compression panels-Theoretical failure analysis, The Structural Engineer. Volume 54A, pp. 489-500, 1976.

Little G. H., The collapse of rectangular steel plates under uniaxial compression, The Structural Engineering, Vol. 58B, pp. 45-60, 1980

Lloyds Rule Book, Test for class 1 and class 2/1 fusion welded pressure vessels, Routine tests and test plates, Chapter 17, Section 3, Paragraph 3.2.11 g. Lloyd's Register of Shipping and International Maritime Organisation, 1996

Manjoine R., Influence of rate of strain and temperature on yield stress of mild steel, Journal of Applied Mechanics, Vol. 11. P. A211, 1944

March K. J., Campbell J. D., The effect of strain rate on the post yield flow of mild steel, Journal of Mesh and Physics of Solids, pp. 11-49. 1963

Minorsky V. U., An analysis of ship collisions with reference to the protection of nuclear powered plants, Journal of Ship Research, Vol. 3, No. 2, pp. 1-4. October 1959

Minorsky V. U., Evaluation of ship-bridge pier impact and of islands as protection, Ship Collisions With Bridges and Offshore Structures, IABSE Colloquium, Copenhagen 1983.

Moolani F. M, Dowling P. J., Ultimate load behaviour of stiffened plates in compression, In Steel Plated Structures, Crosby Lockwood staples, London 1977

Nakamura & Kuroiwa, Experimental study on the failure of ship side structure, Proceedings MARIENV, 1995

NCRE, Plastic and limit design, Committee Report 3E , Proceedings 3rd International Ship Structures Congress, pp 68-67, Hamburg 1967

Ottesen H., Sjogren L., Artificial islands as protection against ship impact, International Offshore and Polar Engineering Conference -94, VOL IV April 10-15 1994

Ohtsubo H., Damage of ship structures in collision and grounding accidents, International Conference Advances In Marine Structures III, Dunfermline, 20-23 May 1997

Ostapenko A., Ultimate strength design of wide stiffened plates loaded axially and normally. Supplementary report No. 164 UC, Transport and Road Research Laboratory, England, pp. 175-180, 1974

Östergaard C., Collision and grounding mechanics, Accidental Loadings on Marine Structures, Risk and Response WEMT-95, Copenhagen. April-1995

Ottesen H. E., Leif S., Artificial islands as protection against ship impact, International Offshore and Polar Engineering Conference-94, vol. IV April 10-15 1994

Paik J. K., Pedersen P. T., Grounding-induced sectional forces and residual strength of grounded ship hulls, International Offshore and Polar Engineering Conference, Los Angeles-96, vol. IV pp. 517-522, 1996

Paik J. K., Wierzbicki T., A benchmark study on crushing and cutting of plated structures, Journal of Ship Research, V41,2, 1997

Parkes E. W., The permanent deformation of an encastre beam struck transversely at any point in it's span, Proceedings of the Institution of Civil Engineers, vol. 10/277, 1958

Pedersen P. T., Yong B., Collision analysis of offshore platforms and bridges, International Symposium on Marine Structures [ISMS]-91, Shanghai CHINA, September 13-14, 1991

Pedersen P. T., Valsgaro S., Ship impacts-bow collisions, International Journal of Impact Engineering Vol. 13, No. 2, pp. 163-187, 1993

Pedersen P. T., Yong B., Elastic-plastic behavior of offshore steel structures under impact loads, International Journal of Impact Engineering Vol. 13, No. 4, pp. 99-115, 1993

Pedersen P. T., Collision and grounding mechanics, Accidental Loadings on Marine structures, Risk and Response WEMT-95, Copenhagen. April-1995

Pedersen P. T., Probability of grounding and collision events, Accidental Loadings on Marine structures, Risk and Response, WEMT-95, Copenhagen. April-1995

Perzyna P., Fundamental problems in viscoplasticity, Advances in Applied Mechanics, Vol. 9, p.243, 1966

Petersen M. J., Dynamics of ship collisions, Journal of Ocean Engineering, Vol. 9. No. 4, pp. 295-329, 1982

Pettersen E, Assessment of import damage by means of a simplified non linear approval, Integrity Of Offshore Structures Applied Science Publishers, /317,1981

Pettersen E., Analysis and design of cellular structures, Report No. UR-79-02, Department of Marine Technology, Norwegian Institute of Technology, 1979

Poudret J., Hunter M., Jean P., Vaughan H., Grounding of a tanker, correlation between damage prediction and observation, Paper presented at Extreme Loads Response Symposium, Arlington, Virginia, October 1981

Reckling K. A., On the collision protection of ships, Practical Design of Ships and Mobile Units, pp. 129-134, Tokyo, October 1977

Reis A. J., Rooda J., The interaction between lateral torsional and local plate buckling in thin walled beams, Preliminary Report of the 2nd International Colloquium on Stability of Ship Structures, Liege, pp.415-425, 1977

Rodd L. J., Large scale tanker grounding experiments, International Offshore and Polar Engineering Conference, Los Angeles-96, vol. IV pp. 483-494, 1996

Rodd L. J., Frame design effects in the rupture of oil tankers during grounding accidents, International Conference Advances in Marine Structures III, Dunfermline, 20-23 May 1997

Rolfe S. T., Barsom J. M., Fracture fatigue control in structures-Application of fracture mechanics, Prentice-Hall, 1977

Ronalds B. F., Dowling P. J., Finite deformations of stringer stiffened plate and shells under knife edge loading, Proceedings of 5th International Conference on Offshore Mechanics and Arctic Engineering, (323), 1986

Saether S., Fracture toughness of ship plates, NVA, NVD, NVE36, Det Norske Veritas, Report No. 80-1014, 1980

Sano et al., A study on the strength of a double hull side structure of a VLCC in collision. Proceedings, MARIENV, 1995

Samuelides E., Structural dynamic and rigid body response coupling in ship collisions, Ph.D. Thesis, Glasgow University, Department of Naval Architecture and Ocean Engineering, Glasgow, 1984

Sanders J. L., Elasto-plastic fracture mechanics, Journal of Applied Mechanics vol. 27, pp. 352, 1960

Sawczuk A., On Initiation of the membrane action in rigid plastic plates, Journal Méchanique, 3 (1), pp 15-23, 1964

Shen W. Q., Dynamic response of a grillage under mass impact, International Journal of Impact Engineering Vol. 13, No. 4, pp. 555-565, 1993

Shuji A., Kentaro O., Evaluation of local brittle zone of offshore structural steels by CTOD and Instrumented Pre-crack charpy impact test, Proceedings of the 4th International Offshore and Polar Engineering Conference, Vol. IV, p.p 198-205, conference, Osaka, Japan, 1994

Simonsen B. C., Wierzbicki T., Grounding bottom damage and ship motion over a rock, International Offshore and Polar Engineering Conference, Los Angeles-96, vol. IV pp. 476-482, 1996

Simonsen B. C., Pedersen P. T., On grounding of fast ships, International Conference Advances In Marine Structures III, Dunfermline, 20-23 May 1997

Smith C. S. et al., Non-linear structural response, Proceedings of the 7th, International Ship Structures Congress, Vol. 1, pp. II, 2-1-II., February 1987

Smith C. S., Compressive strength of welded steel ship grillages, Transactions RINA, pp. 325-359, Vol. 117, 1975

Søreide T. H., Amdahl J., Deformation characteristics of tubular members with reference to impact loads from collision and dropped objects, Norwegian Maritime Research, vol. 10, No. 2, /3/ 1982

Søreide T. H., Bergan P. G., Moan T., Ultimate collapse behaviour of stiffened plates using alternative finite element formulations, In Steel Plated Structures, Crosby Lockwood Staples, London, pp. 618-637, 1977

Soreide T. H., Collapse, Behaviour of stiffened plates using alternative finite element formulations, Report No. 77-3, Division of Structural Mechanics, The Norwegian Institute of Technology, Trondheim, Norway, 1977

Søreide T. H., Moan T., Nordsve N. T., On the behaviour and design of stiffened plates in ultimate limit state, Journal of Ship Research, vol. 22. No. 4, pp. 238-244, 1978.

American Society of Testing And Materials, Standard test method for $J\text{-}_{IC}$, a measure of fracture toughness, , Report ASTM 813-88, 1988

Sumpter J. D. G., Bird J., Clarke J. D., Caudrey A. .J., Fracture toughness of ship steel, The Royal Institution Of Naval Architects, Read in London at a meeting of the RINA on April 20, 1988

Symonds S., Jones N., Impulsive loading of fully clamped beams with finite plastic deformations and strain rate sensitivity, International Journal Mech. Sci. Vol. 14, p.49 1972

American Society of Testing And Materials, Test Method for plain-strain fracture toughness of metallic materials, Report ASTM E399.,

TRRC Report 254, Recommended standard practices for structural testing of steel models, 1977

Tvergaard V. and Needleman A., Buckling of eccentrically stiffened elastic-plastic panels of two simple supports or multiply supported, International Journal of Solids and Structures, Vol. 11, pp647, 1975

Ueda Y., Yao T., Ultimate strength of a rectangular plate under thrust-with consideration of the effects of initial imperfections due to welding, Transactions of Japan Welding research Institute of Osaka University, Vol. 8, No. 2, pp.97-104, 1979

Ueda Y., Murakawa H., Xiang D., Classification of dynamic response of a tubular beam under collision, Proceeding of 8th International Conference on OMAE /645/, 1989

Valsgård S., Pettersen E., Simplified non-linear analysis of ship/ship collisions, Norwegian Maritime Research, vol. 10, no 3,/2/,1982

Vaughan H., Bending and tearing of plate with application to ship bottom damage, The Royal Institution Of Naval Architects, Journal Of The Naval Architect, Issue 97, May 1978

Vredeveldt W. A., Collision and grounding mechanics-Accidental loading on marine structures, Risk and Response, WEMT-95, Copenhagen. April-1995

Ward G. N., Linearised Theory Of Steady High Speed Flow, Cambridge, London, 1955

Watson D. G. M, Gilfillan A. W., Some ship design methods, The Royal Institution of Naval Architects Joint Meeting, Glasgow and evening meeting, London November 1976

Westergard H. M., On fracture mechanics, Transaction, The American Society of Mechanical Engineers, ASME 61, A49, 1939

Wierzbicki T., Crushing behaviour of plate intersections, Structural Crashworthiness, edited by Jones N. and Wierzbicki T., Chapter 3, Butterworth & Co. Ltd., 1983

Woisin G., Design against collision, International Symposium On Advances In Marine Technology, Trodheim, Norway, 1979

Woisin G., The transferability of collision model tests to real collisions, Part 4: Model Test Techniques For Investigating Ship Collision, Unpublished Paper, 1986

Woisin G., Discussion at international symposium on structural crash worthiness, University Of Liverpool, Sept 1983

Wood R. H., Plastic and elastic design of slabs and plates, The Ronald Press, New York, 1961

Yang P. D. C., Caldwell J. B., Collision energy absorption of ships-Bow structures, International Journal of Impact Engineering, Vol. 7, No. 2, 1988

Zhu L., Faulkner D., Dynamic inelastic behavior of plates in minor ship collisions, International Journal of Engineering vol. 15, No. 2 pp. 165-178, 1994

# LIST OF FIGURES

## CHAPTER 1



## CHAPTER 2

CHAPTER 3

CHAPTER 4

CHAPTER 5

# LIST OF TABLES

## CHAPTER 1



## CHAPTER 2



## CHAPTER 3

CHAPTER 5